RELEVANCE OF THE EPIGENETIC REGULATION EXERCISED BY HEPATIC MICRORNAS IN THE FATTY LIVER ARENA: FROM THE BEDSIDE TO THE BENCH

Jèssica Latorre Luque

Universitat de Girona

DOCTORAL THESIS

RELEVANCE OF THE EPIGENETIC REGULATION EXERCISED BY HEPATIC microRNAs IN THE FATTY LIVER ARENA: from the bedside to the bench

Jèssica Latorre Luque

2019

Universitat de Girona

DOCTORAL THESIS

RELEVANCE OF THE EPIGENETIC REGULATION EXERCISED BY HEPATIC microRNAs IN THE FATTY LIVER ARENA: from the bedside to the bench

Jèssica Latorre Luque

2019

Doctoral Programme in Molecular Biology, Biomedicine and Health

Supervised by:
Francisco José Ortega Delgado, Ph. D
José Manuel Fernández-Real Lemos, Ph. D, M.D.

Tutor:
Prof. José Manuel Fernández-Real Lemos

Presented to obtain the degree of PhD at the University of Girona

Universitat de Girona

Dr **Francisco José Ortega Delgado**, principal investigator of the *Biomedical Research Institute of Girona (IDIBGI), Endocrinology, Diabetes and Nutrition Research Unit (UDEN)*. Researcher ascribed to the *CIBER de la Fisiopatología de la Obesidad y la Nutrición (CIBEROBN, ISCIII)*.

Prof. **José Manuel Fernández-Real Lemos**, group leader of the *Biomedical Research Institute of Girona (IDIBGI), Endocrinology, Diabetes and Nutrition Research Unit (UDEN)*, lead investigator of the *CIBER de la Fisiopatología de la Obesidad y la Nutrición (CIBEROBN, ISCIII)*, and professor of medicine at the *University of Girona* (UdG).

WE DECLARE:

That the thesis entitled "***RELEVANCE OF THE EPIGENETIC REGULATION EXERCISED BY HEPATIC microRNAs IN THE FATTY LIVER ARENA: from the bedside to the bench***", presented by Jèssica Latorre Luque to obtain the doctoral degree in *Molecular Biology, Biomedicine and Health* by the *UdG*, has been completed under our supervision and fulfils all the requirements to qualify for an International Doctorate.

For all intents and purposes, we hereby sign this document.

Dr. Francisco José Ortega Delgado Dr. José-Manuel Fernández-Real Lemos

Girona, 2019

Alça el vol, marxa lluny,
I què importa si ningú ho entén?
Que les mateixes pors que ens ceguen
Són finestres plenes de llum.

Oques Grasses (2019)

ACKNOWLEDGEMENTS

Bé, doncs finalment sembla que he acabat la tesi. La veritat és que abans de començar, només de pensar que hauria de doctorar-me, feia bastanta por perquè no dir-ho. I després de quasi cinc anys, puc dir que m'han passat volant i tot i que hem passat moments bons i no tan bons, tot el que m'enduc no ho canviaria per res. Al final, el trajecte no ha estat tan complicat gràcies al suport i la cooperació incondicional de totes i cadascuna de les persones que m'he trobat pel camí.

En primer lloc, vull donar les gràcies al Dr. José Manuel Fernández-Real, director d'aquesta tesi, per ser el primer en parar-me la mà, per la confiança dipositada en mi i per ajudar-me a créixer com a investigadora.

Paco, gràcies per tot. Podria fer una llista molt llarga de tot el que m'has ensenyat i com he arribat a aprendre al teu costat. Gràcies per fer-me veure que la ciència pot ser a vegades frustrant, però també molt gratificant. Gràcies per dir-me sempre les veritats, pels consells, per ajudar-me a calmar els nervis, per fer possible que avui acabi aquesta tesi. Gràcies per ser més que un director, un amic.

José, el teu suport, els teus consells, la teva disposició a ajudar-me en tot moment i la dedicació que has posat en ensenyar-me fan que ara sigui aquí, a punt de dipositar una tesi que sense vosaltres no hagués estat possible.

Quan vaig arribar a UDEN el grup era molt petit. Isa, estar contigo los primeros días cuando empecé me ayudó muchísimo. Després va tornar la Moni, m'havien dit que eres una peça clau del grup i no s'equivocaven. Pacient, enèrgica, amable, atenta, tot un suport i un exemple a seguir.

Aina i Ferran, els meus germans petits. Un gran tàndem dins i fora del laboratori, per la tranquil·litat que m'ha donat saber que éreu sempre allà. Hem compartit moltíssimes coses, des dels mítics esmorzars de bikini al Trueta, colze amb colze als tres ordinadors de baix ben apretadets, infinites converses arreglant el món, hores i hores de poiata, i fins a unes bones nits de festa. De les persones amb qui més hem plorat de riure. Aina, tot i que hem passat un any separades, t'he sentit més a prop que mai. Em considero molt afortunada d'haver-vos tingut al costat tot aquest temps.

Núria i Anna, les noves incorporacions de UDEN, gràcies per l'ajuda desinteressada, els somriures i les estones juntes. Anna, especial menció pels últims dies colze a colze amb les respectives tesis, pels riures que només denotaven estrés, tu a punt de llegir, i jo estirant-me els

cabells amb els últims detalls. I Núria, per ser els meus segons ulls, per cedir-me una mica del teu perfeccionisme. Gràcies a totes dues, en poc temps hem creat un vincle molt especial.

I a tots els membres de UDEN, que han format part de tot això, Estefania, Òscar, Emili, María, Laia, Fer, Luz...gràcies. També agrair a tots els col·laboradors que han format part d'aquest projecte, gràcies a tots per proporcionar les eines necessàries per arrodonir aquesta tesi.

Però com que a l'IdIBGi som pocs i benavinguts, em toca agrair una miqueta més. Rocío, crec que vas ser la primera persona que vaig conèixer fora de UDEN, de seguida vaig pensar, serem amigues. Molts consells, però sobretot una pila de bromes per no parar mai de riure. María! Que haría yo sin ti! Creyendo en mi más de lo que yo haré nunca. Gracias por tu apoyo incondicional, por preocuparte siempre por mi y por lo bien que lo hemos pasado juntas, y junto a Aina, las tres. Marini, l'alegria assegurada, un riure contagiós que et canvia l'estat d'ànim fins i tot quan se't moren les cèl·lules a cultius. Gràcies per transmetre aquesta alegria sempre. I a les noietes de Pedi, Berta i Ari, tant semblants entre vosaltres i molt semblants a mi també, gràcies per la complicitat, pels moments de desconnexió durant el dia, cafès, dinars i estonetes a la tarda si és necessari. Una estona de riures i una mica de xocolata sempre fa les coses més fàcils.

També vull agrair-vos Bet, la veu de l'experiència, Sara, Carme, Sílvia, Ester, Esther, Gerard, Laia...per l'agradable convivència de l'IdIBGi. Moltes gràcies a tots.

Moving to Finland, I am totally grateful to Prof. Vesa Olkkonen for providing me the opportunity to work in his laboratory for three months. I really appreaciate all the scientific help and facilities. I sincerely thank also to Dr. Nidhina Haridas, for your advice, expertise and the great attention on me. And finally Maria, thanks for being there, kind and friendly, willing to help whenever it was necessary.

And I am specially grateful to my dearest friend in Helsinki, Patience, for your constant encouragment and for being a really nice and supportive friend, even at -15 degrees.

El suport no s'acaba a la feina però. Aina i Clara, com hem rigut compartint les penes de ser un "pre-doc", i comparant-nos amb les senyores empresàries Flor i Elena. Gràcies *Ramones* per formar part d'aquest camí de principi a fi. Pels viatges, els sopars i els riures que et fan oblidar de totes les preocupacions. En especial, Aina gràcies per la quantitat de moments compartits al telèfon tot i estar ben a prop, per confiar en mi.

I ja per acabar, agrair a totes i cadascuna de les meves nenes, Gina, Àstrid, Anna, Alba, Pepa, Curi, Alba i Anna, per preguntar-me sempre, per oferir-me ajuda, i sobretot per donar-me els

millors moments de desconnexió. Gràcies per ser la millor colla del món no només ara, sinó des de sempre.

Papes, avis i Èric, sense vosaltres no hauria arribat fins aquí. Pels *tuppers* de l'avi, l'ajuda incondicional, les bromes sobre "com es diu això amb el que treballo", per respectar-me i ser allà, per fer-me sentir recolzada i per animar-me a tirar endavant sempre. Gràcies per ensenyar-me que la constància dóna els seus fruits. Gràcies per creure en mi més del que mai jo arribaré a creure.

I per últim, voldria agrair de manera molt especial a l'Edu el suport incondicional durant tots aquest anys. Gràcies per treure sempre el millor de mi. Per totes les hores que he dedicat a la tesi en comptes de a tu, per la paciència, el suport, les rialles, l'estima, i per tots aquests anys. Perquè aviat podràs fer tu una tesi de microRNAs amb tot el que has hagut d'aguantar. Ara i aquí, sempre al meu costat.

Aquesta tesi és meva però també és vostra, moltes i moltes gràcies a tots i cadascun de vosaltres. M'emporto una tesi, però sobretot, m'emporto amics de veritat.

LIST OF ORIGINAL PAPERS

1. Latorre J, Moreno-Navarrete JM, Mercader JM, Sabater M, Rovira Ò, Gironès J, Ricart W, Fernández-Real JM, Ortega FJ. **Decreased lipid metabolism but increased FA biosynthesis are coupled with changes in liver microRNAs in obese subjects with NAFLD.** *Int J Obes (Lond). 2017 Apr;41(4):620-630.* doi: 10.1038/ijo.2017.21.

2. Latorre J, Ortega FJ, Liñares-Pose L, Moreno-Navarrete JM, Lluch A, Comas F, Ricart W, Höring M, Zhou Y, Liebisch G, Haridas PAN, Olkkonen VM, López M, Fernández-Real JM. **Treatments mimicking NAFLD compromise the biosynthesis of microRNAs required to maintain lipid homeostasis in hepatocytes.** *Under review.*

Articles attached in Appendix II.

ABBREVIATIONS

18S	*18S ribosomal RNA*
36B4	*acidic ribosomal phosphoprotein*
ACACA	*acetyl-CoA carboxylase alpha*
ACLY	*ATP-citrate lyase*
ACSL	*acyl-CoA synthetase long chain*
ACTB	*actin, beta*
AGO	*argonaute*
AGPAT	*1-acylglycerol-3-phosphate*
AGPS	*alkylglycerone phosphate synthase*
ALP	*alkaline phosphatase*
ALT	*alanine aminotransferase*
AMPK	*AMP-activated protein kinase*
ANGPTL3	*angiopoietin like 3*
ANOVA	*analysis of variance*
apoB	*apolipoprotein B*
ARL6IP1	*ADP-ribosylation factor-like 6 interacting protein 1*
ATCC	*American Type Culture Collection*
ATF6	*activating transcription factor 6*
BMI	*body mass index*
BSA	*bovine serum albumin*
BSCL2	*Berardinelli-Seip congenital lipodystrophy 2 lipid droplet biogenesis associated, seipin*
CACT	*acylcarnitine translocase*
CAP	*controlled attenuation parameter*
CAR	*constitutive androstane receptor*
CC	*compound C*
CD36	*CD36 molecule*
CE	*cholesterol ester*
Cer	*ceramides*
ChoRE	*carbohydrate responsive element*
ChREBP	*carbohydrate-responsive element-binding protein*
CKD	*chronic kidney disease*
CPT	*carnitine palmitoyl transferase*
CRP	*C reactive protein*
CRTC2	*CREB regulated transcription coactivator 2*
CT	*computed tomography*
Ct	*cycle threshold*
CVD	*cardiovascular disease*
DAG	*diacylglycerol*

DBP	*diastolic blood pressure*
DDIT3	*DNA damage inducible transcript 3*
DGAT	*diacylglycerol acyltransferase*
DGCR8	*DiGeorge syndrome critical region gene 8*
DICER	*dicer ribonuclease III*
DME	*drug metabolizing enzymes*
DMEM	*Dulbecco's Modified Eagle's Medium*
DMSO	*dimethyl sulfoxide*
DNA	*desoxyribonucleic acid*
DNL	*de novo lipogenesis*
DROSHA	*drosha ribonuclease III*
EDC	*endocrine disrupting compounds*
EDTA	*ethylenediaminetetraacetic acid*
ELOVL5	*ELOVL fatty acid elongase 5*
FA	*fatty acid*
FABP4	*fatty acid binding protein 4*
FASN	*fatty acid synthase*
FATP	*fatty acid transport protein*
FATP5	*fatty acid transport protein 5*
FBS	*fetal bovine serum*
FFA	*free fatty acids*
FFM	*fat free mass*
FIA	*flow injection analysis*
FLI	*fatty liver index*
FoxO1	*forkhead box-containing protein O subfamily 1*
FRET	*fluorescence resonance energy transfer*
GCKR	*glucokinase regulator*
G6P	*glucose-6-phosphate*
G6PC	*glucose 6-phosphatase subunit*
GGT	*γ-glutamyl transferase*
GLP-1	*glucagon-like peptide-1*
GLUT2	*glucose transporter 2*
GNPAT	*glyceronephosphate O-acyltransferase*
GOT	*glutamic oxaloacetic transaminase*
GPAT	*glycerol-3-phosphate acyltransferase*
GPT	*glutamate pyruvate transaminase*
H-MRS	*proton magnetic resonance spectroscopy*
HAMP	*hepcidin*
HbA1c	*glycated haemoglobin*
HCC	*hepatocellular carcinoma*
HDL	*high density lipoproteins*

HexCer	*hexosylceramides*
HG	*high-glucose*
HH	*human hepatocytes*
HL	*hepatic lipase*
HOMA-IR	*Homeostatic model assessment for insulin resistance*
HSL	*hormone sensitive lipase*
HSPA5	*heat shock protein family A (Hsp70) member 5*
IDL	*intermediate-density lipoprotein*
IL-6	*interleukin 6*
INSR	*insulin receptor*
IR	*insulin resistance*
IRS	*insulin receptor substrate*
ITGAX	*integrin subunit alpha X*
JNK-1	*c-Jun N-terminal kinase*
KD	*knockdown*
LBP	*lipopolysaccharide binding protein*
LCFA	*long chain fatty acid*
LD	*lipid droplet*
LDL	*low-density lipoprotein*
let-7	*lethal-7*
LPA	*lysophosphatidic acid*
LPC	*lysophosphatidylcholine*
LPE	*lysophosphatidylethanolamine*
LPL	*lipoprotein lipase*
LSD	*least significant difference*
LSD	*Fisher's least significant difference*
Lv	*lentiviral*
M-CLAMP	*insulin action measured using hyperinsulinemic-euglycemic clamp*
MBOAT7	*membrane bound O-acyltransferase domain containing 7*
MCD	*methionine-choline deficient*
MEM	*minimal essential Eagle medium*
MetS	*metabolic syndrome*
MGAT1	*mannosyl (alpha-1,3-)-glycoprotein beta-1,2-N-acetylglucosaminyltransferase*
miRNA	*microRNA*
MOI	*multiplicity of infection*
MRI	*magnetic resonance imaging*
mRNA	*messenger RNA*
Mtf	*metformin*
MTTP	*microsomal triglyceride transfer protein*

mut	*mutated*
NA	*not available*
NAFL	*non-alcoholic fatty liver*
NAFLD	*non-alcoholic fatty liver disease*
NAS	*NAFLD activity score*
NASH	*non-alcoholic steatohepatitis*
ND	*not detectable*
NEFA	*non-esterified fatty acid*
NR1H3	*nuclear receptor subfamily 1 group H member 3 (or liver X receptor alpha, LXRA)*
NR1H4	*nuclear receptor subfamily 1 group H member 3 (or farnesoid X receptor, FXR)*
nt	*nucleotides*
NT	*non-targeting*
OA	*oleic acid*
OCR	*oxygen consumption rate*
OGTT	*oral glucose tolerance test*
PA	*palmitic acid*
PACT	*protein kinase RNA activator*
PAs	*phosphatidic acids*
PBS	*phosphate buffered saline*
PC	*phosphatidylcholine*
PCA	*principle component analysis*
PCR	*polymerase chain reaction*
PDFF	*proton density fat fraction*
PE	*phosphatidylethanolamine*
PE P	*PE-based plasmalogens*
PEPCK	*phosphoenolpyruvate carboxykinase 1*
PG	*phosphatidylglycerol*
PGC1A	*PPARG coactivator 1 alpha*
PI	*phosphatidylinositol*
PI3K	*phosphatidylinositol-3-kinase*
piRNA	*PIWI interacting RNA*
PKC-ε	*protein kinase c-epsilon*
PKCζ	*protein kinase C-ζ*
PLIN1	*perilipin 1*
PLTP	*phospholipid transfer protein*
PMSF	*Phenylmethanesulfonyl fluoride*
PNPLA3	*patatin-like phospholipase domain-containing 3*
PPARA	*peroxisome proliferator activated receptor alpha*
PPARD	*peroxisome proliferator activated receptor delta*
PPARG	*peroxisome proliferator activated receptor gamma*
PPIA	*peptidylpropyl isomerase A*
PPP2R5C	*protein phosphatase 2 regulatory subunit B'gamma*
PS	*phosphatidylserine*

PXR	*pregnant X receptor*
R.U.	*relative units*
RIN	*RNA integrity number*
RIPA	*radioimmunoprecipitation assay buffer*
RISC	*RNA-induced silencing complex*
RNA	*Ribonucleic acid*
ROC	*receiver-operating characteristics*
ROS	*reactive oxygen species*
SBP	*systolic blood pressure*
SCD	*stearoyl-CoA desaturases*
SDHA	*succinate dehydrogenase complex, subunit A*
SEM	*standard error of the mean*
SGLT2	*sodium-glucose co-transporter 2*
SGMS	*sphingomyelin synthase*
shRNA	*short hairpin RNA*
siRNA	*small interfering RNA*
SLC25A1	*solute carrier family 25 member 1*
SM	*sphingomyelin*
SMPD	*sphingomyelin phosphodiesterase*
SREBF1	*sterol regulatory element binding transcription factor 1*
SS	*simple steatosis*
stRNA	*small temporal RNA*
SULT1A2	*sulfotransferase 1A2*
T2D	*type 2 diabetes*
TAFLD	*toxicant associated fatty liver disease*
TAG	*triacylglyerol*
TCA	*tricarboxylic acid*
TG	*triglycerides*
TGFb	*transforming growth factor beta 1*
TLC	*thin-layer chromatography*
TLDA	*TaqMan Low-Density Array*
TM6SF2	*transmembrane 6 superfamily member 2*
TNFA	*tumor necrosis factor alpha*
TNRC6A	*trinucleotide repeat-containing gene 6A*
TRBP	*transactivation response RNA binding protein*
UCP1	*uncoupling protein 1*
UGCG	*UDP-glucose ceramide glycosyltransferase*
UGT8	*ceramide galactosyltransferase*
US	*ultrasonography*
UTR	*untranslated region*

VLDL *very-low-density lipoproteins*

WHO *World Health Organization*
WHR *waist-to-hip circumference ratio*

XPO5 *exportin 5*

LIST OF FIGURES

LIST OF TABLES

TABLE OF CONTENTS

SUMMARY

Non-alcoholic fatty liver disease (NAFLD) has become the principal cause of chronic liver disease worldwide, involving a spectrum of disturbances mainly characterized by fatty acid infiltration and fat deposition in the liver parenchyma, which can further progress to fibrosis, inflammation, and eventually develop in cirrhosis and hepatocellular carcinoma. Given the impact in the burden of liver disease, the willingness to unravel the underlying pathogenesis of NAFLD is growing, particularly based on identifying altered molecular pathways that trigger the onset and progression of the disease. In this context, impaired epigenetic mechanisms governing gene expression are known to contribute to metabolic disorders in liver. Mounting evidence endorsing the relevance of microRNAs (miRNAs) in the regulation of metabolic issues points towards the future development of medical strategies in the field. These small non-coding RNAs are capable of modulating gene expression, either by translational inhibition or mRNA target decay. Here, a comparative profiling of hepatic miRNAs in obese subjects with NAFLD and age-, gender- and weight-matched controls showed that NAFLD is associated with altered hepatic miRNA expression patterns, and that specific miRNAs are associated with changes in gene expression and impaired glucose and lipid metabolism. Additionally, our experimental approach demonstrated impaired miRNA regulation after direct/indirect AMPK modulation in cultured human hepatocytes and rodent models. The interplay between AMPK and hepatic miRNA expression leading to changes in fatty acid metabolism is sustained by impaired AMPK coupled to decreased miRNA abundance, and the consistent decrease of miRNA candidates together with increased fatty acid accumulation. As the potential targets of miRNAs differentially expressed in NAFLD were involved in molecular mechanisms deregulated in NAFLD such as *de novo* lipogenesis or fatty acid oxidation, disclosing their involvement in the pathogenesis of NAFLD, miR-30b and miR-30c were used for additional investigations targeting their potential for genomic therapies based on the activity of miRNAs. We found that the ectopic replenishment of hepatic miR-30b and miR-30c in conditions mirroring NAFLD partially rescued fatty acid overload and modified lipid profiles within hepatocytes, stressing their potential as epigenetic regulators to combat NAFLD. Altogether, this doctorate thesis provides new progress addressing the role of miRNAs

in NAFLD pathophysiology, including the identification of specific hepatic miRNAs associated with impaired glucose and lipid metabolism in NAFLD, and unravels the activity of miR-30b and miR-30c in tackling inadequate FA accumulation in hepatocytes.

RESUM

La malaltia de fetge gras no alcohòlic (NAFLD) s'ha convertit en la causa principal de les malalties hepàtiques cròniques a nivell mundial, integrant un ventall de trastorns caracteritzats principalment per la infiltració d'àcids grassos al parènquima hepàtic i la deposició de greix, que pot arribar a progressar a estadis de fibrosi, inflamació i, eventualment, cirrosi i carcinoma hepatocel·lular. Atès l'impacte de NAFLD en el global de les malalties hepàtiques, l'interès en desvetllar la patogènesi subjacent a la malaltia està creixent exponencialment, posant en el punt de mira la identificació de les vies moleculars alterades encarregades de desencadenar l'aparició i progressió de la malaltia. En aquest context, es coneix que les alteracions en els mecanismes epigenètics que regeixen l'expressió gènica contribueixen als trastorns metabòlics del fetge. Concretament, nous estudis que avalen la rellevància dels microRNAs (miRNAs) en la regulació de vies metabòliques ja apunten cap al desenvolupament d'estratègies mèdiques en el camp. Els miRNAs són petits RNAs no codificants capaços de modular l'expressió gènica, ja sigui per inhibició de la traducció o per la degradació de la molècula de mRNA diana. En aquesta tesi doctoral, un anàlisi de miRNAs hepàtics comparant pacients obesos amb i sense NAFLD, tenint en compte edat, sexe i pes, ha demostrat que la malaltia està associada amb un perfil de miRNAs alterat, i que l'expressió d'alguns miRNAs concrets està relacionada amb canvis en l'expressió gènica i amb alteracions en el metabolisme glucídic i lipídic. Adicionalment, el nostre plantejament experimental ha demostrat una alteració de la regulació dels miRNAs a través de la modulació directa/indirecta de AMPK en cultiu d'hepatòcits humans i en models de ratolí. La interacció entre AMPK i l'expressió de miRNAs hepàtics que porta a canvis en el metabolisme dels àcids grassos es sustenta per una expressió de AMPK reduïda paral·lela a la disminució de l'abundància dels miRNAs candidats, juntament amb una disminució constant dels miRNAs candidats coincidint amb una major acumulació d'àcids grassos als hepatòcits.

Tenint en compte que les dianes principals dels miRNAs alterats en NAFLD estan involucrades en mecanismes moleculars desregulats en NAFLD, com ara la lipogènesis *de novo* o la oxidació d'àcids grassos, revelant la seva implicació en la patogènesi de la

malaltia, el miR-30b i el miR-30c s'han utilitzat per a posteriors investigacions dirigides al potencial de les teràpies genòmiques basades en l'activitat dels miRNAs. S'ha demostrat que la reposició ectòpica del miR-30b o el miR-30c en condicions que emulen NAFLD, és capaç de rescatar parcialment l'excés d'àcids grassos i modificar els perfils lipídics a l'hepatòcit, posant de relleu el seu potencial com a reguladors epigenètics per combatre el fetge gras en humans. En conjunt, aquesta tesi doctoral proporciona nous progressos abordant el paper dels miRNAs en la fisiopatologia de NAFLD, incloent la identificació de miRNAs específics associats amb el metabolisme glucídic i lipídic alterat en NAFLD, i desvetlla l'activitat de miR-30b i miR-30c per combatre l'acumulació inadequada d'àcids grassos dels hepatòcits.

RESUMEN

La enfermedad de hígado graso no alcohólico (NAFLD) se ha convertido en la causa principal de las enfermedades hepáticas crónicas a nivel mundial, integrando un abanico de trastornos caracterizados principalmente por la infiltración de ácidos grasos en el parénquima hepático y la deposición de grasa, que puede llegar a progresar a estadios de fibrosis, inflamación y, eventualmente, cirrosis y carcinoma hepatocelular. Dado el impacto de NAFLD en el global de las enfermedades hepáticas, el interés en desvelar la patogénesis subyacente a la enfermedad está creciendo exponencialmente, poniendo en el punto de mira la identificación de las vías moleculares alteradas encargadas de desencadenar la aparición y progresión de la enfermedad.

En este contexto, se conoce que alteraciones en los mecanismos epigenéticos que rigen la expresión génica contribuyen a los trastornos metabólicos del hígado. Concretamente, nuevos estudios que avalan la relevancia de los microRNAs (miRNAs) en la regulación de vías metabólicas ya apuntan hacia el desarrollo de estrategias médicas en el campo. Los miRNAs son pequeños RNAs no codificantes capaces de modular la expresión génica, ya sea por inhibición de la traducción o por la degradación de la molécula de mRNA diana. En esta tesis doctoral, un análisis de miRNAs hepáticos comparando pacientes con y sin NAFLD, teniendo en cuenta edad, sexo y peso, ha demostrado que la enfermedad está asociada a un perfil de miRNAs alterado, y que la expresión de miRNAs concretos está relacionada con cambios de expresión génica y con alteraciones en el metabolismo glucídico y lipídico. Adicionalmente, nuestro planteamiento experimental demuestra una alteración de la regulación de los miRNAs a través de la modulación directa / indirecta de AMPK en cultivo de hepatocitos humanos y en modelos de ratón. La interacción entre AMPK y la expresión de miRNAs hepáticos que conduce a cambios en el metabolismo de los ácidos grasos se sustenta por una expresión de AMPK reducida paralela a una disminución de la abundancia de los miRNAs candidatos, juntamente con una disminución constante de los miRNAs candidatos coincidente con una mayor acumulación de ácidos grasos en los hepatocitos.

Teniendo en cuenta que las dianas principales de los miRNAs alterados en NAFLD están involucradas en mecanismos moleculares desregulados en NAFLD, como la lipogénesis

de novo o la oxidación de ácidos grasos, revelando su implicación en la patogénesis de la enfermedad, el miR-30b y el miR-30c se han utilizado para posteriores investigaciones dirigidas al potencial de las terapias genómicas basadas en la actividad de los miRNAs. Se expone que la reposición ectópica del miR-30b o el miR-30c bajo tratamientos que emulan NAFLD, es capaz de rescatar parcialmente el exceso de ácidos grasos y modificar los perfiles lipídicos en el hepatocito, poniendo de relieve su potencial como reguladores epigenéticos para combatir el hígado graso en humanos.

En conjunto, esta tesis doctoral proporciona nuevos progresos abordando el papel de los miRNAs en la fisiopatología de NAFLD, incluyendo la identificación de miRNAs específicos asociados con el metabolismo glucídico y lipídico alterado en NAFLD, y desvela la actividad de miR-30b y miR-30c para combatir la acumulación inadecuada de ácidos grasos de los hepatocitos.

1. INTRODUCTION

1.1. NON-ALCOHOLIC FATTY LIVER DISEASE (NAFLD)

1.1.1. Definition of NAFLD

Non-alcoholic fatty liver disease (NAFLD) is characterized by the excessive accumulation of fat in the liver parenchyma and is defined by hepatic fat content exceeding 5% of liver weight[1] according to the histological analysis, or the proton density fat fraction (PDFF), which provides an estimation of the volume of fatty material in liver samples; or >5.6% assessed by proton magnetic resonance spectroscopy (^{1}H-MRS) or by semi-quantitative fat/water selective magnetic resonance imaging (MRI)[2]. The diagnosis of NAFLD excludes the aetiology of competing liver disease such as viral hepatitis, the use of medications that may induce steatosis such as valproate or anti-retroviral, or excessive alcohol consumption (≥30 g/day for men and ≥20 g/day for women)[3,4].

NAFLD encompasses different clinical entities divided into non-alcoholic fatty liver (NAFL), which includes subjects with simple steatosis (SS) and non-alcoholic steatohepatitis (NASH), characterized by the presence of fat in liver parenchyma but also by the onset of inflammatory issues, fibrosis, hepatocyte ballooning and lobular inflammation[5]. The latter precedes a wide spectrum of disease severity, including cirrhosis and hepatocellular carcinoma (HCC)[5]. While SS barely progresses to advanced diseases, approximately the 20% of patients with NASH would progress to fibrosis and cirrhosis over a 15-year time period[6] (**Figure 1**).

NAFLD has become the major cause of chronic liver disease in Western countries, increasing all-cause of morbidity and mortality when compared to subjects without this condition. The global prevalence of NAFLD has been estimated of ~25% whereas the prevalence of NASH is predicted to range from 3% to 5%[7,8]. Furthermore, the ongoing persistence of sedentary lifestyles and the burden of obesity will increase the current prevalence of NAFLD that will probably emerge as the leading cause of end-stage liver disease in the incoming decades[7,9].

NAFLD is strongly associated with metabolic comorbidities[8,10], including obesity and type II diabetes (T2D)[11], dyslipidaemia and hypertension[12]. In fact, NAFLD is considered the hepatic manifestation of the so-called metabolic syndrome (MetS)[13]. As well, NAFLD

entails higher risk for metabolic disorders and cardiovascular diseases (CVD)[14]. Notwithstanding these evidences, to date there are neither available well-established treatment guidelines nor validated therapies for NAFLD. Thus, the management of this condition is mainly focused on reducing major risk factors to prevent disease progression by means of lifestyle modification and pharmacological therapy[3,15].

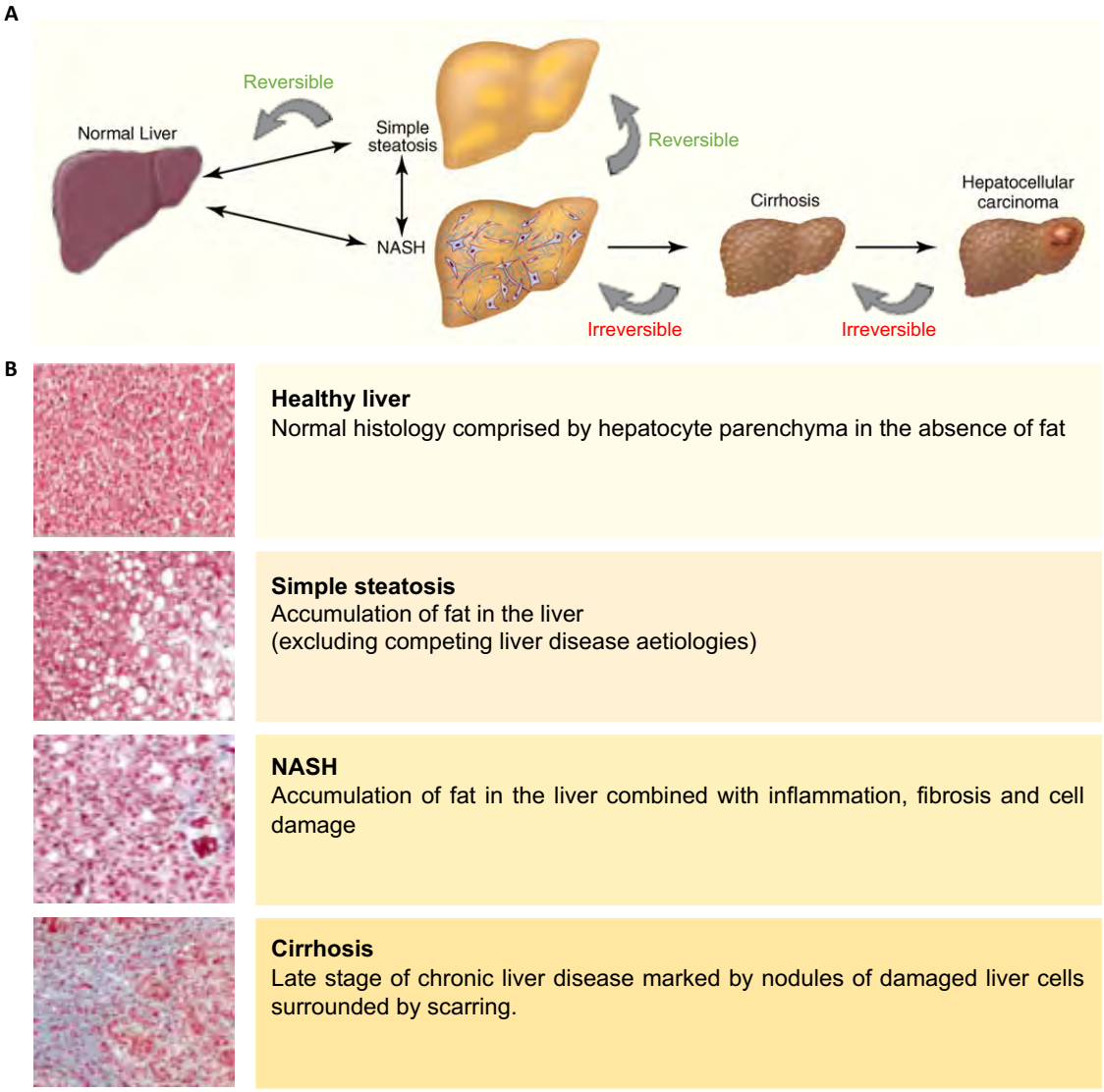

Figure 1. NAFLD spectrum. a) Progression of NAFLD: the accumulation of triglycerides in lipid droplets triggers simple steatosis (SS). When associated with inflammation, fibrosis and cell death, SS progresses in NASH, both stages being likely reversible. NASH can also develop in cirrhosis, with higher risk of HCC. Nowadays these stages are irreversible. **b)** Histological sections illustrating normal liver, SS, NASH and cirrhosis. In NASH and cirrhosis stages, collagen fibbers are present (stained blue with Masson's trichrome stain). *Panel modified from Cohen J. C. et al. (2011)[16].*

1.1.2. Pathogenesis of NAFLD

The main hallmark of NAFLD is triglyceride (TG) accumulation within hepatocyte's cytoplasm. This arises from an imbalance between hepatic lipid input and output, both of which being altered in NAFLD subjects[17]. However, the underlying mechanisms for NAFLD progression are complex and multifactorial. Nowadays, NAFLD is understood as a 'multiple hit' process, involving insulin resistance (IR), oxidative stress, apoptosis and metabolic perturbations prompted by proinflammatory cytokines mainly released by adipose tissue (adipokines)[18]. Before this, an early concept was first proposed as a "two hit theory" in 1998[19]. At the onset of disease, the "first hit" involved the accumulation of TG and free fatty acids (FFAs) in hepatocytes as a consequence of enhanced dietary intake, increased hepatic lipogenesis and progressive hepatic IR. The "second hit" was characterized by lipid peroxidation, mitochondrial dysfunction and inflammatory events that trigger hepatocyte damage and the development of the liver fibrosis that ultimately leads to cirrhosis[19,20]. In parallel with the development of new technologies and extensive research, this view appeared to be too simplistic for recapitulating the complexity of NAFLD where multiple factors act synergistically in the development and progression of the condition[21]. Currently, the more widely accepted theory is the "multiple-hit model", which includes widespread metabolic dysfunction leading to the interaction of multiple genetic and environmental factors as well as changes in the crosstalk between different organs and tissues, including adipose tissue, pancreas, gut, and liver[22]. The "multiple-hit" hypothesis also implements dietary habits, and environmental and genetic factors that can lead to the development of IR, obesity and dyslipidaemia, as well as changes in the intestinal microbiome that can lead to the accumulation of fat in the liver parenchyma[23,24].

Fat availability in the liver relies on lipolytic processes accounting within adipose tissue, the dietary intake, and from *de novo* lipogenesis (DNL). Other pathways involved are impaired hepatic fatty acid (FA) oxidation and reduced synthesis and secretion of very low-density lipoproteins (VLDLs). High levels of FFAs and many other metabolites such as free cholesterols within hepatocytes are known to be lipotoxic[25]. Following this lipotoxicity, mitochondrial dysfunction, characterized by oxidative stress, production of reactive oxygen species (ROS) and endoplasmic reticulum (ER) stress, is activated[25]. The gut can also be involved in the development of steatosis, NAFLD and NASH. Consumption of unbalanced diets of high saturated fat and sugar and low fibber content

can lead to microbiota dysbiosis, facilitating the accumulation of fat in liver, leading to steatosis, inflammation, and alterations of gut barrier. Altered microbiota increases small bowel permeability and increases FAs absorption and circulating molecules such as lipopolysaccharide binding protein (LPS), which contributes to the activation of inflammatory issues[26,27]. All these factors, by altering lipid homeostasis in hepatocytes, can promote an inflammatory environment in liver, leading to a state of chronic inflammation that can be also enhanced by the genetic background and epigenetic modifications[22].

Liver inflammation is commonly associated with hepatocyte death. These forms of cell injury initiate sequences of events that may result in hepatic fibrosis[28]. Apoptotic bodies derived from damaged hepatocytes can activate quiescent hepatic stellate and Kupffer cells, which in turn will activate immune cells that promote inflammatory responses. Activated hepatic stellate cells can develop into myofibroblasts through different stimuli such as transforming growth factor beta 1 (TGFβ1)[29], plateled-derived growth factor[30] and endothelial growth factor[31]. Such inflammatory and immune-mediated responses can induce hepatocyte necrosis and apoptosis, strengthening fibrogenesis[28,32] (**Figure 2**).

An overriding feature of NAFLD would be IR, leading enhanced uptake and synthesis of FFAs, preceding lipotoxicity, oxidative stress and inflammatory activation[21,22]. Nevertheless, rather than a consequence, accumulation of liver fat can also be the cause of hepatic IR. Indeed, FA overload in liver activates protein kinase c-epsilon (PKC-ε) and c-Jun N-terminal kinase (JNK-1)[33], which will be translated into the inability of insulin to activate glycogen synthase, leading enhanced glucose secretion. Not only impaired synthesis of glycogen but also fat accumulation can stimulate gluconeogenesis, contributing to increased glucose secretion[33]. In particular, diacylglycerols (DAGs) and ceramides, two lipids reported as to accumulate in subjects with higher hepatic fat content, have emerged as putative mediators of lipid-induced hepatic IR[34]. DAGs are a class of lipids comprising three-carbon glycerol backbones, with two carbons being linked to fatty acyl chains of varying length. Ceramides comprise a large class of lipids, many of which derive from the condensation of serine and palmitoyl CoA by serine palmitoyltransferases[35]. While DAGs can activate PKC-ε, ceramides activate protein kinase C-ζ (PKCζ) and protein phosphatase 2A, preventing AKT kinase from participating in insulin action[36]. This supports the hypothesis that hepatic steatosis leads to IR by stimulating gluconeogenesis and activating protein kinases that can interfere

the insulin signalling cascade, contributing to the maintenance and worsening of IR in liver[33,35].

Both the "two-hit" and "multiple-hit" hypotheses conceptualise NASH as a condition that is preceded by SS (from a histological standpoint) and IR (from a pathological standpoint)[37]. However, NASH can also be the initial liver lesion, independently of pure fat content found in the liver parenchyma[37]. Therefore, each stage can also be understood as a single condition leading to disease, rather than a continuum of lesion changes of the liver parenchyma over a histological scale[37].

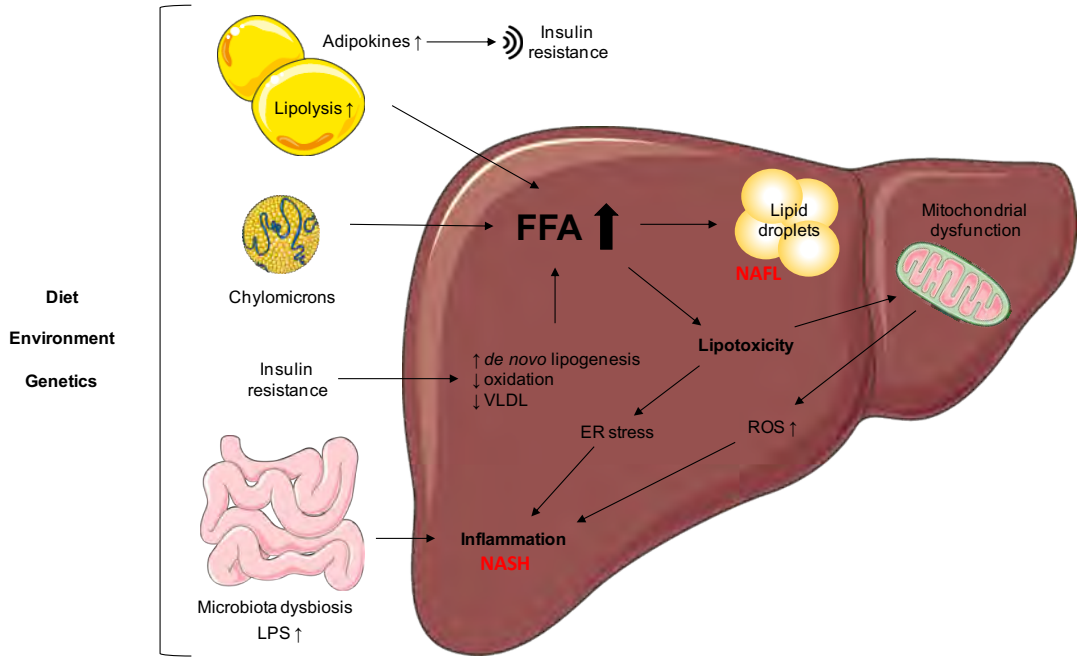

Figure 2. "Multiple-hit" hypothesis for NAFLD progression. Dietary habits, environmental factors and the genetic background can lead to the development of obesity, IR, enhanced FFAs, and changes affecting the microbiome. Adipose tissue lipolysis releases FFAs that can be took and stored by the liver, together with adipokines that may enhance hepatic IR. Chylomicrons are delivered to the liver enhancing FFAs amounts. IR in the liver amplifies DNL and impairs β-oxidation and VLDL secretion, increasing FFAs levels. Altogether, these processes trigger hepatic FFAs intake and deposition, being stored within hepatocytes as lipid droplets, causing NAFL. Impaired FFAs content induces lipotoxicity, mitochondrial dysfunction, and enhanced ROS and ER stress, leading to inflammation and NASH. Microbiota dysbiosis may also trigger increased LPS, contributing to the activation of inflammatory issues. *J Latorre (2019).*

1.1.3. Epidemiology of NAFLD

According to a meta-analysis published in 2016, including 86 studies with a sample size of 8,515,431 participants from 22 countries, the prevalence of NAFLD worldwide is estimated of ~25%[38]. However, as more reliable and replicable diagnostic tools and tests

are required, country-related differences regarding the diagnostic, and the impact of many confounders such as ethnicity, age, gender and the socio-economic status may alter the prevalence currently estimated[38–40]. As well, the prevalence of this condition is fairly increased in patients with T2D to 43-60%[41], more than 90% in severe obese patients[42], and up to 90% in patients with hyperlipidaemia[43].

Despite the fact that the prevalence is increasing globally, the epidemiology and demographic characteristics of NAFLD are not homogeneous worldwide. In terms of geographic location, the three regions with the highest rates of NAFLD are the Middle East, South America and Asia, where the prevalence are 32%, 31% and 27%, respectively[8], followed by a 25% prevalence in USA. In Africa and Europe, NAFLD's prevalence is of 14% and 24%, respectively. Even in Europe, it varies from 5-44% depending on the country[38]. Economic, political and educational levels, together with nutritional and lifestyle factors contribute to the varying prevalence of NAFLD in different locations. The prevalence of NAFLD also varies among ethnic groups. It has been reported that NAFLD is most prevalent in Hispanic Americans, being followed by European and African Americans, although obesity and hypertension are clearly more prevalent in African Americans[8].

Overall, the prevalence of NASH in general population is estimated to range between 1.5% and 6.4%[8]. The increasing prevalence of NAFLD parallels the increase of NAFLD-related risk factors and related diseases. It has been reported that 80% of NASH patients are obese, 44% have T2D, and 72% are dyslipidemic[38]. Patients with these diseases have a higher risk of suffering NAFLD than the general population. Notwithstanding this, apparently healthy non-obese subjects can also show the onset of NAFLD. Different aetiologies such as high-fructose and/or high-fat dietary intake, endocrine disorders, drug-consumption, and the genetic background are also associated with the NAFLD phenotype in lean subjects[44,45].

On the other hand, men are more susceptible to NAFLD than women[46]. One study in Asian subjects disclosed that NAFLD prevalence was 31% in men and 16% in women[47]. Gender is associated with elevated levels of aminotransferase, the presence of histological NASH, hepatic fibrosis and mortality in men patients with NAFLD[46,48]. Despite that, it is worth noting that some old studies suggested that women are more susceptible to NAFLD[49]. In either case, different mechanisms may contribute to gender-

related differences for NAFLD incidence. One explanation for the higher prevalence of NAFLD in men may be increased waist-to-hip ratio (WHR), which is positively associated with the amounts of visceral adipose tissue, which are closely associated with IR[50]. Alcohol consumption may stand as a major precursor as well, as a moderate alcohol intake in men (<30 g/day) is translated into the higher incidence of hepatic steatosis than in their female counterparts[51]. Lifestyle and sex-hormones may also perform significant differences in gender for the prevalence of the condition[52]. Women are "protected" from dysmetabolism because the increased thermogenic activity (also known as browning or "beiging") of their white adipose tissue[52]. Fertile age in women is associated with decreased risk of fibrosis when compared to men, and ovarian senescence during menopause is strongly associated with severe steatosis and NASH. Oestrogen deficiency may be the link of these mechanisms during the development of postmenopausal MetS[52].

NAFLD and NAFLD-related fibrosis increases with age[7]. Old subjects (>70 year-old) have increased risk of NAFLD and NAFLD-related comorbidities such as hypertension, obesity, diabetes and hyperlipidaemia, and show more severe biochemical and histological insights of liver disease[53]. In a meta-analysis published in 2016, the prevalence of NAFLD was 22-27% below 50 year-old but >34% in subjects between 70 and 79 years[38]. In addition, subjects above 70 have a higher likelihood of disease progression and mortality, together with increased risk of developing hepatic fibrosis, HCC and T2D[54–56].

Finally, a number of studies have pointed that the prevalence of NAFLD differs within race and ethnicity, classifying Hispanics as the population most susceptible to NAFLD, hepatic steatosis and elevated aminotransferases. They are followed by non-Hispanic Whites, and the lowest rate has been reported for African Americans[46,57]. Mechanisms for racial/ethnic differences in NAFLD and NASH prevalence include lifestyle, adiposity and genetics. These factors are not mutually exclusive, and may occur and act synergistically. It is important to mention recent evidence connecting genotyping to the epidemiology of NAFLD. Currently, studies of large family-based cohorts indicate that heritability of hepatic steatosis (as being a statistic used to estimate the degree of variation in a population due to genetic variation between individuals, and ranging from 0 to 1) is approximately 0.27[58,59].

1.1.4. Risk factors for NAFLD

1.1.4.1. Obesity and MetS

The metabolic syndrome (MetS) includes a cluster of metabolic abnormalities that may coexist particularly in sedentary obese subjects[60]. Different criteria have been settled down for MetS, but the most recent guidelines define MetS as a disorder that includes any three of the following features: abnormally increased plasma glucose levels at the fasting state (≥100 mg/dl (5.6 mmol/L)), hypertriglyceridemia (≥150 mg/dl (1.7 mmol/L)), low HDL cholesterol (<40 mg/dl (1.0 mmol/L) in men and <50 mg/dl (1.3 mmol/L) in women), high waist circumference (in men >102 cm and in women >88 cm), and hypertension (≥130/85 mmHg)[61,62]. Patients with MetS commonly have high fat accumulation in liver and hepatic IR. The liver is responsible for two of the key components more likely related to MetS: fasting plasma glucose and VLDL[61]. Moreover, fatty liver may release at the same time many other biomarkers of cardiovascular risk, such as C-reactive protein (CRP), fibrinogen and coagulation factors[63]. Thus, the liver is a key determinant of metabolic disturbances leading to MetS. On the other hand, NAFLD and obesity overlap in many aspects, including the spectrum of diseases that may be triggered under such conditions[61]. For instance, a meta-analysis comprised of 21 cohort studies with a total of 381,655 participants suggested that obese individuals (BMI≥30 kg/m^2) had 3.5-fold increased risk of NAFLD than non-obese subjects, and there was a clear correlation between BMI and NAFLD risk[64].

1.1.4.2. Dietary intake and gut microbiota

As an innovative concept, the gut-liver axis has appeared to be a key triggering factor of obesity and NAFLD. It has been suggested that consumption of obesogenic diets may alter gut microbiota and the intestinal barrier function favouring the occurrence of metabolic endotoxemia and low-grade inflammation[65]. As a consequence, they may contribute to the development of obesity and fatty liver disease. The role of gut microbiota is understood as multifactorial. Microbiota can improve or aggravate NAFLD through different mechanisms, including changes in intestine permeability, changing the amount of energy absorbed from diet, altering the expression of genes in the DNL and choline and bile acid metabolic pathways, producing ethanol or interacting with innate immunity[27,66]. With that, intestinal host-microbiome communications can play various roles in the development and progression of NAFLD or NASH. Thus,

manipulation of the microbiome, mainly through the diet, towards a healthy state that is protective against NAFLD is currently being considered as an effective therapeutic approach in the field of fatty liver diseases[67].

1.1.4.3. Sedentarism

A sedentary lifestyle holds strong physiological and epidemiological associations with the onset of NAFLD. Sedentarism is likely to be prevalent in people with risk of MetS, excessive adiposity and T2D[68]. Several cross-sectional studies have found that people with NAFLD perform less physical activity than their counterparts without this condition, being also more prone to fatigue[69,70]. Physical training is thought to be beneficial for patients with MetS since it improves muscle insulin sensitivity[71]. Moreover, regular exercise decreases intrahepatic TG content and VLDL secretion. Actually, a cross-sectional retrospective study comprising 72,359 participants showed the association between regular exercise, reduced risk of NAFLD and decreased liver enzymes[72]. Furthermore, physical activity promotes an increase in postprandial net muscle glycogen synthesis, improves muscle insulin sensibility and decreases hepatic DNL[73].

1.1.4.4. Xenobiotics

As the liver is the first-line defence against harmful xenobiotics, hepatocytes are usually affected by many chemicals and pollutants of the environment. Recently, it has been described a new disease entity as toxicant associated fatty liver disease (TAFLD), a form of NAFLD related to exposure to chemical compounds found in food and water[74]. The intracellular accumulation of xenobiotics is regulated at different stages including uptake, biotransformation and elimination by drug metabolizing enzymes (DME). Pregnane X receptor (PXR) and constitutive androstane receptor (CAR) are ligand-activated nuclear receptors that actively regulate a wide range of DMEs, responding to many xenobiotics and endobiotics[74].

Air pollution, soil, water and a wide variety of chemical compounds are acquiring importance as risk factors contributing to the onset of NAFLD. Studies published in both mice and human have reported that air pollution, embracing smoke, vapours, sand, combustion derivatives, and so on, may trigger oxidative stress, worsening obesity and IR[75,76]. Despite the fact that most of this research has been focused on the inflammatory

response of respiratory airways, continuous exposition to a polluted air is also associated with systemic and chronic low-grade inflammation, increased plasma triglycerides, LDL and VLDL, worsening IR. Once in the liver, Kupffer cells may be activated, triggering the inflammatory cascade that may contribute hepatic lipid accumulation[77].

Besides air pollution, water, contaminants found in water, soil and food can also alter glucose and lipid homeostasis in liver. Pesticides and herbicides, and many other endocrine disrupting compounds (EDCs) have been reported to contribute to NAFLD progression[78]. Pesticides and herbicides cause mitochondrial dysfunction and participate in the activation of PXR, which increase intestinal and hepatic lipid contents. Such EDCs may promote lipid peroxidation, lowering antioxidant defences and rising the inflammatory response, contributing to the metabolic dysfunction that leads to liver steatosis and other morbidities[74,77].

1.1.4.5. Genetic background

Genetic factors may contribute to how individuals respond to the challenge of an excessive caloric intake and metabolic disturbances. The "multiple-hit" hypothesis of NAFLD considers multiple insults acting together against genetically predisposed subjects to cause NAFLD[22]. Within the last years, multiple genome-wide association studies (GWAS) and candidate gene studies have increased our understanding of genetic variations contributing to the onset of NAFLD. Nowadays, genetics are believed to contribute to 30-50% of the risk of metabolic disturbances such as obesity, T2D or cirrhosis. Heritable component of NAFLD comes from familial aggregation and twin studies, and it ranges from 22 to 38%[79].

Susceptibility to complex disorders is determined by the combined effects of multiple single nucleotide polymorphisms (SNPs), each of them contributing to disease risk. Genome-wide approaches are nowadays more likely to identify moderate-risk genetic variants associated with NAFLD. Studies focused on specific candidate genes linked to a given phenotypic trait, based on the known functions and biological relevance of the encoded protein, are also pretty common in the field[80,81]. Thereby, genes involved in IR, lipid metabolism and oxidative stress have been identified as plausible candidates and potential therapeutic targets. SNP arrays have allowed to profile the most common variants and paved the way for GWAS, which have brought the four genetic variants showing the strongest associations with NAFLD: patatin-like phospholipase domain-

containing 3 (*PNPLA3*)[59], transmembrane 6 superfamily member 2 (*TM6SF2*)[82], membrane bound O-acyltransferase domain containing 7 (*MBOAT7*)[83,84] and glucokinase regulator (*GCKR*)[85].

PNPLA3 is located on chromosome 22. Its variant rs738409 c.444 C>G is a non-synonymous cytosine to guanine nucleotide transversion mutation that encodes an isoleucine-to-methionine substitution at codon 148 (I148M). Little is known about the physiological functions of *PNPLA3* or how the amino acid change I148M alters function. In homozygous carriers, hepatic fat content is more than two-fold higher than in non-carriers. Accordingly, this allele is most prevalent in Hispanics (0.49), the group most susceptible to NAFLD[58,59]. *PNPLA3* encodes for adiponutrin. Even amino acid 148 does not lie within the catalytic site, it might prevent the substrate from accessing to the site. It appears to sensitize the liver to metabolic stressors of excess calories and adiposity. Proper activity of *PNPLA3* is acylglycerol hydrolase[86] together with lysophosphatidic acid activity[87]. It seems that I148M variant would reduce the first and increase the second, which consequently would reduce hepatic secretion of VLDL and increase synthesis of triacylglycerol (TAG), respectively[59,88].

TM6SF2 is located on chromosome 19. Its variant rs58542926 c. 449 C>T is also a non-synonymous cytosine to thymine nucleotide mutation that encodes a glutamate-to-lysine substitution at codon 167 (E167K). *TM6SF2* protein is localized in ER and ER-Golgi, functioning as a lipid transporter and interacting with proteins involved in intestinal absorption. *In vitro* experiments have disclosed that knockdown of *TM6SF2* reduced the secretion of triglyceride-rich lipoproteins and ApoB, leading to increased cellular triglyceride accumulation and consequently, an increase in number and size of lipid droplets. The E167K variant confers a loss of function to the protein, thus triggering similar effects as in knockdown models. On a background of IR and metabolic stress, *TM6SF2* acts as a determinant of MetS, while it protects the liver, it increases the cardiovascular risk and vice versa. Individuals carrying the minor allele (167K) appear to have increased NAFLD risk with advanced fibrosis and liver-related morbidity, while major allele (167E) is associated with increased risk for dyslipidaemia and cardiovascular disease[83].

It has been postulated that *MBOAT7*, membrane bound O-acyltransferase domain containing 7, is associated with increased fat content and liver damage. This gene

encodes for an enzyme involved in phosphatidylinositol acyl-chain remodelling, and its lower hepatic protein expression has been associated with NAFLD spectrum[89]. A GWAS study identified the rs641738 C>T SNP in *MBOAT7* locus that was associated with reduced *MBOAT7* expression, predisposing to cirrhosis development and HCC[89].

GCKR is able to control the influx of glucose in hepatocytes, regulating DNL pathway. Its variant rs1260326 is a missense loss-of-function mutation, encoding a proline-to-leucine substitution at codon 446 (P446L). This variant affects GCKR activity, which is focused on inhibiting glucokinase function in response to fructose-6-phosphate, resulting in enhanced glucokinase activity and the generation of substrates for DNL[85,90].

1.1.5. NAFLD Diagnosis

NAFLD stands for SS and NASH according to some histological and biochemical features. NAFLD can be also defined into "primary" or "secondary" depending on the main cause. While primary NAFLD is related to obesity, T2D and dyslipidaemia; secondary NAFLD is associated with hypothyroidism, hypogonadism, obstructive sleep apnoea, polycystic ovary syndrome, hypopituitarism, pancreatoduodenal resection, drug-induced, total parenteral nutrition or short bowel syndrome[91].

NAFLD diagnosis is based on the presence of the following criteria: i) detection of hepatic steatosis, either by imaging or histology, ii) no causes for secondary hepatic fat accumulation such as significant alcohol consumption, steatogenic medications (e.g. valproate, amiodarone, methotrexate or tamoxifen) or hereditary disorders, and iii) exclusion of co-existing aetiologies for chronic liver disease such as hemochromatosis, chronic viral hepatitis, autoimmune liver disease and Wilson's disease[44,92].

Early diagnosis and treatment of hepatic steatosis can prevent the development of progressive states, including NASH, liver fibrosis, cirrhosis and HCC[93]. Liver biopsy has been traditionally considered as the gold standard for steatosis assessment. However, liver biopsy is an invasive and potentially harmful procedure that can eventually develop in severe complications. Thus, non-invasive techniques are still required in order to improve the diagnosis and follow-up of subjects with NAFLD.

1.1.5.1. Non-invasive NAFL diagnosis

1.1.5.1.1. Clinical features

Many subjects with NAFLD are commonly asymptomatic and may just show generic symptoms (e.g. fatigue, sleep disturbances, right upper quadrant discomfort). The most common physical insight is hepatomegaly, explored by abdominal palpation during clinical examination, while advanced liver disease can also be associated with portal hypertension, characterized by increased in blood pressure within the portal venous system. Overall, given the lack of biomarkers for an accurate early diagnosis, NAFLD requires the exclusion of many known typical causes of chronic liver disease and steatosis. In addition, as NAFLD is tightly linked to MetS, this condition must be suspected in all individuals who show any of the MetS signs, since MetS itself is found in as many as 30% of subjects with NAFLD[94].

1.1.5.1.2. Biochemical variables

The diagnosis of NAFLD rises as a result of abnormalities pointing at the liver biochemistry[95]. Alanine aminotransferase (ALT) and aspartate aminotransferase (AST) are surrogate markers of liver injury, together with γ-glutamyl transferase (GGT). ALT and AST are responsible for the catalysis of an amino acid to α-ketoglutarate, being both important in energy homeostasis. GGT is also an enzyme transferase that catalyses γ-glutamyl functional groups forming glutamate. It is believed that increased aminotransferases in plasma are due to cell damage coupled with plasma membrane disruption[96,97], and thus a valuable biomarker of liver damage.

The sensitivity and specificity of elevated ALT levels for NASH are 45% and 85%, respectively. Based on the current threshold values (<40 IU/L in males and <31 IU/L in females)[95], ALT levels above 60 IU/L may indicate higher likelihood of NASH. Additionally, it has been reported that elevations in ALT level within subjects with NASH may be associated with IR and intrahepatic fat content[95]. Despite that, it must be taken into account that 30-60% of patients with biopsy-proven NASH would display normal ALT levels[95], pointing at the great variability and current understanding of this condition.

1.1.5.1.3. Imaging

Imaging biomarkers integration is at the spotlight of resources aimed at assessing liver steatosis, and it is based on determining the lipid content of liver parenchyma as a common feature in NAFLD[98]. It is not only important to recognize fatty liver on imaging, but also to discriminate fatty liver *per se* from other pathologies[91]. Different techniques are available in the assessment of hepatic steatosis, including ultrasonography, computed tomography and magnetic resonance.

1.1.5.1.3.1. Ultrasonography

The most common method employed for the semi-qualitative assessment of hepatic steatosis is ultrasonography (US), being the most affordable and reliable non-invasive technique, widely used around the world. US is a first-line screening procedure for detection of steatosis, which leads to increased hepatorenal contrast, liver brightness, deep attenuation and vascular blurring[91,93]. It has been reported that, according to US, steatosis correlates with metabolic derangements and histological changes affecting liver samples[99]. Nevertheless, the coefficient of variation regarding repeatability is limited, especially when there is a low-mild degree of steatosis[45]. Thus, a new attenuation parameter was developed recently, aimed at detecting and quantify low degrees of steatosis. It was named as controlled attenuation parameter (CAP), designed to provide quite immediate and reproducible results, and is able to measure the attenuation of the ultrasound beam as it traverses the hepatic parenchyma, taking into account that ultrasound energy is likely more blunted by fat than by non-fatty tissues. Hence, a greater attenuation implies a greater fat content[100].

1.1.5.1.3.2. Computed tomography

Computed tomography (CT) is a technique that uses a more objective approach for steatosis quantification. During CT, the liver-to-spleen attenuation ratio is measured. Deposition of fat in liver is likely characterized by a reduction in the attenuation of hepatic parenchyma, which in physiological conditions is higher than spleen. During hepatosteatosis, the liver parenchyma may show quite less density. Subsequently measures of CT can quantify the presence of fat within liver parenchyma[101,102]. As in US procedure, CT techniques are not sensitive to mild degrees of steatosis[101].

1.1.5.1.3.3. Magnetic resonance

Magnetic resonance imaging (MRI) is more sensitive than CT for the assessment of hepatosteatosis. It is considered a highly validated and reproducible method for hepatic measurement of triglyceride contents, thus being the gold standard within non-invasive methods to assess fatty liver. The quantitative biomarker would be PDFF (providing a rough estimation of the volume fraction of fatty material in the liver), which measures the proportion of mobile protons that are attributable to fat rather than to water. Here, the inter/intra-observer repeatability and reliability are considered to be quite adjusted[103].

1.1.5.2. Non-invasive NASH diagnosis

The most difficult challenge is to distinguish between NAFL and NASH, being the latter at a greater risk for developing progressive fibrosis. It is postulated that NASH diagnosis is based on the presence of steatosis, together with hepatocyte ballooning and lobular inflammation during liver biopsy. Nevertheless, several non-invasive procedures have been tested for the non-invasive assessment of NASH, including but not limited to plasma levels of cytokeratin 18, which is considered a biomarker of hepatic apoptosis[104,105]. Still, elevated levels of ALT and AST have limited specificity in clinical settings, and their sensitivity makes them not useful for identifying NASH[95]. Therefore, non-invasive diagnosis of NASH is still an issue requiring further investigation.

1.1.5.3. Histological diagnosis of NAFLD

Liver biopsy is considered the gold-standard procedure for proper assessment of both NAFLD and NASH[95,106]. Nevertheless, this is an invasive procedure, potentially harmful, also being largely limited by errors in sampling, evaluation and assessment[107]. Thus, clinical risk factors as well as emerging biomarkers are still required to identify subjects who may benefit from a liver biopsy[95].

On one hand, NAFL is commonly diagnosed when there is SS, steatosis plus lobular or portal inflammation without ballooning, and SS with ballooning but without portal inflammation. On the other hand, NASH requires simultaneous presence of SS, ballooning and lobular inflammation. Moreover, NASH can also show additional features such as polymorphonuclear infiltrates and apoptotic bodies, even though they are not required for diagnosis[45].

Scoring systems developed for chronic liver diseases are useful, showing higher reproducibility between pathologists, and therefore supplying an easier way to compare different hepatic lesions. Thus, the Pathology Committee of the NASH Clinical Research Network designed and validated a histological feature scoring system that addresses the full spectrum of NAFLD lesions and provide a NAFLD activity score (NAS) useful for many clinical trials[106].

NAS comprises 14 histological features, measured qualitatively or semi-quantitatively. First, these are evaluated to assess the severity of hepatic lesions. Grading involves the assessment of the disease activity: steatosis, hepatocyte ballooning and inflammation, while staging involves the assessment of fibrosis and vascular remodelling. NAS score was postulated as the concept of necroinflammatory grading being potentially more reversible than the fibrosis stage[108]. Four of these histological features are measured semi-quantitatively in scales with different degree of relevance: steatosis (0-3), lobular inflammation (0-3), hepatocellular ballooning (0-2) and fibrosis (0-4). Steatosis is more likely macrovesicular, when lipid vacuole fills hepatocytes, even though sometimes it can be both mediovesicular (several vacuoles per hepatocyte), or microvesicular (the hepatocyte cytoplasm is replaced by a great number of small lipid vacuoles)[106]. Mild-lesions associate with steatosis and can be classified within NAFL diagnosis, being a common feature the presence of a few inflammatory immune cells or ballooned hepatocytes[108]. Inflammation is mainly provided by mononuclear and Kupffer cells, being this degree usually low-mild, since a higher rate of inflammation suggests different aetiologies. Finally, ballooned hepatocytes picture quite clear, without vacuolar cytoplasm and finely rounded shapes. In early NASH stages, lesions are allocated around the terminal hepatic vein, while during advanced fibrotic stages the lesions may lose the acinar localization[91,106]. The rest of them are miscellaneous features qualitatively measured, recorded as present or absent[108]. This scoring system leads to a diagnostic categorization that classifies subjects as "not NASH", "borderline" and "NASH" subjects. NAS ≥5 indicates diagnosis of NASH, and scores below 3 are diagnosed as "not NASH", while values in the middle belong to "borderline". Being steatosis, inflammation and ballooning the features that best correlate with NASH diagnoses, the proposed NAS enables strong reproducibility (**Table 1**).

Table 1. NASH Clinical Research Network Scoring System Definitions. Semi-quantitative histological features utilized to categorise NAFLD. *Table taken and adapted from Kleiner D.E. (2005)*[108].

NAFLD activity score (NAS)		
Feature	Definition	Score
Steatosis		
Grade	Presence of fat	
	<5%	0
	5-33%	1
	34-66%	2
	>66%	3
Inflammation		
Lobular inflammation	Assessment of inflammatory foci	
	No foci	0
	<2 foci per 200x field	1
	2-4 foci per 200x field	2
	>4 foci per 200x field	3
Liver cell injury		
Ballooning	None	0
	Few balloon cells	1
	Many cells/prominent ballooning	2
Fibrosis		
Stage	None	0
	Perisinusoidal or periportal	1
	Perisinusoidal and portal/periportal	2
	Bridging fibrosis	3
	Cirrhosis	4

1.2. THE HEPATOCYTE AND EXPERIMENTAL MODELS OF NAFLD

The liver is a critical hub for a wide variety of physiological processes related to digestion, detoxification, fluid balance and metabolic homeostasis[109,110]. The hepatic parenchyma synthesizes a number of molecules, metabolizes nutrients and xenobiotics, and stores, exports and secretes metabolic compounds, neutralizing foreign antigens[110]. The liver executes crucial functions in fasting and feeding, assembling glucose via

gluconeogenic pathway and storing glycogen, respectively. Hepatocytes can also oxidize lipids, and package them for secretion and storage in peripheral tissues. The liver regulates the metabolism of many amino acids, being responsible for the vast majority of proteins secreted into circulation. All these procedures take place in a structurally complex and multicellular tissue composed by the liver parenchyma, the functional tissue, integrated by at least seven different cell types arranged in a matrix that facilitates their interaction[109,110]. Hepatocytes, cholangiocytes, sinusoidal endothelial cells, macrophages, lymphocytes and dendritic and stellate cells comprise the liver parenchyma. Hepatocytes represent up to 80% of the total cell population in the liver parenchyma, and they are considered the primary hepatic effector cell, since the majority of liver functions can be attributed to hepatocyte's activity[110,111]. They are large polygonal cells (averaging about 25-30 μm in cross section and 5000-6000 μm^3 in volume), acutely polarized by molecular specializations, possessing apical and basolateral plasma membrane domains composed of distinct surface proteins, channels and receptors. As befits their numerous metabolic functions, they contain abundant mitochondria, peroxisomes, lysosomes, Golgi complexes, aggregates of rough and smooth ER and a great amount of microtubules/microfilaments[112]. Hepatocytes are challenged to orchestrate nutrient uptake and blood detoxification, while controlling the packaging and secretion of key proteins, lipids and bile acids[111], and reacting to the infiltration of immune and endothelial cells. Thus, taking into account the relevance of the hepatocyte within the liver parenchyma, *in vitro* experimental approaches have mainly employed this cell type to elucidate molecular mechanisms involved in the progression of NAFLD[113].

1.2.1. *In vitro* models of NAFLD

Modelling the progressive disease spectrum of NAFLD *in vitro* or *ex vivo* can be challenging given the multifactorial nature of the condition[114]. Primary cell cultures, immortalized cell lines, liver slices and perfused liver are considered well-established tools to model NAFLD pathophysiology[115].

While immortalized cell lines (including hepatocytes, hepatic stellate cells, sinusoidal endothelial cells and Kupffer cells) grow steadily, have unlimited life-span, stable phenotypes, and show quite standardized culture conditions, primary human hepatocytes are closer to resemble the clinical conditions, despite the short-term viability

and specific culture requirements[113]. The most widely used immortal cell lines are Huh7 (human hepatoma) and HepG2 (human hepatocellular carcinoma) cells. Additional alternatives also include primary rodent cell lines, but they do not always mirror what we found in human liver samples[113].

To achieve the complexity of hepatic tissue, co-culture models offer high reproducibility mimicking cell-to-cell interactions. The most recent studies have also used three-dimensional liver cell cultures mimicking the physiological settings of disease progression rather than single-cell monolayers[116]. The more complex is the biological model, the better it resembles the quite complex liver cytoarchitecture, while their complexity limits extended therapeutic and research-based applications. Therefore, the vast majority of *in vitro* models of NAFLD have developed in lines and primary cell cultures to study disease onset and progression.

The first model used to mirror steatosis in hepatocytes took advantage of the toxicity of tetracycline, which triggers hepatic dysfunction, reduced mitochondrial β-oxidation and fat accumulation in animals[117]. The following experimental designs included treatments of hepatoma cell lines with high concentrations of glucose as common features of NAFLD and T2D[118].

However, among the different factors involved in the pathogenesis of NAFLD, the most widely used approach is the use of FFAs, being the major mediator of hepatic steatosis[119]. FFA sources include dietary FAs, increased lipolysis of peripheral fat stored in adipose and newly synthesized FAs via DNL[120]. Exposing hepatocytes to high concentrations of FFAs will result in the formation of intracytoplasmic lipid droplets, at the same time it sensitizes hepatocytes to apoptosis[121] and transcription of proinflammatory cytokines[122]. The impact of FFAs may differ according to the moiety of FAs used, being stearic > palmitic > palmitoleic > oleic acid the scale from more-to-less lipotoxic activity. Hence, differential effects caused by palmitic acid (PA) or oleic acid (OA) will influence cell activity and viability. Such treatments consist of the use of monounsaturated and/or saturated FAs. These models employ PA (C16:0), OA (C18:1) or the mixture of both at a common ratio 3:1, as a reflection of what happens in Western diets. PA and OA are also the most abundant FAs in human liver. Since OA is by its own quite less lipotoxic than PA, some results indicate that treatments of OA on PA-treated hepatocytes can prevent to some extent PA-induced lipotoxicity, while increasing TAG synthesis[123].

Envisaging the possibility that IR may result from accumulation of liver fat, several models have been focused on reducing liver lipids to prevent disease progression[124]. In this context, AMP-activated protein kinase (AMPK) has become a potential target to study NAFLD, due to its ability to improve metabolic homeostasis and decrease liver fat content[124]. Hence, cell models have employed AMPK inhibitors such as Compound C, a potent and reversible inhibitor of AMPK that mimics to some extent NAFLD condition[125–128]. On the other side, AMPK activation is linked to metabolic improvement, and has been tested through various pharmaceuticals or nutraceuticals compounds such as metformin[129] and resveratrol[130].

So far, *in vitro* models employed to analyse the molecular events leading NAFD have been thoroughly studied, but different experimental approaches should be taken in consideration when extrapolating data from one model to the other. In addition, little studies have been published using primary human hepatocytes to resemble NAFLD condition. Nevertheless, rat and mice hepatocyte primary cultures have been used instead[131,132].

Not only *in vitro*, but also *in vivo* models, and particularly rodent models (being genetic or diet-induced) to study the onset and progression of NAFLD to later stages of the disease have been extensively used to verify mechanisms underlying the development of NAFLD and as tools to assess new therapeutic strategies. Despite that, the available models, either *in vitro* or i*n vivo* only mimic certain insults of the disease found in humans and the appropriate model selection remains to be uncertain since inadequateness in resembling the precise stage wanted to study will make it challenging to translate to the clinics[133].

1.3. METABOLISM AND NAFLD

As a central regulator of metabolism, the liver plays an important role in the regulation of systemic glucose and lipid fluxes during fasting and feeding states, encompassing synthesis, export and redistribution to other tissues, and the utilization of substrates for its own energy needs[134]. Food is digested in the gastrointestinal tract, and glucose, FA,

and amino acids are absorbed and directly transported to the liver through the portal vein circulation system.

In the feeding state, glucose is stored in liver as glycogen or used for the synthesis of FAs and amino acids. These FAs are esterified by means of the glycerol-3-phosphate to generate triacylglycerols (TAGs), which are stored in lipid droplets within hepatocytes or secreted to the circulation through VLDL particles. TAGs are then transported to fat depots for energy storage, or to the muscle for energy metabolism. Also amino acids are metabolized in the liver to provide energy surplus, or used for the synthesis of proteins and glucose[135].

In the fasted state glucose and TAGs are transported from liver to the muscle, adipose tissue and other tissues where such substrates are metabolized. The liver glycogen becomes glucose through glycogenolysis, being released into bloodstream for the intake of other cells. In muscle, glycogen and proteins are metabolized to lactate/alanine and amino acids, respectively. These products are released and delivered to the liver to synthesize glucose again, process known as gluconeogenesis. In adipose tissue, TAGs storage may become FFAs and glycerol through lipolysis, and travel to the liver and muscle, respectively, as energy. Non-esterified fatty acids (NEFAs) are oxidized inside mitochondria through fatty acid β-oxidation, producing ketone bodies (ketogenesis), and glycerol is utilized for glucose production (**Figure 3**).

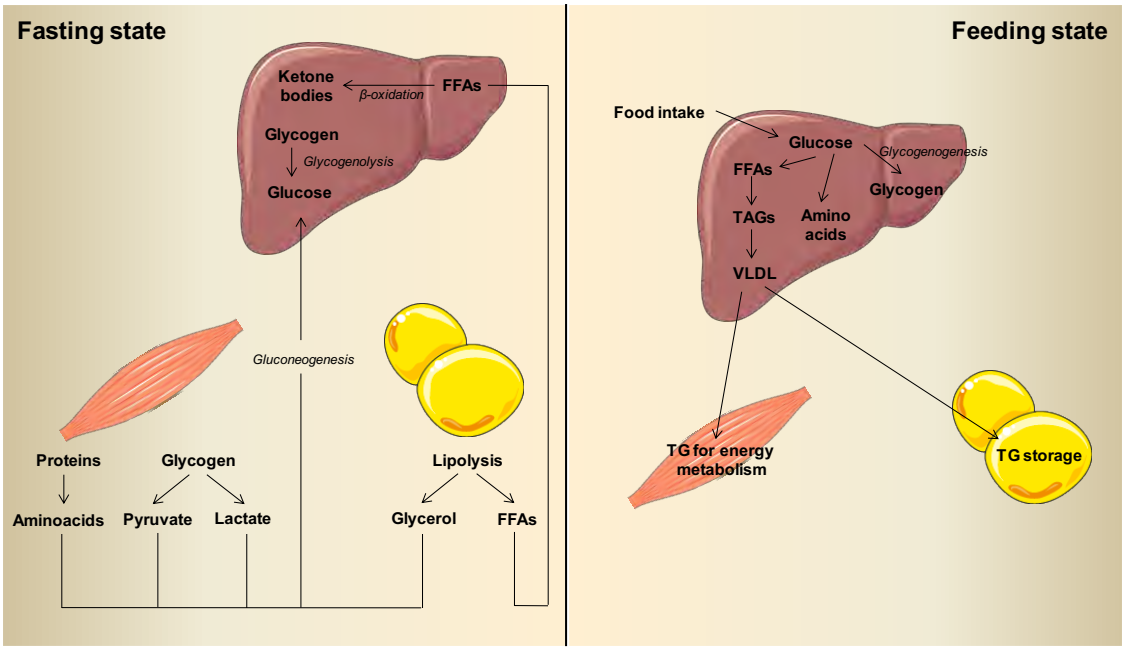

Figure 3. Energy homeostasis: fasted versus feeding state. In a fasted or post-absorptive state, catabolic pathways achieve glucose homeostasis. Adipose tissue releases FFAs and glycerol after degradation of lipids (lipolysis). FFAs can be collected by the liver and undergo β-oxidation, releasing ketone bodies. In muscle, glycogen is metabolized to either pyruvate or lactate, and proteins are defragmented into single amino acids. Amino acids, pyruvate and lactate together with glycerol from adipose tissue, are carried to the liver and used to make glucose via gluconeogenesis. Glucose can also be obtained by glycogenolysis in the liver. In contrast, after feeding, glucose levels increase and enter within hepatocyte, where FA are synthesized from glucose. After conversion into TAG, fat particles are packed within VLDL and released to adipose tissue (for energy storage), and to muscle (as fuel). Glucose molecules can also be used for the synthesis of amino acids, or to increase glycogen storage through glycogenogenesis. *J Latorre (2019).*

Under physiological conditions, these procedures are highly coordinated to carbohydrate and lipid inflow from feeding, and uptake of FAs derived from adipose tissue lipolysis during fasting[135]. Disruption of any of these pathways, triggering fat accumulation within hepatocytes, can lead to the development of NAFLD[136].

1.3.1. Glucose metabolism in liver

The liver is a major site of glucose utilization at the postprandial state. Molecules of glucose moves in and out hepatocytes via the glucose transporter 2 (GLUT2), also known as solute carrier family 2 (facilitated glucose transporter), member 2 (SLC2A2), a transmembrane carrier protein that enables glucose transport across cell membranes. Inside hepatocytes, glucose is phosphorylated by the glucokinase to glucose 6-phosphate (G6P). G6P can participate in many metabolic pathways, including glycogen synthesis, ATP or FA synthesis through pyruvate (glycolysis product) or pentose

phosphate pathway. In a fasted state, G6P would be dephosphorylated by the G6Pase to release glucose. Moreover, G6P cannot be transported by glucose transporters, so it will remain inside cells[134].

Under physiological conditions, glucose from carbohydrate intake stimulates the secretion of insulin by the pancreas, which will travel via the portal vein eliciting key actions in hepatocytes. Insulin binds to the insulin receptor (INSR) and activates the tyrosine kinase activity triggering the phosphorylation of insulin receptor substrates (IRSs), IRS-1 and IRS-2, which are highly expressed in liver. Tyrosine-phosphorylated IRSs bind and activate phosphatidylinositol-3-kinase (PI3K), which in turn activates the serine/threonine Akt kinase[137]. Akt inactivates the hepatic forkhead box-containing protein O subfamily-1 (*FoxO1*), avoiding the translocation of this transcription factor to the nuclei. Notably, activated *FoxO1* triggers the expression of genes involved in gluconeogenesis, so the blockade of its translocation downregulates the transcription of genes that are required for gluconeogenesis, such as the phosphoenolpyruvate carboxykinase (*PEPCK*) and glucose 6-phosphatase (*G6Pase*). On the other hand, insulin activates another transcription factor that enhances the transcription of FA biosynthesis pathway, sterol regulatory element binding transcription factor 1 (*SREBF1)*. Once activated, this transcription factor enhances the expression of acetyl-coenzyme A carboxylase (*ACC*) and fatty acid synthase (*FASN*)[138]. Thus, insulin secreted during fed states promotes glycogen synthesis and lipogenesis, while it suppresses hepatic glucose production and inhibits gluconeogenesis and glycogenolysis. Suppression of insulin signalling during fasting promotes gluconeogenesis and glycogenolysis, maintaining glucose levels. Synthesized TGs[139] are secreted as VLDLs, that are eventually stored the adipose tissue, or consumed in muscle[140] (**Figure 4**).

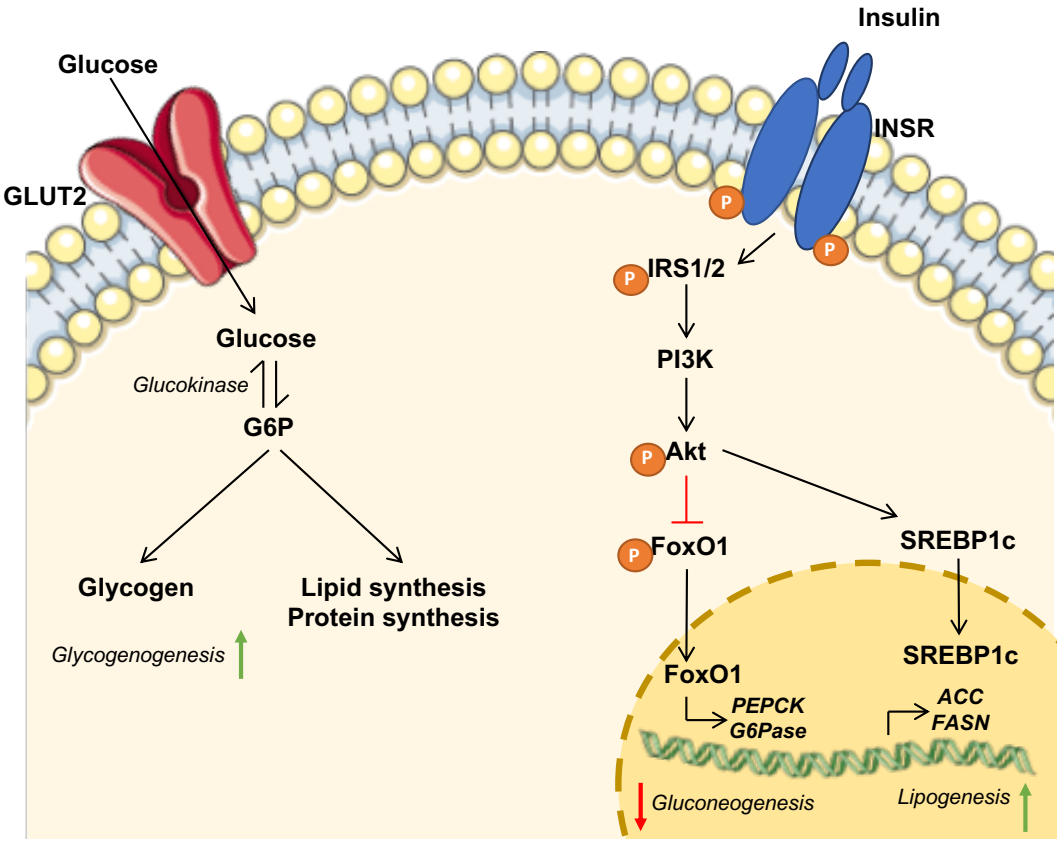

Figure 4. Glucose and insulin signalling in hepatocytes. After transformed into G6P, glucose is used for the biosynthesis of glycogen, lipids or proteins, and insulin controls transcriptional regulation and activation of genes involved in lipid and carbohydrate metabolism. Insulin binds to INSR triggering IRS phosphorylation, and the activation of PI3K and Akt, which in turn activates SREBF1 and inactivates FoxO1. The result is decreased gluconeogenesis and enhanced biosynthesis of lipids. *J Latorre (2019).*

1.3.2. Impaired glucose homeostasis in NAFLD

Hepatic IR is one of the features of NAFLD development and progression. IR is the condition through which the cellular response to insulin is significantly decreased. Insulin can control lipid metabolism and it enhances FA re-esterification into TG. The islets of Langerhans under IR condition are stimulated to secrete insulin to overcome the defect in plasma glucose absorption and to reduce glucose generation in the liver. Therefore, glucose metabolism is tightly regulated by insulin, which is also regulated by glucose concentrations in plasma[141]. The liver is the source of 90% of endogenous glucose, and hepatic IR occurs when insulin-induced suppression of glucose production is impaired[36].

During steatosis, hepatic IR is limited to suppression of hepatic glucose production, which is referred to as selective IR. In this case, insulin do not suppress glycogenolysis

and gluconeogenesis yet it is still stimulating cholesterol and TG synthesis. The expression of *PEPCK* and *G6Pase* remain increased in patients with steatosis, so gluconeogenesis continues. Despite the impairment in the FoxO1 signalling, the SREBP-1c pathway remains active, making TGs accumulate in the liver. As in normal glucose homeostasis, TGs are secreted into circulation and will worsen the insulin-resistant state in adipose tissue and muscle. The result will be the classic triad composed by hyperglycaemia, hyperinsulinemia and hypertriglyceridemia[139,140].

1.3.3. Lipid metabolism in liver

Under physiological conditions, FAs, together with glucose and amino acids, are absorbed at the small intestine, where they are resynthesized into TAG. Subsequently, they are assembled into chylomicrons and delivered through the lymphatic system[142]. The steady state of hepatic TGs in liver is low since this organ is not intended for fat depot and storage. However, there is a considerable traffic between adipose tissue and liver in response to feeding and fasting states[143]. FAs in liver can be stored as lipid droplets within hepatocytes or converted into other lipid species (e.g. glycerolipids, glycerophospholipids) and packed into VLDL particles that will be secreted to the circulation (**Figure 5**).

During the fasting state, FAs are released from adipose tissue, or oxidized in the mitochondria to generate energy. After feeding, in a situation of carbohydrates surplus, FAs will be also synthesized *de novo* within the liver. Thus, different pathways need to be highly adapted to maintain homeostasis in liver, since the hallmark of NAFLD is TG accumulation, happening when there is an imbalance between lipid acquisition (regulated by DNL and FA uptake) and lipid removal (regulated by mitochondrial oxidation and export as VLDL particles)[134,144].

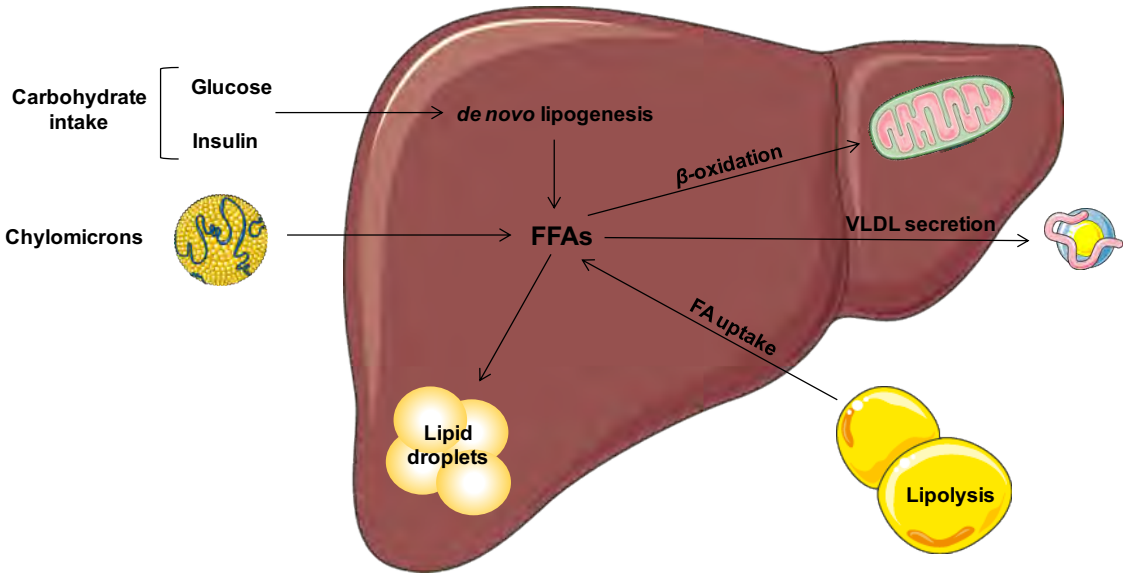

Figure 5. Lipid metabolism in the liver. Carbohydrate intake may increase glucose and insulin levels, which together promote DNL in liver. FFAs also come from adipose tissue lipolysis, and from circulating chylomicrons. The balance between lipid acquisition and removal, represented by β-oxidation and VLDL secretion will be decisive for the deposition of FFAs within hepatocytes. *J Latorre (2019).*

1.3.4. Lipid homeostasis in NAFLD

The balance of hepatic triglycerides is controlled by hepatic uptake and consumption of FAs. FFAs can be generated from several pathways including DNL, adipose tissue lipolysis that will deliver FFAs, dietary fat or reduced FA oxidation. When the energy storage capacity of adipose tissue is exceeded, there is increased lipid flux to non-adipose organs, causing lipotoxicity and IR[145]. The accumulation of lipid droplets within hepatocytes results in hepatic steatosis. As a major consequence, multiple dysfunctions such as alterations in mitochondrial dysfunction with oxidative stress, impaired secretion of VLDL or FA biosynthesis may be apparent (**Figure 6**).

1.3.4.1. *De novo* lipogenesis

DNL is the cluster of metabolic pathways aimed at synthesize FAs from carbohydrates. After feeding and in IR states, DNL increases substantially, therefore contributing to the development of NAFLD[146], accounting for approximately 26% hepatic TG accumulation[147].

DNL starts with glucose, which enters the glycolytic pathway and is hydrolysed into pyruvate. Pyruvate enters the mitochondria and is metabolized into acetyl-CoA that

feeds the tricarboxylic acid (TCA) cycle. Acetyl-CoA is combined with oxaloacetate by citrate synthase to form citrate. Citrate exits the mitochondria and it is converted back into acetyl-CoA and oxaloacetate by the ATP-citrate lyase (*ACLY*). In the cytoplasm, acetyl-CoA is converted to malonyl-CoA by acetyl-CoA carboxylase alpha (*ACACA)*, which is subsequently utilized as a substrate for the production of 16-carbon saturated palmitate by the main biosynthetic enzyme, the *FASN*[148]. After additional and more specific reactions, palmitate is further converted into more sophisticated FAs. Specifically, palmitate or palmitic acid is elongated by long chain fatty acid elongase family members in the ER to generate long-chain fatty acids (more than 16 carbon-chain), and desaturated by stearoyl-CoA desaturases (*SCDs*) to generate mono- and poly-unsaturated LCFAs that will eventually be the major source of FAs. Then, glycerol-3-phosphate acyltransferase (*GPAT*) catalyses the esterification of glycerol-3-phosphate from glycolysis and combines this compound with new synthesized FAs to generate lysophosphatidic acids (LPAs), which would be converted to phosphatidic acids (PAs) by 1-acylglycerol-3-phosphate (*AGPAT*). Finally, PAs are processed to diacylglycerols (DAGs) through lipin 1, and triacylglycerols through acyl-CoA:diacylglycerol acyltransferase (DGAT)[144,149] (**Figure 6**). Exacerbated DNL may cause hepatic steatosis, and may also lead steatohepatitis, since saturated FAs can cause inflammation and apoptosis[150].

DNL is orchestrated primarily through transcriptional regulation of glycolytic and lipogenic genes. After feeding, glucose and insulin increase in concentration, both required for lipogenesis. Plasma glucose levels can stimulate lipogenesis via glycolysis, providing a carbon source for FA synthesis, or inducing the expression of enzymes involved in the lipogenic pathway through activation of carbohydrate response element binding protein (*ChREBP*)[151]. This activation will translocate *ChREBP* to the nucleus, where binds to carbohydrate responsive elements (ChoREs), present in protomers of lipogenic genes. On the other side, glucose *per se* will also increase insulin concentration, which will help promoting lipogenesis via activation of *SREBF1*[152]. Here again, the activation of *SREBF1* will translocate it to the nucleus and bind to sterol regulatory elements that will promote lipogenesis. So, both *ChREBP* and *SREBF1* are considered to be the master transcription factors that regulate lipogenic process. While the phenotypic IR state in NAFLD would be expected to counteract insulin-mediated SREBP-1c activation, selective IR ensures that insulin retains its ability to induce DNL through SREBP-1c, while being unable to supress gluconeogenesis. At the same time, DNL can

contribute to IR, since harmful lipid species accumulation may interfere insulin signalling cascade[153].

1.3.4.2. Fatty acid oxidation

Since the main objective is the generation of ATP for hepatocytes, FA β-oxidation is high during fasting, while it decreases after feeding. β-hydroxybutyrate, acetoacetate and acetone are common ketone bodies produced in the mitochondria, being used as fuel for extrahepatic tissues when necessary[134]. β-oxidation requires FAs to be transported from the cytoplasm to the mitochondrial matrix. To allow translocation through the mitochondrial membrane, activation of FAs by fatty acyl-CoA synthetase (ACS) in the cytoplasm is required. Subsequently, LCFA-CoAs are able to enter the mitochondria in a carnitine-dependent manner, which is the rate-limiting step for FA β-oxidation. The main controller of FA entry and β-oxidation flux is carnitine palmitoyl transferases (CPT), consisting of three proteins: *CPT1*, acylcarnitine translocase (*CACT*) and *CPT2*. CPT1 is the key enzyme during FA oxidation and it is tightly regulated by malonyl-CoA, being also the first intermediate for DNL pathway. High concentrations of malonyl-CoA trigger the inhibition of *CPT1*. Mammal tissues express three isoforms of CPT1: *CPT1A*, *CPT1B* and *CPT1C*, mainly expressed in liver, muscle and heart, and brain, respectively. CPT1 is specifically located in the inner zone of the mitochondrial outer membrane, and it can catalyse the formation of fatty acyl-carnitine from fatty acyl-CoA and free-carnitine. Acyl-carnitines can be shuttled across the inner mitochondrial membrane by carnitine translocase and enter the mitochondrial matrix[154]. Within the mitochondrial matrix, acyl-CoAs are broken down into acetyl-CoAs, which are further oxidized during TCA cycle where NADH and $FADH_2$ are generated for ATP synthesis by the electron transport chain. When there is a surplus of these metabolites, acetyl-CoAs are converted to ketone bodies[144,155].

The master regulator of fatty acid β-oxidation is the peroxisome proliferator activated receptor alpha (*PPARα*), a nuclear receptor activated by LCFAs and phosphatidylcholines, that is highly expressed in liver, specifically in mitochondria and peroxisomes[134]. PPARG coactivator 1 alpha (*PGC1α*) is a coactivator of *PPARα* that enhances β-oxidation, even though multiple factors can regulate β-oxidation through *PPARα*, like hepatic fibroblast growth factor 21 (*FGF21*), stimulated by glucagon[156]. Glucagon can also activate AMP-activated protein kinase (AMPK), which

phosphorylates and inhibits *ACACA*. As a result, malonyl-CoA synthesis is then blocked and unable to inhibit *CPT1*[157]. The opposite situation is observed after feeding, when insulin facilitates DNL upregulating *SREBP-1c,* consequently activating *ACACA* and impairing FA oxidation. Additionally, insulin also stimulates the phosphorylation of PGC1α by Akt, impairing its ability to act as a coactivator of FA β-oxidation (**Figure 6**)[157].

The contribution of FA oxidation in NAFLD is still not fully understood. While the expected consequence of hepatic lipid accumulation would be increased FA oxidation, studies of FA oxidation in subjects with NAFLD have reported enhanced, unchanged or even decreased rates of oxidation pathways[136].

1.3.4.3. VLDL secretion

Hepatic TGs can be stored within the hepatocytes or secreted into the circulation as very low-density lipoproteins (VLDL) particles, triglyceride-rich lipoproteins containing a hydrophobic core, composed of TGs and cholesterols, and a hydrophilic coating of phospholipids and unesterified cholesterols. VLDLs may transport triglycerides, phospholipids, cholesterol and cholesteryl esters. Once in the target tissue, VLDL is converted to higher-density lipoproteins and smaller-size atherogenic particles the by lipoprotein lipase, as intermediate- density lipoproteins (ILD) and low-density lipoproteins (LDL)[158].

The VLDL secretion rate varies according to the hepatic TG content and the overall capacity for VLDL assembly[158]. VLDL assembly requires the action of microsomal triglyceride transfer protein (*MTTP*), and it relies on two steps. The first step implies partial lipidation of newly synthesized apolipoprotein (apo) B-100 during translation within the lumen of ER. This process forms a small dense precursor. The second step involves the merge of this precursor within a large triglyceride droplet to form a mature triglyceride-rich VLDL. While the first step requires *MTTP*, the second one is modulated by phospholipases D and A2[159]. Thus, apoB100 is essential to export VLDL from liver since each VLDL particle is stabilized by a single apoB 100 molecule. When TGs are less abundant, apoB 100 is degraded[159].

In subjects with NAFLD, impaired VLDL assembly and secretion will result in intrahepatic FA accumulation. Steatosis has been reported in patients with

hypobetalipoproteinemia (<5th percentile plasma levels of LDL-cholesterol and/or total apoB)[160] or abetalipoproteinemia (with mutations in *MTTP*)[161]. Same observations have been detected in *MTTP* knockout mice[162]. On the other hand, it has been reported that subjects with NAFLD have an overproduction of VLDL particles in response to increased DNL and higher FAs in blood, despite apoB 100 molecules do not increase in number[163] (suggesting that VLDL particles in NAFLD subjects may contain more triglycerides than VLDL particles in subjects without this condition). The increased availability of TGs can increase the assembly of VLDL, eventually resulting in hypertriglyceridemia, a common feature of NAFLD. Nevertheless, even VLDL secretion rate is higher, this it is not enough to eradicate the TG accumulation in the liver parenchyma.

Insulin also plays a role in regulating VLDL assembly, since this hormone can promote degradation of apoB 100 together with the downregulation of *MTTP* expression. It has been reported that *MTTP* is a target gene of *FoxO1*, which binds to MTTP promoter regions increasing the transcription. During the onset of NAFLD, the failure of insulin to supress VLDL production can increase VLDL assembly, as insulin would not stand against apoB and the nuclear localization of *FoxO1* would enhance *MTTP* transcription[164]. Hence, IR is associated with increased secretion of VLDL and hypertriglyceridemia, as well as with hepatic steatosis (**Figure 6**).

1.3.4.4. Fatty acid uptake

Hepatic FAs uptake stands for substrate delivery and transport into hepatocytes[158]. Excessive intake of FAs can trigger TGs storage, resulting in steatosis. The major source of lipids within hepatocytes is circulating FFAs, coming from dietary fat intake and lipolysis of TGs in adipose tissue. Excessive fat intake will increase plasma concentrations of TGs and FFAs, which would consequently increase their uptake into hepatocytes. Within adipose tissue, insulin has the dual effect of increasing adipocyte lipoprotein lipase (*LPL*), which increases the ability of adipocytes to disaggregate triglycerides to FFAs, while it decreases the activity of the hormone sensitive lipase (*HSL*), which does the opposite converting stored triglycerides to FFAs and glycerol for export. Altogether, insulin action is related to the intake of more FFAs and less delivery. During the IR state, hepatocytes are exposed to more FFAs for uptake[165,166]. Thus, lipids got at the surface of hepatocyte in different forms. Some lipoprotein particles are taken by receptor-mediated endocytosis, while TGs are usually disaggregated by hepatic

lipases (*HL*) generating FFAs that traverse plasma membranes by diffusion. Within hepatocytes, FFAs can be converted into TGs or oxidized.

The hepatocyte capacity for FA uptake depends on many transporter proteins located at the cell membrane. The key contributors of this process are FA transporter proteins (*FATPs*) and fatty acid translocase, also known as *CD36*, which is activated by Pregnane X receptor (*PXR*)[167]. Different FATPs isoforms have been identified, being *FATP2* and *FATP5* the most significant in hepatocytes. Despite the fact that *CD36* is expressed in a wide variety of tissues, its gene expression in hepatocytes is quite low, being its effects less crucial. In fact, previous data have shown that while genetic deletion of *FATP5* reduced FA uptake[168], *CD36* absence is not enough to abolish hepatic steatosis[169].

After entering the hepatocyte cytoplasm, FFAs are converted into acyl-CoAs. The molecular mechanism of this conversion is not fully understood. It is suggested that *FATPs* have some sort of fatty acyl-CoA synthetase activity or that they are able to activate the long acyl-CoA synthetases (*ACSLs*) to generate acyl-CoAs. As with FATPs, different ASCL isoforms have been identified, still 50% of ACSL activity in the liver belongs to *ACSL1*, located in ER and mitochondria. Even *ACSLs* appear to be involved in FA uptake, they also channel FA from FA oxidation to lipid biosynthesis[170]. Other proteins to take into account are fatty acid binding proteins (*FABPs*), which bind to long-chain fatty acids (LCFAs) acting as chaperones and carriers. Acyl-CoAs can be oxidized to generate acetyl-CoAs and energy, synthesized to triglycerides and stored within hepatocytes, being precursors of DNL or secreted as VLDL particles[143] (**Figure 6**).

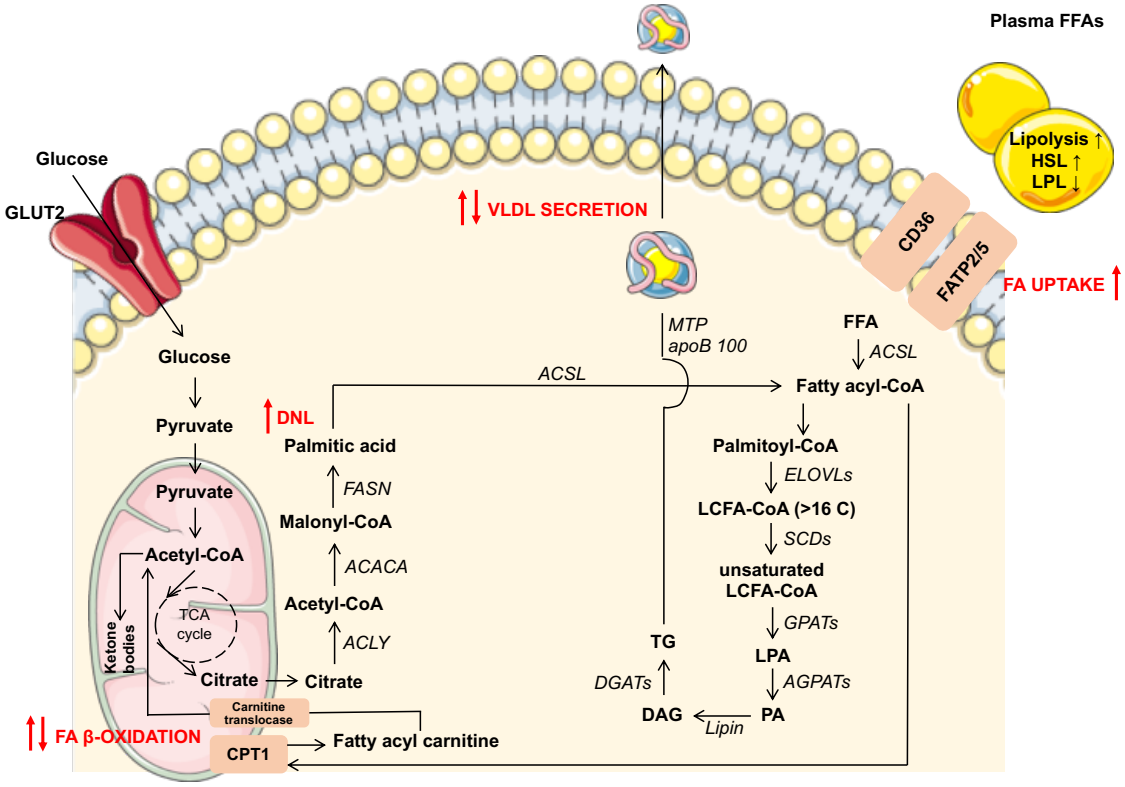

Figure 6. Molecular mechanisms for TG accumulation during NAFLD. DNL, FA uptake, FA β-oxidation and VLDL secretion are the main pathways controlling FA accumulation within hepatocytes. Imbalance between these mechanisms contributes to NAFLD onset and progression. *J Latorre (2019).*

1.3.5. The role of AMPK

The AMP-activated protein kinase (AMPK) is a heterotrimeric complex consisting of an α catalytic subunit (two different isoforms), together with two regulatory subunits β and γ (two and three isoforms respectively). The AMPK α subunit contains the catalytic phosphorylation site on threonine 172 (Thr^{172}), and the β subunit is required for maintaining the structure of AMPK heterotrimer, while γ subunit acts as a regulatory subunit due to nucleotide-binding properties that allow the allosteric control of this complex. AMPK is primarily activated by increased AMP/ATP ratio as a result of energetic challenges that interfere ATP production and enhance energy consumption, while high levels of ATP will inhibit the activity of this kinase[171]. Thus, AMPK senses changes in the AMP/ATP ratio by binding such metabolites in a competitive manner. Once activated, AMPK inhibits ATP-consuming processes and activates catabolic processes (i.e. proteolysis, lipolysis and β-oxidation).

AMPK-mediated phosphorylation of substrates plays a key role in homeostasis regulation and maintenance. To improve NAFLD, increased levels of AMPK activity in the liver would supress DNL and increase FA oxidation, through the phosphorylation and inactivation of ACC[172]. AMPK activation can also reduce TG accumulation in liver due to its ability to inhibit DNL. AMPK phosphorylates ACC1 at Ser^{79} and ACC2 at Ser^{221}. Such phosphorylations block the polymerization of ACC. Lower ACC activity is translated into lower malonyl-CoA levels, so DNL is compromised[173]. AMPK can also phosphorylate SREBPF1 at Ser^{372}, inhibiting the proteolytic cleavage and nuclear translocation, suppressing again DNL. As proof of concept, a mouse model with serine to alanine knock-in mutations affecting active sites, rendered the inability to be phosphorylated and disclosed highly active ACC function, with the subsequent accumulation of TGs in liver, leading to NAFLD and impaired metabolism[129]. These data point that AMPK-mediated phosphorylation and inactivation of ACC leads to enhanced shuttling of carbohydrates through DNL[129] (**Figure 7**).

Referring to FA oxidation, the ability of AMPK in phosphorylating ACC leads the reduction in malonyl-CoA. Being malonyl-CoA the allosteric inhibitor of CPT1, the rate-limiting enzyme for mitochondrial FA oxidation, AMPK also increases FA oxidation by impeding malonyl-CoA to inhibit CPT1, which will be able to supply FAs into the mitochondrial matrix[174,175]. Here again, knock in mutations in ACC active sites disclosed lower rates of FA oxidation, demonstrating the involvement of AMPK[129] (**Figure 7**).

AMPK can also play a role in the regulation of gluconeogenesis by phosphorylating CREB regulated transcription coactivator 2 (CRTC2), blocking its nuclear translocation. Nuclear CRTC2 promotes the expression of gluconeogenic genes such as *PEPCK* and *G6Pase*, so its blockade may trigger inhibition of this pathway[134] (**Figure 7**).

Altogether, AMPK is considered an essential cellular energy sensor of cellular energy status, maintaining cell energy balance. Even ATP levels are reduced in NAFLD, liver AMPK activity is reduced in NAFLD subjects, suggesting the role of different pathways modulating AMPK activity[176,177].

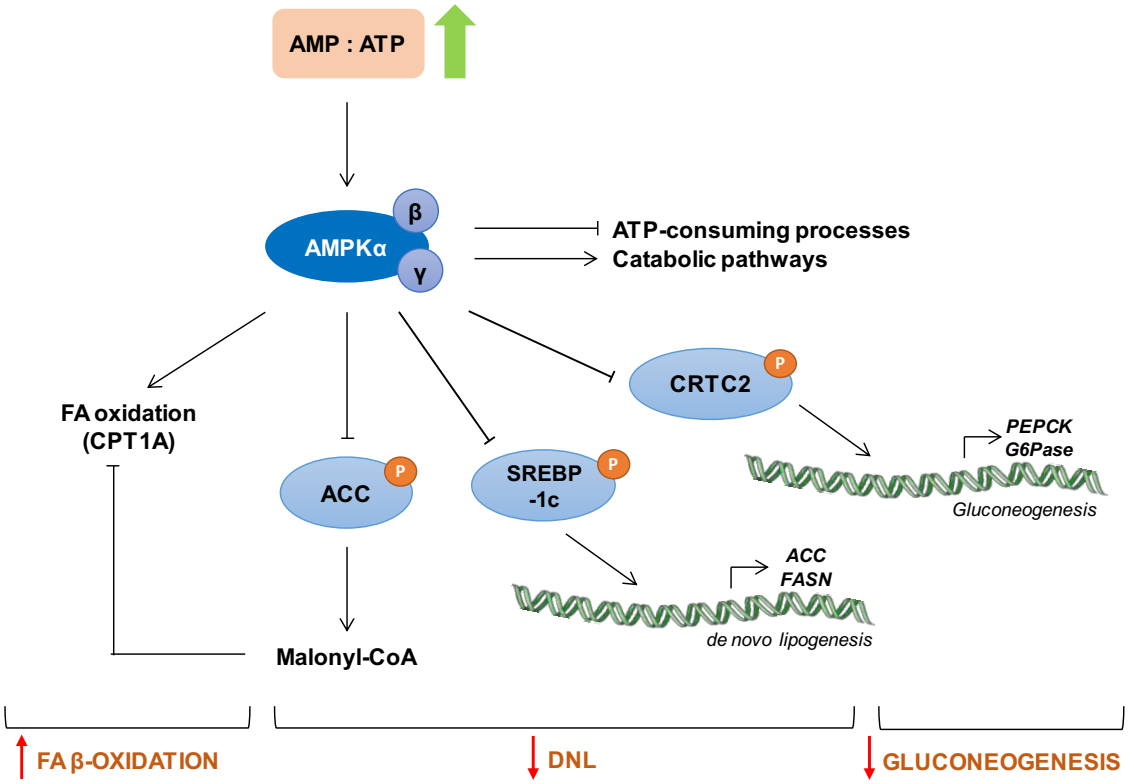

Figure 7. The role of AMPK in hepatocytes. AMPK activation can counteract NAFLD through its ability to mitigate pathways involved in TG accumulation: inhibiting ACC, SREBPF1 and CRTC2, decreasing DNL and gluconeogenesis. At the same time, AMPK can stimulate catabolic pathways such as FA β-oxidation. *J Latorre (2019)*

Several studies have used metformin as an activator of AMPK to test its efficacy in humans. Most of them show an improvement in liver aminotransferases and liver histology. However, since monitoring the efficacy of metformin therapy is still unclear, new sensitive an noninvasive markers of response to validate preclinical data are needed[178].

1.4. MicroRNAs

1.4.1. Tiny giants in the regulation of cell fate

In 1993, Victor Ambros and colleagues discovered that *lin-4*, a gene known to control the timing of *Caenorhabditis elegans (C. elegans)* larval development, was producing a pair of small RNAs that were not translated into a protein[179]. These small *lin-4* RNAs were approximately of 22 and 61 nt in length, and they had antisense complementarity to different sites in the 3′ untranslated region (UTR) of the lin-14 mRNA. This discovery

supported a model in which the *lin-4* RNAs pair to the *lin-14* 3'UTR to specifically repress translation and reduce the amount of lin-14 protein. This novel method of regulating gene expression at the post-transcriptional stage was first thought to be unique and exclusive of *C. elegans*. However, in 2000, lethal-7 (let-7) was the second miRNA discovered in *C. elegans*. Let-7 was found to be implicated in the late larval transition to adult, and in contrast to *lin-4*, homologues of this gene were discovered in many organisms, including humans[180]. Firstly, as lin-4 and let-7 were components of the gene regulatory network that controlled the timing of *C. elegans*, they were also referred to as small temporal RNAs (stRNAs). Later it was shown that many 21- and 22-nt expressed RNAs, existed also in invertebrates and vertebrates, and some of them were highly conserved. In the following years, small RNAs were cloned from humans, flies and worms, derived from a longer precursor with a stem-loop and evolutionarily conserved across species. These findings reported a new class of non-coding RNAs, and the term microRNA was introduced for define this collective. It was suggested that the sequence-specific, posttranscriptional regulatory mechanisms mediated by small RNAs were more substantial than previously thought[181–183]. Hence, the shorter *lin-4* is now recognized as the founding member of an abundant class of regulatory RNAs called microRNAs (miRNAs)[179].

Nowadays, miRNAs are defined as a class of non-coding RNAs that are processed from step-loop regions of longer transcripts, with the ability of regulate the expression of complementary messenger RNAs[184]. They comprise small 19–24 polynucleotides in length, endogenous, evolutionarily conserved oligonucleotides that function as posttranscriptional regulators of gene expression[185]. A miRNA registry named miRBase, set up in 2002, serves as an online repository for miRNA sequences and annotations[186]. The current release (22.1) contains 38,589 miRNA entries (October 2018), representing a predicted hairpin portion of a miRNA transcript with information on the location and sequence of the mature miRNA sequence[186].

Together with other short non-coding RNAs species, including interfering RNAs (siRNAs), small nucleolar RNAs (snoRNAs), and PIWI interacting RNAs (piRNAs), miRNAs constitute one of the most abundant forms of gene-regulatory elements in animals. To understand its regulatory function, it is mandatory to determine which messenger RNAs can be targeted. miRNA targets can be predicted by searching for conserved 6-8mer matches to miRNA seed region. Four type of matches are known to

be selectively conserved: the 6-mer site (matching perfectly the 6-nt miRNA seed), the 7mer-m8 site (comprising the seed match plus a Watson-Crick match to miRNA nucleotide 8), the 7mer-A1 site (comprising the seed match supplemented by an A across from miRNA nucleotide 1 and the 8mer site (comprising the seed match plus both m8 and A1). The four canonical sites share six contiguous Watson-Crick matches to the miRNA seed, which are the nucleotides that occupy the positions 2 to 7 (**Figure 8**). Taking into account the seed-matched target predictions, mRNAs that either decrease after miRNA addition or vice versa, increase following miRNA disruption are plausible to contain seed matches. The hierarchy of site efficacy is the following: 8mer > 7mer-m8 > 7mer-A1 > 6mer. Knowing that, miRNAs can have a wide variety of different targets often repressing multiple genes at different points in the same biological pathway. Furthermore, multiple miRNAs are able to target the same mRNA[187,188]. In total, more than 45,000 miRNA target sites within 3'UTR are present in human, and more than 60% of human protein-coding genes have been under selective pressure to maintain complementarity to miRNAs[188].

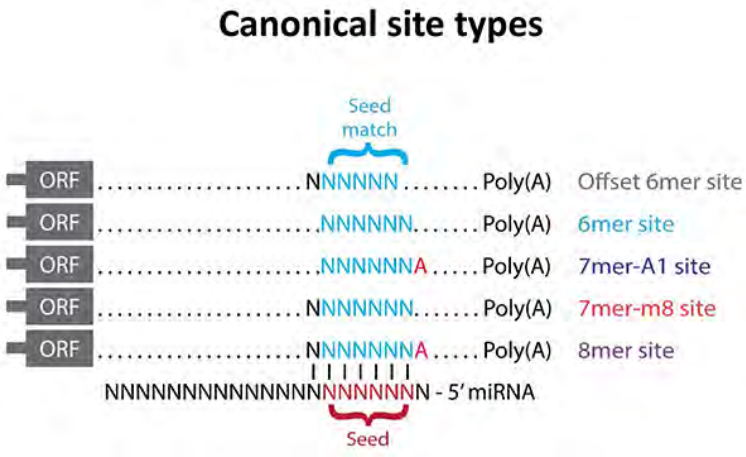

Figure 8. Canonical site types for miRNA:mRNA interaction. Plausible site types of interaction between miRNA and the 3'UTR seed sequence of target mRNA. *Image taken from Targetscan database*[189].

At first, miRNAs were thought to bind to complementary target sequences in mRNAs and interfere with the translational machinery, thereby preventing or altering the production of the protein[190]. Later it was also found that in addition to translational repression, miRNAs could bind to its target mRNA, triggering the recruitment of mRNA decay factors[191]. As a consequence, these association would lead to mRNA destabilization, degradation and decreased expression. Therefore, the main role of

miRNAs is to induce mRNA degradation and decay, also inhibiting the translation to protein[191].

Given their regulatory activity, miRNAs are regarded as attractive tools for therapeutic approaches and new researches based on these molecules as therapeutic candidates. Taking into account that their expression can be enhanced or impaired, therapeutic approaches are focused on either replacing or disrupting its expression. miRNA replacement is based on restoring miRNA amounts by short RNA duplexes that mimic endogenous miRNAs, and it is used when the quantities of the specific miRNA are downregulated in disease but higher expressed in control situation[190]. While miRNA mimics are double-strand, chemically synthesized, but mimic mature endogenous miRNA, miRNA inhibitors are chemically modified, being single-stranded oligonucleotides able to antagonize specific miRNA. They are used when the endogenous miRNA is overexpressed. Depending on its function, they are called antagomirs or antimiRs. While antagomirs are entirely complementary to the entire mature miRNA, antimiRs are complementary to the seed region of the mature miRNA. Therefore, antagomirs degrade miRNA target, while antimiRs sequestrate them[190].

1.4.2. miRNA biogenesis

The biogenesis of miRNA biogenesis follows a two-step process including both nuclear and cytoplasmic cleavage events[192]. In metazoan, miRNAs are transcribed by RNA polymerase II (Pol II) as part of much longer primary transcripts called "pri-miRNAs", whose maturation occurs through sequential processing events. Each pri-miRNA has at least one region that folds back on itself to form a hairpin substrate. Then, the pri-miRNA is processed into ~70- to 120-nucleotide-long precursor RNA called pre-miRNA by a multiprotein complex called Microprocessor. Microprocessor is highly conserved in animals, but not in plants. This multiprotein complex contains drosha ribonuclease III (DROSHA), which is the core RNAse III enzyme that executes the nuclear cleavage of the pri-miRNA. It has been demonstrated that immunopurified DROSHA cleaved pri-miRNA to release pre-miRNA *in vitro,* and RNA interference of DROSHA resulted in accumulated pri-miRNAs coupled with a strong reduction of pre-miRNAs and mature miRNAs[193]. Drosha forms a dimer with DiGeorge syndrome critical region gene 8 (DGCR8). The transcribed pre-miRNA is subsequently exported into the cytoplasm by exportin 5 (EXP5). EXP5 is able to bind pre-miRNAs in the presence of the Ran-GTP

cofactor. Therefore, not only EXP5 is required for miRNA biogenesis, but also its cofactor[194]. Once in the cytoplasm, pre-miRNAs are processed into mature duplexes of ~18-23 nucleotides by dicer ribonuclease III (DICER), another RNAse III enzyme which is able to cleave the loop region of the pre-miRNA. DICER recognizes the 5' phosphate and 3' overhang approximately at the two helical turn away from the base, and then cuts the double strand. The cleavage separates the loop from the double strand, acting together with transactivation response RNA binding protein (TRBP). Then, the 2 miRNA strands are separated, giving a miRNA strand with unstable base paring at the 5' that will constitute the guide strand, and the other one with a stable base pairing at the 5' end that is usually dysfunctional and eventually degraded. The guide strand, along with TRBP will associate with catalytic Argonaute (AGO) proteins. This complex will receive the name of RNA-induced silencing complex (RISC). Occasionally, the other strand can also associate with AGO proteins, thus serving both strands as functional. Therefore, TRBP will facilitate the entry of DICER-miRNA complex into RISC, containing AGO2, protein kinase RNA activator (PACT), trinucleotide repeat-containing gene 6A (TNRC6A) and other binding proteins. Once the guide strand is into the RISC, it is guided to the 3'UTR of the target mRNA, triggering two plausible repression mechanisms. In case of perfect base complementarity, it will degrade the mRNA, while multiple sequence mismatches will trigger translational inhibition. Nevertheless, there are exceptions where almost perfect complementarity will lead to translational suppression but not cleavage. The target recognition is done by conserved seed sequence of miRNA where 2-8 residues are complementary to 3'UTR motifs (**Figure 9**)[192,195].

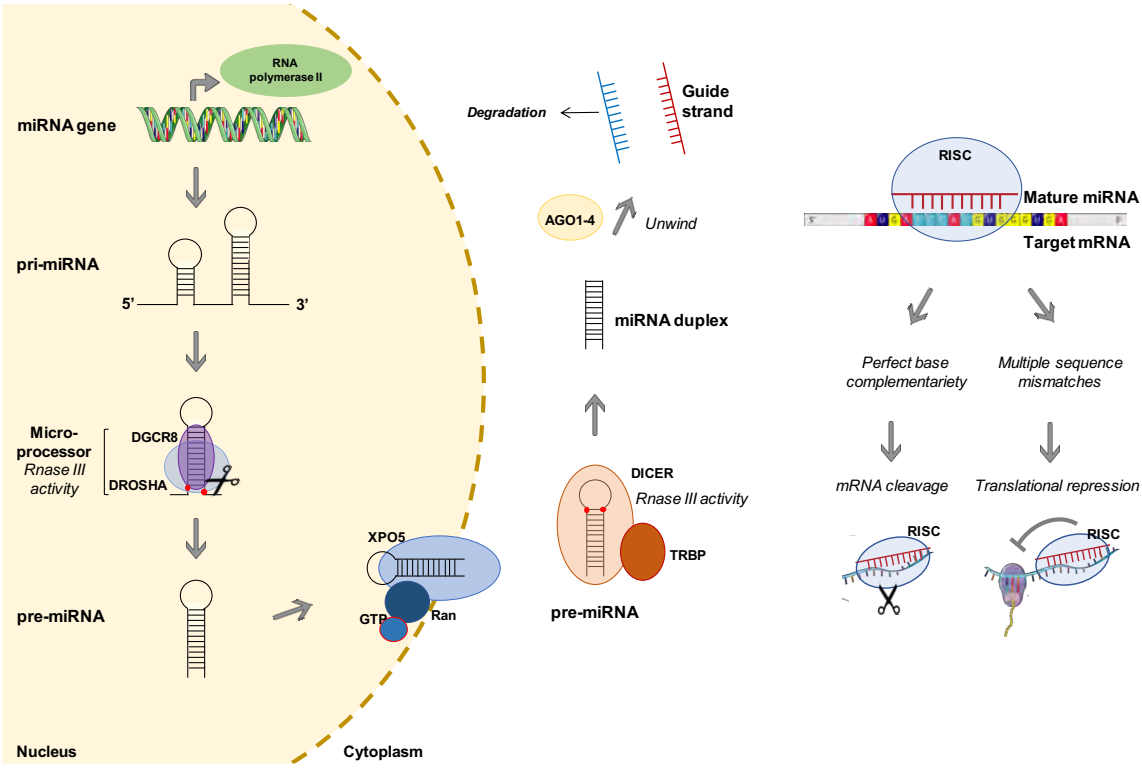

Figure 9. miRNA biogenesis. miRNAs are transcribed as pri-miRNAs by RNA polymerase II within the nucleus. The pri-miRNA is then cleaved by the Microprocessor, containing DROSHA and DGCR8, producing the pre-miRNA. This 60-70 nucleotide precursor is exported to the cytoplasm by XPO5, and processed by DICER and TRBP to produce mature miRNAs. Subsequently, the two strands are unwinded and the guide strand is loaded into RISC. Once within the complex, either degradation or translational repression will be mediated according to base complementarity[195]. *J Latorre (2019).*

1.4.3. miRNA function and prediction of target genes

A single miRNA can bind a great variety of 3'UTRs found in many mRNAs. On the other hand, a single mRNA can be targeted by a great number of miRNAs. It is worth stressing that although the most common binding site is 3'UTR, miRNAs can also bind coding sequence (CDS) or 5'UTR of mRNAs. As epigenetic modulators, the transcriptome of a specific cell type can be completely shaped by miRNA activity[196].

The way to address it is the utilization of *in silico* tools that predict miRNA:mRNA interactions, and subsequently validate them. There are different databases trying to predict miRNA target genes. Nevertheless, bioinformatic tools have a limited predictive power to identify all targets. Algorithms used by each database are different, but the vast majority are based on seed complementarity between miRNA and mRNA, while others take into account different parameters such as thermodynamic principles[197].

1.4.4. miRNAs and liver disease

Taking into account that about 60% of human genes can be regulated by miRNAs[188], it can be postulated a key regulatory role of miRNAs in multiple physiological processes and disorders, also including fatty liver disease[198–200].

Dysregulation of various miRNA expression profiles have been reported to be a key pathogenic factor in many liver diseases, including viral hepatitis, AFLD and HCC[201]. Not only studies have been done on hepatic miRNAs, but also circulating miRNAs profiles have been shown to reflect histological changes and molecular events in the liver, presumably suggesting that circulating miRNAs could be potential NAFLD biomarkers[198].

1.4.4.1. miRNA profiling of subjects with NAFLD

Some studies have focused on describing miRNA profiles trying to provide new insights into the potential involvement of miRNAs in NAFLD. Cheung *et al.*[202] profiled 474 mature miRNA species in liver samples from obese individuals with NASH and subjects with normal liver histology, reporting an altered hepatic miRNA expression profile associated with NASH. 46 miRNAs were found to be differentially expressed between groups. Among them, upregulation of miR-34a and miR-146b, and downregulation of miR-122 were confirmed in an extended sample comprised of 50 subjects (18% men, age = 46 ± 9 years, body mass index (BMI) = 37.3 ± 3.2 kg/m^2). Noteworthy, miRNA levels were not associated with NASH severity, suggesting a role in biological processes not related to fibrosis itself[202].

Another study disclosed significant downregulation of two hepatic miRNA candidates (miR-122 and miR-192) in obese patients with NASH and/or NAFLD when compared to lean subjects with normal liver histology (n=65; 43% men, age=50 ± 6 years, BMI=30.1 ± 4.2 kg/m^2)[203].

Additional research has analysed miRNAs expression in liver samples from morbid obese females with (n=15; age=51 ± 8 years, BMI=44.4 ± 6.6 kg/m^2) and without (n=15; age=47 ± 6 years, BMI=41 ± 4.6 kg/m^2) hepatic fibrosis, disclosing significant changes in miRNAs that completely differed from those reported before, identifying an

upregulated expression of miR-182, miR-183, miR-31, miR-224, miR-150 in fibrotic liver, and downregulation of miR-590, miR-378i, miR-17 and miR-219a[204].

Another study selected subjects (n=30; 33% men, age=48 ± 10 years, BMI=45.9 ± 5.4 kg/m^2) with the highest (30%) and lowest (0%) liver fat and profiled liver biopsies on microarrays able to identify 1438 miRNAs. While the screening method revealed a total number of 42 miRNAs upregulated and 2 miRNAs downregulated in NAFLD subjects compared to controls, and 4 out of 44 were validated: miR.103a-2*, miR-106b*, miR-576-5p and miR-892a[205].

The last compiled study profiled 233 miRNAs in a cohort classified as NAFL, NASH, cirrhosis and controls (n=36; age from 26 to 59, BMI ≥ 40 kg/m^2). Three miRNAs were found to be differentially regulated (miR-301a-5p and miR-34a-5p increased and miR-375 decreased) with disease progression[206].

miRNA expression profiling studies published in patients with NAFLD have reported inconsistent results, mainly due to the diagnostic accuracy distinguishing individuals with NAFLD, NAFL, NASH or fibrosis. Despite that, all these analytical results suggested that NAFLD severity is associated with a specific pattern of altered hepatic miRNA expression that may drive the hallmark of the disorder, being altered lipid and carbohydrate metabolism (**Table 2**)[199].

Table 2. Summary of hepatic miRNA profiles previously associated with NAFLD in humans. Values represent the mean ± SD. [a]NAFLD include patients with NAFL, NASH and cirrhosis. *J Latorre (2019).*

Study	**Ref#**[202]	**Ref#**[203]	**Ref#**[204]	**Ref#**[205]	**Ref#**[206]
N	50	65	30	30	36
Men/Women	9/41	28/37	0/30	10/20	0/36
Age (years)	46.4 ± 8.6	49.8 ± 5.7	49.2 ± 2.9	48 ± 10	26 to 59
BMI (kg/m^2)	37.3 ± 3.2	30.1 ± 4.2	42.7 ± 2.4	45.9 ± 5.4	BMI ≥ 40 kg/m^2
Identification by (all miRNAs)	Microarray (474)	-	Sequencing	Microarray (1,438)	Sequencing
NAFLD/Controls (identification)	15/15	-	15/15	15/15	26/10
Validation by (miRNA candidates)	RT-PCR (4)	RT-PCR (2)	RT-PCR (11)	RT-PCR (8)	RT-PCR (3)
NAFLD/Controls (validation)	25/25	51/14	15/15	10/10	26/10[a]
Upregulated	miR-34a, miR-146b	-	miR-182, miR-183, miR-150, miR-224, miR-31	miR-103a-2*, miR-106b*, miR-576-5p, miR-892a	miR-34a, miR-301a
Downregulated	miR-122, miR-139-5p	miR-122, miR-192	miR-378i, miR-590, miR-17, miR-219	-	miR-375

Since miRNAs have been proposed as an attractive diagnostic tool, profiles have been performed in both liver and serum, searching for plausible targets and associations with common features of NAFLD, respectively. Despite that, the miRNA expression correlation between serum and liver usually tends to be inconsistent[207].

1.4.4.2. miRNAs and NAFLD

Besides general profiles, it is of special interest the great number of studies that have disclosed differences in specific miRNA expression between liver samples from NAFLD subjects compared to controls. So far, NAFLD subjects widely show upregulation of the

following miRNAs: miR-21, miR-31, miR-34a, miR-103/107, miR-144, miR-146b, miR-150, miR-182, miR-183, miR-200a, miR-224 and miR-301a, and downregulation of: let-7, miR-17, miR-26, miR-29, miR-33a/b, miR-122, miR-296, miR-373, miR-375 and miR-378c[190,200,201,208].

miRNA expression is tissue-specific and it is recognised that miR-122 constitutes more than half of the total amount of miRNA expressed in the liver. Therefore, miR-122 is thought to play an important role in the liver. However, a variety of studies targeting miR-122 have revealed controversial results. While most of the investigations reported that silencing miR-122 induced overexpression of genes related to lipogenic pathways[209–211], others disclosed that the inhibition of miR-122 through antagomirs resulted in a reduced expression of lipogenic genes together with an increase in FA oxidation, mediated by the activation of AMPK[212]. Discrepancy between studies should be attributed to distinct animal models and methodological approaches.

Apart from studies based on the functional role of miR-122, some other miRNAs have been studied based on the functional impact held by their targets. miR-33a and miR-33b contribute to the modulation of FA metabolism and insulin signalling pathways. Specifically, miR-33 deficient mice develop obesity and liver steatosis presumably due to SREPB1, which appears overexpressed in the absence of miR-33a, and concomitantly it elevates plasma HDL levels[213].

miR-34a has also been studied in liver disease, which main target is sirtuin 1 (SIRT1). It appears to be upregulated in both mice fed a high-fat diet and liver and serum from patients with NAFLD[200]. SIRT1 is a direct target of miR-34a and a key mediator of energy metabolism via multiple signalling pathways. The inhibition of miR-34a restored SIRT1 expression and activation of AMPK, suggesting a fundamental role for miR-34a in NAFLD lipid metabolism dysregulation[214]. miR-34a levels are linked to NAFLD severity and as miR-122, it may serve as a novel biomarker for NAFLD progression (**Table 3**)[215].

1.4.4.3. miRNAs linked to advanced NAFLD stages

Considering that miRNAs can regulate cell proliferation and survival, understanding the miRNA modulation in NASH may promote new evidences of disease progression. miR-21 has been studied in NASH pathophysiology. Previous studies have suggested that miR-21 was upregulated in NASH livers and low-density lipoprotein receptor-

deficient high-fat diet mice, and it has been proven that its inhibition or suppression decreases liver injury, inflammation and fibrosis, by restoring PPARα expression[216]. miR-21 levels are reported to be different throughout different stages of NAFLD, indicating that certain miRNAs can play different roles in the progression of NAFLD-related liver injury. miR-103 and miR-107, which differ by one nucleotide, have been reported to be increased in NASH patients. Their overexpression induced impaired glucose tolerance and conversely, their silencing in mice lead to improved glucose homeostasis and insulin sensitivity (**Table 3**)[217].

Fibrosis stage is triggered by a complex network of signalling pathways that regulate the deposition of proteins in the extracellular matrix and fibrogenesis, where hepatic stellate cells and Kupffer cells are the main contributors. Several studies have focused on the role of miR-29 family in fibrosis development. miR-29 is reported to be related to cell proliferation, extracellular matrix homeostasis and gluconeogenesis its major effect in the liver is its involvement in fibrosis. A mouse model of carbon tetrachloride (CCl4) induced hepatic fibrogenesis revealed that miR-29 family was significantly downregulated in treated-mice livers[218], appearing to have an antifibrotic activity by targeting fibrotic genes such as collagen type I alpha 1 (*COL1A1*)[219]. Moreover, its levels were found to be significantly lower in NAFLD patients[220]. Studies relating miR-122 with fibrosis also disclosed that deficiency of miR-122 contributes to NASH-induced liver fibrosis through tissue-remodeling genes (**Table 3**)[221].

miRNA dysregulations in human HCC have been described with only few miRNAs in common, pointing to the high heterogeneity of HCC. Downregulated miRNAs identified in more than one studies include let-7, miR-122, miR-26 and miR-101, while miR-221 and miR-181 are reported to be upregulated in HCC[190]. The functional relevance of miR-122 is not only important in early stages of disease, but also in fibrosis and HCC. miR-122 is reported to be repressed in HCC, whereas its restoration was able to revert this phenotype[222]. Another well-known tumour-supressive miRNA is let-7. It is known to directly target LIN28/28B, which at the same time inhibit let-7. Inflammation triggers enhanced expression of LIN28/28B, suppressing let-7 and triggering oncogenic events[223]. Finally, miR-26 is also linked to HCC prognosis, exhibiting reduced expression. miR-26 is known to be a tumour suppressor by targeting cyclins D2 and E2. In fact, systemic administration of miR-26 in a mouse model of HCC resulted in

inhibition of cancer cell proliferation and protection from disease progression, therefore classifying miR-26 as a useful tool for the prevention or treatment of HCC (**Table 3**)[224].

Altogether, there is growing evidence supporting the notion that hepatic miRNAs are deregulated in fatty liver, and suggests a mechanistic relevance and therapeutic utility in the field. Thus, research assessing the regulation and activity of hepatic miRNAs is of great interest. Such studies may provide further insight into the specific role of miRNAs in fatty liver and associated diseases.

Table 3. Deregulated miRNAs in hepatic tissues and circulation in different models of NAFLD stages. Compilation of different studies based on describing specific miRNA expression pattern in different stages of NAFLD, including NAFL, NASH, fibrosis or HCC. *J Latorre (2019).*

miRNA	*Regulation in disease*	*Model*	*Findings*	*Reference*
		NAFL		
miR-122	Decreased	Mice fed with methyl-deficient diet	Steatosis progression	209
		Mice with Mir122a deletion	Increased cholesterol and triglyceride content in the liver	210
			Decreased serum cholesterol and triglycerides	
		Cultured hepatocytes silencing miR-122	Overexpression of lipogenic genes	211
		Cultured hepatocytes overexpressing miR-122	Downregulation of lipogenic genes	
miR-33	Decreased	Mice with miR-33 deficiency	Obesity and steatosis development	213
miR-34a	Increased	High-fat diet mice	Association with NAFLD features	214
		NAFLD livers	Dyslipidaemia (positive association with VLDL and TG)	215
		NASH		
miR-21	Increased	Mouse model of NASH with miR-21 deficiency	Reduced liver cell injury, inflammation and fibrogenesis	216
miR-103/107	Increased	Gain of miR-103/107 in mice	Impaired glucose homeostasis	225
		Silencing of miR-103/107 in mice	Improved glucose homeostasis and insulin sensitivity	

		Fibrosis		
miR-29	Decreased	Carbon tetrachloride-treated mice	Fibrosis progression	226
		NAFLD serum	Negative association with fibrotic features	220
miR-122	Decreased	Methionine-choline deficient (MCD)	Increased liver fibrosis	221
		HCC		
let-7	Decreased	Cancer cell lines	IL-6 overexpression and oncogenic events	223
miR-26	Decreased	Gain of miR-26 in NASH models	Cancer cell proliferation inhibition	224
miR-122	Decreased	Silencing miR-122 in mice	Growth of HCC and increased migration and invasive activity	222

2. HYPOTHESIS

1. **MicroRNAs are associated with hepatic fat overload and impaired metabolism, contributing to the pathogenesis of non-alcoholic fatty liver disease (NAFLD)**

NAFLD represents a spectrum of disturbances encompassing fatty acid (FA) infiltration of the liver parenchyma, which often leads to the activation of inflammatory pathways and insulin resistance. In the context of impaired metabolism, the association between hepatic microRNA profiles and NAFLD is poorly recognized. Providing association of specific microRNAs linked to the pathophysiology of fatty liver disease could pave future investigations, targeting new biomarkers and genomic therapies based on the microRNA-related post-transcriptional regulation.

2. **Treatments mirroring NAFLD compromise the biosynthesis of microRNAs required to maintain lipid homeostasis in hepatocytes**

The balance between FA biosynthesis, uptake and clearance is of utmost importance for maintaining lipid homeostasis in hepatocytes, the most common parenchyma cells in the liver. Genes involved in these mechanisms could be targets for microRNAs that are differentially expressed in subjects with NAFLD. Here we postulate the significant alteration of microRNAs required to maintain lipid homeostasis in hepatocytes under conditions mimicking NAFLD.

3. **Impaired AMPK function may be at the forefront of significant changes in microRNA patterns found in hepatocytes challenged with conditions mirroring NAFLD**

AMP-activated protein kinase (AMPK) is a master metabolic regulator that inhibits lipogenesis and other ATP-consuming processes. Previous studies have reported that treatments enhancing its expression increase the expression of DICER, a key enzyme of microRNA biosynthesis. Therefore, AMPK could regulate FA metabolism through the regulation of hepatic microRNA availability.

4. **Ectopic replenishment of microRNA candidates can restore lipid homeostasis in hepatocytes, tackling the progression of NAFLD**

Impaired hepatic microRNA expression in NAFLD may lead to an inadequate control of target genes involved in the acquisition of fatty liver. We hypothesize that the ectopic replenishment of regulatory microRNAs significantly diminished in NAFLD patients could restore the control of lipid metabolism in hepatocytes.

3. OBJECTIVES

1. To assess the hepatic microRNA (miRNA) signature in obese subjects with and without non-alcoholic fatty liver disease (NAFLD)

1.1. To analyse the expression profile of mature miRNAs found in liver samples from subjects with and without NAFLD

1.2. To identify associations with anthropometrical, biochemical and clinical features taking into account confounding factors such as age, sex and the body mass index (BMI)

2. To validate experimental models mimicking NAFLD

2.1. To design *in vitro* models of primary human hepatocytes and cell lines as HepG2 challenged with different agents able to trigger or reduce lipid accumulation within hepatocytes, thus mimicking NAFLD *in vitro*

2.2. To analyse gene and miRNA expression values in these models

3. To characterize the potential mechanisms linking NAFLD to the miRNA signature of hepatocytes

3.1. To analyse the expression of genes related to molecular mechanisms altered in NAFLD, mainly those related to lipid and glucose metabolism and inflammation

3.2. To assess the relationship between hepatic miRNAs and gene expression to identify epigenetic mechanisms related to impaired fatty acid accumulation

4. To evaluate functional and mechanistic significance of hepatic miRNA candidates

4.1. To identify target key-genes also altered in liver pathophysiology

4.2. To test miRNA transfection effects in hepatocytes challenged with agents triggering lipid accumulation, and analyse the impact upon adverse conditions leading to FA overload

4.3. To employ miRNA mimics to transfect hepatocytes under normal and conditions leading to impaired metabolism and evaluate the impact of this gain of function

4.4. To perform *in silico* research of potential gene targets and mechanistic development downstream the ectopic expression of miRNA candidates

4. MATERIALS AND METHODS

4.1. STUDY POPULATION

The study population was comprised of 60 non-consecutive obese subjects (20% male) eligible for bariatric surgery (age=46 ± 9 years, BMI = 45.2 ± 6.6 kg·m^{-2}) with (28.3%) or without NAFLD. NAFLD was first suspected in participants with abnormal liver enzymes and/or radiological evidence of fatty liver, coupled with negative insights of other causes standing for liver disease, and the absence of significant amounts of alcohol consumption (≥20 g per day for women, and ≥30 g per day for men). Each participant underwent clinical assessment, radiological, haematological and biochemical testing prior to laparoscopic Roux-en-Y gastric bypass. At the moment of surgery, subjects underwent a percutaneous core liver biopsy with a 15-gauge microvasive biopsy device and laparoscopic guidance.

A subcohort comprised by 19 obese women belonging to the study population group was used as an identification sample. It was formed by 8 obese women (age=44 ± 9 years, BMI = 43.6 ± 8 kg m^{-2}) with normal liver histology, ultrasound and liver enzymes, and 11 obese and NAFLD female patients (age = 48 ± 6 years, BMI = 44.8 ± 7 kg m^{-2}).

NAFLD classification was made based on liver biopsies using NAS, a designed and validated scoring system designed by the Pathology Committee of the NASH Clinical Research Network. As it has been explained, NAS comprises different histological features, where four of them are measured semi-quantitatively, being steatosis, lobular inflammation, hepatocellular ballooning and fibrosis. The NAS system allowed to perform a diagnostic categorization that classified patients as "not NAFLD", "borderline" or "NAFLD". More detailed information about the scoring system in the subsection "*1.1.5.3. Histological diagnosis of NAFLD*". All liver specimens from the extended sample of 60 Caucasian men (20%) and women (17 NAFLD, 24 borderlines and 19 obese participants with no signs of liver dysfunction) were obtained from non-consecutive obese patients following bariatric surgery in the Surgery Service of the Hospital Universitari Dr Josep Trueta (Girona, Spain). The study protocol was approved by the Ethics Committee and the Committee for Clinical Investigation (CEIC) of the Hospital Universitari Dr Josep Trueta. All subjects provided written informed consent before entering the study.

Liver samples were snap frozen in liquid nitrogen for genomic analyses, and fixed in formalin for histological assessment. Fixed samples were stained with haematoxylin-

eosin and Masson's trichrome stain, and all the specimens were evaluated by the same pathologist according to NAFLD clinical research network criteria. Exclusion criteria included fatty liver alone, cirrhosis or bridging fibrosis, and the use of statins.

4.1.1. Clinical measurements

4.1.1.1. Anthropometric characterization

The **Body mass index** (BMI) is calculated as the weight divided by the square of the body height (kg/m^2). **Fat mass percentage** was measured by densitometry, an approach that distinguishes fat mass (FM) from total fat free mass (FFM). Together with densitometry, the Deurenberg formula[227] and electrical bioimpedance (TANITA® MC-190 Body Composition Analyzer; *Tanita Corporation, Tokyo, Japan*) have been used to estimate body fat percentage. Blood pressure was measured by both **systolic blood pressure** (SBP) and **diastolic blood pressure** (DBP) in the upper arm. All participants included in the study are morbid obese subjects (BMI>40 kg·m^{-2}) according to WHO guidelines (*https://www.who.int/es/news-room/fact-sheets/detail/obesity-and-overweight*).

4.1.2.2. Biochemical characterization

Fasting **glucose** concentrations in serum were obtained by means of an oxidation reaction and the consequent colorimetric variation, monitored with a Beckman Glucose Analyzer II spectrophotometer (*Beckman Instruments, California, USA*).

Total cholesterol was also measured by spectrophotometry and the peroxidase-catalysed esterification/oxidation reaction in a BM/Hitachi 747-100 analyser (*Roche Diagnostics, Indianapolis, USA*). **High- and low-density lipoproteins** (HDL and LDL respectively) were measured directly in serum by precipitation of apoB containing lipoproteins, and polyethylene glycol-coupled cholesteryl esterase and cholesterol oxidase for the HDL-cholesterol measurement, while LDL is most often determined using the "Friedewald formula", which takes into account measured values for total cholesterol, HDL and triglycerides: LDL-C = (TC) - (HDL-C) - (TG/5), where units are mg/dL. **Triglycerides** were analysed by the glycerol phosphate oxidase/peroxidase reaction. Circulating concentrations in both cases were measured by spectrophotometric methods.

Total haemoglobin (Hb) and **C-reactive protein** (CRP) are also routine biochemical determinations obtained by spectrophotometry in plasma samples with ethylenediaminetetraacetic acid (EDTA) (*Coulter Electronics, Florida, USA*), a common anticoagulant. It is common that Hb binds free glucose molecules in plasma thanks to a covalent attachment. The percentage of these proteins with attached glucose molecules is called **glycosylated haemoglobin** (HbA1c), and it is an indicator of glucose concentrations in the bloodstream during the half-life of Hb (from 6 to 8 weeks) and an indirect marker of impaired glucose tolerance (>6%). HbA1c was measured by chromatographic, immunological and electrophoretic methods in an erythrocyte's lysate. The oral glucose tolerance test (OGTT) allows to determine the degree of glucose intolerance of a subject, an inversely proportional parameter of **insulin sensitivity**. The OGTT takes into account the circulating glucose values in fasting, and 30, 60, 90 and 120 minutes after ingesting 75 g of glucose. Normotolerance established levels range from 60 to 100 mg of glucose per decilitre (dL) of fasting blood, less than 200 mg / dL 1 hour later, and less than 140 mg / dL at the end of the OGTT.

IR can be calculated according to the homeostatic model assessment for insulin resistance (HOMA-IR)[228] which uses the fasting glucose and insulin values according to the formula $HOMA_{IR}$ = (insulin x glucose)/22.5, where insulin is presented as μU/ml and glucose in mmol/L.

The levels of **aspartate aminotransferase** or **glutamic oxaloacetic transaminase** (AST/GOT) and **alanine aminotransferase** or **glutamic pyruvic transaminase** (ALT/GPT) are primarily used to diagnose liver disease. **Gamma-glutamyl transferase** (GGT) is also commonly measured to evaluate a possible liver damage. The most specific method couples the formation of pyruvate and oxaloacetate – the products of the aminotransferase reactions – to their enzymatic reduction to lactate and malate. GGT measurement uses p-nitrophenol phosphate as substrate.

4.1.2.3. Hyperinsulinemic-Euglycemic Clamp Technique

The plasma insulin concentration is acutely raised to a new plateau and maintained at 100 μU/ml by a continuous infusion of insulin for 120 min. This level would result in profound, rapidly developing hypoglycaemia if the plasma glucose concentration were not maintained at its euglycemic level. But meanwhile, the plasma glucose concentration

is held constant at basal levels by a variable glucose infusion. When the steady-state is achieved, the glucose infusion rate equals glucose uptake by all the tissues in the body and is therefore a measure of tissue **insulin sensitivity**.

4.2. ANIMAL MODELS

C57BL6 mice (10 weeks old) were held in a specific restrainer for intravenous injections Tailveiner (TV-150; *BiosebLab, France*). Tail-injections were carried out using a 27G X 3/8" (0.40 mm x 10 mm) syringe. Mice were injected with either 100 µl of null (sh-luciferase, n=8) or AMPKα1-DN lentiviral particles (n=9), diluted in saline. The protein-coding sequence of AMPKα1-DN was cloned from pVQAd SF1-AMPKα1-DN (Material serial reference number 24603; *ViraQuest Inc., IA, USA*) into the pSIN-Flag vector. To generate lentiviral (Lv) particles, the pSIN-Flag vector containing AMPKα1-DN was cotransfected with packaging vectors (psPAX2 and pMD2G) into HEK293T as previously described[229]. psPAX2 and pMD2G were a gift from Didier Trono (*Addgene Plasmids, Massachusetts, USA*).

4.3. CELL CULTURE

4.3.1. Primary human hepatocytes

Primary human hepatocytes (HH) were commercially obtained (P10651; *Innoprot, Bizkaia, Spain*). They are isolated from human liver and cryopreserved immediately after isolation. Hepatocyte Medium (HM; *Innoprot, Bizkaia, Spain*) is a complete medium designed for optimal growth of normal human hepatocytes *in vitro*. It is supplemented with 5% FBS, 1% hepatocytes growth supplement (that is, the combination of growth factors, hormones and proteins necessary for culture of primary hepatocytes), and 100 units·ml^{-1} penicillin and streptomycin, following manufacturer's recommendations. HH grew on poly-L-lysine pre-coated cell dishes at 37ºC and 5% CO_2.

4.3.2. HepG2 cell culture

HepG2 cells were purchased from American Type Culture Collection (HB-8065™; *ATCC, Virginia, USA*). HepG2 cells are derived from a liver hepatocellular carcinoma of a 15-year-old Caucasian male[230]. They are epithelial in morphology and have an

adherent growth as monolayers and in small aggregates. HepG2 were cultured in Dulbecco's Modified Eagle's Medium (DMEM; *Thermo Fisher Scientific, Massachusetts, USA*) supplemented with 10% fetal bovine serum (FBS, *Thermo Fisher Scientific, Massachusetts, USA*), 100 units·ml^{-1} penicillin and streptomycin, 1 % glutamine and 1% sodium pyruvate, at 37ºC and 5% CO_2 atmosphere. The proliferation rate of HepG2 is 48 h, subcultivation ratio of 1:4 to 1:6 and medium has to be renewed twice per week.

4.3.3. Huh7 cell culture

Huh7 cells (a gift from Professor Vesa Olkkonen) are derived from a liver tumour in a 57-year-old Japanese male[231]. They are a well-differentiated hepatocyte derived cellular carcinoma cell line, epithelial-like, adherent to the surface of flasks or plates and typically grow as 2D monolayers. Huh7 cells were cultured in Minimal essential Eagle medium (MEM AQ™; *Sigma-Aldrich, Missouri, USA*) with 10% FBS (*Thermo Fisher Scientific, Massachusetts, USA)*, 100 µg/ml streptomycin and 100 units·ml^{-1} penicillin, at 37ºC and 5% CO_2 atmosphere. The doubling time of Huh7 cells is 24 h and medium has to be renewed 2-3 times a week.

4.3.4. Treatments *in vitro*

Treatments were performed in both primary HH and HepG2 cells. In HepG2, treatments with high glucose and high insulin (HG; *Sigma-Aldrich, Missouri, USA*), palmitic acid (PA; *Sigma-Aldrich, Missouri, USA*) or the combination of PA and oleic acid (OA; *Sigma-Aldrich, Missouri, USA*) were tested. HepG2 cells and/or HH were treated with PA, PA+OA, HG or with a combination of these treatments. In both HepG2 and primary HH, Compound C (CC; *Sigma-Aldrich, Missouri, USA*) was used as an AMPK inhibitor. Metformin (Mtf; *Sigma-Aldrich, Missouri, USA*) was used as an AMPK activator.

4.3.4.1. High-glucose

HepG2 cells were initially treated with a combination of glucose (33 mM) and insulin (100 nM) for 24 h. Both HepG2 and HH were treated equally.

4.3.4.2. Palmitic acid and/or oleic acid

Hepatocytes were treated with PA (0.2 to 0.5 mM) conjugated to bovine serum albumin (BSA; *Sigma-Aldrich, Missouri, USA*) as follows: 27.84 mg of PA were dissolved in 1 ml sterile water to make a 100 mM stock solution. An aliquot of 5% BSA was prepared in serum-free DMEM. 100 mM PA stock solution and 5% BSA were mixed for at least 1 hour at 40 °C to obtain a 5 mM solution, as previously described[232]. While HepG2 were treated with PA 500 μM during 72 h, primary human hepatocytes were treated with PA 200 μM for 24 h. BSA supplemented medium was used for all control conditions.

Since plasma FFAs are composed of the saturated FA PA (about 30-35%) and the monounsaturated FA OA (40-50%)[233], in addition to the treatment of exclusive PA in HepG2, a combination of PA (200 μM) and OA (300 μM). Both FAs were complexed to BSA at 5% prior to addition to cell culture medium. BSA supplemented medium was used for all control conditions.

4.3.4.3. Compound C

Compound C (CC; *Sigma-Aldrich, Missouri, USA*) was applied using dimethyl sulfoxide (DMSO; *Sigma-Aldrich, Missouri, USA*) 0.08% as vehicle. CC, also known as dorsomorphin, acts as a potent, selective, reversible and ATP-competitive inhibitor of AMPK[234]. Treatments with CC were performed at 10 μM.

4.3.4.4. Metformin

Metformin (Mtf; *Sigma-Aldrich, Missouri, USA*) is an antihyperglycemic agent that acts lowering the hepatic output of glucose. It does not stimulate insulin secretion[235]. Moreover, it is reported to stimulate AMPK. Treatments with metformin were performed at 1 mM. Phosphate buffered saline (PBS; *Thermo Fisher Scientific, Massachusetts, USA*) was used as a vehicle.

After treatments, cells were washed with PBS and collected with QIAzol® Lysis Reagent (*QIAgen, Hilden, Germany*) for RNA purification.

4.3.5. miRNA mimic transfection

Both hepatocyte cell lines and primary cultures were transfected with miRNA mimics or a non-targeting control siRNA in 12 or 24-well plates for 48h using HiPerfect

Transfection Reagent (*QIAgen, Hilden, Germany*). Transfections were performed using reverse-transfection protocol, where cell seeding, complex formation and transfection are all performed at the same day. First, miRNA mimics were added to plate wells, followed by HiPerfect Transfection Reagent. After complex formation in the wells, cells were added. The amount of miRNA mimic was optimized for each cell model, as well as the ratio of HiPerfect Transfection Reagent to miRNA mimic. 1:3 miRNA mimic: HiPerfect Transfection Reagent was the ratio used in our experiments. The optimal cell confluency did not exceed 80% at the moment of transfection.

The miRNA mimics (*QIAgen, Hilden, Germany*) used were: AllStars Negative Control siRNA (1027280), miR-10a-5p (MSY0000253), miR-16-5p (MSY0000069), miR-26a-5p (MSY0000082), miR-29c-3p (MSY0000681), miR-30b-5p (MSY0000420), miR-30c-5p (MSY0000244), miR-34a-5p (MSY0000255), miR-122-5p (MSY0000421), miR-139-5p (MSY0000250), miR-146b-5p (MSY0002809), miR-222-3p (MSY0000670) and miR-422a (MSY0001339).

4.3.6. Lentiviral infection

Knockdown (KD) of AMPKα1/2 and DICER were performed using lentiviral particles expressing short hairpin RNAs (shRNAs) targeting AMPKα1/2, DICER and control shRNA (sc-45312, sc-40489 and sc-108080 respectively; *Santa Cruz Biotechnology, Texas, USA*) following manufacturer's instructions. For infection, HepG2 cells were plated at a density of $2x10^5$ cells/well in 6-well plates and viruses were added at the multiplicity of infection (MOI) of 1 with 7 µg/ml polybrene (*Santa Cruz Biotechnology, Texas, USA*) for 24h. Polybrene is a cationic polymer used to increase the efficiency of infection in cell cultures by neutralizing the charge repulsion between the virons and cell surface[236]. After 24h of infection, media was replaced with fresh media without polybrene, and 24h forward, stable clones expressing the shRNA were selected via puromycin dihydrochloride (*Life Technologies, California, USA*). The specificity of interference was checked by either mRNA expression or western blot.

4.4. MITOCHONDRIAL FUNCTION

Seahorse XF Analyse (*Agilent Technologies, California, USA*) is able to measure oxygen consumption rate (OCR), mirroring key cellular functions such as mitochondrial

respiration or glycolysis, in living cells using a multi-well plate. XF Analysers perform compound addition and mixing, label-free analytical detection, and automatic measurement of OCR in real time.

Seahorse XF kits and reagents help simplify running and XF assay by providing pre-calibrated, pre-tested reagents together with specific cell culture plates and sensor cartridge for measuring mitochondrial respiration, glycolysis and FA oxidation in cells. The XF Cell Mito Stress Test, which is the standard for measuring mitochondrial function in cells, uses modulators of respiration that target components of the electron transport chain in the mitochondria. The compounds (oligomycin, FCCP, and a mix of rotenone and antimycin A) are serially injected to measure ATP-linked respiration, maximal respiration, and non-mitochondrial respiration, respectively (**Figure 10**). The measurement is carried out by dispensing compounds that have been loaded into injector ports within the cartridge, and results are given with pmol/min.

Agilent Seahorse XF Assays were performed in an Agilent Seahorse 96-well XF Cell Culture Microplate in conjunction with an XF96 Sensor Cartridge. The seeding surface of each well is 0.106 cm^2. 15000 cells/well were seeded and cultured for 48 h with the transfection complexes in 80 µl of growth medium. The sensor cartridge is the critical component of the XF assay platform, where each probe tip is spotted with a solid-state sensor material that detects changes in both pH and O_2 concentration over time to calculate rates. Moreover, compounds affecting mitochondrial function are also located in the sensor cartridge previous to the assay.

The day prior to the assay the XFp Analyzer was turned on and warmed up overnight or for a minimum of 5 h, together with the hydration of the sensor cartridge in XF Calibrant at 37°C in a non-CO_2 incubator. Before performing the assay, growth medium had to be replaced with a suitable assay medium. It was obtained by supplementing XF Base Medium with 1 mM pyruvate, 2 mM glutamine and 10 mM glucose, filter-sterilized and pH adjusted to 7.4. The assay medium was pre-warmed at 37°C and then growth medium was replaced by assay medium to a total volume of 180 µl. Cells were placed in a 37°C incubator without CO_2 for one hour prior to the assay. During this hour, Seahorse XFp sensor cartridge had to be loaded with compounds. Its ability to inject compounds during the assay and see results in real time is accomplished by dispensing compounds that have been loaded into injector ports within the cartridge prior to placement in the

instrument. Each series of ports must contain the same volume. Compounds had to be diluted in prepared and pH-adjusted assay medium before being loaded into the sensor cartridge. The compounds were added as follows: oligomycin in port A (0.5 µM), FCCP in port B (0.5 µM) and a mix of rotenone (0.5 µM) and antimycin A (0.5 µM) in port C, leaving port D empty. Three-min cycles were measured for each condition and the output gave the OCR measures. These measures were normalized to total protein content of each well, which was determined by Pierce™ BCA Protein Assay Kit (*Thermo Fisher Scientific, Massachusetts, USA*).

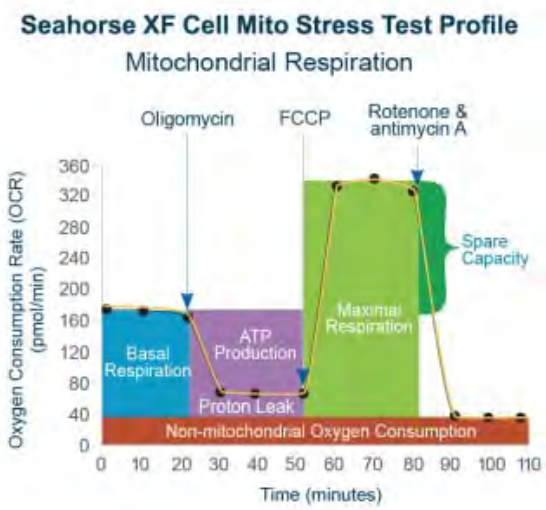

Figure 10. XFp Cell Mito Stress Test profile of the key parameters of mitochondrial function. Sequential compound injections measure basal respiration, ATP production, proton leak, maximal respiration, spare respiratory capacity, and non-mitochondrial respiration. *Image taken from Agilent website.*

4.5. CLONING AND MUTAGENESIS FOR DUAL LUCIFERASE ASSAYS

ACSL1- and ANGPTL3- 3'UTR constructs were commercially acquired (*GenScript, New Jersey, USA*). ACSL1-3'UTR was 1548 bp (1.5 kb) and ANGPTL3-3'UTR was 1360 bp (1.3 kb). Both were delivered inserted in pUC57 vector, and XhoI and EcoRI as restriction enzymes were flanking the insert. Previously, it was checked that restriction sites were not present in the interest sequences. To obtain wild-type clones of 3'UTR sequences downstream of firefly luciferase in the dual luciferase vector pEZX-MT06 (*GeneCopoeia, Rockville, USA*), the following steps were necessary:

4.5.1. Bacterial transformation

NEB-5-alpha competent *E. coli* cells (*New England Biolabs, Massachusetts, USA*) were used for transformation. Cells had to be thawed on ice for 10 min. 20 ng of plasmid DNA containing ACSL1- and ANGPTL3- 3'UTR were added to the cells and carefully flicked the tube to mix cells and DNA. The mixture was placed on ice for 30 min, heat shocked at exactly 42ºC for 40 sec and again on ice for 5 min more (no mixing). After that, 500 µl of uper Optimal broth with Catabolite repression (SOC) medium were added and the mixture was placed at 37ºC for 60 min in constant shaking at 250 rpm, in order to obtain maximal transformation efficiency supplying a high concentration of glucose. Selection plates were warmed at 37ºC and transformed cells were spread onto the selection plate and incubated overnight at 37ºC.

4.5.2. Bacterial culture and isolation of plasmid DNA

Luria broth (LB) was added to a tube or flask, together with the ampicillin antibiotic. A single colony from the selection plate was selected and added to the LB. Bacterial culture was incubated at 37ºC for 12-18 h in a shaking incubator. After incubation, growth was confirmed by the presence of a cloudy haze in the media. This bacterial culture was then used for isolating plasmid DNA using EndoFree Plasmid Maxi Kit (*QIAgen, Hilden, Germany*), according to manufacturers' protocol. Briefly, the starter culture was centrifuged at 6,000 x g for 15 min at 4ºC to harvest the bacterial cells. Then, the bacterial pellet was resuspended in three consecutive buffers which enable the proper lysis of the bacterial cells, which was then applied to a cartridge for filtering and get rid of protein, genomic DNA and cell debris. The filtered lysate was then applied to a column, washed to remove contaminants and large amounts of carbohydrates, and eluted. The eluted DNA was precipitated with isopropanol, and centrifuged at 15,000 x g for 30 min at 4ºC. Supernatant was decanted and DNA pellet was washed with 70% ethanol and centrifuged again at 15,000 g for 10 min. Finally, supernatant was decanted, pellet was air-dried and re-dissolved in a suitable volume of water. Final product was ready for DNA quantification.

4.5.3. Double digestion

3'UTR sequences were flanked by restriction enzymes and inserted in pUC57 vector; therefore, the aim was inserting them into pEZX-MT06 dual luciferase vector. Double digestion protocol was needed to first separate the construct from the original vector and next inserting in the interest vector. The double digestion was performed using the following reaction mix: 2 µg of DNA sample, 1 µl of EcoRI, 1 µl of XhoI, 2 µl of 10x FastDigest Green Buffer (*Thermo Fisher Scientific, Massachusetts, USA*) and water to bring the final volume to 20 µl. DNA was digested by incubating the reaction mixture at 37ºC for 15 min. The FastDigest Green Buffer is a digestion buffer which supports 100% activity of all FastDigest reaction enzymes.

4.5.4. Purifying DNA from an Agarose Gel

The resulting fragments from digestion were analysed by gel electrophoresis. Our fragment of interest was identified helped by UV light. Then, it was sliced and placed in a microfuge tube. The gel slice had to be previously weight, since its weight indicate the proportional liquid volume needed, as well as the amount of each buffer necessary during the DNA isolation step. Finally, isolation of the DNA from the gel was achieved by using a commercial gel purification kit, in this case, Nucleospin® Gel and PCR Clean-up (*Macherey-Nagel, Düren, Germany*), following manufacturer's instructions.

4.5.5. DNA Ligation

Ligation was performed by the T4 DNA ligase enzyme (*Thermo Fisher Scientific, Massachusetts, USA*). It catalyses the formation of covalent phosphodiester linkages, which permanently join the nucleotides together. We combined the following: 50 ng vector, 20-25 ng of cut insert, 1 µl of T4-ligase, 2 µl of Ligase Buffer and water to bring the final volume to 20 µl. The reaction was incubated overnight at 16ºC. After ligation, the insert DNA is physically attached to the backbone and the complete plasmid can be transformed into bacterial cells for propagation.

4.5.6. Final vectors

Bacterial transformation, bacterial culture, isolation of plasmid DNA and double digestion protocols had to be repeated to verify that the interest cut insert has been optimally inserted into the correct vector.

4.5.7. Mutagenesis

ACSL1- and ANGPTL3- 3'UTR constructs acquired from *GenScript* (*New Jersey, USA*) were mutated in order to verify the specific binding between miRNAs and mRNAs from ACSL1 and ANGPTL3. The miR-16, miR-30b and miR-30c target sequences of ACSL1 and ANGPTL3 were mutagenized using QuikChange XL kit (*Agilent Technologies, California, USA*), which allows site-specific mutation in virtually any double-stranded plasmid. First, mutagenic oligonucleotide primers for use were designed individually according to the required mutation. Primers had to contain the mutation, flanked by unmodified nucleotide sequence. ACSL1 3'UTR had different binding regions for miR-16 and for miR-30b/c (sharing same seed region). Thus, two different set of mutagenic primers had to be designed for ACSL1, while only one for ANGPLT3 was used, with a predicted binding site for miR-30b/c. The mutagenic primer sequences were the following:

ACSL1	
miR-16 ACSL1 F WT	5'-GCAAATTCTGCAGCTGTCTGCTGCTCTAAAGAGTACAGTGCA-3'
miR-16 ACSL1 F MUT	5'-GCAAATTCTGCAGCTGTCGCTATGCCTAAAGAGTACAGTGCA-3'
miR-16 ACSL1 R MUT	5'-TGCACTGTACTCTTTAGGCATAGCGACAGCTGCAGAATTTGC-3'
ACSL1	
miR-30 ACSL1 F WT	5'-ACCTCATGTTGCAGACCATGTTTATGGTAATACACACTTT-3'
miR-30 ACSL1 F MUT	5'-ACCTCATGTTGCAGACCGCCGGGGTGGTAATACACACTTT-3'
miR-30 ACSL1 R MUT	5'-AAAGTGTGTATTACCACCCCGGCGGTCTGCAACATGAGGT-3'
ANGPTL3	
miR-30 ANGPTL3 F WT	5'-TTAAACATACAATCACATAACCTTAAAGAATACCGTTTACATTTCTCAATCAAAATTCTT-3'
miR-30 ANGPTL3 F MUT	5'-TTAAACATACAATCACATACGGCTAAAGAATACCCGGGGGGTTTCTCAATCAAAATTCTT-3'
miR-30 ANGPTL3 R MUT	5'-AAGAATTTTGATTGAGAAACCCCCCGGGTATTCTTTAGCCGTATGTGATTGTATGTTTAA-3'

The sample reaction had to be prepared by mixing 5 µl of 10x reaction buffer, 25 ng of dsDNA template, 125 ng of oligonucleotide primer #F, 125 ng of oligonucleotide primer #R, 2 µl of dNTPs mix, 0.5 µl of MgCl2, 2 µl of Phusion DNA polymerase (*Thermo Fisher*

Scientific, Massachusetts, USA), and water to bring the final volume to 25 µl. Thermal cycling consist of denaturing DNA template, annealing mutagenic primers containing wanted mutation, and extend the primers with the Phusion DNA polymerase.

4.5.8. *DpnI* digestion

After mutagenesis, 1 µl of *Dpn I* restriction enzyme (10 U/µlM; *Thermo Fisher Scientific, Massachusetts, USA*) was added directly to each amplification reaction and incubate 1 h at 37ºC to digest parental DNA. The *Dpn I* endonuclease (target sequence: 5'-Gm^{6}ATC-3') is specific for methylated and hemi-methylated DNA and it was used to digest the parental DNA template and to select for mutation-containing synthesized DNA[237].

4.5.9. Acquisition of mutant vectors

1 µl of the *Dpn I*-treated DNA from each sample reaction was transformed into competent cells. Colonies obtained were the input for bacterial cultures growth and acquisition of plasmid DNA, which was subsequently send for sequencing to confirm that the mutation had been properly inserted. Once mutations had been verified by sequencing reaction, the mutated ACSL1 and ANGPLT3 3'UTR had to be cloned downstream of firefly luciferase in the dual luciferase vector pEZX-MT06 (*GeneCopoeia, Rockville, USA*) (**Figure 11**). Thus, the same steps as in the wild-type vectors had to be performed, including: DNA digestion, purification of DNA from an agarose gel and DNA ligation to put the mutated inserts into the correct vector. Maxi-preps of both wild-type and mutant vectors were finally performed to obtain big quantities of the final constructs.

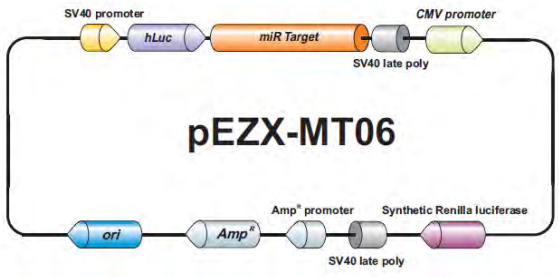

Figure 11. pEZX-MT06 vector. *Image taken from Genecopoeia website.*

4.5.10. Dual luciferase assay

The Dual-Luciferase® Reporter (DLR™) Assay System provides an efficient way of performing dual-reporter assays. In this assay, the activities of firefly and *Renilla* luciferases are measured sequentially from a single sample by using the dual Luc kit (*Promega, Wisconsin, USA*). The firefly reporter is obtained by adding Luciferase Assay Reagent II (LAR II) to generate a stabilized luminescent signal. After its quantification, this reaction is quenched, and the *Renilla* luciferase reaction is simultaneously initiated by adding Stop&Glo® Reagent to the same tube. It also produces a stabilized signal from the *Renilla*, which decays slowly over the course of the measurement (**Figure 12**).

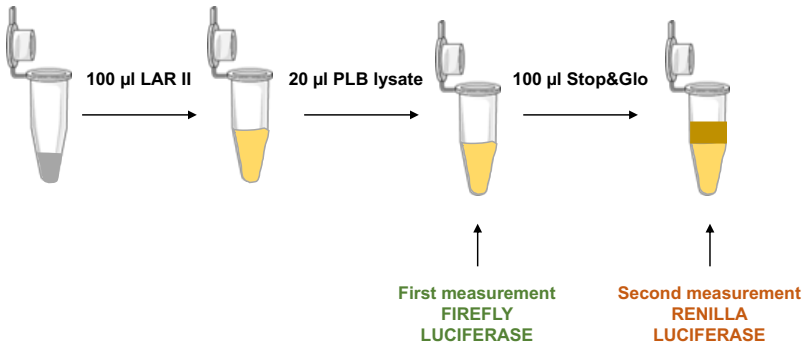

Figure 12. Dual luciferase reporter assay system protocol workflow.

Huh7 cells grown in 96-well plates were transfected for 24 h with the Luc-ACSL1 or Luc-ANGPTL3 wild-type or mutated construct (50 ng of DNA) together with miR-16, miR-30b or miR-30c mimics (100 nM) or with non-targeting control siRNA (100 nM) by means of Lipofectamine™ 2000 (*Invitrogen, California, USA*). One day before transfection, cells were seeded at 30,000 cells/well in 100 µl of growth medium without antibiotics. For each transfection sample, DNA - Lipofectamine™ 2000 complexes were prepared by diluting DNA (including miRNA mimic and dual luciferase vector) in 25 µl of Opti-MEM, at the same time that Lipofectamine™ 2000 was diluted in 25 µl of Opti-MEM. After 5-minute incubation, the diluted DNA and the diluted Lipofectamine™ 2000 were combined at a total volume of 50 µl. The solution was mixed gently and incubated for 20 minutes at room temperature to allow the DNA- Lipofectamine™ 2000 complexes to form. Complexes were added to each well containing cells and medium so as the final volume was 100 µl per well. The ratio of DNA (in µg): Lipofectamine™ 2000 (in µl) to use when preparing complexes should be 1:2.

After 48 h transfection, the growth medium was removed and a sufficient volume of PBS enough to was the surface of the culture vessels was added. After removing PBS, it was dispensed 25 µl of passive lysis buffer (supplied by the kit at 5X concentrate) in a 96-well culture plate. This volume was enough to completely cover the cell monolayer. Once added, the plate had to be placed on a rocking platform for 15 min at 4,000 rpm to ensure complete coverage of the cell monolayer with 1X PLB. Reporter assay could be performed directly or lysates could also be transferred to a tube for further handling and storage. The assays for firefly luciferase activity and *Renilla* were performed sequentially using one reaction well using GloMax® 96 Microplate Luminometer, which can detect as little as $1x10^{-19}$ moles firefly luciferase enzyme using Luciferase Assay Reagent II (LAR II) and $1x10^{-18}$ moles *Renilla* enzyme using Stop&Glo® Reagent. For that, previous to the assay, the injectors had to be prepared. The intake tubing for injector 1 must be placed into the bottle of LAR II, while the intake tubing for injector 2 into the bottle of Stop&Glo® Reagent (**Figure 12**). Results were given in an Excel spreadsheet, both firefly luciferase and *Renilla* measurements. Since cells were transfected with both 3'UTR downstream of the dual-luciferase vector (being wild-type or mutant) together with the miRNA mimic, we would expect that if there is a specific binding between miRNA-mRNA, the translation will be inhibited and the luminescent signal will be lower. On the other side, if no interaction is happening (in case of mutant 3'UTR), the luminescent signal will be same as control (**Figure 13**).

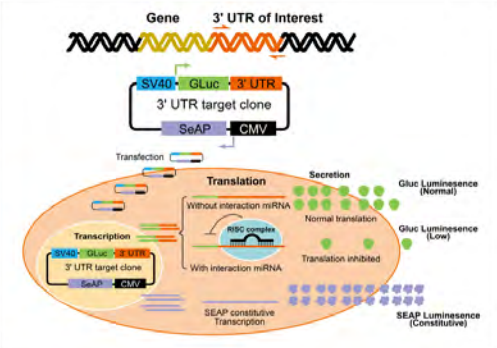

Figure 13. Dual luciferase reporter system with 3'UTR clones. 3'UTR clones are introduced in mammalian expression vectors. If there is a specific binding between miRNA and 3'UTR, the translation will be inhibited and the luminescence signal will be lower. On the other side, it there is no interaction, translation and luminescence signal will be normal. *Image taken from Genecopoeia website.*

4.6. GENE EXPRESSION ANALYSIS

4.6.1. RNA extraction

Total RNA can be purified from up to 30 mg animal or human tissues, from 100 to 10^7 animal or human cells, or yeast using RNeasy® Mini Kit (*QIAgen, Hilden, Germany*). This procedure represents a well-established technology for RNA purification which combines phenol/guanidine-based lysis of samples and silica-membrane-based and the speed of micro spin technology.

Liver samples (~50 mg) and cells were first lysed and homogenized in 1 mL or 0.6 mL respectively, of QIAzol® Lysis Reagent (*QIAgen, Hilden, Germany*) before RNA extraction. QIAzol is the monophasic solution of phenol and guanidine thiocyanate, designed to facilitate lysis of tissues, to inhibit RNases and remove most of the cellular DNA and proteins from the lysate by organic extraction, thus ensuring the purification of intact RNA. Liver samples were lysed and homogenized with the help of TissueLyzer (*QIAgen, Hilden, Germany*), while this step was not necessary with cells. After homogenization, 0.2 volumes of chloroform were added, and the homogenate was separated into aqueous and organic phases by centrifugation (15 min, 4°C, 12,000 rpm). RNA partitions to the upper, aqueous phase, while DNA partitions to the interphase and proteins to the lower, organic phase or the interphase. The upper, aqueous phase was extracted to a new RNAse-free tube, and 1:1 100% ethanol volume was added to provide appropriate binding conditions for all RNA molecules from 18 nucleotides (nt) upwards. The sample was then applied to the RNeasy Mini spin column (*QIAgen, Hilden, Germany*), where the total RNA bound to the membrane and phenol and other contaminants were efficiently washed away thanks to wash buffers. High-quality RNA is finally eluted in RNase-free water. Purity and concentration of the obtained RNA were estimated by a spectrophotometer. NanoDrop™ ND-Spectrophotometer (*Thermo Fisher Scientific, Massachusetts, USA*) allows to assess the RNA concentration of the final solution and its purity. RNA integrity was checked with the Nano lab-on-a-chip assay for total eukaryotic RNA using Bioanalyzer 2100 (*Agilent Technologies, California, USA*). This is a microfluidic platform for quantifying the degradation degree of the genomic material through the measurement of the main ribosomal subunits (18S and 28S), measured by the RIN (RNA integrity) number.

4.6.2. Retrotranscription of mRNA

Between 0.1 and 1 µg RNA/sample were used as the input for reverse transcription reaction. RNA was reverse transcribed to cDNA using High Capacity cDNA®Reverse Transcription Kit (*Applied Biosystems, California, USA*), according to the manufacturers' protocol. The kit provides individual reagents (10X RT Buffer, 25X dNTP Mix 100 mM, 10X RT Random Primers, MultiScribe™ Reverse Transcriptase and RNase Inhibitor) that when combined, 2X Reverse Transcription Master Mix is ready to use (**Table 4**). The random primer method ensure that the synthesis occurs efficiently with all species of mRNA molecules present. The Retrotranscription reaction consists of 2 stages, one of melting or association of complementary sequences (primers with mRNAs molecules), of 10 min at 25ºC, and another of elongation of sequences and degradation of mRNA molecules, directed by the action of the retrotranscriptase enzyme, during 120 min at 37ºC (**Table 5**). The last step consists of incubation at 85ºC during 5 min to stop the reaction. Obtained cDNA was stored at -20ºC until being used.

Table 4. 2X RT reaction mix for cDNA synthesis

RT Reaction Mix Components	Volume for One Sample (µL)
10X RT Buffer	2.0
25X dNTPs (100mM)	0.8
10X RT Random Primers	2.0
MultiScribeTM Reverse Transcriptase	1.0
Rnase Inhibitor	1.0
Nuclease-free water	3.2
Total	10.0

Table 5. Thermal cycling conditions for cDNA synthesis

	Step 1	Step 2	Step 3	Step 4
Temperature	25ºC	37ºC	85ºC	4ºC
Time	10 min	120 min	5 min	∞

4.6.3. Retrotranscription of miRNA

4.6.3.1. Megaplex™ Pools

miRNAs were reverse transcribed by TaqMan MicroRNA Reverse Transcription Kit (*Applied Biosystems, California, USA*). Kit components are the same as those from cDNA Reverse Transcription Kit, excluding the primers. Megaplex™ RT Primers Pools streamline the workflow for quantitating up to 380 miRNAs in parallel by enabling reverse transcription in a single reaction. miRNAs included in each RT pool are shown in **Appendix I**.

An aliquot of 3 µl containing 350-1000 ng of purified RNA was used into the RT using the TaqMan miRNA Reverse Transcription kit, together with TaqMan miRNA Multiplex RT assays (**Table 6**), which are required to run the TaqMan Array human MicroRNA A+B Cards Set (*Life Technologies, Darmstadt, Germany*). The final reaction volume was 7.5 ul. The retrotranscription reaction consists of 2 stages, the first comprised by 40 cycles (2 min at 16ºC, 1 min at 42ºC and 1 sec at 50ºC), followed by a last step of incubation at 85ºC during 5 min to stop the reaction (**Table 7**).

Table 6. RT reaction mix for running Megaplex™ Pools

RT Reaction Mix Components	Volume for One Sample (µL)
Megaplex RT Primers (10X)	0.8
dNTPs with dTTP (100mM)	0.2
Multiscribe Reverse Transcriptase (50 U/µL)	1.5
10X RT Buffer	0.8
$MgCl_2$ (25 mM)	0.9
Rnase Inhibitor (20 U/µL)	0.1
Nuclease-free water	0.2
Total	4.5

Table 7. Thermal cycling conditions for running Megaplex™ Pools

Stage	Temp	Time
Cycle (40 Cycles)	16°C	2 min
	42°C	1 min
	50°C	1 sec
Hold	85°C	5 min
Hold	4°C	∞

4.6.3.2. Custom RT using TaqMan® MicroRNA Assays

Customised RT enables to compose pools of RT primers. Each TaqMan® MicroRNA Assay contains one 5X RT primer. Up to 96 can be pooled into one RT reaction as follows: combining 10 ul of each individual 5X RT primer and adding Nuclease-free water to bring the final volume to 1 mL. Here, again an aliquot of 3 ul containing 350-1000 ng of purified RNA was used into the RT together with 12 ul of RT reaction mix containing the RT primer pool, dNTPs, transcriptase, buffer and inhibitor (**Table 8**). The final volume is 15 ul and the reaction consists of two stages: 30 min at 16°C followed by 30 min at 42°C. The last step of incubation is 5 min at 85°C to stop the reaction (**Table 9**).

Table 8. RT reaction mix for running Custom RT Pools

RT Reaction Mix Components	Volume for One Sample (µL)
RT Primer Pool	6.
dNTPs with dTTP (100mM)	0.3
Multiscribe Reverse Transcriptase (50 U/µL)	3
10X RT Buffer	1.5
Rnase Inhibitor (20 U/µL)	0.19
Nuclease-free water	1.01
Total	12

Table 9. Thermal cycling conditions for running Custom RT Pools

Stage	Temp	Time
Hold	16°C	30 min
Hold	42°C	30 min
Hold	85°C	5 min
Hold	4°C	∞

4.6.4. TaqMan Low Density Arrays (TLDAs)

TLDAs were used in both liver samples belonging to the identification cohort, as well as in primary HH treated with PA, CC or Mtf. TaqMan Array miRNA 384-well Cards (*Applied Biosystems, California, USA*) are pre-loaded with TaqMan miRNA Expression Assays. The coverage of the most relevant miRNAs for human or rodent species, aligned with Sanger miRBase v21, with over 740 primer/probe assays enabled across the sets of TaqMan miRNA Array Cards. TaqMan® Array Human MicroRNA Card Set v3.0 is comprised by a two-card set (A+B) containing a total of 384 TaqMan® MicroRNA Assays per card. Included on each array are three TaqMan MicroRNA Assay endogenous controls to aid in data normalization and one TaqMan® MicroRNA Assay not related to human as a negative control. This approach requires the use of Megaplex™ Primer Pools for miRNA reverse transcription. Panels with plates design (A+B) and miRNA assay ID are available in **Appendix I**.

Each card can run one sample against 384 TaqMan® Assay targets (**Figure 14**). Each fill reservoir was filled with 100 µl of sample-specific PCR reaction mix, 8 times, according to **Table 10**. Loaded cards were then centrifuged and sealed. Thermal-cycling conditions comprise three steps: enzyme activation, denaturing, and annealing/extending (**Table 11**).

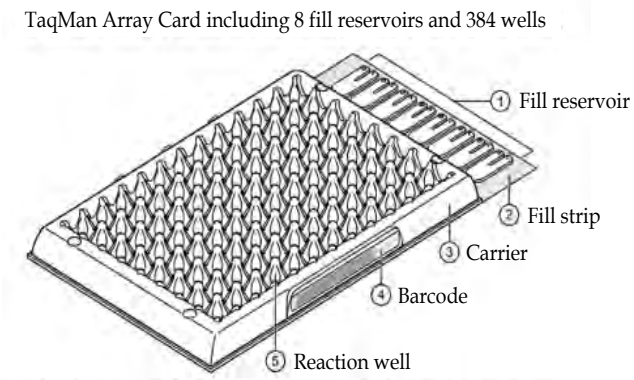

Figure 14. TaqMan® Array Card template. *Adapted from Thermo Fisher Scientific, "User Guide: Megaplex Primer Pools - For MicroRNA expression analysis with TaqMan Array Cards.*

An aliquot of 10 ul of the Megaplex™ RT product was diluted in 440 ul of nuclease-free water and combined in with the master mix in same amounts. Normalized values were obtained as the raw Ct value-average of raw Cts for all miRNAs with reliable results (Ct values ≤ 35) in each sample.

Table 10. Real-time PCR (RT-PCR) reaction for running TaqMan MicroRNA Array

Component	Volume for One Array (µL)
TaqMan Universal PCR Master Mix, No AmpErase® UNG 2X	450
Megaplex™ RT product	10
Nuclease-free water	440
Total	900

Table 11. Thermal cycling conditions for running TaqMan MicroRNA Array

Stage	Temp	Time
Hold	50°c	2 min
Hold	95°c	10 min
Cycle	95°c	15 sec
(40 cycles)	60°c	1 min

4.6.5. Quantitative Real-time PCR

Real-time polymerase chain reaction (PCR) uses DNA polymerases to amplify target cDNA, using sequence-specific primers. It allows the sensitive, specific and reproducible

quantitation of nucleic acids. The amount of cDNA is revealed after each cycle through fluorescent dyes that yield increasing fluorescence proportional to the number of PCR product molecules generated, which are called amplicons. Real-time PCR consist of three major steps and reactions are generally run for 40 cycles. The three steps are the following:

- **Denaturation:** at the beginning of the technique, the temperature is raised in order to bring double-stranded DNA into single strands and loosen secondary structure. The highest temperature that *Taq* DNA polymerase is able to withstand is typically used (95ºC) in denaturation step.
- **Annealing:** during this step, complementary sequences will hybridize. An appropriate temperature is used, based on the calculated melting temperature of the primers (usually 5ºC below the melting temperature of the primers).
- **Extension:** this step is catalysed by *Taq* DNA polymerase at 70-72ºC. The primer extension occurs at rates of up to 100 bases per second.

The most widely used chemistries for real-time quantitative PCR are the double-stranded DNA-intercalating agent SYBR® Green and TaqMan® hydrolysis probes. Both pre-validated TaqMan primer/probe sets for gene and miRNA (*Applied Biosystems, California, USA*) and gene-specific primer pairs (*Sigma-Aldrich, Missouri, USA*) were used for gene expression using the LightCycler®480 (Roche Diagnostics, Barcelona, Spain) and QuantStudio™ 7 Flex Real-Time PCR System (*Applied Biosystems, California, USA*), using both TaqMan and SYBR Green® approaches.

SYBR Green® is based on binding the fluorescent dye to double-stranded deoxyribonucleic acid. When SYBR dye is added to a sample, it is immediately bound to all the double-stranded DNA present. During PCR, DNA polymerase amplifies the target sequence creating PCR products. SYBR dye will bind to each new copy of double-stranded DNA. As PCR progresses, more PCR product is created, resulting in an increase in fluorescence intensity proportional to the amount of PCR product produced.

TaqMan method is based on 5′ nuclease chemistry, and each assay contains the primer and probe set for your target of interest. The oligonucleotide probe is constructed containing a fluorescent dye at 5′ and a suppressor dye at 3′.

While the probe is intact, the proximity of the suppressor dye blocks the fluorescence emitted by the indicator dye by fluorescence resonance energy transfer (FRET). At the start of real-time PCR reaction, temperature is raised in order to denature the double-stranded cDNA. When the reaction temperature is lowered to allow the primers and probes to anneal to their target sequences, when the target sequence is present, *Taq* polymerase will synthesize a complementary DNA strand using unlabelled primers and template. Once the polymerase reaches the TaqMan probe, its endogenous 5′ endonuclease activity will cleave the probe, separating the dye from the quencher and therefore resulting in an increase in fluorescence intensity proportional to the amount of amplicon synthesized with each cycle of PCR.

TaqMan and SYBRGreen LightCycler® master mixes are ready-to-use reaction compounds specifically developed for the hydrolysis probe detection format in multi-well plates on the LightCycler®480 Instrument or QuantStudio™ 7 Flex Real-Time PCR System. Both contain FastStart Taq DNA Polymerase for hot start PCR, which significantly improves the specificity and the sensitivity of PCR by minimizing the formation of nonspecific amplification products (**Table 12** for gene expression and **Table 13** for miRNA expression).

Table 12. RT-PCR reaction for gene expression analysis

Component	Volume for one well (µl)
Lightcycler® taqman® master	3.3
Taqman® hydrolysis probe	0.3
Nuclease-free water	1.3
cDNA	2

Table 13. RT-PCR reaction for miRNA expression analysis

Component	Volume for one well (µl)
Lightcycler® taqman® master	4.5
Taqman® hydrolysis probe	0.5
cDNA	5

Relative expression values per gene and sample are given as number of times in which the target gene is expressed with respect to an endogenous control, defined as those whose expression is not altered by the parameters subjected to study[238]. As

housekeeping references, PPIA (peptidylprolyl isomerase A or cyclophilin)[238], 36B4 (acidic ribosomal phosphoprotein)[239] and SDHA (succinate dehydrogenase complex, subunit A)[240] genes were used for gene expression for human samples, while Ppia (peptidylprolyl isomerase A or cyclophilin)[241], Actb (actin, beta)[242] or 18S (18S ribosomal RNA)[242] were used for rodent models. RNU6b was used as housekeeping for miRNA expression in both human and mice.

During the RT-PCR each sample originates a sigmoidal curve for all the studied genes, and a level of fluorescence determined for each Ct at over the 40 amplification cycles (**Table 14**). From the curves, one can determine the threshold. The value Ct is then defined as the number of cycles needed in the RT-PCR to reach a certain level of fluorescence, which is inversely proportional to the number of copies of the original transcript. Hence, the greater number of copies, the less Ct values will be necessary to reach the arbitrary threshold.

Table 14. Thermal cycling conditions for running quantitative real time PCR

Stage	Temp	Time
pre-incubation	95°c	10 min
amplification	95°c	10 sec
(45 cycles)	60°c	30 sec
cooling	95°c	10 sec

Finally, ΔCt is calculated as the difference between the Cts of the target gene and the Cts of the endogenous control from the same cDNA sample[243]. Variations in the expression of the different genes for each sample with respect to the endogenous control are quantified by the value $2^{-\Delta Ct}$.

4.7. PROTEIN ANALYSIS

4.7.1. Protein extraction and Western blot

Cultured cells were lysed in Cell Lysis Buffer (*Cell Signaling, Massachusetts, USA*) with phenylmethylsulfonyl fluoride (PMSF; *Sigma-Aldrich, Missouri, USA*) at 1:200 dilution as protease inhibitor, sonicated and centrifuged to remove the insoluble material. Protein concentrations were subsequently measured from the supernatants. Protein determination was performed using Pierce™ BCA Protein Assay Kit (*Thermo Fisher*

Scientific, Massachusetts, USA). It is a two-component, high-precision, detergent-compatible assay reagent set to measure at 562 nm total protein concentration compared to a protein standard. After quantification, equal amounts of total proteins were subjected to electrophoresis on 10% SDS poly-acrylamide gels. After separation, proteins were transferred onto Nitrocellulose (*Bio-Rad Laboratories, California, USA*). The following antibodies were used: ACSL1, AMPKα1/2, FAS, p-ACC, ACC, p-Akt, Akt, ANGPTL3 and β-actin. All primary antibodies were used at 1:1000 dilutions, and anti-rabbit or anti-mouse IgG, HRP-linked were used as secondary antibodies (**Table 15**). Blots were visualized by enhanced chemiluminescence (ECL; *Thermo Fisher Scientific, Massachusetts, USA*) and signals were quantified by using Image J software (*https://imagej.nih.gov/ij/*).

Table 15. Primary and secondary antibodies used for Western Blot

Primary Antibody	**Dilution**	**Trading House**
ASCL1	1:1000	Ab178419 (*Abcam, Cambridge, UK*)
AMPKα1/2	1:1000	sc-25792 (*Santa Cruz Biotechnology, Texas, USA*)
FAS	1:1000	sc-20140 (*Santa Cruz Biotechnology, Texas, USA*)
Phospho-ACC (Ser^{79})	1:2000	11818 (*Cell Signaling, Massachusetts, USA*)
ACC	1:1000	3676 (*Cell Signaling, Massachusetts, USA*)
Phospho-Akt (Ser^{473})	1:1000	4058 (*Cell Signaling, Massachusetts, USA*)
Akt	1:1000	9272 (*Cell Signaling, Massachusetts, USA*)
ANGPTL3	1:1000	prepared in-house
β-actin	1:1000	sc-47778 (*Santa Cruz Biotechnology, Texas, USA*)
Secondary Antibodies	**Dilution**	**Trading House**
Anti-rabbit IgG / HRP	1:2000	7074S (*Cell Signaling, Massachusetts, USA*)
Anti-mouse immunoglobulins / HRP	1:1000	P0260 (*CiteAb, Bath, UK*)

4.7.2. Enzyme-linked ImmunoSorbent Assay

Media from transfected cells in 12-well plates was collected and stored in -20°C. Cells were lysed and used for protein determination by Pierce™ BCA Protein Assay Kit (*Thermo Fisher Scientific, Massachusetts, USA*). Cell media were analysed using Human Apolipoprotein B ELISA^{PRO} kit (*Mabtech AB, Nacka Strand, Sweden*) according to

manufacturer's protocol. The absorbance was measured at 450 nm in a microplate reader and a 4-parameter curve fitting program was used for data analysis.

4.8. LIPID ANALYSIS

4.8.1. Thin-layer chromatography

Cultured transfected cells were grown on 12-well plates. Cells were then incubated with 5 μCi/well [3H]-acetic acid (*GE Healthcare, Illinois, USA*) in complete media for 3 h. After incubation, cells were washed twice and scraped in 2% cold sodium chloride. Total lipids were extracted according to Bligh and Dyer. At first, 2 ml methanol and 1 ml chloroform were added followed by vortex and centrifugation at 2500 rpm at 4ºC for 10 min. Supernatants were then transferred to fresh tubes. 1 ml water and 1 ml chloroform were subsequently added. Vortex and centrifugation steps were repeated at 2500 rpm at 4ºC. The upper layer containing aqueous phase with some polar species was be discarded, while the lower phase, being the organic one containing TAGs, membrane lipids and other neutral lipids was transferred to a fresh tube, and samples were evaporated with nitrogen gas. Immediately after evaporation, 40 μl chloroform: methanol at 9:1 ratio were added to dissolve lipid species. Using a Hamilton syringe, samples were applied on thin layer silica-based chromatography using hexane: diethyl ether: acetic acid: water (65:15:1:0.25) as the solvent system. Triacylglycerol (TAG) and cholesterol ester (CE) standards were run on thin-layer chromatography (TLC) along with the samples to identify the corresponding species. TAG, diacylglycerol (DAG) and CE bands were scraped to scintillation tubes and the [3H] radioactivity was measured by liquid scintillation counting, and the results normalized for total cell protein.

4.8.2. Triglyceride and cholesterol quantification assay

Cultured transfected cells were lysed using Cell Lysis Buffer (*Cell Signaling, Massachusetts, USA*) with PMSF (*Sigma-Aldrich, Missouri, USA*) at 1:200 dilution as protease inhibitor and centrifuged at 12,000 rpm for 15 min at 4ºC. The supernatant was then subjected to triglyceride and cholesterol analysis using the GPO-PAP Triglyceride assay kit or CHOD-PAP Cholesterol assay kit (*Roche/Hitachi, Tokyo, Japan*). The results were normalized to the total protein concentration.

The extraction procedure for triglyceride quantification of mice livers was adapted from methods described previously[244]. Approximately 200 mg of livers were homogenized for 2 minutes in ice-cold chloroform-methanol (2:1, vol/vol). Triglycerides were extracted during 5h shaking at room temperature. For phase separation, H_2SO_4 was added, samples were centrifuged, and the organic bottom layer was collected. The organic solvent was dried using a Speed Vac and re-dissolved in chloroform. Hepatic TG levels of each sample were measured in duplicate after evaporation of the organic solvent by using Spinreact Triglycerides Quantitation kit according to manufacturer's protocol (Spinreact S.A.).

4.8.3. Lipid droplet staining

4.8.3.1. *Bodipy 493/503*

Probes incorporating the lipophilic fluorescent BODIPY® (4,4-difluoro-3a,4adiaza-s-indacene) (*Molecular Probes, Oregon, USA*) fluorophore is intrinsically lipophilic. Consequently, probes incorporating this fluorophore are more likely to mimic the properties of natural lipids. Both HepG2 and Huh7 transfected cells with miRNA mimics were seeded on coverslips. The optimal cell number should be determined to achieve confluence of 30-50% at the time of staining to permit proper imaging. At the time-point of interest (48 h post-transfection), 2 μM BODIPY solution in DMSO (*Sigma-Aldrich, Missouri, USA*) was prepared and used to stain cells for 1 h, and then changed to normal media for 3 h. Cells were washed twice with PBS and fixed with 4% paraformaldehyde for 30 min. After washing twice, coverslips were mounted using Mowiol (*Calbiochem, California, USA*) containing 5 μg/ml 4',6-diamidino-2-phenylindole (DAPI; *Molecular Probes, Oregon, USA*). After mounting coverslips onto glass slides, they were kept overnight at room temperature before imaging. Imaging was done with oil 63X objective and Colibri laser (*Carl Zeiss Imaging Solutions GmbH, Oberkochen, Germany*), with the same exposure time for non-targeting control siRNA or miRNA mimics, and images were captured with Zen 2 software (Zeiss). Cell number, area and size of lipid droplets were quantified with FIJI (Image J) software with a set cut-off threshold (total signal intensity/number of cells in the field).

4.8.3.2. Oil Red O

Cells and mice livers lipid content was analysed by Oil Red O staining. Cells were washed with PBS and fixed with 4% paraformaldehyde for 1 h. Then cells were dipped

in isopropanol 60% before being dried and stained with Oil Red O (*Sigma-Aldrich, Missouri, USA*) for 10 min at room temperature. After staining, cells were washed repeatedly with water and pictures were taken using an inverted microscope. After imaging, 100% isopropanol was added to elute the Oil Red dye and absorbance was measured at 500 nm Cytation 5 Cell Imaging Multi-Mode Reader (*BioTek Instruments, Vermont, USA*).

Hepatic frozen sections were cut (8 μm) and fixed in 10% buffered formaldehyde. Sections were stained in filtered Oil Red O (*Sigma-Aldrich, Missouri, USA*), washed in distilled water, counterstained with Harris hematoxylin (*Bio-Optica, Milan, Italy*) and washed again in distilled water. Sections were mounted in aqueous mountain medium (*Bio-Optica, Milan, Italy*). Images were taken with a digital camera Olympus XC50 (*Olympus Corporation, Tokyo, Japan*) at 40x. Digital images were quantified with ImageJ Software (*National Institutes of Health, Bethesda, MD, USA*).

4.8.4. Lipidome analysis

Lipid extraction was performed according to the method of Bligh and Dyer[245] in the presence of not naturally occurring lipid species as internal standards. Thus, the following lipid species were added as reference control: PC 14:0/14:0, PC 22:0/22:0, PE 14:0/14:0, PE 20:0/20:0 (di-phytanoyl), PS 14:0/14:0, PS 20:0/20:0 (di-phytanoyl), PI 17:0/17:0, LPC 13:0, LPC 19:0, LPE 13:0, Cer d18:1/14:0, Cer 17:0, D7-FC, CE 17:0 and CE 22:0. HepG2 cell lysates consisting of 100 μg protein were extracted. Chloroform phase was recovered by a pipetting robot and vacuum dried. The residues were dissolved in either in 10 mM ammonium acetate in methanol/chloroform (3:1, v/v) (for low mass resolution tandem mass spectrometry) or chloroform/methanol/2-propanol (1:2:4 v/v/v) with 7.5 mM ammonium formate (for high resolution mass spectrometry). The analysis of lipids was performed by direct flow injection analysis (FIA) using either a triple quadrupole mass spectrometer (FIA-MS/MS; QQQ triple quadrupole) or a hybrid quadrupole-Orbitrap mass spectrometer (FIA-FTMS; high mass resolution). FIA-MS/MS (QQQ) was performed in positive ion mode using the analytical setup and strategy described previously[246,247]. A fragment ion of m/z 184 was used for phosphatidylcholine (PC), sphingomyelin (SM)[246] and lysophosphatidylcholine (LPC)[248]. The following neutral losses were applied: Phosphatidylethanolamine (PE) 141, phosphatidylserine (PS) 185, phosphatidylglycerol (PG) 189 and phosphatidylinositol

(PI) 277[249]. PE-based plasmalogens (PE P) were analyzed according to the principles described by Zemski-Berry[250]. Sphingosine based ceramides (Cer) and hexosylceramides (HexCer) were analyzed using a fragment ion of m/z 264[251]. Lipid species were annotated according to the recently published proposal for shorthand notation of lipid structures that are derived from mass spectrometry[252]. For these data glycerophospholipid species annotation was based on the assumption of even numbered carbon chains only. SM species annotation is based on the assumption that a sphingoid base with two hydroxyl groups is present.

The Fourier Transform Mass Spectrometry (FIA-FTMS) setup has been previously described[253]. Triacylglycerol (TG), diacylglycerol (DG) and cholesteryl ester (CE) were recorded in positive ion mode FTMS in m/z range 500 - 1000 for 1 min with a maximum injection time (IT) of 200 ms, an automated gain control (AGC) of 1*106, three microscans and a target resolution of 140,000 (at 200 m/z). The mass range of negative ion mode was split into two parts. LPC and lysophosphatidylethanolamine (LPE) were analyzed in the range 400 - 650 m/z. PC, PE, PS, SM and Cer were measured in m/z range 520 - 960. Multiplexed acquisition (MSX) was used for, the [M +NH4]+ of free cholesterol (404.39 m/z) and D7-cholesterol (411.43 m/z) 0.5 min acquisition time, with a normalized collision energy of 10 %, an IT of 100 ms, AGC of 1*105, isolation window of 1 m/z, and a target resolution of 140,000. Data processing details were described in in Höring et al. using the ALEX software[254] which includes peak assignment and intensity picking. The extracted data were exported to Microsoft Excel 2010 and further processed by self-programmed Macros.

4.9. *IN SILICO* TOOLS

Putative miRNA binding sites in 3'UTR messenger RNAs were identified using TargetScan (http://www.targetscan.org), miRanda (http://www.microrna.org/), and miRWalk (http://zmf.umm.uni-heidelberg.de/apps/zmf/mirwalk2/). TargetScan predicts biological targets of miRNAs by searching for the presence of conserved 8mer, 7mer and 6mer sites that match the seed region of each miRNA[255]. miRanda is a comprehensive resource of miRNAs target predictions, which are based on miRanda algorithm incorporating current biological knowledge on target rules and usage of an up-to-date compendium of mammalian microRNAs. miRWalk is a comprehensive archive supplying the largest available collection of predicted and experimentally verified miRNA-target interactions. It was developed to generate possible miRNA interactions

with all regions of a gene by gathering 13 prediction data sets from existing miRNA-target resources. miRpath v.3 was employed to perform miRNA pathway analysis through experimentally validated miRNA interactions derived from DIANA-TarBase v6.0[256]. Finally, it was also performed gene annotation enrichment analysis through the Database for Annotation, Visualization and Integrated Discovery (DAVID). It provides a comprehensive set of functional annotation tools to understand biological meaning behind large list of genes[257,258].

4.10. ETHICAL CONSIDERATIONS

Animal experiments were performed in agreement with the International Law on Animal Experimentation and were approved by the USC Ethical Committee (project ID 15010/14/006) and the University of Iowa Institutional Animal Care and Use Committee.

4.11. STATISTICS

Normally distributed data are presented as mean ± *standard error of the mean* (SEM) or mean ± *standard deviation* (SD). Before statistical analysis, normal distribution and homogeneity of the variances were evaluated using *Levene's test*. *Student's t-test* was used to determine if the means of two sets of data were significantly different from one to each other. *One-way analysis of variance* (ANOVA) for multiple comparisons was used to compare groups with respect to continuous variables, using post hoc by *Fisher's least significant difference* (LSD) procedures for two by two comparisons. Lineal relationship between quantitative variables was analysed with bivariable models using *Pearson* and *Spearman's tests*. *Receiver-operating characteristics* (ROC) curves were generated to evaluate the ability of chosen miRNAs to distinguish between borderline participants and NAFLD patients versus controls with no sign of liver disease[259]. *Multiple linear regression or multiple regression* is a statistical technique that uses several explanatory variables to predict the outcome of a response variable. The goal was to model the linear relationship between the explanatory (independent) variables and response (dependent) variables. Herein, we used multiple linear regression to evaluate the contribution of miRNAs to NAFLD variance, considering the effect of age, BMI, etc. Level of significance was set at p-value < 0.05. Detection of miRNAs *in vivo/in vitro* under different experimental conditions was established at 35 Cts or less for all replicates.

Statistical analyses were performed with the SPSS (*SPSS v12 Inc., Illinois, USA*), Prism 6 (*Graphpad Software, California, USA*) and R Statistical Software (*http://www.r-project.org/*). The SL qPCRNorm Package (*Bioconductor*) was used for the analysis of arrays, as previously[260].

5. RESULTS

5.1. THE BEDSIDE: COMPREHENSIVE miRNA PROFILING AND GENE EXPRESSION IN SUBJECTS WITH AND WITHOUT NAFLD

The main objective of this part was to investigate variations in hepatic miRNAs in obese patients with or without NAFLD. miRNA expression patterns were first analysed in an identification sample formed by 19 obese women and miRNA candidates were subsequently validated in an extended sample of 60 participants in association with clinical and biochemical parameters. Additionally, the expression of genes related to glucose metabolism (*GLUT2, G6PC, PEPCK*), *de novo* FA biosynthesis (*ChREBP, SREBP1c, LXRα, FXR, FASN, ACACA, PPP2R5C*) FA uptake and transport (*PPARγ, PGC1α, CD36, FABP4, FATP5, PLTP*), FA oxidation (*PPARa*), inflammation (*ITGAX, PPARδ, HAMP, TNFa*) and endoplasmic reticulum stress (*ATF6, DDIT3, HSPA5*) were analysed taking into account miRNA involvement in gene regulation. miRNA profiles were obtained through TLDAs and validation analyses were performed by qRT-PCR.

5.1.1. Comprehensive miRNA profiling of human liver samples

Clinical and biochemical data of study participants are shown in **Table 16**. Liver miRNA profiling was first performed in a subgroup of 19 obese women classified according to the presence or absence of NAFLD. Previous surgery and histological evaluation, eleven of these participants, being 58% of the total, were suspected of NAFLD based on the laboratory and sonographic findings. NAFLD patients and age, sex and weight-matched controls with no sign of hepatic disturbances differed in parameters of IR, such as fasting insulin (17.4 ± 10 and 9 ± 3, p=0.023), HOMA-IR (4.4 ± 2.8 and 2 ± 0.8, p=*0.036*) and M-clamp (3.1 ± 1.5 and 6.6 ± 2.9, p=0.011).

Table 16. Anthropometric and biochemical data of subjects included in identification sample. Values represent the mean ± SD. Bold indicates significant results (p-value < 0.05).

Clinical outputs (units)	No NAFLD (n=8)	NAFLD (n=11)	Student t-test
Sex (M/W)	0/8	0/11	
Fatty liver (Yes/No)	0/8	0/11	
Dyslipidemia (Yes/No)	2/6	3/8	
T2D (Yes/No)	0/8	0/11	
NAFLD activity score (% 5 grade)	0	10.5	
Lobular activity (>2 focus/field, %)	0	26.4	
Ballooning degeneration (%)	0	0	
Fibrosis staging (%)	0	10.6	
Age (years)	44 ± 9	48 ± 6	0.251
BMI (kg/m2)	43.6 ± 8	44.8 ± 7	0.726
SBP (mmHg)	127.3 ± 24.4	143.1 ± 16.7	0.110
DBP (mmHg)	73.4 ± 12.4	82.9 ± 8.8	0.065
Fat mass (%, densitometry)	46 ± 3.1	47.2 ± 6	0.643
Fasting glucose (mg/dl)	93.1 ± 12.8	97.7 ± 10.2	0.395
Fasting insulin (µIU/ml)	**9 ± 3**	**17.4 ± 10**	**0.023**
Glycated hemoglobin (%)	5.3 ± 0.4	5.6 ± 0.4	0.193
HOMA-IR index	**2 ± 0.8**	**4.4 ± 2.8**	**0.036**
M (mg/(kg ·min))	**6.6 ± 2.9**	**3.1 ± 1.5**	**0.011**
Cholesterol (mg/dl)	188 ± 37.2	198.7 ± 34.1	0.523
HDL Cholesterol (mg/dl)	48.8 ± 9.7	46.5 ± 12.1	0.665
LDL Cholesterol (mg/dl)	120 ± 29.3	126.2 ± 32.1	0.673
Triglycerides (mg/dl)	95.9 ± 44.7	130.6 ± 39	0.089
GGT (IU/l)	28.8 ± 22.8	30.5 ± 26.5	0.885
GPT (IU/l)	22.9 ± 9.5	23.8 ± 10.6	0.844
CRP (mg/dl)	0.62 ± 0.32	0.84 ± 0.45	0.259
LBP (µg/ml)	23.7 ± 6.1	26.9 ± 9.3	0.413

Once the patients were characterized and classified based on NAFLD presence or absence, liver miRNA profiling was performed using TLDAs, that allow the analysis of 744 mature miRNAs in human samples. Concurrently with increased IR and signs of NAFLD, such as NAFLD activity score, lobular activity, and/ or fibrosis staging, deregulation of 14 hepatic miRNAs was identified (**Table 17**) (**Figure 15**).

Table 17. miRNAs differentially expressed in subjects with or without NAFLD. Values represent the mean ± SD. Bold indicates significant results (p-value < 0.05).

miRNAs	No NAFLD (n=8)	NAFLD (n=11)	Student t-test
miR-155	0.284 ± 0.116	0.483 ± 0.173	0.003
miR-1201	0.083 ± 0.025	0.055 ± 0.023	0.004
miR-886-5p	0.051 ± 0.046	0.136 ± 0.076	0.005
miR-378	2.09 ± 0.45	1.34 ± 0.43	0.015
miR-30b-5p	5.68 ± 2.09	3.48 ± 1.04	0.020
miR-34a	0.346 ± 0.163	0.5 ± 0.188	0.022
miR-122-5p	89.8 ± 42.5	52.0 ± 20.6	0.024
miR-125b	2.79 ± 0.69	1.93 ± 0.41	0.034
miR-422a	0.34 ± 0.155	0.2 ± 0.081	0.036
miR-139-5p	1.45 ± 0.57	0.9 ± 0.52	0.039
miR-146b-5p	3.3 ± 1.6	5.6 ± 3.2	0.044
miR-204	0.137 ± 0.051	0.09 ± 0.03	0.046
miR-708	0.01 ± 0.004	0.023 ± 0.012	0.047
RNU48	28.3 ± 21.9	15.2 ± 11.2	0.048

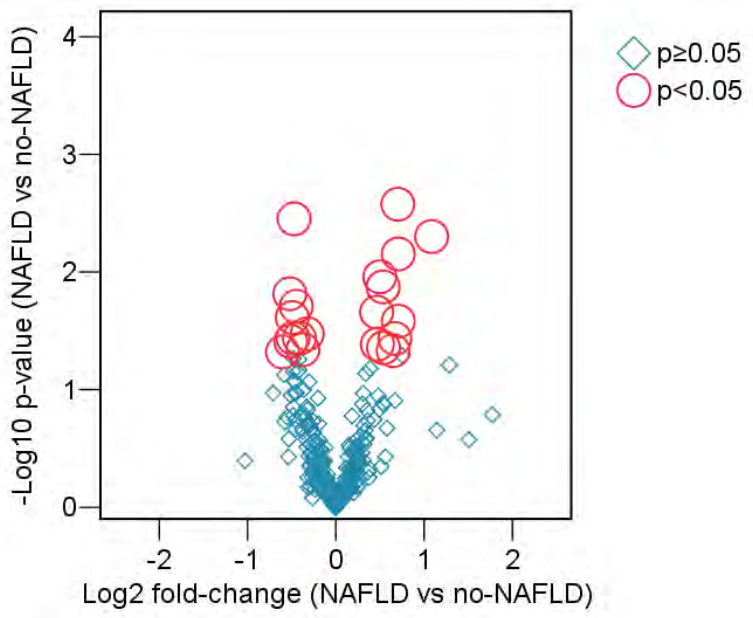

Figure 15. miRNA profiles in NAFLD versus non-NAFLD subjects. Volcano plots representing changes in miRNA expression assessed in subjects with and without NAFLD. Red circles stand for statistically significant changes (p<0.05).

In order to validate miRNA regulation in an extended cohort, all miRNA candidates found in the identification sample by TLDAs were analysed using TaqMan miRNA hydrolysis probes in liver biopsies from the extended validation sample of 60 participants, including the subjects selected for the identification sample. The extended

sample was classified in three different groups based on pathological anatomy: No NAFLD (meaning no signs of steatosis), NAFLD and borderline group (classified in between by the presence of few signs of steatosis) (**Table 18**). Here, groups differ in clinical data such as SBP, DBP, M-clamp, triglycerides and GGT. The validation procedure shortlisted five hepatic miRNAs that differed significantly between NAFLD patients and controls (**Table 19**). Decreased expression of miR-139-5p, miR-30b-5p, miR-122-5p and miR-422a, and increased miR-146b-5p were confirmed in obese NAFLD patients and/or borderline subjects, when compared to gender, age and weight-matched controls, while the rest of the miRNAs that appeared in the identification sample lost significance in the validation procedure.

Table 18. Anthropometric and biochemical data of study participants (extended sample). Fisher's least significant difference (LSD) post-hoc test was performed by comparing NAFLD vs. no NAFLD participants. Data is presented as mean ± SD. Bold indicates significant results (p-value < 0.05).

Clinical outputs (units)	No NAFLD (n=19)	Borderline (n=24)	NAFLD (n=17)	ANOVA	LSD[a]
Sex (M/W)	2/17	6/18	4/13		
Fatty liver (Yes/No)	1/18	4/20	2/15		
Dyslipidemia (Yes/No)	7/12	8/16	6/11		
T2D (Yes/No)	6/13	5/19	6/11		
NAFLD activity score (% 5 grade)	0	0	12.5		
Lobular activity (>2 focus/field, %)	0	8.3	12.6		
Ballooning degeneration (%)	0	4.2	18.8		
Fibrosis staging (%)	0	16.7	43.7		
Age (years)	45.9 ± 9.6	47.1 ± 9.2	49.9 ± 6.4	0.376	0.172
BMI (kg/m2)	44.5 ± 7.6	46.4 ± 5.5	44.5 ± 6.9	0.538	0.999
SBP (mmHg)	132.6 ± 17.6	139.0 ± 12.3	151.5 ± 19.4	**0.004**	**0.001**
DBP (mmHg)	74.3 ± 10.3	76.5 ± 11.8	86.9 ± 13.7	**0.006**	**0.003**
Fat mass (%, densitometry)	44.9 ± 5.0	47.5 ± 6.5	44.7 ± 4.5	0.205	0.881
Fasting glucose (mg/dl)	98.3 ± 17.7	107.3 ± 32.4	125.2 ± 54.2	0.092	**0.032**
Fasting insulin (µIU/ml)	10.6 ± 4.2	23.9 ± 24.9	31.1 ± 41.0	0.074	**0.026**
Glycated hemoglobin (%)	5.66 ± 0.56	6.04 ± 1.25	6.49 ± 1.38	0.092	**0.030**
HOMA-IR index	2.63 ± 1.54	7.69 ± 14.24	13.43 ± 25.46	0.148	0.052
M (mg/(kg ·min))	5.20 ± 3.16	3.32 ± 1.62	2.40 ± 1.23	**0.003**	**0.001**
Cholesterol (mg/dl)	179.9 ± 30.5	201.1 ± 36.2	186.3 ± 27.9	0.095	0.558
HDL Cholesterol (mg/dl)	47.2 ± 10.4	46.0 ± 9.6	48.1 ± 15.0	0.852	0.817
LDL Cholesterol (mg/dl)	113.3 ± 26.5	129.7 ± 33.8	108.9 ± 22.7	0.053	0.646
Triglycerides (mg/dl)	97.7 ± 36.7	126.7 ± 47.5	146.4 ± 52.0	**0.008**	**0.002**
GGT (IU/l)	20.3 ± 7.7	28.7 ± 12.7	43.2 ± 38.0	**0.011**	**0.003**
GPT (IU/l)	23.9 ± 15.3	27.6 ± 19.7	30.4 ± 17.6	0.554	0.282
CRP (mg/dl)	0.63 ± 0.42	0.92 ± 0.57	0.96 ± 0.82	0.196	0.105
LBP (µg/ml)	26.7 ± 10.3	23.7 ± 8.1	30.4 ± 13.4	0.160	0.302

Table 19. Validation of miRNA differentially expressed between groups. Fisher's least significant difference (LSD) post-hoc test was performed by comparing NAFLD vs. no NAFLD participants. Data is presented as mean ± SD. Bold indicates significant results (p-value < 0.05) and r.u. relative units.

miRNAs	No NAFLD (n=19)	Borderline (n=24)	NAFLD (n=17)	ANOVA	LSD[a]
miR-139-5p (r.u.)	1.43 ± 0.54	1.00 ± 0.37	1.08 ± 0.47	**0.009**	**0.023**
miR-30b-5p (r.u.)	1.48 ± 0.39	1.15 ± 0.42	1.18 ± 0.43	**0.028**	**0.036**
miR-122-5p (r.u.)	715.1 ± 361.0	499.9 ± 261.9	494.8 ± 253.7	**0.038**	**0.032**
miR-146b-5p (r.u.)	5.23 ± 1.66	5.64 ± 1.65	6.82 ± 2.3	**0.038**	**0.014**
miR-422a (r.u.)	3.96 ± 1.69	2.8 ± 1.52	2.92 ± 1.44	**0.042**	**0.048**

5.1.2. Gene expression in liver samples

Taking into account that miRNAs are able to modulate gene expression, either by translational inhibition or mRNA target degradation[184], the next approach aimed to evaluate gene expression in the liver to be further associated with miRNA candidates. Since NAFLD is characterized by fat deposition in hepatocytes and inflammation, being in close association with IR, a wide variety of genes related to these processes were analysed in the extended cohort. First, a set of genes expressed in association with fatty liver disease was identified based on previous literature[261,262]. Gene expression measures were assessed in the whole cohort using TaqMan mRNA hydrolysis probes by qRT-PCR. The 'DeltaCt' normalized values were obtained as the raw Ct value for each gene – the raw Cts for the endogenous control (*PPIA*) in each sample. Associations with clinical outputs and/or NAFLD were tested for genes related to glucose metabolism (*GLUT2, G6PC, PEPCK*), *de novo* FA biosynthesis (*ChREBP, SREBF1, LXRA, FRX, FASN, ACACA, PPP2R5C*), FA uptake and transport (*PPARG, PGC1A, CD36, FABP4, FATP5, PTLP*), FA oxidation (*PPARA*), inflammation (*ITGAX, PPARD, HAMP, TNFA*) and endoplasmic reticulum stress (*ATF6, DDIT3, HSPA5*). In addition, *ARL6IP1* and *SULT1A2*, two genes that have been reported in close association with NAFLD[263,264] were also analysed, showing significant variations in NAFLD patients *vs.* controls. All these measurements disclosed the significant modification of at least 15 genes in liver samples from NAFLD patients when compared to sex, age and weight-matched controls (**Table 20**).

Table 20. Gene expression in liver. Fisher's least significant difference (LSD) post-hoc test was performed by comparing NAFLD vs. no NAFLD participants. Data is presented as mean ± SD. Bold indicates significant results (p-value < 0.05).

Gene expression (r.u.)	No NAFLD (n=19)	Borderline (n=24)	NAFLD (n=17)	ANOVA	Ratio	LSD[a]
Glucose metabolism						
GLUT2	0.998 ± 0.256	1.005 ± 0.373	0.621 ± 0.232	**<0.0001**	0.62	**0.001**
G6PC	0.465 ± 0.215	0.417 ± 0.234	0.237 ± 0.175	**0.007**	0.51	**0.003**
PEPCK-C	2.92 ± 1.05	2.24 ± 1.63	1.22 ± 0.69	**0.001**	0.42	**<0.0001**
***De novo* FA biosynthesis**						
ChREBP	0.466 ± 0.108	0.42 ± 0.104	0.398 ± 0.16349	0.265	0.85	0.115
SREBP1c	0.0024 ± 0.0008	0.0024 ± 0.0007	0.0026 ± 0.0011	0.842	1.06	0.611
NR1H4	0.02 ± 0.007	0.019 ± 0.007	0.015 ± 0.005	0.062	0.75	**0.028**
NR1H3	0.05 ± 0.011	0.046 ± 0.014	0.04 ± 0.014	0.145	0.82	**0.049**
FASN	0.052 ± 0.049	0.083 ± 0.096	0.042 ± 0.038	0.166	0.82	0.701
ACACA	0.02 ± 0.01	0.023 ± 0.009	0.02441 ± 0.017	0.496	1.23	0.268
PPP2R5C	0.026 ± 0.008	0.026 ± 0.008	0.019 ± 0.006	0.012	0.73	**0.01**
FA uptake and transport						
PPARγ	0.00036 ± 0.00013	0.00042 ± 0.00014	0.00033 ± 0.00012	0.111	0.92	0.512
PGC1a	0.082 ± 0.052	0.067 ± 0.031	0.049 ± 0.016	**0.037**	0.60	**0.01**
CD36	0.108 ± 0.04	0.114 ± 0.033	0.086 ± 0.027	**0.046**	0.80	0.069
FABP4	0.0034 ± 0.003	0.0064 ± 0.0105	0.0095 ± 0.0085	0.111	2.79	**0.037**
FATP5	0.609 ± 0.158	0.472 ± 0.128	0.409 ± 0.169	**0.001**	0.67	**<0.0001**
PLTP	0.011 ± 0.005	0.012 ± 0.005	0.008 ± 0.004	0.059	0.73	0.054
FA oxidation						
PPARa	0.132 ± 0.051	0.114 ± 0.028	0.099 ± 0.03	**0.036**	0.75	**0.011**
Inflammation						
ITGAX	0.0045 ± 0.0016	0.0063 ± 0.0028	0.0072 ± 0.0046	0.056	1.60	**0.021**
PPARδ	0.013 ± 0.003	0.0157 ± 0.0054	0.0119 ± 0.003	**0.020**	0.94	0.600
HAMP	0.724 ± 0.553	0.898 ± 0.668	0.693 ± 0.599	0.517	0.96	0.885
TNFa	0.0023 ± 0.0024	0.0038 ± 0.0034	0.0037 ± 0.0034	0.276	1.60	0.213
ER stress						
ATF6	0.025 ± 0.014	0.022 ± 0.0087	0.025 ± 0.013	0.433	0.888	0.339
DDIT5	0.01 ± 0.006	0.0082 ± 0.0042	0.0138 ± 0.0136	0.134	1.0	0.992
HSPA5	0.072 ± 0.044	0.066 ± 0.031	0.079 ± 0.033	0.524	0.98	0.93
Others						
ARL6IP1	0.402 ± 0.109	0.322 ± 0.048	0.325 ± 0.064	**0.003**	0.81	**0.005**
SULT1A2	12.009 ± 2.578	9.370 ± 2.546	9.176 ± 3.139	**0.016**	0.76	**0.009**

5.1.3. Association with clinical outputs

Expression in liver samples of miRNA candidates was associated with anthropometric and clinical measures such as BMI (that is, let-7a, miR-125b, miR-122-5p, miR-422a and miR-378, all of them inversely associated with increased weight), HDL (miR-122-5p and miR-34a associated positively, while miR-146b showed inverse relationship with HDL), LDL (miR-125b and miR-155, with direct association) and circulating levels of inflammatory markers, such as LBP (inversely related to hepatic let-7a) and CRP (that shown negative association with hepatic miR-30b and miR-204) (**Table 21**).

Table 21. Single correlations of candidate miRNA with clinical outputs. r stands for Spearman's rho. Bold indicates significant results (p-value < 0.05).

	BMI (kg/m²)		HDL (mg/dl)		LDL (mg/dl)		LBP (µg/ml)		CRP (mg/dl)	
	r	*p*	r	*p*	r	*p*	r	*p*	r	*p*
let-7a	**-0.326**	**0.011**	-0.055	0.674	-0.143	0.275	**-0.299**	**0.024**	-0.098	0.463
miR-125b	**-0.324**	**0.012**	-0.06	0.648	**0.301**	**0.020**	0.012	0.931	-0.022	0.867
miR-122-5p	**-0.291**	**0.025**	**0.29**	**0.026**	-0.064	0.628	-0.234	0.083	-0.144	0.284
miR-422a	**-0.281**	**0.029**	-0.112	0.396	0.178	0.172	-0.077	0.570	-0.211	0.112
miR-378	**-0.276**	**0.033**	-0.093	0.480	<0.001	0.998	-0.26	0.051	-0.147	0.270
miR-30b	-0.221	0.090	-0.059	0.657	<0.001	0.998	-0.161	0.231	**-0.27**	**0.040**
miR-204	-0.197	0.132	0.019	0.888	0.093	0.482	0.002	0.990	**-0.271**	**0.040**
miR-146b	0.185	0.160	**-0.262**	**0.045**	0.001	0.994	0.241	0.073	0.004	0.976
miR-155	-0.146	0.271	-0.038	0.778	**0.278**	**0.033**	-0.229	0.090	-0.048	0.724
miR-34a	-0.05	0.708	**0.543**	**<0.001**	-0.049	0.711	-0.161	0.236	0.029	0.828
miR-139-5p	0.029	0.826	-0.197	0.132	0.003	0.982	0.171	0.203	-0.146	0.274

To perform multiple linear regression models, borderline and NAFLD participants were joined in NAFLD variable group (thus representing risk of NAFLD). NAFLD contributed to explain the variance of miR-139-5p (13%, p=0.028), miR-30b-5p (15.3%, p=0.018), miR-122-5p (18.8%, p=0.018) miR-146b (15.4%, p=0.037) and miR-422a (17.7%, p=0.011), after adjusting for gender, age, weight, dyslipidaemia (that is, circulating HDL and/or LDL) and inflammation (LBP and/or CRP) (**Table 22**). Only decreased miR-139-5p and miR-122-5p in liver explained together 29.2% (p=0.005) of the variance of NAFLD (borderline + NAFLD patients) after correcting for many confounders.

Table 22. Multiple linear regression of the hepatic miRNAs related to NAFLD. Beta is the standardized regression coefficient, which allows evaluating the relative significance of each independent variable in multiple linear regression analyses. Adjusted R2 express the percentage of the variance explained by the independent variables in the different models (that is, 0.50 is 50%). Significant associations are indicated in bold. [a]NAFLD variable group is defined here as Borderline + NAFLD group *vs.* control.

	miR-139-5p		**miR-30b-5p**		**miR-122-5p**		**miR-146b-5p**		**miR-422a**	
	Beta	*p*	Beta	*p*	Beta	*p*	Beta	*p*	Beta	*p*
Gender	0.018	0.887	-0.222	0.081	-0.083	0.526	0.09	0.501	-0.15	0.227
Age (years)	-0.12	0.343	0.049	0.693	-0.012	0.928	0	0.998	-0.073	0.56
Bmi (kg/m²)	0.021	0.868	-0.191	0.129	**-0.288**	**0.05**	0.286	0.059	**-0.285**	**0.022**
Hdl (mg/dl)	-0.179	0.167			0.214	0.112	**-0.273**	**0.045**	-0.082	0.52
Ldl (mg/dl)									0.221	0.078
Crp (mg/dl)					0.193	0.22	-0.289	0.082		
Lbp (µg/ml)			-0.13	0.297	-0.239	0.063	0.229	0.071		
NAFLD[a]	**-0.37**	**0.005**	**-0.368**	**0.005**	**-0.348**	**0.021**	**0.3**	**0.033**	**-0.342**	**0.007**
Adjusted R square	**13% (p=0.028)**		**15.3% (p=0.018)**		**18.8% (p=0.018)**		**15.4% (p=0.037)**		**17.7% (p=0.011)**	

In order to determine the level of discrimination provided by each hepatic miRNA, the area under the curve was estimated. All miRNA candidates presented discriminatory capacity between subjects with signs of NAFLD and gender, sex and BMI-matched controls: miR-139-5p (area=0.74 (95% CI= 0.61-0.87), *p*=0.003), miR-30b-5p (area=0.71 (95% CI= 0.57-0.84), *p*=0.008), miR-122-5p (area= 0.68 (95% CI= 0.53-0.83), *p*=0.028), miR-422a (area= 0.70 (95% CI= 0.57-0.84), *p*=0.013), miR-146b (area= 0.67 (95% CI= 0.51-0.82), *p*=0.041) (**Figure 16a**). It is worth mentioning that among clinical outputs, only SBP (area= 0.75 (95% CI= 0.59-0.92), *p*=0.006) and M-clamp (area= 0.70 (95% CI= 0.51-0.89), *p*= 0.027) provided significant discriminatory capacity for NAFLD variance (**Figure 16b**). Nevertheless, no significant associations were identified between hepatic miRNAs and parameters of IR, triglycerides, SBP or DBP and plasma liver enzymes.

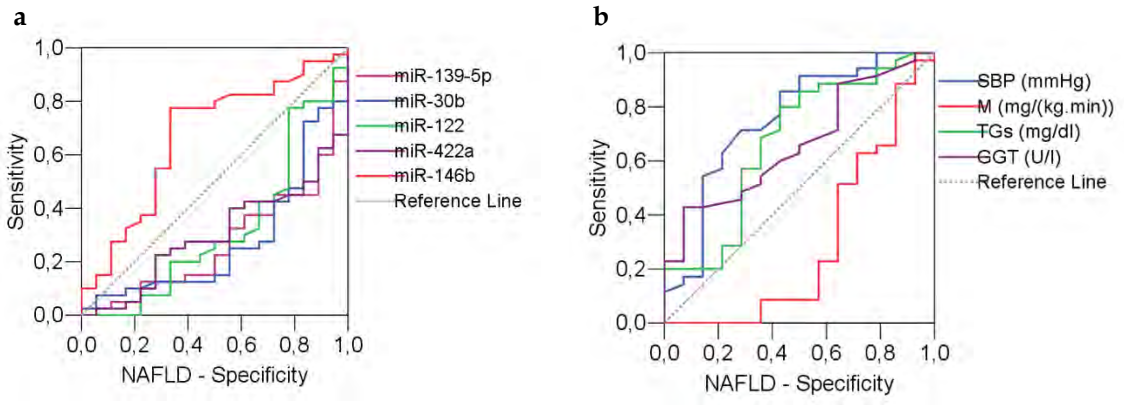

Figure 16. ROC curve for a) liver miRNAs and b) clinical outputs as surrogates of NAFLD. NAFLD variable includes borderline and NAFLD group, based on the laboratory, sonographic and histological findings. Grey continued line (diagonal) indicating area under the curve (AUC) = 0.5.

5.1.4. Association with gene expression

Significant regulation of genes appeared to be in close association with changes in miRNAs. Currently, decreased miR-122-5p in NAFLD was associated with decreased FA metabolism and transport in the liver, including lower *ChREBP* (r= 0.36, p= 0.007), *PPARG* (r= 0.27, p= 0.048), *PPARA* (r= 0.398, p= 0.002), *LXRA* (r= 0.32, p= 0.016) and *FATP5* (r= 0.47, p= 0.0003) gene expression. On the other hand, an increased macrophages-related gene such as *ITGAX* (r= -0.381, p= 0.006) and *FABP4* (r= -0.310, p= 0.018) associated with decreased miR-30b-5p. *ITGAX* was also inversely associated with miR-422a expression (r= -0.40, p= 0.004), while increased miR-146b-5p expression was related to *FABP4* (r= 0.38, p= 0.004), and decreased *GLUT2* (r= -0.34, p= 0.011), *FATP5* (r= -0.37, p= 0.004), *FABP4* (r= -0.38, p= 0.004) and *ChREBP* (r= -0.36, p= 0.006) (**Figure 17**).

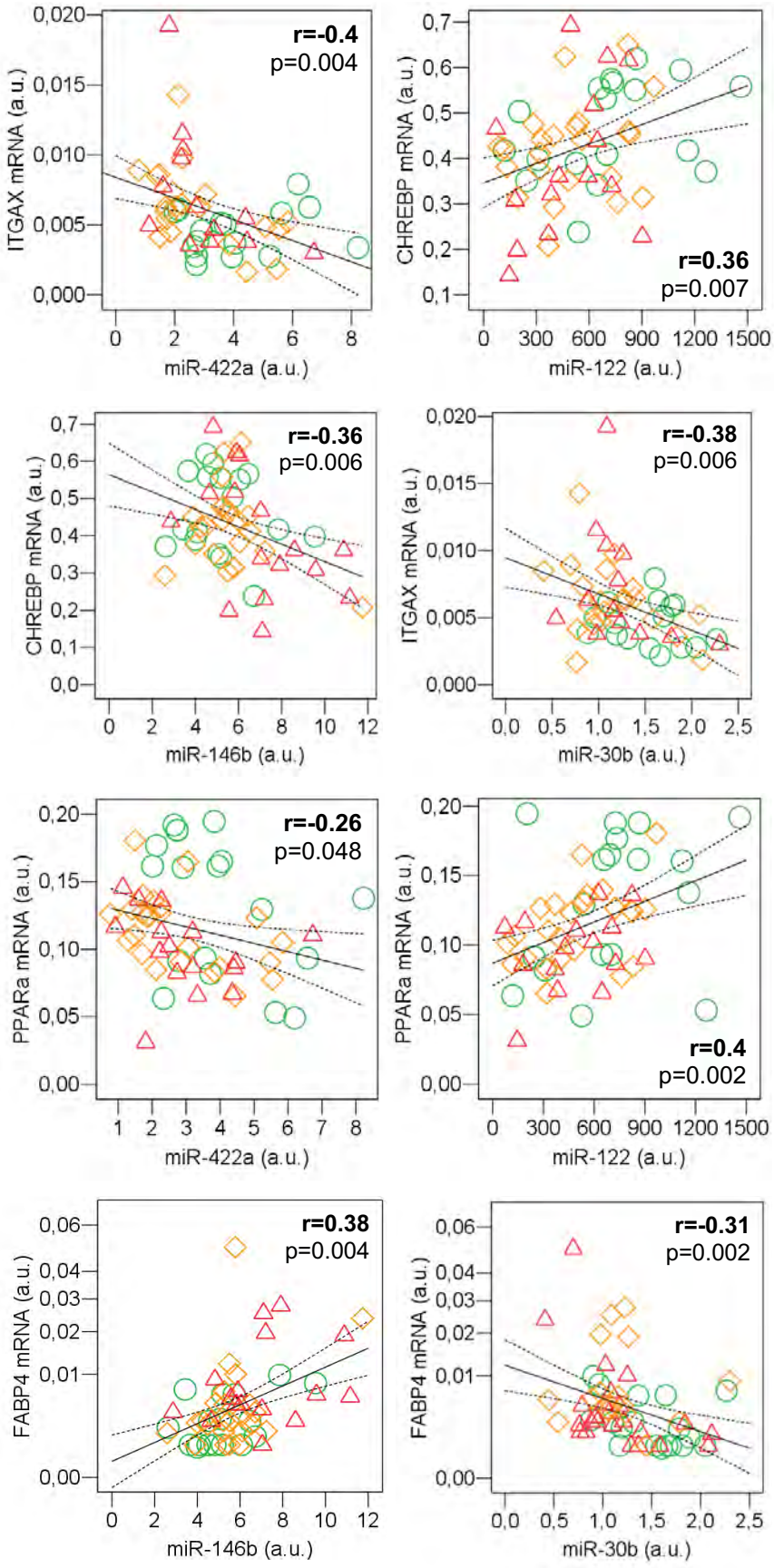

Figure 17. Relationship between gene expressions and hepatic miRNA candidates. Values for control subjects are represented as green circles (O); borderline are yellow diamonds (◊); and red triangles for NAFLD patients (Δ).

5.2. THE BENCH: HEPATOCYTE MODELS TO STUDY NAFLD *IN VITRO*

Molecular mechanisms and pathophysiology involved in the progression of NAFLD were first obtained from animal models (genetic or diet-induced models). Nevertheless, cell models are important tools in research to elucidate the molecular pathways involved in the progression of disease. Immortalized cell lines and primary cell cultures are widely used to develop *in vitro* models for research. While primary culture is the closest *in vitro* model to human liver, immortalized cell lines have continuous growth, unlimited lifespan, stable phenotype and high availability. Different treatments were used in both HepG2 and hepatocyte primary culture trying to resemble NAFLD in the cells. The effort to set up reliable *in vitro* models for the study of NAFLD greatly contributed to the understanding of mechanisms, triggering factors and causal effectors.

5.2.1. Fine-tuning of *in vitro* models

To further validate cross-sectional findings in liver samples, and to test whether values of miRNA candidates for NAFLD may respond to FA deposition in hepatocytes, the objective was to find *in vitro* models that mirror what we found in humans. The main aim was to perform functional studies to figure out whether the miRNA candidates can restore normal lipid accumulation within hepatocytes. We explored different models of FA-induced steatosis and conditions of high-glucose (HG) and insulin mimicking IR in HepG2 and primary human hepatocytes (HH). Gene and miRNA expression measures were assessed in order to see whether expression profiles were representative of *in vivo* findings.

5.2.1.1. High-glucose (HG)

HepG2 cells (**Figure 18**) and HH (**Figure 19**) were treated with a combination of glucose (33 mM) and insulin (100 nM) for 24 h. HG treatment did not show lipid accumulation, and *de novo* FA biosynthesis genes were not responding to treatment, and neither did miRNA expression pattern. Few changes were detected at gene expression level, only coinciding in the decrease of *PGC1A* expression. In HH, the expression of genes related to the insulin pathway such (e.g. *GLUT2*) was decreased. This was in agreement with decreased phosphorylated Akt serine/threonine kinase vs total Akt upon HG (-54%, $p<0.0001$) (**Figure 20**). Despite HG and high-insulin stimulation was not enough to

trigger lipid accumulation *in vitro*, the treatment showed to be efficient referring to insulin pathway at protein level.

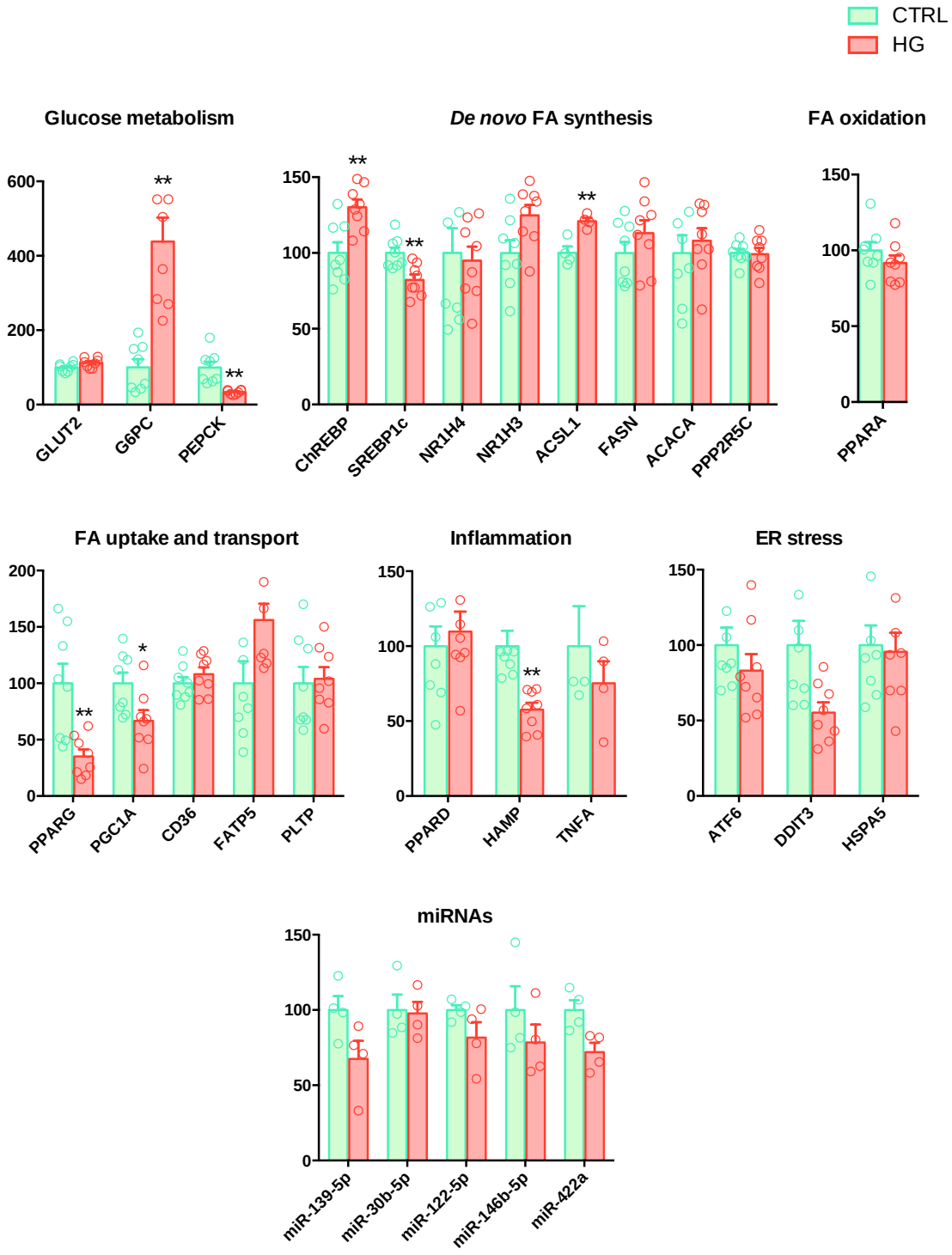

Figure 18. HepG2 cells upon high glucose and high insulin. Mean ± SEM. *p<0.05, **p<0.01.

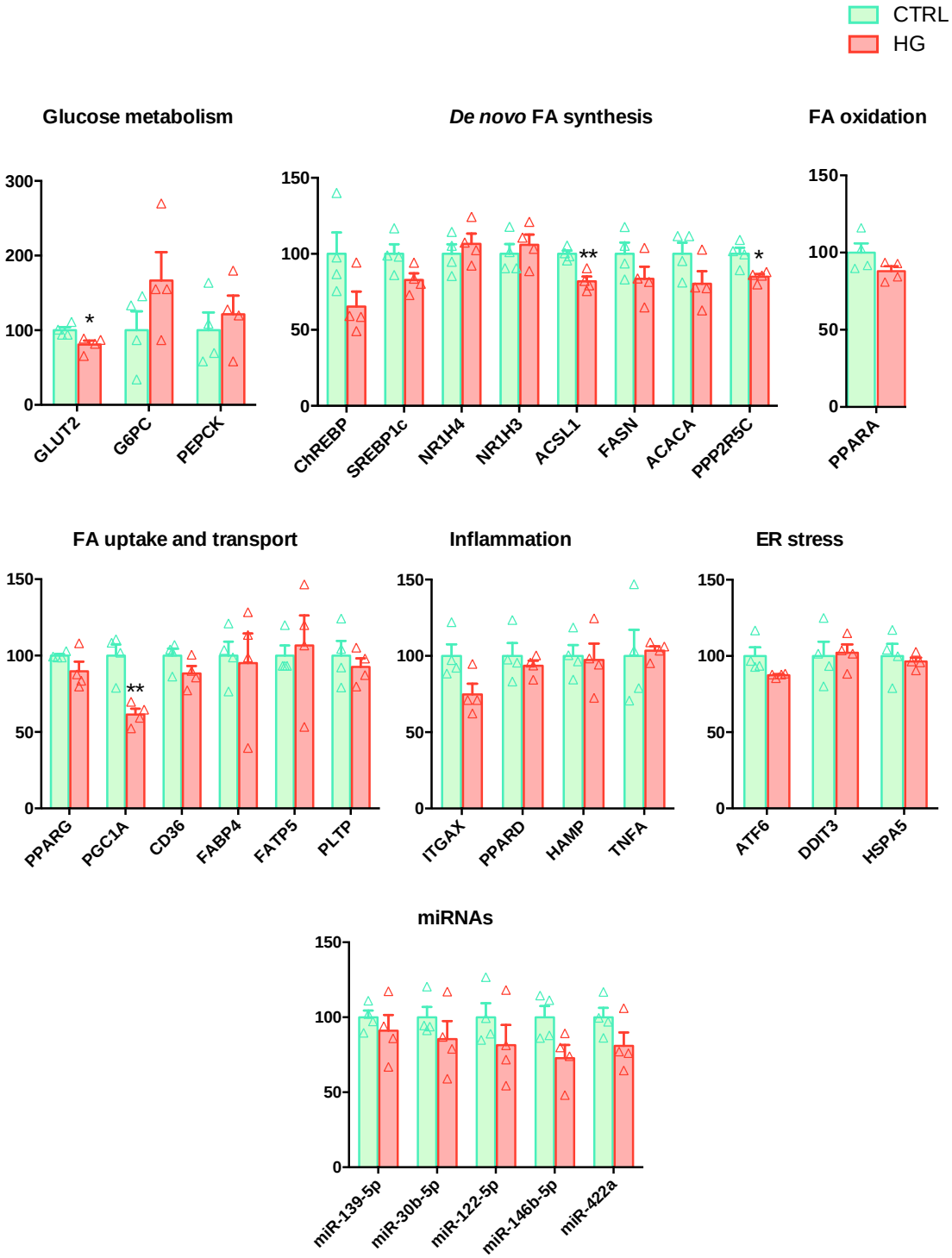

Figure 19. HH upon high glucose and high insulin. Mean ± SEM. *p<0.05, **p<0.01.

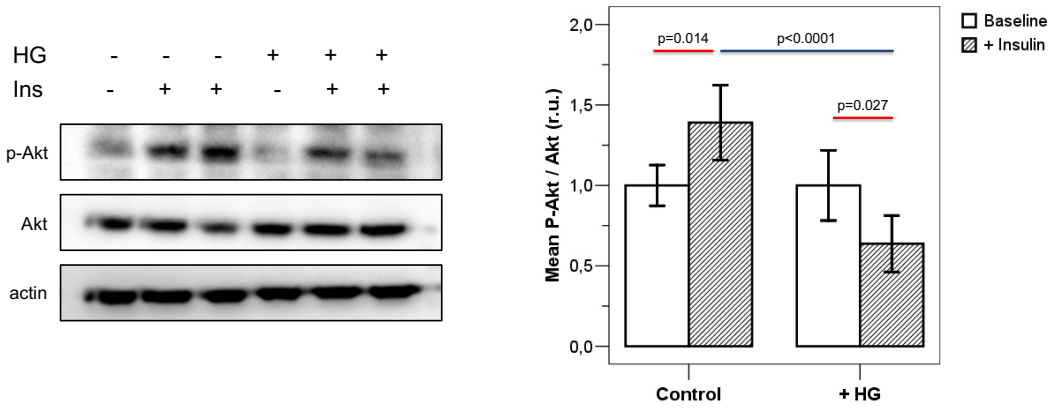

Figure 20. Decreased phospho-Akt signalling upon insulin stimulation in HG-treated HH. Ratio between phosphorylated (Ser473) Akt serine/threonine kinase (pAkt) and total Akt in HH stimulated (HG) or not (control) with high glucose (33 mM) and insulin (100 nM) mimicking conditions of IR in NAFLD patients. Mean ± SEM. *p<0.05, **p<0.01.

5.2.1.2. Palmitic acid (PA)

To trigger SS and inflammation, HepG2 and HH were treated with palmitate 0.5/0.2 mM PA, 72/24h respectively. Among the genes evaluated, thirteen showed significant changes upon PA in HepG2 and fifteen in HH. Higher expression of genes codifying for key enzymes in FA biosynthesis such as *ACSL1*, *FASN*, *ACACA* and *ChREBP* with fold changes of 3.1, 3.7, 1.7 and 1.6, respectively were detected in HepG2 cells, with a p-value <0.05. Apart from detecting significant transcriptome changes suggestive of enhanced DNL, genes related to FA uptake and lipid transport also showed differential expression patterns, namely increased *CD36* and *PLTP* running together decreased *PPARG* and *PGC1A*. Concomitantly, decreased expression of genes related to FA oxidation such as *PPARA* and gluconeogenesis represented by *PEPCK* was found in PA-treated HepG2 cells. High saturated FAs may induce oxidative stress and ER stress leading to cell death[265]. In fact, ER stress contributes to cell death in hepatocytes exposed to high concentrations of saturated FAs[266]. Nevertheless, ER stress, measured by the expression of genes such as the DNA damage inducible transcript 3 (*DDIT3*), heat shock protein family A member 5 (*HSPA5*), and the activating transcription factor 6 (*ATF6*), disclosed a significant decrease upon PA in HepG2 cells. However, increased expression of the antiapoptotic *BCL2* and decreased levels of the tumour suppressor gene *BAX* (2.5 and 0.5-fold change) reflected changes in signalling pathways aimed at regulating cell growth and proliferation, which are opposite to the activation of apoptosis. Concurrently with all these changes, FA-induced significant decreased expression of

miRNAs candidates, except for miR-122-5p, which showed no significant variation in cells upon treatment (**Figure 21**).

Similar expression profiles were assessed in HH after 24h of treatment with PA (**Figure 22**). Increased *de novo* FA synthesis was marked by *ACSL1* and *FASN* higher expressions ($p<0.01$), with fold changes of 1.4 and 1.7, respectively. FA uptake and lipid transport gene expression was also altered showing increased expression of *CD36*, *FABP4* and *PLTP*, and glucose metabolism represented by *GLUT2* disclosed decreased expression. On the other hand, in primary cell line *PGC1A* appeared to be increased upon PA treatment, as well as *PPARA*. According to its higher sensitivity upon treatment, inflammation and ER stress markers were significantly increased upon PA, including higher expression of *ITGAX*, *HAMP*, *TNFA* as inflammatory markers, and *ATF6*, *DDIT3* and *HSPA5* as ER stress indicators. In parallel to all these changes, FA-induced decreased expression of all miRNA candidates (**Figure 22**).

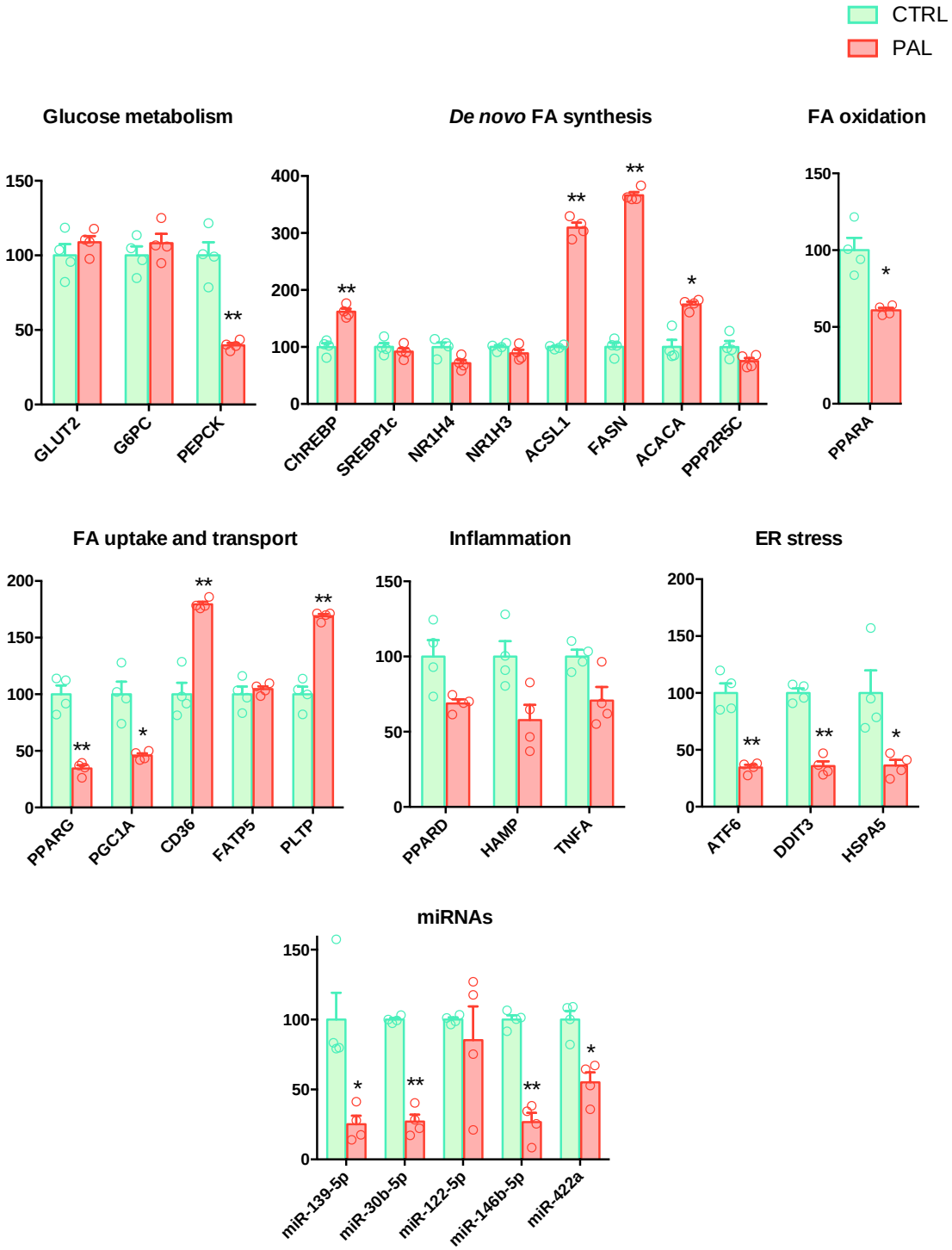

Figure 21. HepG2 cells upon palmitic acid. Mean ± SEM. *p<0.05, **p<0.01.

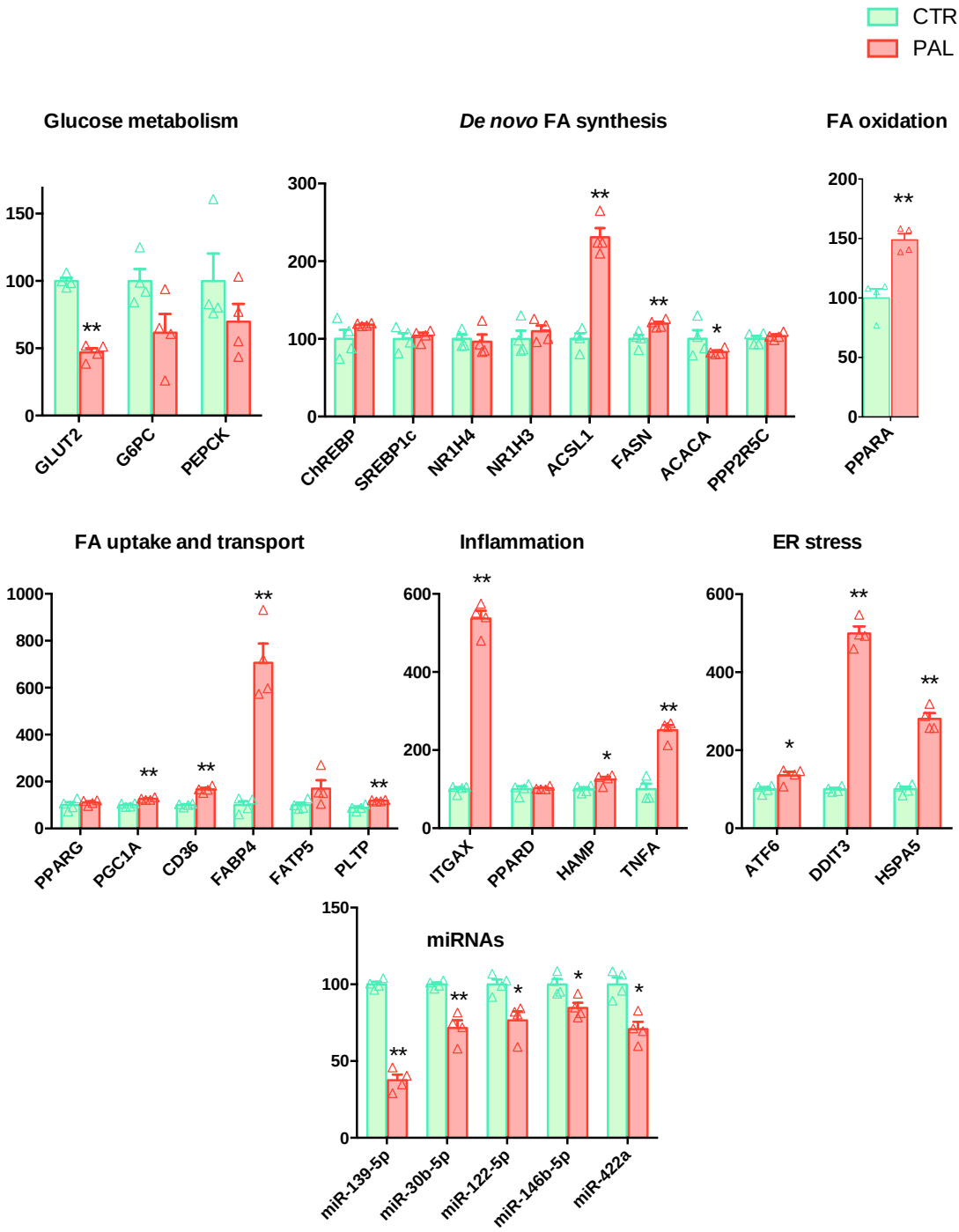

Figure 22. HH cells upon palmitic acid. Mean ± SEM. *p<0.05, **p<0.01.

5.2.1.3. Palmitic acid plus oleic acid (PA+OA) / Palmitic acid plus high glucose (PA+HG)

HepG2 were also challenged with a combination of PA (200 µM) and oleic acid (OA, 300 µM). Here we found significant changes in seventeen (**Figure 23**). The major difference between PA alone and PA combined with OA was that genes related to DNL were less enhanced upon PA+OA than by PA alone, even though *NR1H3 (a.k.a. LXRA)*, known to

precede genes involved in hepatic FA synthesis[267], was clearly upregulated. Despite that, genes upstream DNL such as *ChREBP*, *SREBP1c, ACSL1* and *ACACA* appeared to be significantly downregulated (0.68, 0.81, 0.74 and 0.83-fold change, respectively) (**Figure 23**). Here, two genes related to FA uptake such as *CD36* and *FATP5*[268] were decreased, and *PPARG* and *PGC1A* disclosed the same pattern as HepG2 cells upon treatments of PA. In parallel, decreased expression of genes related to FA oxidation such as *PPARA* and gluconeogenesis was also found in PA+OA-treated cells. Inflammatory response, as suggested by *PPARD*, *HAMP* or *TNFA* mRNA was downregulated together with biomarkers of ER stress markers, suggesting that induction of lipotoxicity was less apparent than after PA alone. miRNA analysis disclosed significant downregulation of miR-30b-5p, miR-146b-5p and miR-422a (**Figure 23**).

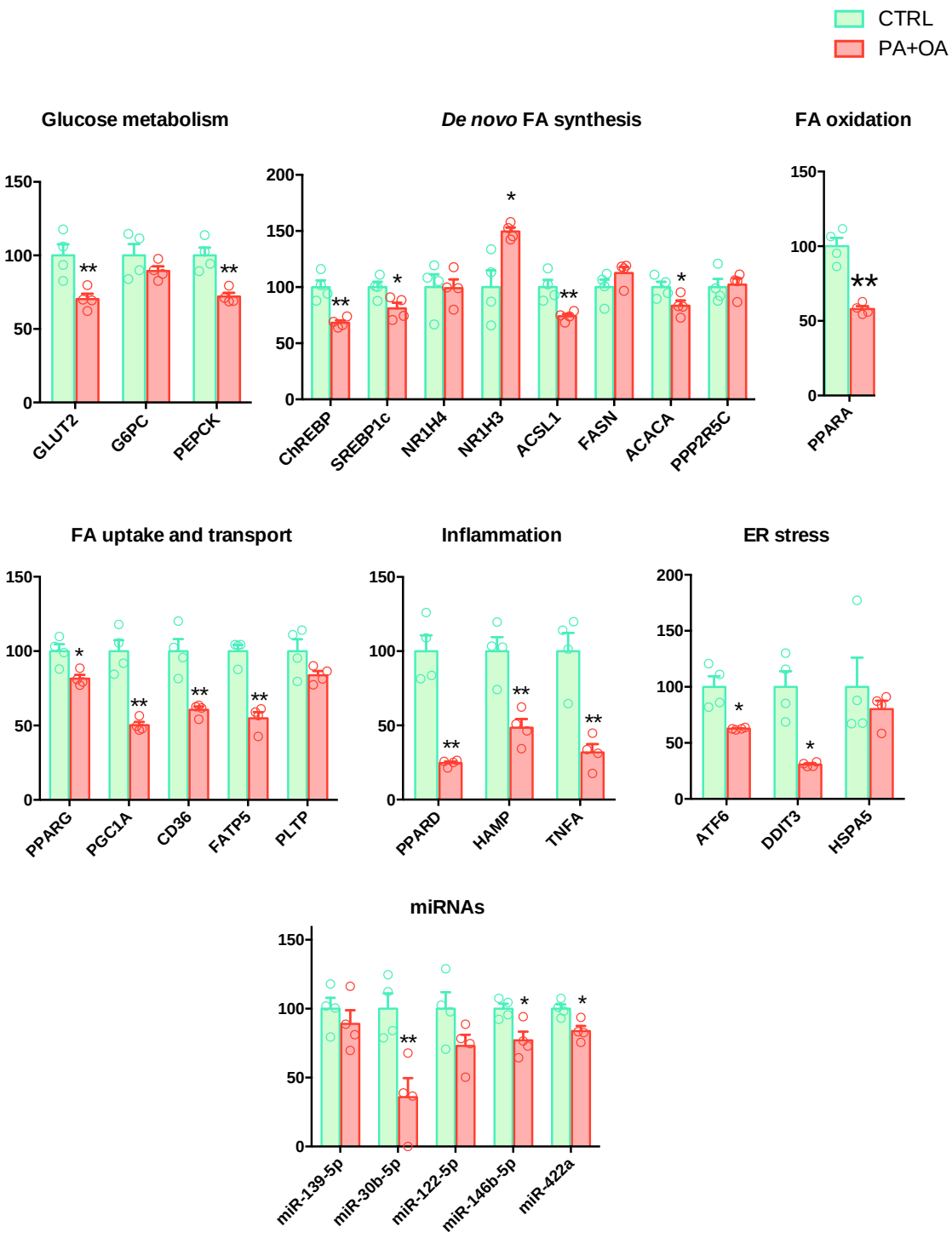

Figure 23. HepG2 cells upon palmitic acid plus oleic acid. Mean ± SEM. *p<0.05, **p<0.01.

On the other hand, HH were challenged with a combination of HG and PA. In partial agreement with HepG2, HH cultured under conditions of a combination of HG and PA reported increased fat overload. These changes were coupled to significant variations in target miRNAs. Noteworthy, HH stimulated with PA alone or in combination with HG showed very similar results for genes and miRNAs, suggesting that PA alone was

enough to stimulate NAFLD-related variations in HH. As in HepG2, increased expression of genes associated with FA metabolism, uptake and transport was identified, including significant changes of *ACSL1*, *FASN*, *CD36*, *FABP4*, *FATP5*, *PLTP* and *PPARA*. In addition, biomarkers of inflammation, as expression levels of *ITGAX*, *HAMP* and *TNFA* were also increased, together with ER stress markers such as *DDIT3* and *HSPA5*. This indicate some degree of lipotoxicity in this *in vitro* model, as it was found in PA-treated cells. A significant downregulation of *GLUT2* was found in parallel to these changes, suggesting impaired glucose metabolism. Concomitantly with variations in gene expression, downregulation of hepatic miRNAs was demonstrated in this model (**Figure 24**).

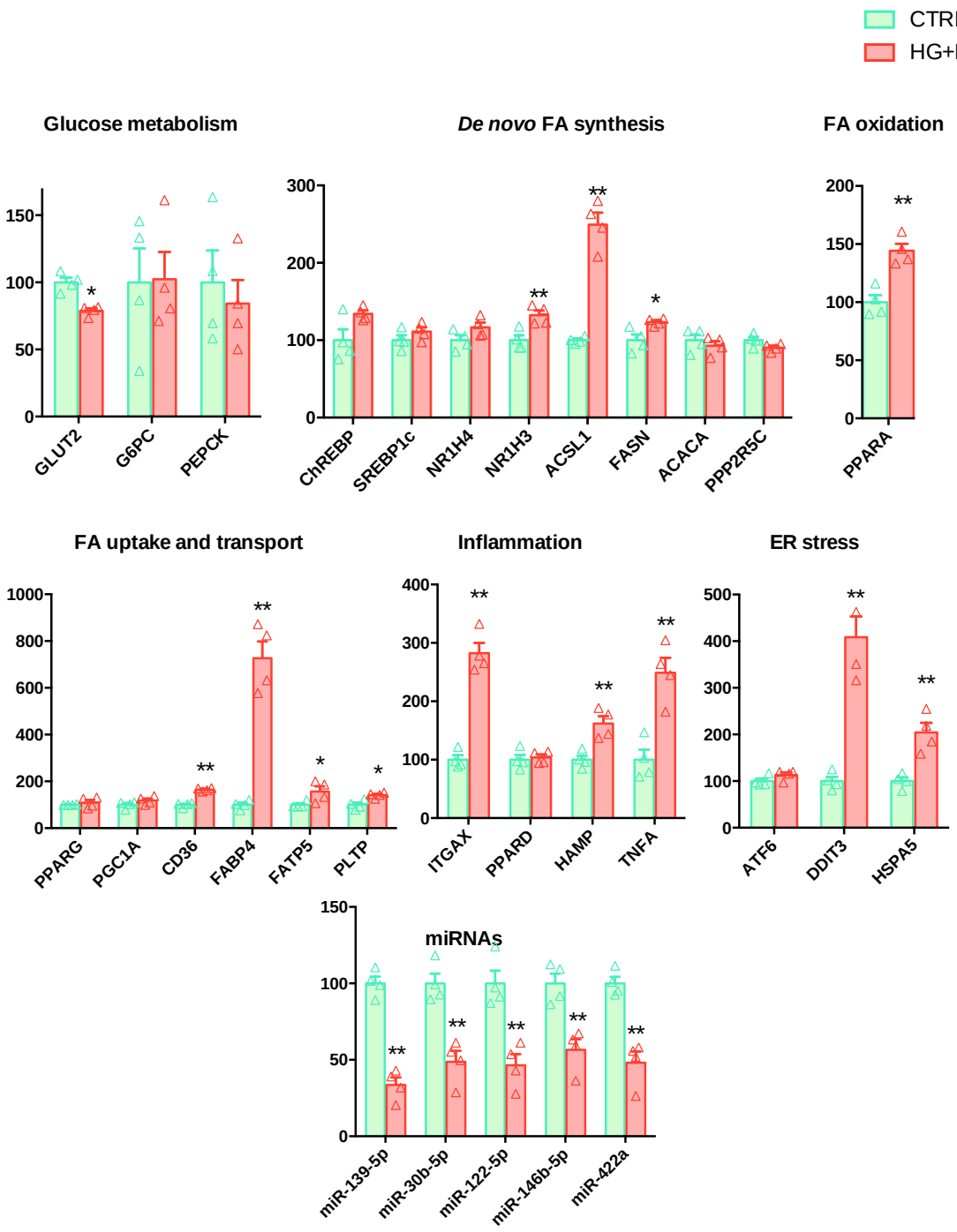

Figure 24. HH upon high glucose plus palmitic acid. Mean ± SEM. *p<0.05, **p<0.01.

5.2.1.4. Compound C

Taking into account that AMPK is able to regulate hepatic lipid metabolism and its activation has been widely proposed to lower hepatic triglyceride content[269], HepG2 and HH were subjected to compound C (CC) treatment, known to inhibit AMPK activity[270]. Thereby, it was shown that CC was able to trigger DNL in both HepG2 and HH by increasing *ACSL1* and *FASN* with fold changes of 1.65 and 2.17 respectively in HepG2

cells and 1.37 and 1.67 in HH. Referring to FA synthesis, CC in HepG2 was also triggering an increase in *SREBP1c* transcription factor and *PPP2R5C*, as well as downregulated expression of *NR1H4*, a bile acid receptor known to regulate lipid homeostasis. Despite increasing FA synthesis, FA uptake and transport were partially compromised in both cell models, represented by decreased expression of *CD36* and *FATP5* in HepG2, and *CD36* exclusively in HH. On the other side, *PPARG* was upregulated in HepG2 and *PLTP* in HH. Proper glucose metabolism represented by *GLUT2* expression was jeopardized in both *in vitro* models, with a significant downregulation of its expression. Inflammation and ER stress was more marked in HepG2-treated cells, while HH only disclosed a significant increase in *DDIT3* expression, a specific ER stress marker. Coupled to gene expression changes, CC was triggering a stressed downregulation of miRNA candidates, more significantly in HH (**Figures 25 and 26**).

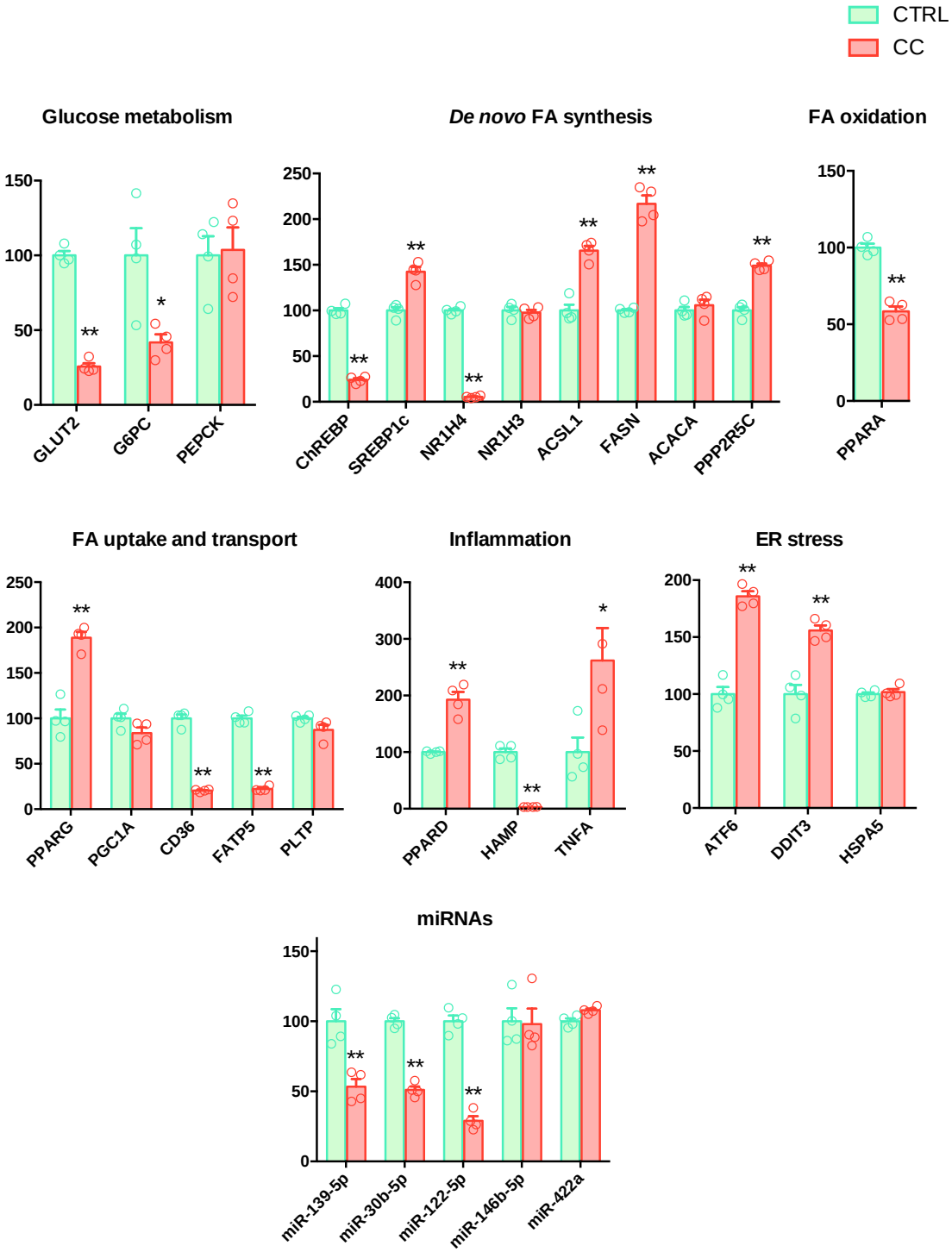

Figure 25. HepG2 cells upon Compound C. Mean ± SEM. *p<0.05, **p<0.01.

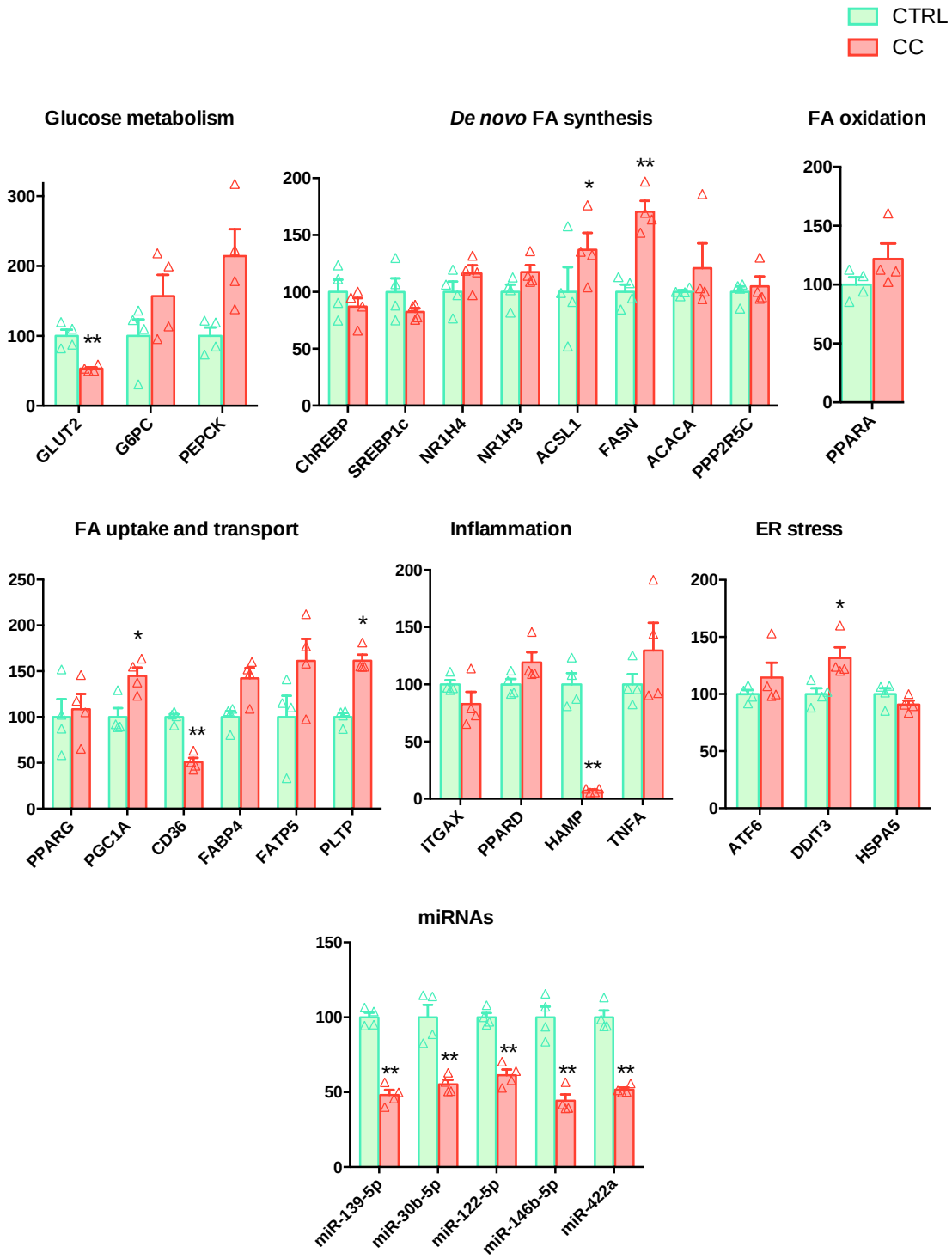

Figure 26. HH upon Compound C. Mean ± SEM. *p<0.05, **p<0.01.

5.2.1.5. Metformin

The impact of the antidiabetic drug metformin in hepatocytes leads to FA oxidation and decreased lipogenesis[271], mainly accomplished through the activation of AMPK[272]. Here, treatments of metformin were aimed at confirm that gene and miRNA expression patterns behave accompanying the beneficial effects on lipid homeostasis. Thereby, we

found a slight but significant decrease of *ChREBP* and *SREBP1c*, as well as reduced *ACSL1* expression in HepG2 cells challenged with this drug (**Figure 27**). Some of the genes involved in FA uptake and transport also disclosed decreased expression patterns (*CD36* and *FATP5*). In addition, genes involved in gluconeogenesis, being *PEPCK* and *G6Pase* were also downregulated, meaning that gluconeogenesis was disrupted upon the treatment (**Figure 27**). On the other hand, inflammatory genes appeared to be fairly downregulated upon metformin. These changes were linked to an improvement in cell homeostasis, and were coupled to a significant increase in miR-30b-5p and miR-122-5p (**Figure 27**).

Accordingly, changes in HH showed a significant decrease of *ACSL1*, *FABP4* and *TNFA*, together with an increase in *GLUT2* and *PPARA* (linked to FA oxidation). C*hREBP* and *NR1H3* expression levels disclosed higher activity in HH challenged with metformin. Here, miR-30b-5p, miR-146b-5p and miR-422a were significantly upregulated (**Figure 28**).

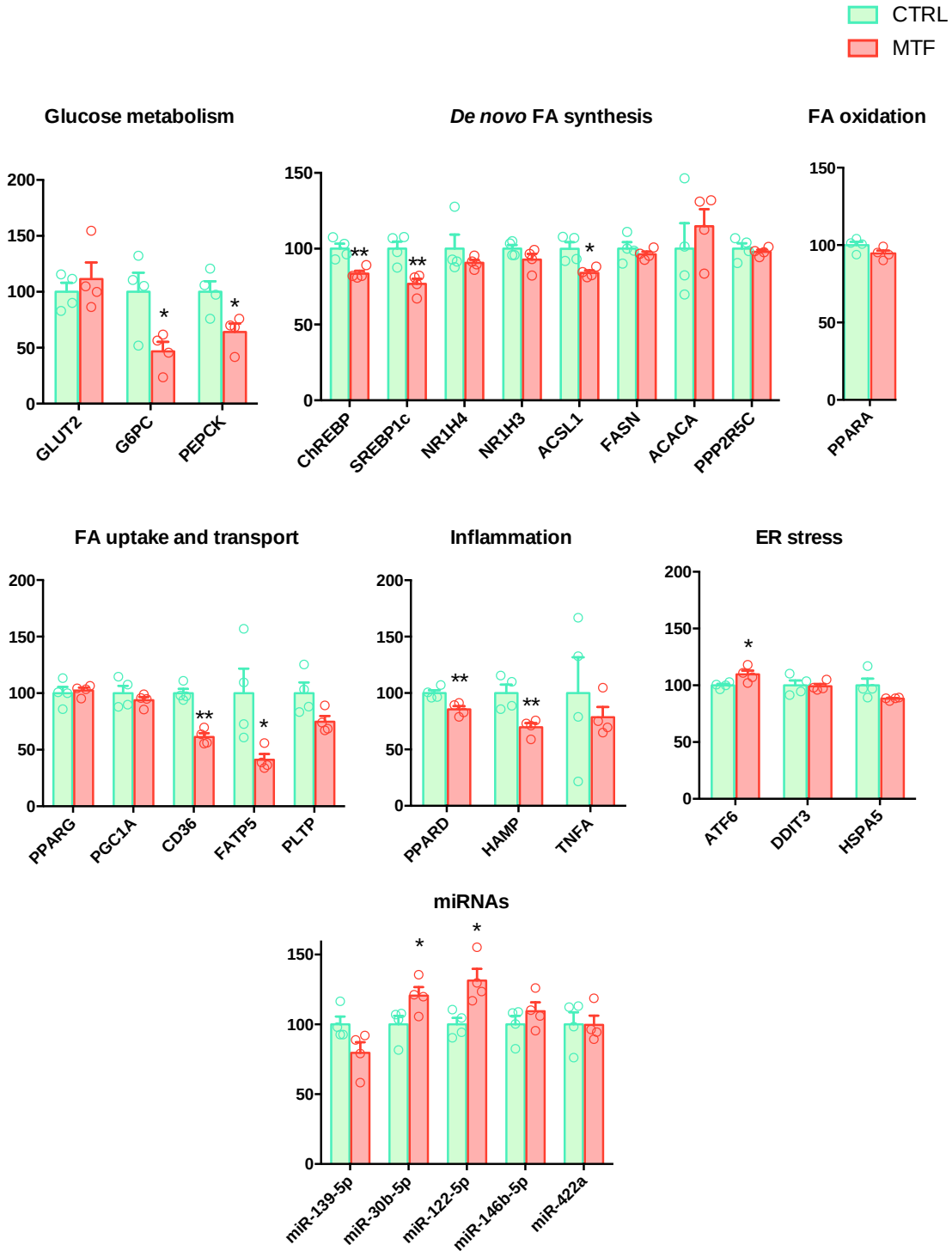

Figure 27. HepG2 cells upon metformin. Mean ± SEM. *p<0.05, **p<0.01.

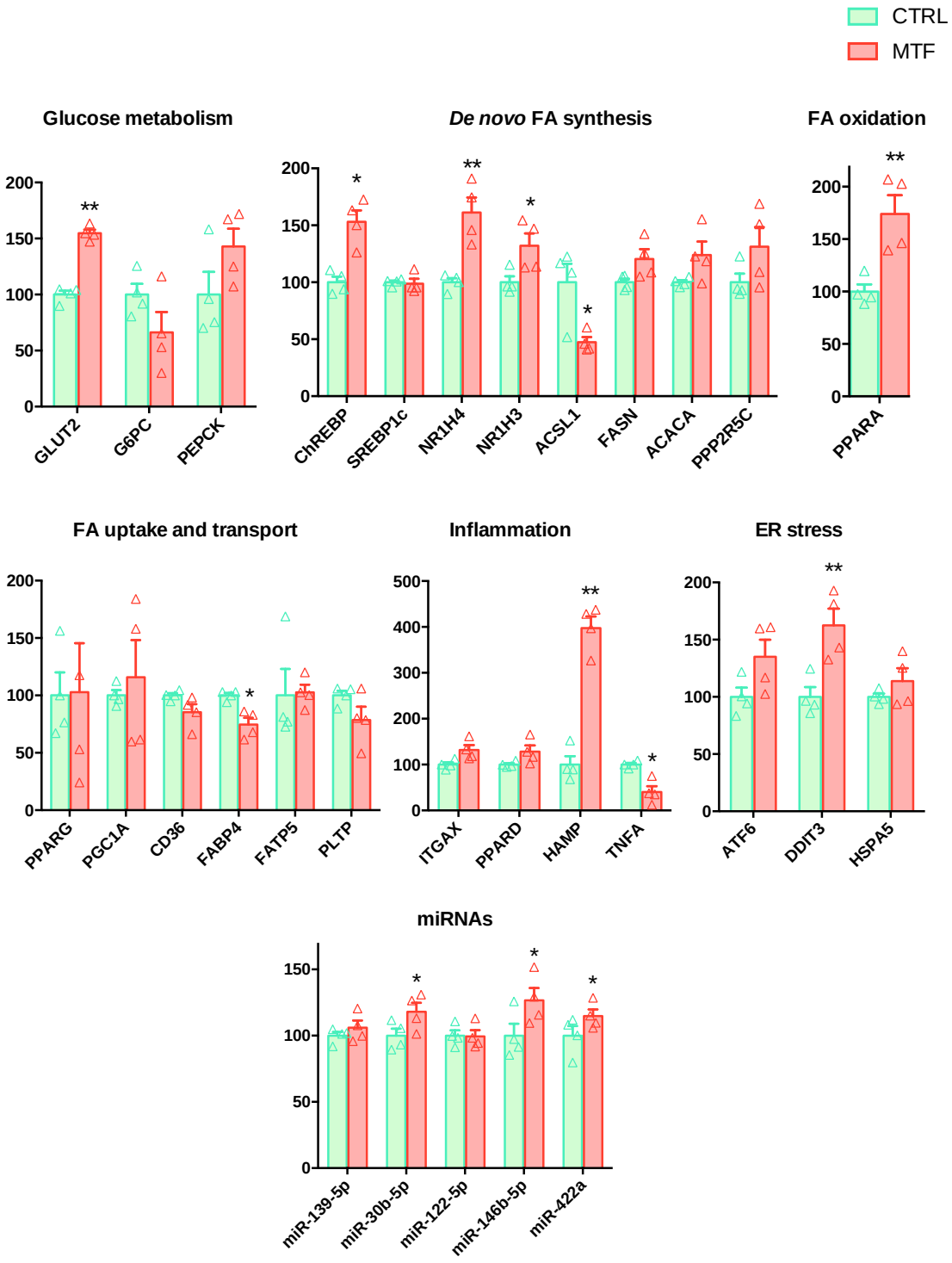

Figure 28. HH upon metformin. Mean ± SEM. *p<0.05, **p<0.01.

5.2.2. Modulation of AMPK and FA metabolism in hepatocytes

The balance between FA biosynthesis, uptake and clearance is of crucial importance for maintaining lipid homeostasis function of hepatocytes, being the most common parenchyma cells in the liver. Besides circulating FA intake, impaired β-oxidation occurring at the inner mitochondrial membrane[273] and enhanced DNL substantially contribute to hepatic FA deposition[274]. These processes are directly or indirectly modulated by the energy sensor AMP-activated protein kinase (AMPK), a master metabolic regulator that blocks the transcription of lipogenic enzymes[275], while actively inhibits biosynthetic pathways and increases FA oxidation[276]. Therefore, a number of AMPK activating compounds have been reported to have beneficial effects as therapeutic interventions in the fatty liver arena[124]. In particular, metformin, a common antidiabetic drug, can decrease hepatic steatosis in models by activating hepatic AMPK[277]. Consistent with this notion, inhibition of AMPK leads to the activation of lipogenesis as a central event in the development of chemical-induced fatty liver[278]. In this context, dorsomorphin or compound C (CC), a pyrazolopyrimidine related to protein kinase inhibitors, is occasionally used as a cell-permeable ATP-competitive inhibitor of AMPK to rescue the positive effect of AICAR and metformin[279]. Despite the controversy about the selectivity of this reagent, known to inhibit a number of kinases other than AMPK[280], CC is still being used to provide a proof of AMPK involvement in the regulation of lipid accumulation by other bioactive molecules both in vivo and *in vitro*[281,282].

Results from "Section 5.2.1: *In vitro models of NAFLD*" disclosed PA and CC as the best agents to resemble NAFLD *in vitro*, triggering increased expression of genes related to lipid deposition and a significant downregulation in targeted hepatic miRNAs.

Once our *in vitro* models were ready, both HH and HepG2 were exposed in parallel to metformin as an inducer, and to PA or CC, as inhibitors for 24h. Herein, gene expression were analysed in parallel with lipid droplet staining, to assess FA deposition through different approaches.

As expected, lipid droplet staining showed that PA and CC-treated HepG2 (**Figure 29a**) and HH (**Figure 29b**) disclosed a significant increase in lipid droplets and fat deposition, while metformin decreased the amount of lipid.

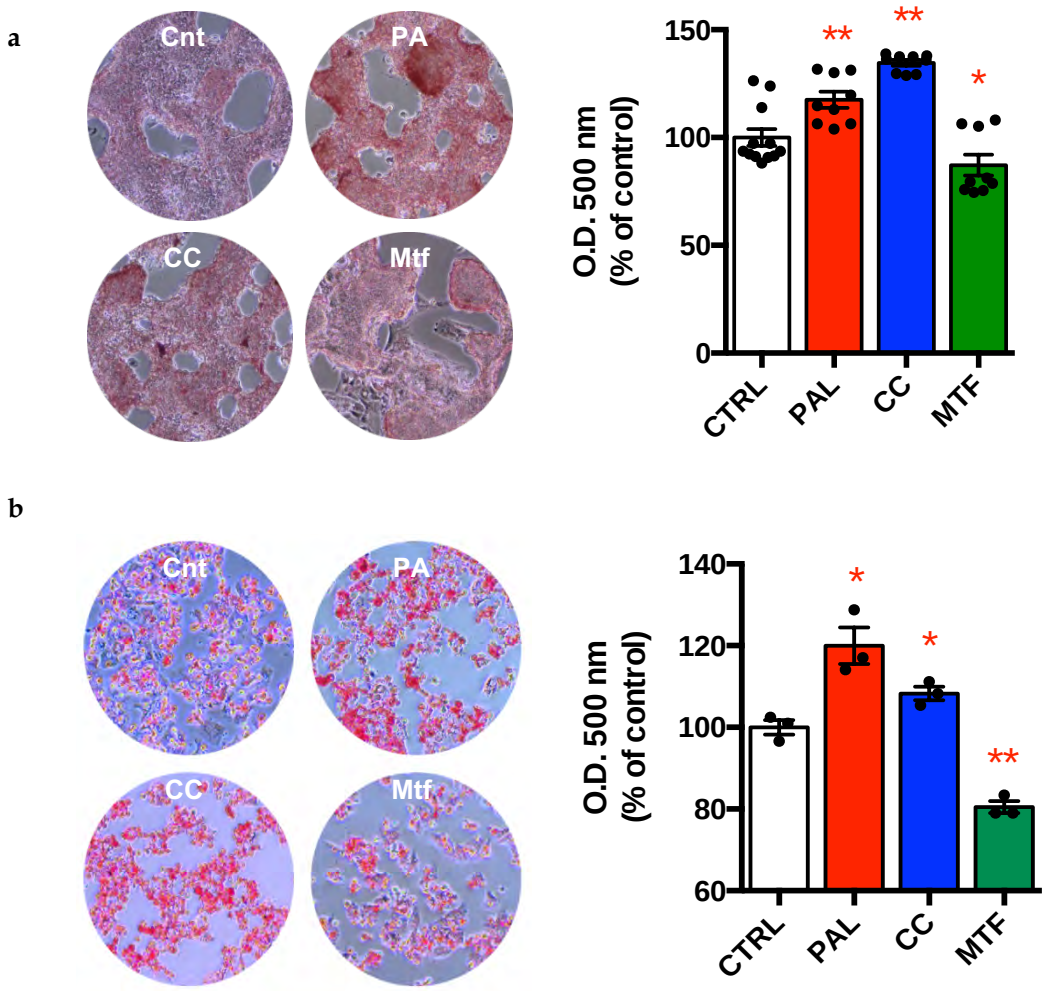

Figure 29. Lipid staining (Oil Red O) in HepG2 cells (a) and primary human hepatocytes (b) challenged with palmitate (PA), compound C (CC) and metformin (Mtf), and non-treated controls (Cnt). Optical density (OD) was measured at 500 nm and relative quantification of the staining is shown in the right-hand panels. Mean ± SEM. * $p<0.05$, ** $p<0.01$.

As previously, treatments with PA and CC enhanced the expression of gene related to lipid accumulation and shortlisted increased *ACSL1* and *FASN* mRNA, while *GLUT2* was compromised. In parallel, inflammatory activation was evident in hepatocytes challenged with PA, as suggested by enhanced expression levels of *IL8* in HH, *ITGAX* in both cell models or *TNFα* in HepG2 cells. On the other hand, metformin led to the significant downregulation of *ACSL1* in both HH and HepG2, together with decreased *FATP5* and *CD36* in HepG2 cells, and reduced *TNFα* mRNA in HH (**Table 23**). Concomitant to these effects, a significant downregulation of miRNA synthetic machinery (*DROSHA, XPO5, DICER* and *AGO2*) was strongly coupled to AMPK inhibition in HH, while metformin enhanced their expression (**Table 23**).

Table 23. Changes of gene expression in HepG2 and HH under treatments of PA (500 and 200 µM respectively), CC (10 µM) and metformin (Mtf) (1 mM). Data is expressed as percentage of change versus control. Color-scales go from red (increased) to green (decreased). *p<0.05, **p<0.01.

HepG2 cells

Genes	PA	CC	Mtf
De novo fatty acid (FA) biosynthesis			
ACSL1	**214.47****	**65.46****	**-15.37***
FASN	**29.84****	**116.76****	-3.63
LPL	**52.38****	55.16	-2.51
FA uptake and transport			
FATP5	**30.8***	**-77.7****	**-58.8***
CD36	**45.5****	**-79.5****	**-38.7****
PLTP	4.1	-12.6	-25.2
Glucose metabolism			
GLUT2	**-16.1***	**-74.3****	11.4
Inflammation			
TNFα	**227.8****	**162.0***	-21.4
ITGAX	**304.0***	56.2	5.2
IL8	19.7	-62.3	7.3
miRNA processing machinery			
DROSHA	**-19.9***	3.6	-13.3
XPO5	-4.5	-18.9	**-13.9***
DICER	**-11.7***	**-15.3****	1.1
AGO2	**63.4****	**266.2****	10.8

Primary human hepatocytes (HH)

Genes	PA	CC	Mtf
De novo fatty acid (FA) biosynthesis			
ACSL1	**154.9****	**37***	**-50.8***
FASN	**16.2****	**66.8***	22.5
LPL	6	**73.2****	22.2
FA uptake and transport			
FATP5	**115.8***	62.3	5.6
CD36	**56.0****	**-49.1****	-14.6
PLTP	**26.7****	**61.5***	-21.3
Glucose metabolism			
GLUT2	**-34,5****	**-16,6****	55.2
Inflammation			
TNFα	151.2	29.6	**-59.9***
ITGAX	**286.8****	-17.2	31.7
IL8	**635.6***	**-39.9***	12.6
miRNA processing machinery			
DROSHA	**-30.5****	**-31.9****	27
XPO5	**-16.0****	**-13.4***	**28.4***
DICER	**-28.8****	**-14.6***	**32.8***
AGO2	-13.5	-11.8	**48.2***

5.2.3. Treatments mimicking NAFLD modify miRNA profiles

5.2.3.1. Comprehensive miRNA profiling in hepatocytes

In order to investigate which mechanism could underlie the observed effects, we focused on miRNA expression patterns. TLDAs were used to characterize the expression of 754 common mature miRNAs in HH challenged with PA, CC or metformin. First, we identified hepatic miRNA detectable (threshold Cts <35) in all samples. The normalized value was obtained by calculating the average of all analysed miRNAs. *In vitro* cultured HH expressed as many as 305 miRNAs, representing 40.5% of the total miRNAs analysed. Qualitative analysis disclosed that the overall profile comparing hepatocytes at the baseline and after treatment was marked by a substantial increase upon PA and metformin treatments (67.3% and 70.9%, respectively), and an outstanding downregulation following CC treatment (-69.4%) (**Figure 30a**). Of note, qualitative analysis through Venn diagrams and assessment of those miRNAs with p-value lower than 0.05 reported that chemical modulation of AMPK modulation clearly impacted on miRNA expression patterns, where 136 miRNAs appeared downregulated under CC (27 with p-values<0.05), while 139 appeared upregulated under metformin, 18 of them being statistically significant (**Figure 30b**).

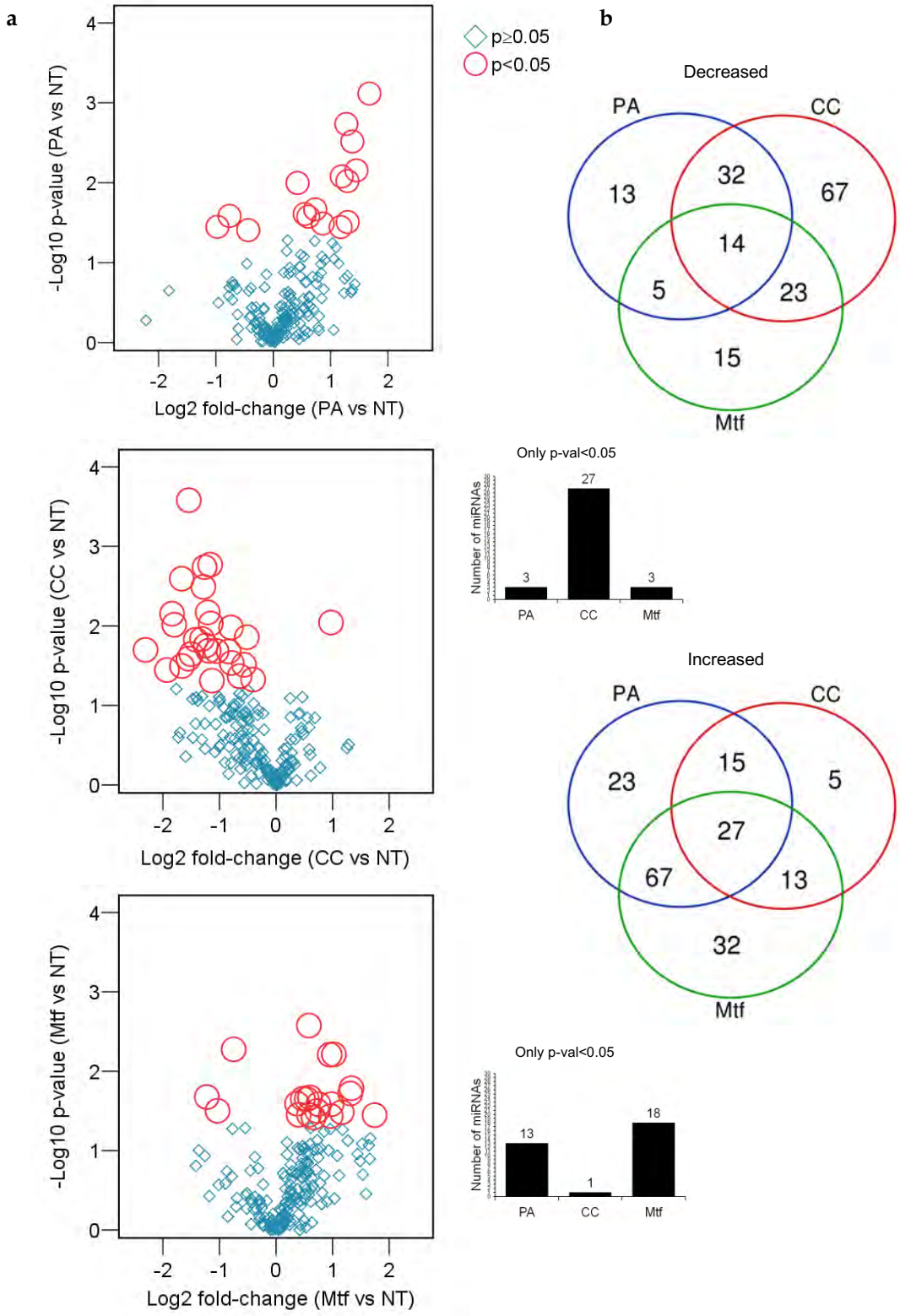

Figure 30. Treatments modulating AMPK impact miRNA expression patterns in hepatocytes. **a)** Volcano plots representing changes in miRNA expression assessed in HH challenged with palmitate (PA), compound C (CC) or metformin (Mtf). Red circles stand for statistically significant miRNAs ($p<0.05$). **b)** Venn diagrams plot the number of decreased/increased miRNAs upon treatments with PA (blue), CC (red) and Mtf (green). The numbers of hepatic miRNAs showing significant alterations (p-value<0.05) are depicted in bar plots.

Such remarkable differences accounted in the context of 59 hepatic miRNA with significant variations upon at least one of the treatments (**Table 24**). Intriguingly, even though PA and CC triggered lipid accumulation in cell models mimicking liver steatosis, quite few coincidences regarding miRNA deregulation were found between two treatments.

MicroRNAs	PA	CC	Mtf
hsa-let-7b	**-26.4***	19.0	-22.1
hsa-miR-100	20.4	**-68.8****	22.7
hsa-miR-106a	23.6	**-55.4****	40.8
hsa-miR-10a	59.6	**-71.9****	163.7
hsa-miR-1225-3P	**142.5****	-39.4	-41.1
hsa-miR-1227	-53.9	-37.4	**-52.2***
hsa-miR-1255B	**121***	-12.5	-14.2
hsa-miR-126	8.9	-33.9	**66***
hsa-miR-1274A	**175****	4.4	-0.5
hsa-miR-1274B	**143****	35.2	9
hsa-miR-1290	**68.1***	-26.1	-4
hsa-miR-130a	**34***	-31.1	-0.2
hsa-miR-130b	-41.8	**-56.7****	10.5
hsa-miR-132	2.9	0.1	**29.6***
hsa-miR-139-5p	-3.7	-13.3	**38.4***
hsa-miR-146a	107.7	**-59.1****	**146.2***
hsa-miR-146b	7.9	**-55.2****	95.2
hsa-miR-149#	**139.1***	18.9	98
hsa-miR-151-5P	19.1	-41.5	**92.2****
hsa-miR-152	**-50***	58	347.7
hsa-miR-16	34.9	**-72.7****	60.3
hsa-miR-17	13.7	**-58.5****	39.1
hsa-miR-199a-3p	14	**-67.1***	41.3
hsa-miR-200b	7.4	**-56***	20.8
hsa-miR-206	12.3	-29.1	**32.5***
hsa-miR-20a	10.8	**-60.2***	17.6
hsa-miR-20b	-15.4	-22.5	**104****
hsa-miR-21	8.3	**-58.5***	2.3
hsa-miR-22#	124.6	-74.7	**56.7***
hsa-miR-221	0.2	**-44.6***	**49.4****
hsa-miR-222	23.7	**-29.9***	26.3
hsa-miR-24	22.8	**-32.8***	44.3
hsa-miR-26a	5.1	**-52.2***	**96.8***
hsa-miR-27a	**52.8***	-21.5	**50.4***
hsa-miR-29a	20.9	**-36.6***	27.5
hsa-miR-30a-3p	48.9	-50.1	**51***
hsa-miR-30a-5p	-20.3	-49	**91.5***
hsa-miR-30b	18.9	**-42.2***	63.5
hsa-miR-30c	21.6	-32.7	**66.6***
hsa-miR-331-5p	-93.9	36	**-57.5***
hsa-miR-365	66.7	**-55.8***	55.4
hsa-miR-370	**162.2****	20.4	62.9
hsa-miR-374-5p	14.6	**-74.4***	-35.4
hsa-miR-375	**221.4****	13.4	-21.1
hsa-miR-376c	2.9	**-63.3***	0.5
hsa-miR-378	40.9	**-42.5***	**45.6***
hsa-miR-379	-39.6	-75.1	**258.9***
hsa-miR-411	**81.3***	**-67.2***	31.4
hsa-miR-432	**47.2***	-5.6	-1.4
hsa-miR-454	-25.3	**-65.9***	83.8
hsa-miR-489	**-40.8***	-5	-57
hsa-miR-505#	74.8	5.5	**129.9***
hsa-miR-532	95.4	-48.2	**151.4***
hsa-miR-655	-22.6	**-81.3***	26
hsa-miR-661	116.5	43.6	**-40.5****
hsa-miR-720	**128.9****	25.3	11.5
hsa-miR-744	18.5	**-24.7***	-31.8
hsa-miR-886-3p	46.5	**94.8****	-11.5
hsa-miR-99a	-3.4	**-65.6****	79.1

Table 24. Significant variations detected in miRNA quantities with at least one treatment. Data is expressed as percentage of change versus control. Color-scale goes from red (increased) to green (decreased). *p<0.05, **p<0.01.

miRNA candidates were also assessed in HepG2 cells (**Figure 31**). These candidates were selected after a procedure based on previous data to select miRNAs linked with NAFLD pathophysiology. This validation confirmed significant downregulation of miR-26a, miR-30b, miR-30c, and miR-34a during treatments of PA and CC, while reduced miR-29c, miR-146b, miR-222, and miR-422a accounted only upon PA, and miR-16 and miR-139a levels were significantly decreased in HepG2 challenged with CC (**Figure 31**). On the contrary, metformin led to enhanced expression of miR-16 and miR-30b (**Figure 31**). Hence, treatments mirroring NAFLD and AMPK modulation in HH and HepG2 cells appears to have a significant impact on miRNA regulation.

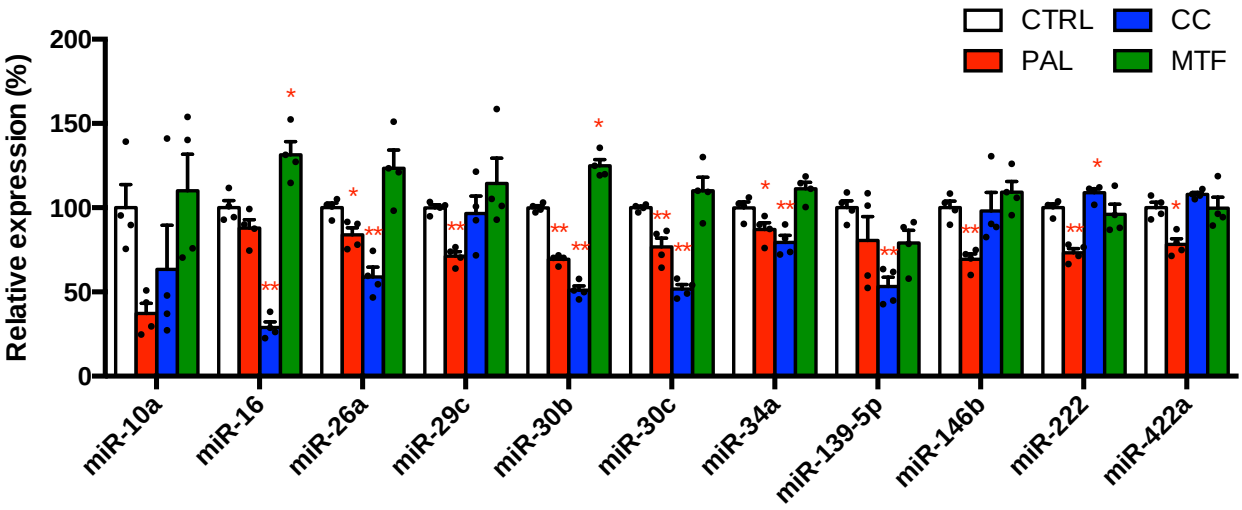

Figure 31. Altered expression levels of miRNA candidates in HepG2 treated cells. Mean ± SEM. *p<0.05, **p<0.01.

5.2.3.2. AMPK silencing: effects *in vitro*

As miRNA profiles in hepatocytes were so widely affected by treatments mirroring NAFLD and leading to AMPK modulation, next experiments were focused on investigating which mechanism could underlie the observed effects, linking treatments mirroring NAFLD to AMPK disruption. Taking into account that CC is not a completely specific AMPK inhibitor, and thus part of its impact could represent off-target effects, HepG2 were subjected to lentiviral particles containing short-hairpin able to inhibit AMPKα1/2 isoforms. miRNA expression and the metabolic commitment of the cells subjected to AMPK knockdown were assessed.

Lipid droplet staining disclosed a significant overload in FA accumulation when AMPK was inhibited (**Figure 32a**).

AMPK KD was verified through qRT-PCR, where expression of *PRKAA1* gene, codifying for AMPK protein, was significantly downregulated in knockdown cells compared to control (fold-change 0.77, $p<0.01$) (**Figure 32b**). In agreement with our previous results, partial ablation of AMPK resulted in enhanced lipogenesis represented by increased expression of genes related to FA biosynthesis (*ACSL1*, fold-change 1.21 and *FASN*, fold-change 1.35), and FA uptake (*CD36*, fold-change 1.24). No changes were reported in *GLUT*2, while inflammation markers analysed disclosed a significant decrease in *TNFA* and increase in *ITGAX* (**Figure 32b**).

miRNA analysis of candidates previously validated in HepG2 challenged with PA, CC and Mtf, disclosed again an overall downregulation in AMPK-KD cells compared to controls, where 9 out of 12 miRNAs analysed (miR-10a, miR-26a, miR-29c, miR-30b, miR-34a, miR-139, miR-146b, miR-222 and miR-422a) appeared to be significantly downregulated in AMPK-KD condition (**Figure 32c**).

Finally, AMPK KD was also confirmed at protein level, together with a significant increase in FAS protein levels (**Figure 32d**). Protein analysis results matched therefore with gene expression data, where *PRKAA1* and *FASN* expression was downregulated in AMPK-KD HepG2 cells.

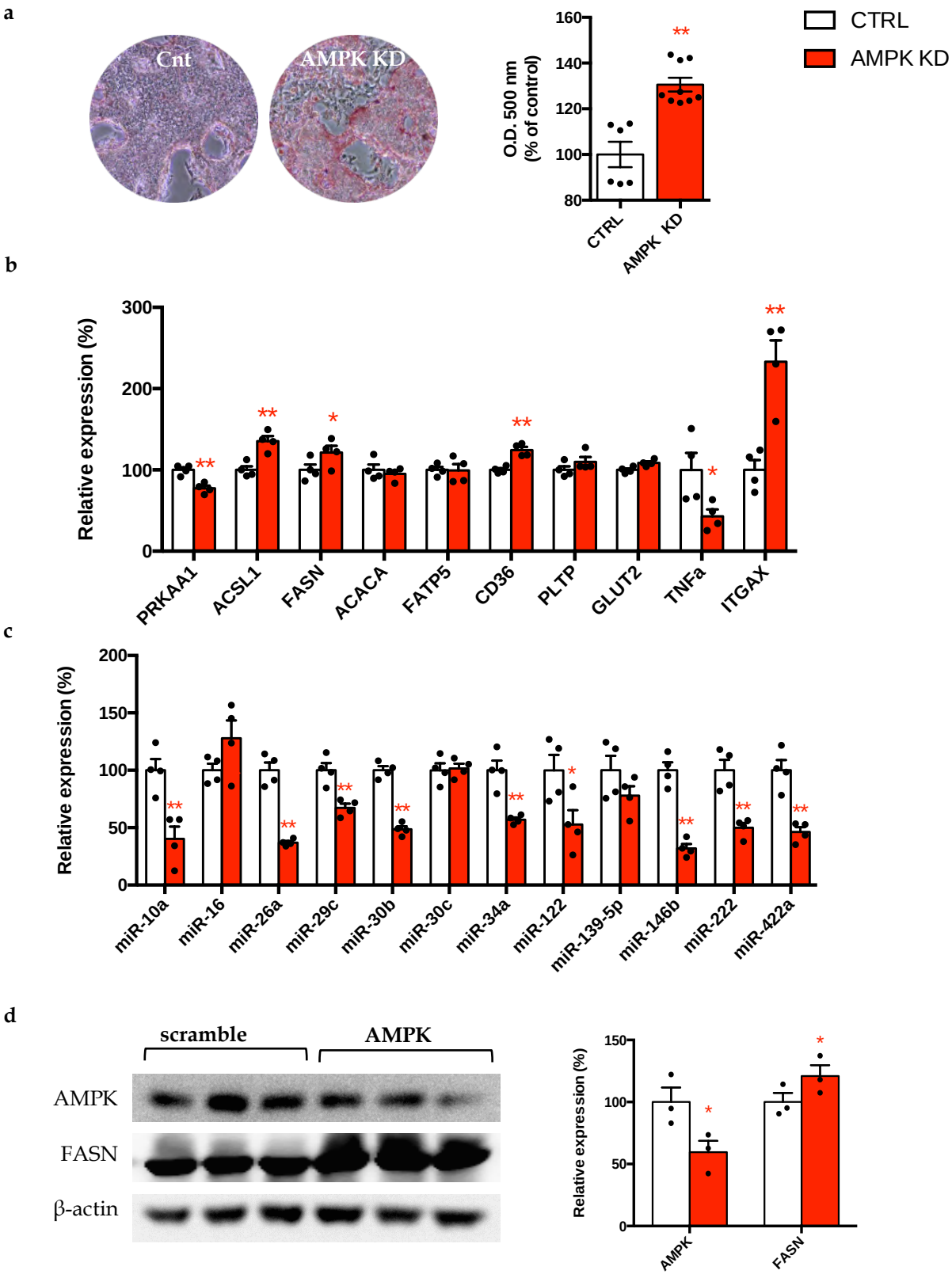

Figure 32. AMPK knockdown (KD) induce lipid accumulation in hepatocytes. a) Oil Red O staining of AMPK KD and control cells. Optical density (OD) was measured at 500 nm. **b)** Gene expression measures in AMPK (a.k.a. PRKAA1) KD vs. control. **c)** Impact of genetic modifications on the expression levels of miRNA candidates in AMPK KD vs. control. **d)** Representative western images of AMPK, FASN and β-actin (as endogenous control) of AMPK-KD HepG2 cells compared to scramble control (left panel) and quantification of AMPK and FAS protein levels with respect to β-actin (right panel). Mean ± SEM. *p<0.05, **p<0.01.

5.2.3.3. AMPK silencing: effects *in vivo*

To elucidate the contribution of AMPK activity on miRNA regulation *in vivo*, rodent models of AMPK modulation were performed. Tail vain injection was the approach employed to achieve liver-specific AMPK knockdown through lentiviral particles harbouring a dominant negative isoform of AMPKα (AMPK-DN).

In order to confirm AMPK silencing, hepatic levels of pACC protein were analysed. AMPK is known to mitigate triglyceride accumulation in the liver due to its ability to phosphorylate ACC and consequently block its dimerization[283]. These will be translated in reduced DNL rates. Western blot disclosed that pACC levels were significantly reduced after the injection of lentiviral particles harbouring AMPK-DN when compared with mice treated with GFP lentivirus (**Figure 33a**).

In keeping with the inhibition of the liver AMPK and the reduced pACC levels, increased hepatic triglyceride content was detected in mice treated with Lv-AMPK-DN lentivirus, measured either by Oil Red staining (**Figure 33b**) or triglyceride quantification in hepatic tissue by immunohistochemistry (**Figure 33c**)

Referring to gene expression, after injection of Lv-AMPK-DN it was detected an increase in lipogenic genes such as *Acsl1* or *Fasn*, and decreased *Glut2* mRNA. At the same time, genes involved in miRNA biosynthesis were also analysed, disclosing a significant downregulation of *Drosha* and *Ago2* and upregulation of *Dicer* and *Xpo5* (**Figure 33d**).

As expected, coupled with gene expression modulation, it was detected a marked decrease in miRNA levels, being miR-10a, miR-16, miR-26a, miR-30b, miR-30c, miR-34a, miR-222 and miR-422a statistically significant compared to control mice (**Figure 33e**).

Thus, impaired AMPK activity resulted also in a significant deregulation of overall miRNA levels *in vivo*, being tightly linked to increased FA metabolism. Hence, current *in vivo* analysis strongly supported our findings *in vitro*, linking AMPK to miRNA biosynthesis.

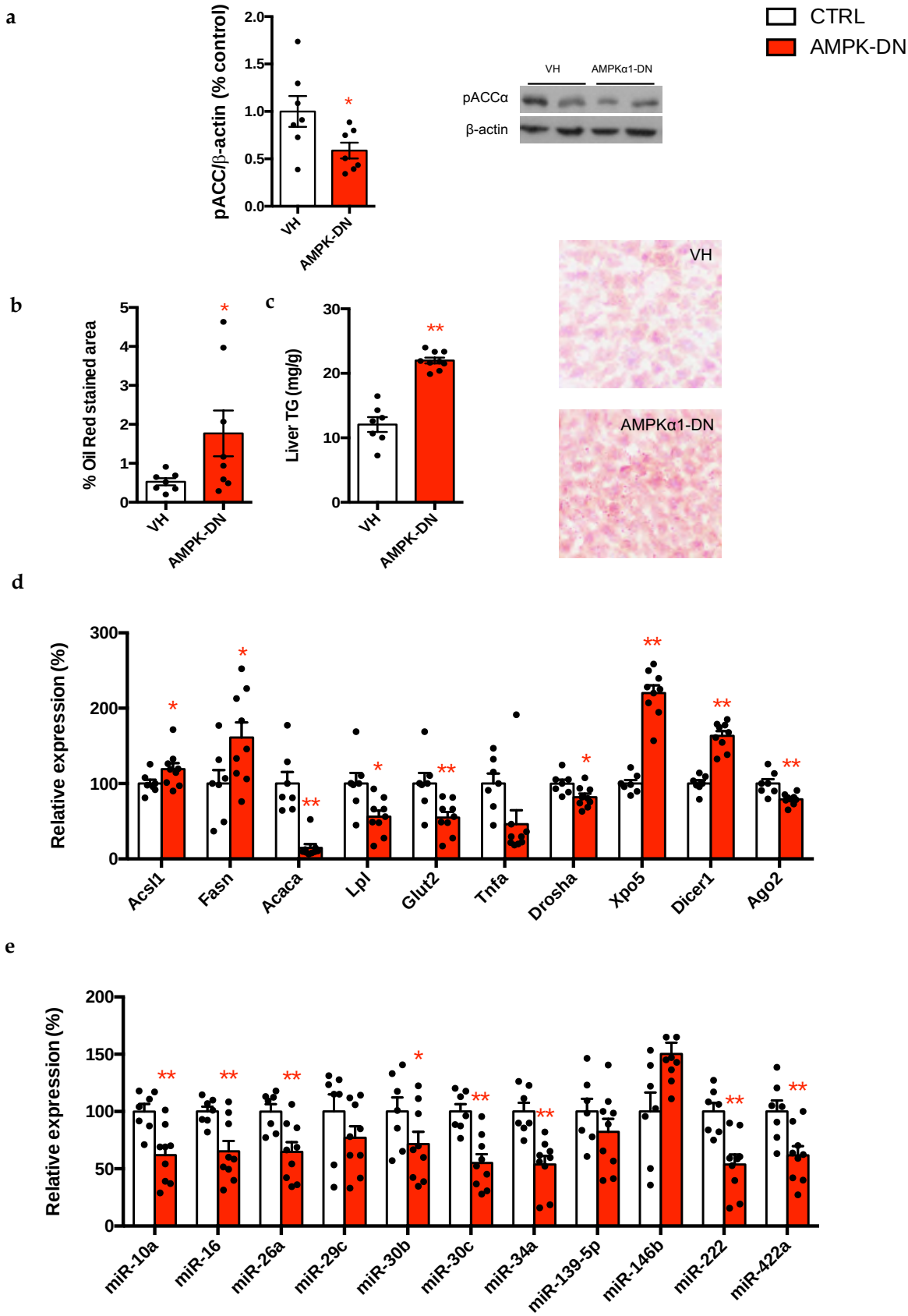

Figure 33. AMPK knockdown (KD) *in vivo*. a) Hepatic levels of phosphor (p)-ACC protein levels normalized by actin levels. **b)** Percentage of the Oil Red O stained area in the liver. **c)** Triglyceride content in the liver normalized by grams of tissue. **d)** Gene and **e)** miRNA expression in mice subjected to tail-injection of AMPK sh-RNA lentivirus (AMPK-DN, n=9) vs. vehicle (VH, n=7). Mean ± SEM. *p<0.05, **p<0.01, ***p<0.001.

5.3.3. DICER may be required for the regulatory activity exercised by AMPK

Given that so far direct AMPK inhibition resulted in miRNA downregulation and higher lipogenesis, associated with dysregulation of genes involved in miRNA biosynthesis pathway, independent knockdown of *DICER* through lentiviral particles in HepG2 cells was also performed. While previously AMPKα1/2 KD was tested to confirm that chemical inhibition of AMPK pathway through CC antagonist was specific *in vitro*, DICER KD was used to ascertain that miRNA downregulation could trigger similar effects on cell phenotype, thus meaning increased FA load. Notably, decreased *DROSHA* and *DICER* in both HH and HepG2 cells upon PA or CC treatments was further highlighted by the opposite upregulation exercised by Mtf at least in HH (**Table 23**). Therefore, given that chemical inhibition of AMPK resulted in impaired expression of miRNA-processing enzyme *DICER*, it was sought to study whether this key regulator was also involved in lipid deposition.

Lipid droplet staining disclosed a significant overload in FA accumulation when DICER was inhibited (**Figure 34a**).

Specific KD of DICER was accomplished in HepG2 cells by shRNA expressing lentiviral particles. DICER KD was verified through qRT-PCR, where expression of *DICER* gene, codifying for DICER enzyme, was significantly downregulated in knockdown cells compared to controls (fold-change 0.79, $p<0.01$). Interestingly, decreased *DICER* depicted similar effects as the knockdown of AMPK in hepatocytes, including enhanced expression of *ACSL1, FASN, CD36* and *PLTP* (**Figure 34b**).

Accordingly, anomalous gene expression levels were coupled to an overall miRNA downregulation, with consistent decrease of miR-16, miR-26a, miR-29c, miR-30b, miR-30c, miR-34a, miR-146b and miR-222 (**Figure 34c**).

Thus, impaired AMPK and/or DICER activity may play functional roles in decreased miRNA biosynthesis and the metabolic disruption affecting hepatocytes under conditions leading to increased FA deposition and the acquisition of NAFLD traits.

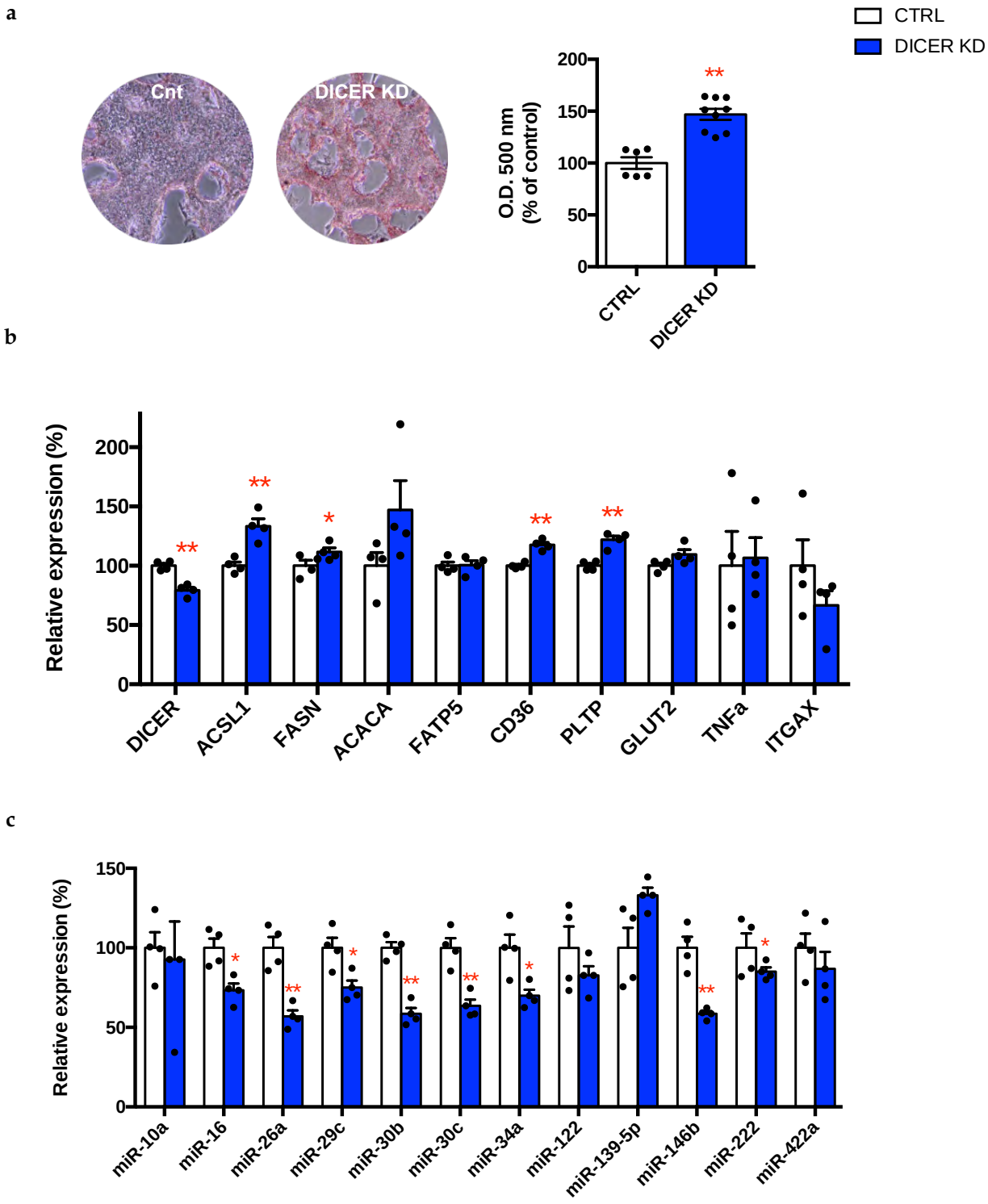

Figure 34. DICER knockdown (KD) induce lipid accumulation in hepatocytes. a) Oil Red O staining of DICER KD and control cells. Optical density (OD) was measured at 500 nm. **b)** Gene expression measures in DICER KD vs. control. **c)** Impact of genetic modifications on the expression levels of miRNA candidates in DICER KD vs. control. Mean ± SEM. *p<0.05, **p<0.01.

5.3. miRNA CANDIDATES MAY RESCUE FATTY ACID OVERLOAD IN HEPATOCYTES

The main objective of this part was to assess whether impaired hepatic miRNA expression detected previously both in human samples, animal and cellular models was at the forefront of changes in gene expression and subsequent synthesis and deposition of FA in hepatocytes. As previously mentioned in "*Introduction*" section, miRNA function is based on transcriptional regulation, and miRNA targets can be predicted by searching for complementarity regions in 3'UTR of plausible target genes. Once matched, miRNAs have the ability to trigger either translational repression or mRNA cleavage, both eventually disclosing mRNA decreased expression.

Taking into account that our previous results, including human samples or models resembling NAFLD, reported mostly a downregulated miRNA profile associated with NAFLD condition, only mimic miRNAs (meaning chemically synthesized, double-stranded RNAs which mimic mature endogenous miRNAs after transfection into cells) were specifically employed to perform next experiments.

Thus, to study miRNA candidates' functionality, both HepG2 and Huh7 hepatoma cell lines were transfected with mimic miRNAs or a non-targeting control siRNA in order to test which of them deserved further investigations based on their effects at cellular level. The most appealing miRNAs were subjected to an extensive study focused on their involvement in all pathways involved in FA deposition in the liver.

5.3.1. Selection of miRNA candidates involved in lipid metabolism

5.3.1.1. Lipid droplet staining

To study whether the observed changes in candidate miRNAs had a functional significance, HepG2 and Huh7 hepatoma cell lines were transfected with mimic miRNAs or a non-targeting control siRNA (NT). The first approach was based on screening the overall phenotype of the cell upon transfections through lipid droplet (LD) quantification using *Bodipy 493/503*.

It was found that, of twelve miRNA candidates, only treatments with miR-16, miR-30b or miR-30c mimics led to a significant reduction in the content and size of lipid droplets in hepatocytes (**Figure 35**).

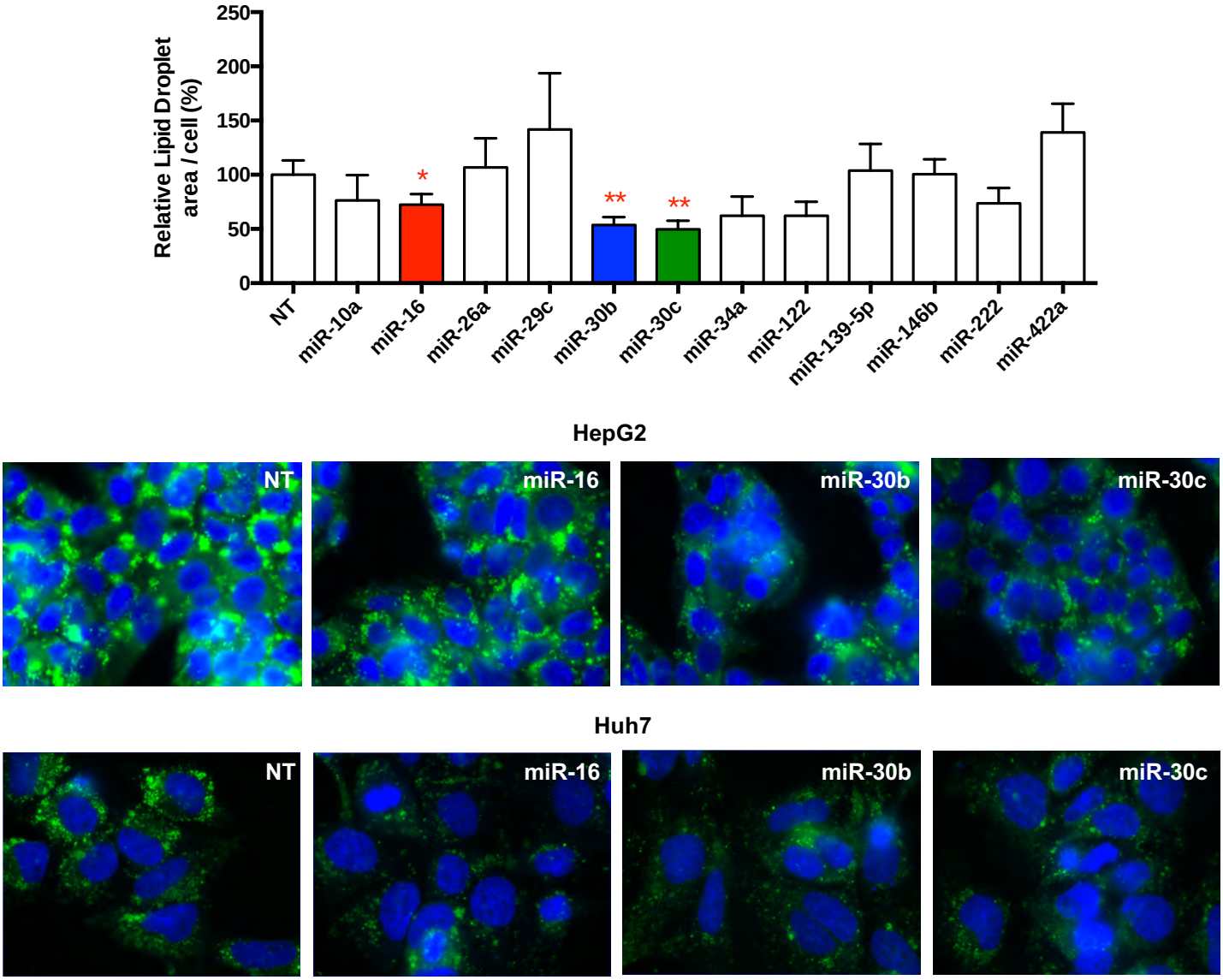

Figure 35. Impact of miRNA candidates on hepatocytes lipid droplets. Lipid droplet staining staining in Huh7 and HepG2 cells transfected with non-targeting (NT) or either miR-16, miR-30b or miR-30b mimic miRNAs. *Bodipy 493/503* (green) and DAPI (blue) report lipid droplets and nuclei, respectively. Bar plots show the average of lipid droplet area vs cell number. *Bodipy 493/503* (green) and DAPI (blue) report lipid droplets and nuclei, respectively. Mean ± SEM. *p<0.05, **p<0.01.

5.3.2. Overexpression of miRNA candidates improves lipid homeostasis

5.3.2.1. Analysis of DNL

Analysis performed by thin layer silica-based chromatography (TLC) showed that ectopic expression of miR-16, miR-30b and miR-30c drove reduced triglycerides, diacylglycerols and cholesterol ester storage in the cells (**Figure 36**).

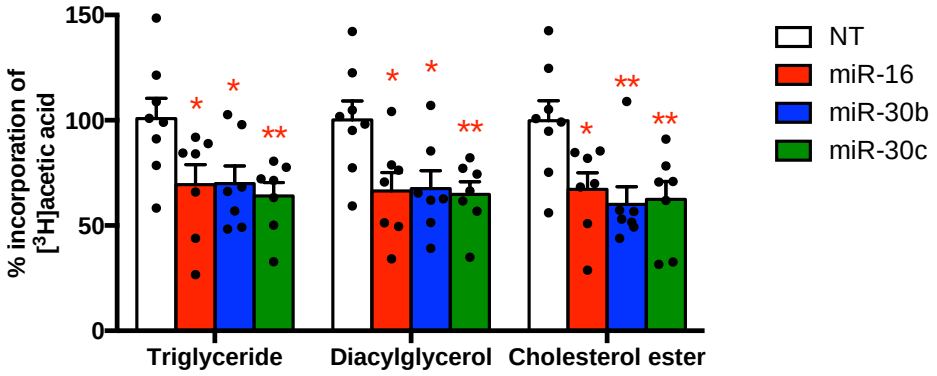

Figure 36. Impact of miRNA candidates on lipid synthesis. Triglyceride, diacylglycerol, and cholesterol esters (c.p.m. per ng protein) measured in transfected HepG2 by thin-layer chromatography. Results were normalized for total protein Mean ± SEM. *p<0.05, **p<0.01.

5.3.2.2. Analysis of triglyceride and cholesterol

Immunosorbent assessment of triglyceride and cholesterol in cell culture media verified significant decreases when cells were treated with miR-30b and miR-30c mimics, but not upon miR-16 mimic (**Figure 37**).

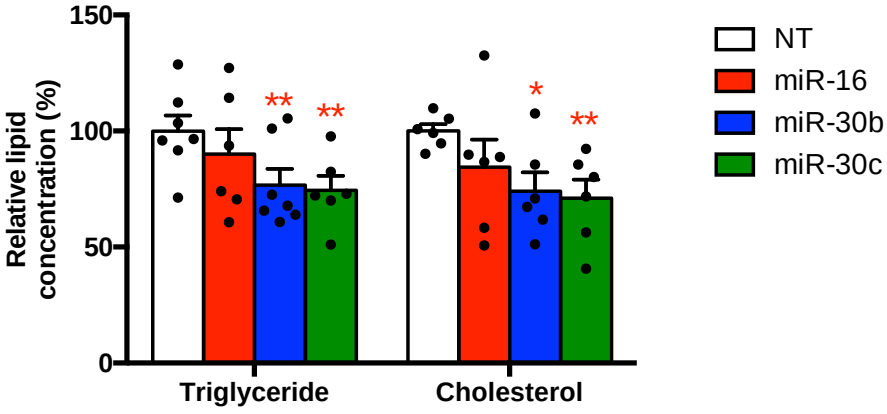

Figure 37. Impact of miRNA candidates on triglyceride and cholesterol. Triglycerides and cholesterol content (mmol/L per ng protein) were measured in culture supernatants. Results were normalized for total protein. Mean ± SEM. *p<0.05, **p<0.01.

5.3.2.3. Analysis of the mitochondrial function

Quantitative analysis of the mitochondrial function (oxygen consumption rate, OCR) of HepG2 transfected cells disclosed that hepatocytes transfected with miR-30b and miR-30c mimics accomplished 26% (p-value<0.05) and 35% (p-value<0.05) increase, respectively, while no significant change of OCR was found in cells transfected with miR-16 mimic (**Figure 38**).

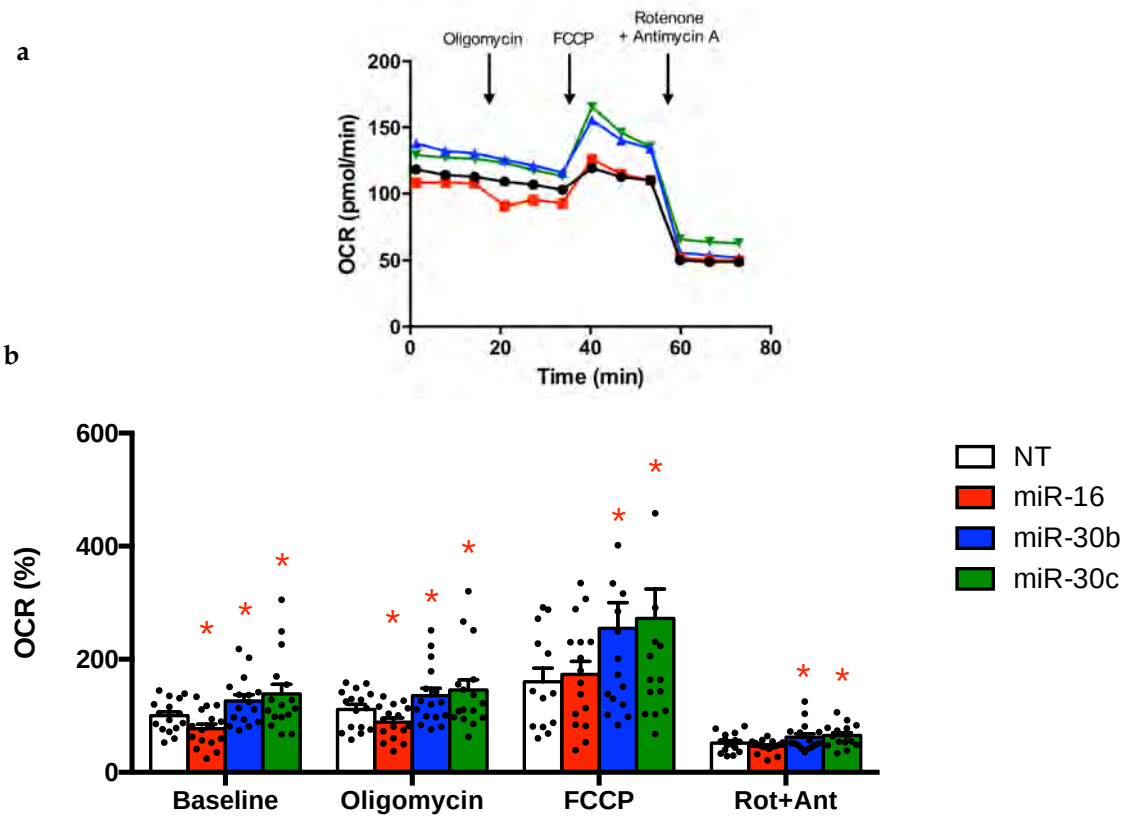

Figure 38. Impact of miRNA candidates on mitochondrial function. a) Oxygen consumption rate (OCR) in NT control (black dots), and HepG2 cells transfected with either miR-16 (red squares), miR-30b (blue triangles), or miR-30c (green inverted triangles) mimics. **b**) Relative oxygen consumption rate normalized by µg protein (pmol/min/µg protein). Mean ± SEM. *p<0.05, **p<0.01.

5.3.2.4. Analysis of VLDL secretion

Levels of apoB were assessed in the media of HepG2 transfected cells, as an indicator of VLDL secretion rates. Results disclosed that miR-30b and miR-30c mimic miRNAs led to decreased apoB levels (**Figure 39**).

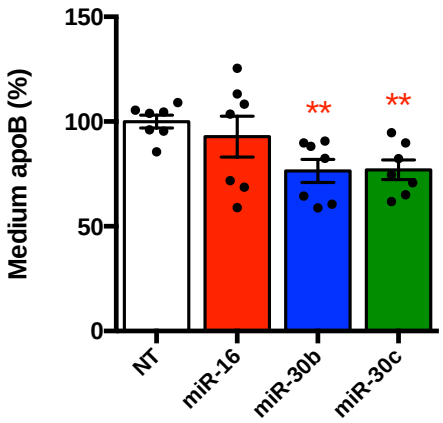

Figure 39. Impact of miRNA candidates on apoB concentration. Apolipoprotein B (apoB) measures (ng/µg protein) in transfected HepG2 and control cells. Mean ± SEM. *p<0.05, **p<0.01.

Altogether, current results pointed that after transient transfections with miR-30b and miR-30c mimics, there was a significant decrease in lipid deposition within hepatocytes, coupled with an increased mitochondrial activity in HepG2 cells. These effects were less prominent after transfection of miR-16.

5.3.3. Overexpression of hepatic miRNA candidates regulates proteins that activate FA metabolism and controls storage

Next, we focused on investigating which mechanisms could underlie the observed effects at the molecular level. Herein, the main objective was to investigate which target genes of miRNA candidates may contribute to the apparent regulation of lipid homeostasis in hepatocytes.

5.3.3.1. *In silico* approaches

miRWalk 2.0 was the chosen database to perform *in silico* predictions of targets from miR-16, miR-30b and miR-30c, since it combines its own algorithm based on prediction within the complete sequence of the target gene, with other 12 existing miRNA-target prediction programs (DIANA-microTv4.0, DIANA-microT-CDS, miRanda-rel2010, mirBridge, miRDB4.0, miRmap, miRNAMap, doRiNA, PITA, RNA22v2, RNAhybrid2.1 and Targetscan)[284]. Besides prediction approaches, miRWalk also collects experimentally verified miRNA-target interaction information.

With that, miRWalk2.0 was employed to extract predicted targets from miR-16, miR-30b and miR-30c. Subsequently, Venn Diagram tool was used to calculate the intersection between the lists of predicted targets for each miRNA. As expected, miR-30b and miR-30c, belonging to the same miRNA family, where sharing most of their targets (5624), while 91 genes were exclusive targets of miR-30b and 107 can be specifically regulated by miR-30c. On the other side, miR-16 has 4170 targets. Nevertheless, the three candidates were sharing 3286 plausible targets, including a wide variety of genes involved in lipid homeostasis (**Figure 40**).

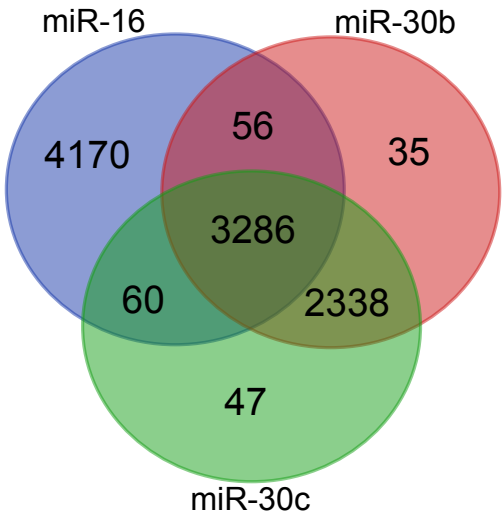

Figure 40. Venn Diagram of predicted target genes for hepatic miRNA candidates. Target genes were combined to elucidate common targets between miRNA candidates.

mirPath v.3 was used to perform miRNA pathway analysis, using both predicted and validated miRNA target genes. Of note, while mirPath can use as input predicted miRNA targets, it can also utilize experimentally validated miRNA interactions derived from Tarbase. Herein, Tarbase was the chosen algorithm to predict the pathways in which the three miRNA candidates could be mostly involved. miR-30b was predicted to be involved in FA biosynthesis (i.e. FASN and other key genes in this pathway are potential target genes) in the highest position, followed by FA metabolism. Same pathways were predicted for miR-30c. With regard to miR-16, it seems to be also potentially involved in these pathways. Merging the three miRNA candidates, FA biosynthesis and metabolism pathways appeared on the top of the list (**Table 25, Figure 41**).

Table 25. Pathways prediction for miR-30b, miR-30c and miR-16.

Position	KEGG pathway	p-value	Genes	miRNAs
hsa-miR-30b-5p				
1	Fatty acid biosynthesis	$1.6x10^{-22}$	FASN, ACSL1, ACSL4	1
2	Fatty acid metabolism	$2.8x10^{-10}$	FASN, ELOVL5, CPT2, FADS2, ACSL1, ACSL4, HSD17B12	1
hsa-miR-30c-5p				
1	Fatty acid biosynthesis	$3.4x10^{-21}$	FASN, ACSL1, ACSL4	1
2	Fatty acid metabolism	$2.9x10^{-9}$	FASN, FADS1, ELOVL5, CPT2, FADS2, ACSL1, ACSL4, HSD17B12	1
hsa-miR-16-5p				
2	Fatty acid biosynthesis	$7.7x10^{-11}$	FASN, ACSL1, ACSL4, ACACA	1
9	Fatty acid metabolism	$1.5x10^{-5}$	FASN, ACADSB, ACSL3, ACOX1, ACOX3, HADHA, CPT1A, PPT1, ELOVL5, FADS2, PPT2, ACSL4, ACACA	1
hsa-miR-30b-5p, hsa-miR-30c-5p, hsa-miR-16-5p				
1	Fatty acid biosynthesis	$<1e^{-325}$	FASN, ACSL1, ACSL3, ACSL4, ACACA	3
2	Fatty acid metabolism	$<1e^{-325}$	FASN, ACADSB, ACSL3, ACOX1, ACOX3, FADS1, HADHA, CPT1A, PPT1, ELOVL5, CPT2, FADS2, PPT2, ACSL4, ACSL1, HSD17B12, ACACA	3

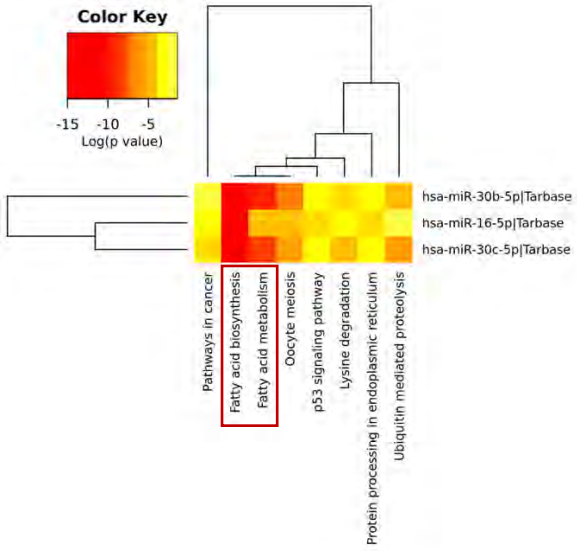

Figure 41. Heatmap and clustering of pathways likely modulated by miRNA candidates in humans. Pathway analysis were performed using experimentally validated miRNA interactions derived from DIANA-TarBase v6.0. Color-scale goes from red (higher significance) to yellow (lower significance).

5.3.3.2. Gene expression

HepG2 transfected cells with miR-16, miR-30b or miR-30c mimics depicted decreased expression of genes coding for factors involved in the synthesis of TAGs. miR-16 transfection disclosed significant decrease of *ACSL1*, *ELOVL5*, *ANGPTL3, AGPAT4*, *SCD5* and *UCP1*, while MBOAT7 appeared upregulated (**Figure 42**). miR-30b and miR-30c reported similar results, showing decreased expression of *ACSL1*, *ELOVL5, ANGPTL3*, *AGPAT4*, *SCD5, DGAT1, DGAT2* and *UCP1*. Both miRNAs also reported a significant upregulation of *MBOAT7* and *CPT1a* (**Figure 42**).

Of note, expression of two genes directly related to the development of NAFLD, angiopoietin like 3 (*ANGTPL3*), a liver-secreted protein recently identified as a marker of NAFLD in both mice and humans[285], and the membrane-bound O-acyltransferase 7 (*MBOAT7*), the disruption of which has been linked to liver disease[85], showed significant down and upregulation, respectively (**Figure 42**). In line with changes affecting mitochondrial activity, we found an increase of *CPT1a* mRNA in cells treated with miR-30b or miR-30c mimic.

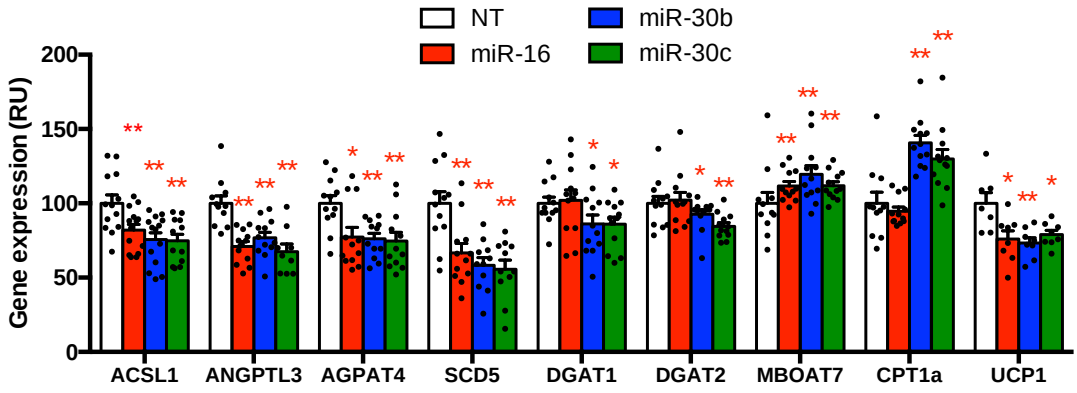

Figure 42. Impact of miRNA candidates on gene expression. Expression of genes involved in lipid metabolism upon treatments with mimic miRNA candidates. Mean ± SEM. *p<0.05, **p<0.01.

5.3.3.3. Validation of miRNA target genes

5.3.3.3.1. The luciferase assay

Once identified a wide variety of genes that were affected after transient transfection of miRNA mimics, 3'UTR binding sites for our miRNA candidates were pursued in order to be experimentally validated. It is worth mentioning that downregulation of a gene does not imply a direct interaction with the miRNA. Plausible 3'UTR binding sites for

candidate miRNAs were explored along genes involved in lipid metabolism. In fact, 3'UTR binding sites were identified in the mRNA coding for ACSL1. Consequently, miR-16, miR-30b and miR-30c target sequences of ACSL1 were mutagenized triggering site-specific mutation that will eventually block the binding between the miRNA and the 3'UTR of the gene (**Figure 43**).

ACSL1 WT 3'UTR	5'- AUUCUGCAGCUGUC**UGCUGCU**C -3'
miR-16-5p	3'- GCGGUUAUAAAUGC**ACGACGA**U -5'
ACSL1 mut 3'UTR	5'- AUUCUGCAGCUGUC**GCUAUGC**C -3'
ACSL1 WT 3'UTR	5'- UCAUGUUGCAGACC**AUGUUUA**UG -3'
miR-30b-5p	3'- UCGACUCACAUCC**UACAAAU**GU -5'
miR-30c-5p	3'- CGACUCUCACAUCC**UACAAAU**GU -5'
ACSL1 mut 3'UTR	5'- UCAUGUUGCAGACC**GCCGGGG**UG -3'

Figure 43. Wild-type and mutated 3'UTR of ACSL1. Specific binding sites for either miR-16 or miR-30b/c were mutagenized to trigger site-specific mutations.

Huh7 cells were subsequently transfected with the wildtype (WT) ACSL1 3'UTR dual luciferase reporter or mutated ACSL1 3'UTR (mut), together with the miRNA mimics. Results showed a significant reduction of the luciferase signal upon transfection with miRNA mimic candidates. Notably, luciferase activity was not modified in cells transfected with a mutated ACSL1 3'UTR reporter construct, hence confirming specific binding between the current miRNA candidates (**Figure 44**).

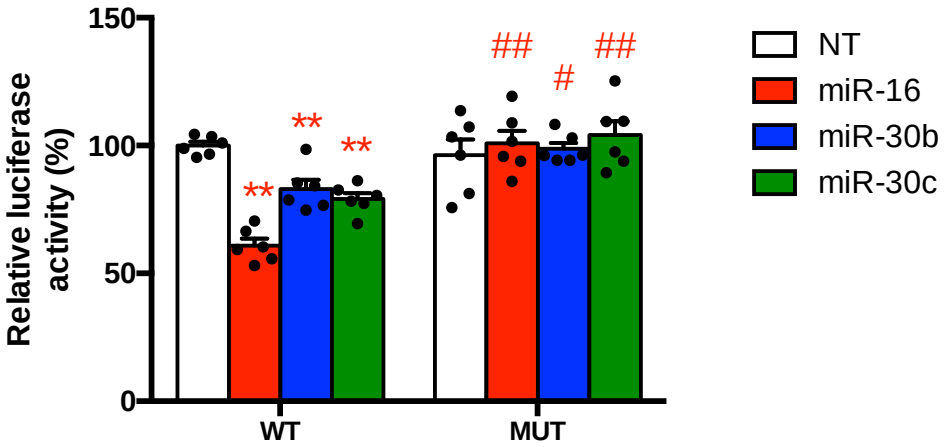

Figure 44. miR-16, miR-30b and miR-30c directly targeted the 3'UTR of ACSL1. Huh7 cells transfected with a wildtype control (WT) ACSL1 3'UTR dual Luc reporter or mutated ACSL1 3'UTR (MUT), together with a non-targeting control siRNA (NT) or miRNA mimics (miR-16, miR-30b, miR-30c). Firefly Luc activity normalized for Renilla signal is shown. Mean ± SEM. *p<0.05, **p<0.01.

5.3.3.3.2. Protein target validation by immunobloting

Western blot was also performed to validate target gene regulation by miRNA candidates. Accordingly, ACSL1 protein analysis endorsed the luciferase results, thus confirming the causal relationship suggested by the complementary sequences (**Figure 45**).

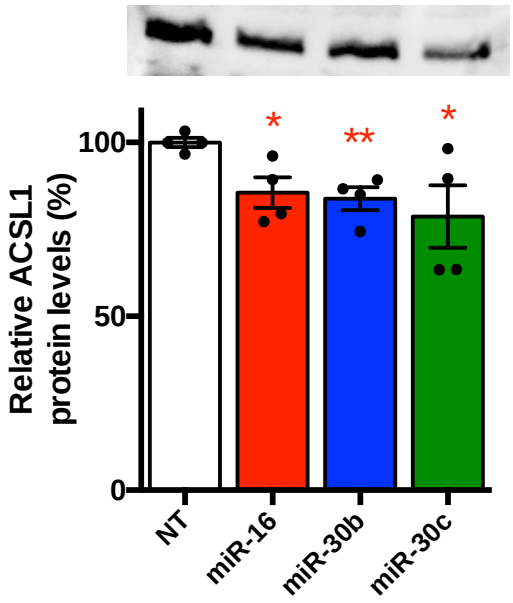

Figure 45. miR-16, miR-30b and miR-30c downregulate ACSL1 protein levels. Western blot results for ACSL1 in HepG2 cells after transfection with NT control or miRNA mimics. The ACSL1 signal was quantified and normalized against total protein in 2 independent experiments. Mean ± SEM. *p<0.05, **p<0.01.

These data depicted the involvement of the negative regulation of this enzyme in mechanisms leading to decreased lipogenesis upon treatment of hepatocytes with miR-16, miR-30b and miR-30c mimics.

5.3.4. Overexpression of potential miRNA candidates modulates the sphingomyelin/ceramide ratio

To obtain an overview of the effects accomplished by miRNA mimic transfections on the cellular lipidome of human hepatocytes, total lipids directly extracted from the cells were subjected to quantitative direct flow injection electrospray ionization tandem mass spectrometry (ESI-MS/MS). Results obtained from treatments with miR-16, miR-30b and miR-30c mimics were individually compared to control. Principle component analysis (PCA) discriminated miR-16 from miR-30b and miR-30c treatments (**Figure 46**).

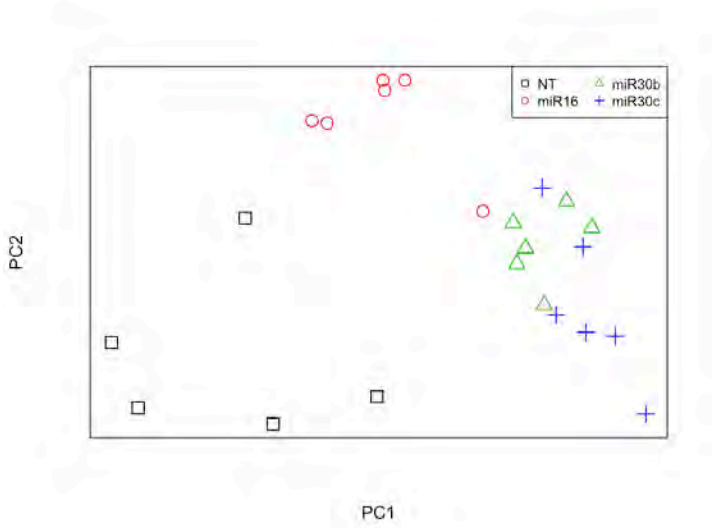

Figure 46. Principle component analysis (PCA) discriminates miR-16 from the miR-30 family. Global lipidome results were subjected to PCA analysis. Six replicates per group were analysed. Squares representing non-targeting (NT) control, circles for miR-16, triangles for miR-30b and crosses for miR-30c.

Accordingly, heatmap analysis also reported a similar lipidome profile when HepG2 were transfected with either miR-30b or miR-30c mimics, discriminating from miR-16 transfected cells. Consistent reduction of phosphatidylethanolamine plasmalogens (PE P) and ceramides (Cer), together with an increase of sphingomyelins (SM), were observed after the ectopic overexpression of miR-30b and miR-30c, the changes accomplished by miR-16 being less prominent (**Figure 47a, Figure 47b**).

a

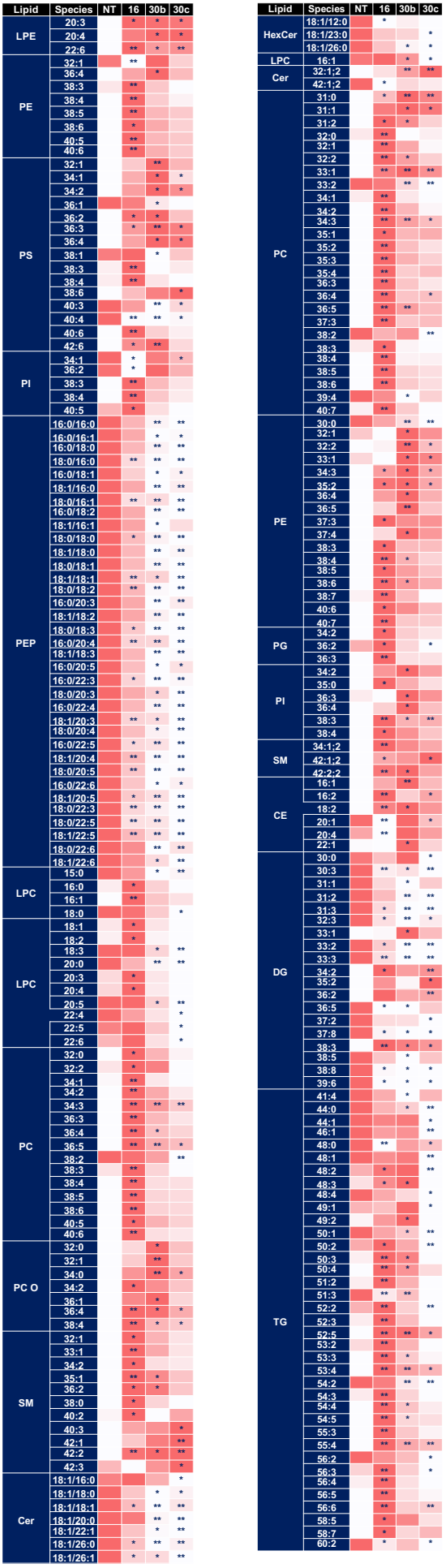
Lipid
Species
NT
16
30b
30c
LPE
PE
PS
PI
PEP
LPC
PC
PC O
SM
Cer
HexCer
Low levels
High levels
* p-val<0.05
** p-val<0.01

b

Abbrev.	Lipid Class	Lipid Category	Method	miR-16	miR-30b	miR-30c
LPE	Lysophosphatidylethanolamine	Glycerophospholipids	QQQ	37.6	34.7	34.1
PE	Phosphatidylethanolamine	Glycerophospholipids	QQQ	7*	3.9	-0.3
PS	Phosphatidylserine	Glycerophospholipids	QQQ	7.5*	2.6	-1.1
PG	Phosphatidylglycerol	Glycerophospholipids	QQQ	26.8	19.4	11.4
PI	Phosphatidylinositol	Glycerophospholipids	QQQ	7.1*	4.1	0.2
PE P	based plasmalogens	Glycerophospholipids	QQQ	-33.2**	-51.6**	-55.4**
LPC	Lysophosphatidylcholine	Glycerophospholipids	QQQ	23.6*	-1.6	-7.6
PC	Phosphatidylcholine	Glycerophospholipids	FTMS	12.5	4.7	0.7
PC O	Phosphatidylcholine-ether	Glycerophospholipids	FTMS	-4.8	-19.7	-17
SM	Sphingomyelin	Sphingolipids	FTMS	15.1**	15.1*	10.4*
Cer	Ceramide	Sphingolipids	QQQ	-1.7	-7	-11.6*
HexCer	Hexosylceramide	Sphingolipids	QQQ	-24.3**	-25.6**	-30.1**
CE	Cholesteryl Ester	Sterol Lipids	FTMS	1.5	6.9	2.2
DG	Diacylglycerol	Glycerolipids	FTMS	-6	-7.8	-9.4
TG	Triacylglycerol	Glycerolipids	FTMS	10.8**	0.8	-9**
FC	Free Cholesterol	Sterol Lipids	FTMS	-1.4	-3.6	-6.3

* p-val<0.05
** p-val<0.01

Figure 47. Impact of miR-16, miR-30b and miR-30c on specific lipid species. a) Lipid classes and families significantly affected by treatment in HepG2 cells. The color-scale indicates the intensity of changes. **b)** Lipid species grouped in families significantly affected by miR-16, miR-30b and/or miR-30c mimics.

The findings at lipidome level were further investigated at gene expression level. Taking into account the most modified lipid species based on the cellular lipidome, next investigations were focused on analysing the gene expression modulation of key genes involved in the synthesis or degradation of such species, hypothesizing the plausible role of miRNA candidates in post-transcriptionally modulating them.

Herein, genes involved in either synthesis and/or degradation of lipid species were analysed by qRT-PCR. Glyceronephosphate O-acyltransferase (GNPAT) and alkylglycerone phosphate synthase (AGPS) were analysed as enzymes involved in the biosynthesis of PE P (**Figure 48a**). Sphingomyelin synthases (SGMS) isoforms, SGMS1 and SGMS2, were analysed as the ones involved in the synthesis of sphingomyelins. Referring to ceramides class, sphingomyelin phosphodiesterases (SMPD) isoforms, SMPD2 and SMPD3 were analysed for their involvement in ceramides synthesis from sphingomyelins, and UDP-glucose ceramide glycosyltransferase (UGCG) and ceramide galactosyltransferase (UGT8) involved in hexosyl-ceramides synthesis. Therefore, lipidome findings were strongly supported by consistent changes in the expression of key enzymes related to the synthesis/degradation of sphingomyelins and ceramides, disclosing elevated expression of SGMS1 and SGMS2 mRNAs, and decreased SMPD1 in HepG2 cells treated with miR-30b or miR-30c mimics (**Figure 48c, Figure 48d**). Besides these gene expression makers and considering previous results of miRNA candidates on

LD formation, several key genes involved in this procedure were also analysed: perilipin 1 (PLIN1), seipin (BSCL2), solute carrier family 25 member 1 (SLC25A1) and mannosyl (alpha-1,3-)-glycoprotein beta-1,2-N-acetylglucosaminyltransferase (MGAT1). Results reported that the expression of PLIN1, SLC25A1 and MGAT1 was also compromised by both miR-30b and miR-30c, while miR-30b also reduced BSCL2, an endoplasmic reticulum-resident protein of key importance in neutral lipid storage in lipid droplets, droplet morphology and the morphological changes in adipocytes and hepatocytes resulting from increased lipid accumulation[286] (**Figure 48b**).

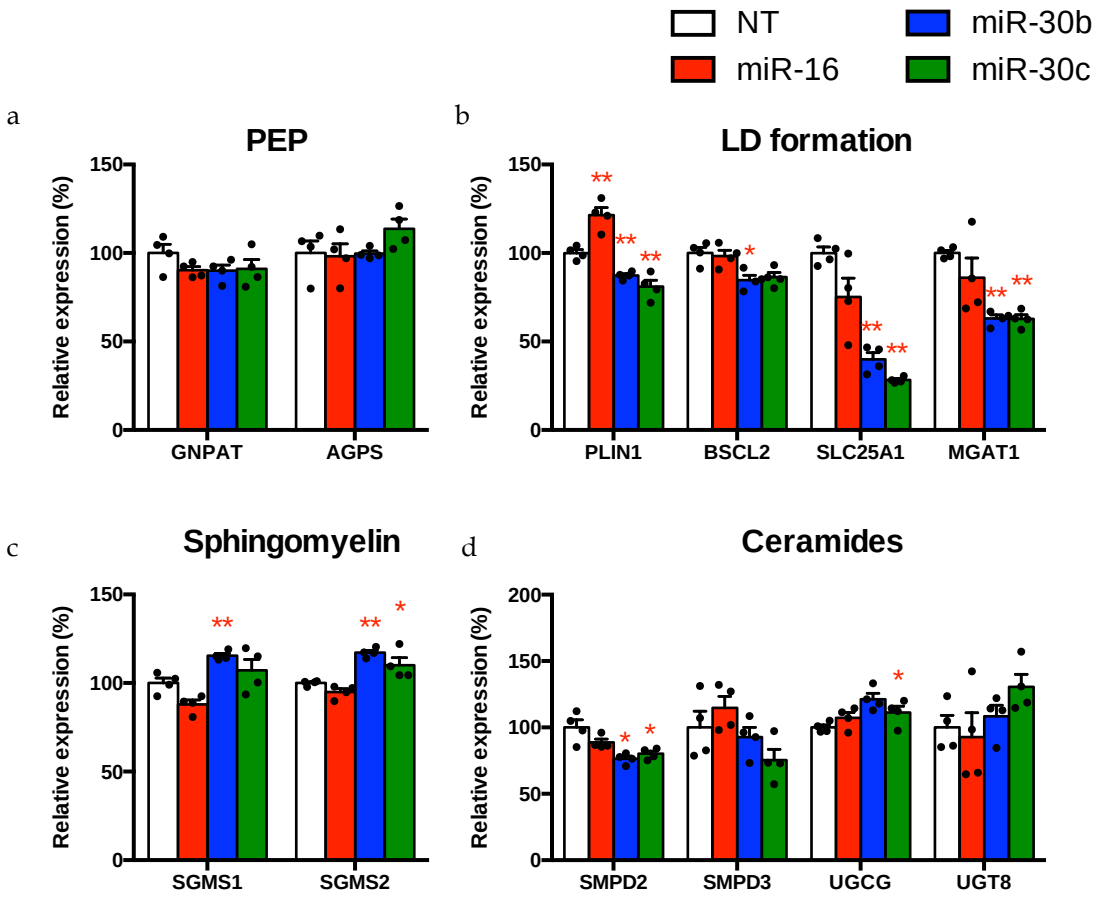

Figure 48. Impact of miR-16, miR-30b and miR-30c on key genes involved in the amount of different lipid species. mRNA expression measures of genes related to the synthesis and degradation of **a)** phosphatidylethanolamine plasmalogens (PEP), **b)** lipid droplet (LD) formation, **c)** sphingomyelins and **d)** ceramides. Mean ± SEM. *p<0.05, **p<0.01.

5.3.5. Recovery of miR-30b and miR-30c acts against FA accumulation in hepatocytes

Considering that the most consistent results appeared to be using miR-30b and miR-30c mimics, and its downregulation was found to be associated with NAFLD and treatments that mimicked this condition (pointing the loss of these unique miRNA species at the forefront of the imbalance of lipid homeostasis in hepatocytes), we wanted to see whether their recovery restored lipid deposition after treatments triggering FA overload. Consequently, conditions triggering FA overload were combined with transfections with miR-30b and miR-30c mimics. AMPK and DICER KD HepG2 cells used, together with HepG2 control cells challenged with CC, all of them triggering lipid droplet accumulation in the cells.

First, the ectopic expression of both miRNAs was confirmed by qRT-PCR (**Figure 49**).

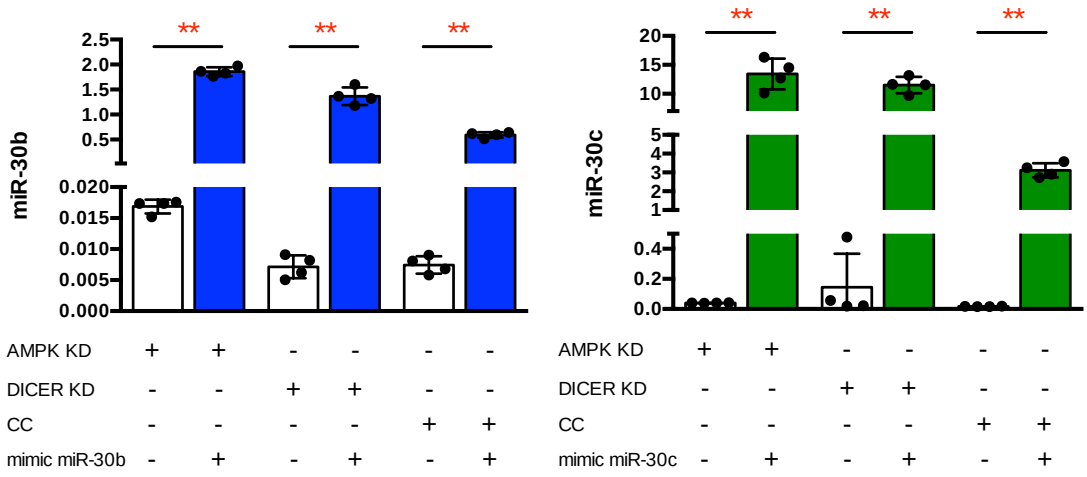

Figure 49. miR-30b and miR-30c expression validation after miRNA mimics in HepG2 cells challenged with treatments inducing FA accumulation. Quantification of miRNAs after mimic transfections in treatments leading to increased FA deposition (i.e. AMPK and DICER knockdown (KD), and Compound C). Mean ± SEM. *p<0.05, **p<0.01.

Once validated miRNA overexpression, lipid droplet staining revealed the ability of miR-30b and miR-30c to reduced TG storage in hepatocytes challenged with CC or knockdown of AMPK and DICER expression (**Figure 50**). Replenishment of miR-30b in hepatocytes lacking AMPK, and treatments of HepG2 cells with either miR-30b or miR-30c challenged with CC, reduced the lipid droplet area (**Figure 50**).

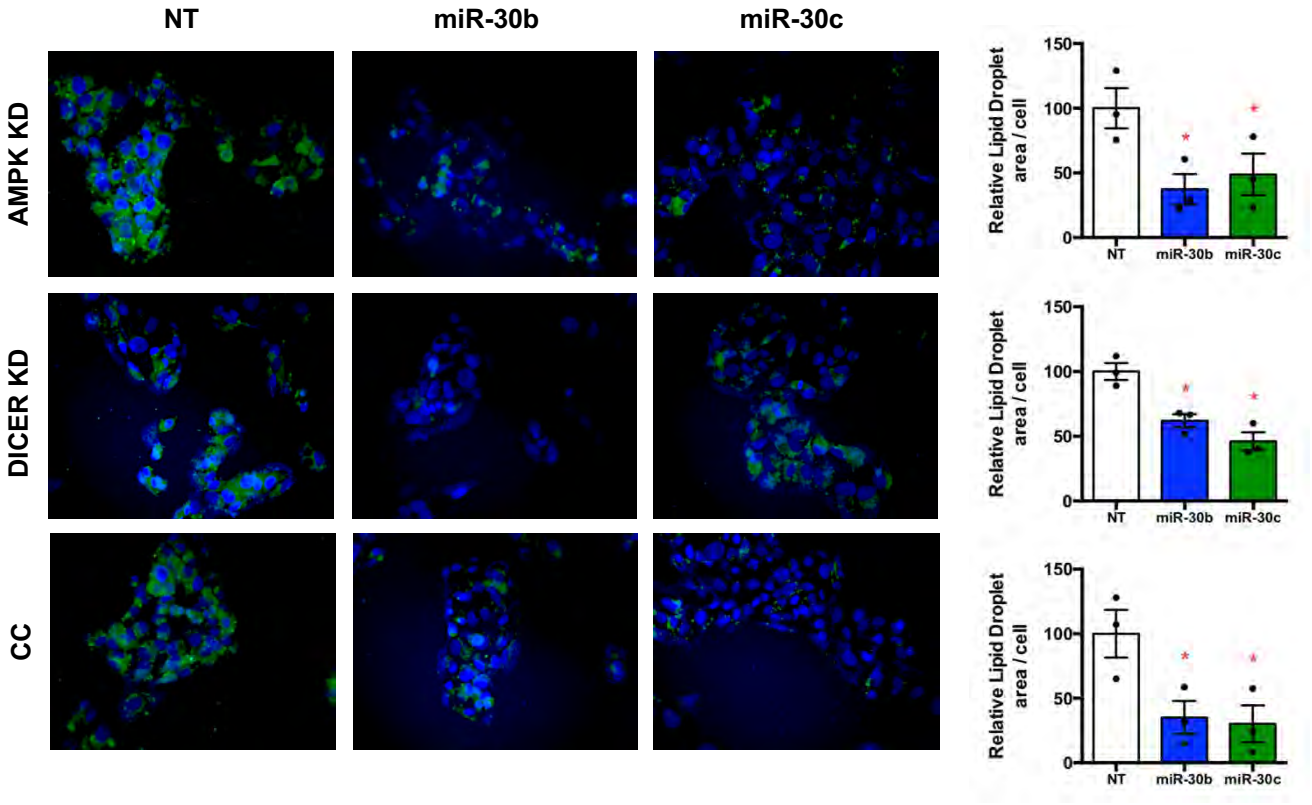

Figure 50. Recovery of miR-30b and miR-30c *in vitro* protects against lipid deposition in hepatocytes. Lipid droplet staining in cells transfected with non-targeting control (NT), miR-30b or miR-30c mimics. *Bodipy 493/503* (green) and DAPI (blue) report lipid droplets and nuclei, respectively. At the bottom, bar plots representing lipid droplet area per cell, the value of NT being set at 100. Mean ± SEM. * $p<0.05$, ** $p<0.01$.

In concordance with LD staining results, transfection of miR-30b or miR-30c mimics into hepatocytes was able to modulate genes involved in FA deposition in hepatocytes. Together with miRNA expression values, it was analysed the expression of genes involved in lipid homeostasis (*ACSL1, FASN, CD36* and *PTLP*) and *GLUT2* representing glucose metabolism. Accordingly, transfection of miR-30b or miR-30c mimics into hepatocytes decreased the expression of *ACSL1* and *FASN* in the three conditions. Additionally, it was reported elevated *GLUT2* mRNA in hepatocytes with AMPK knocked down, suggesting at least partial restoration of glucose intake in this cell model (**Figure 51**).

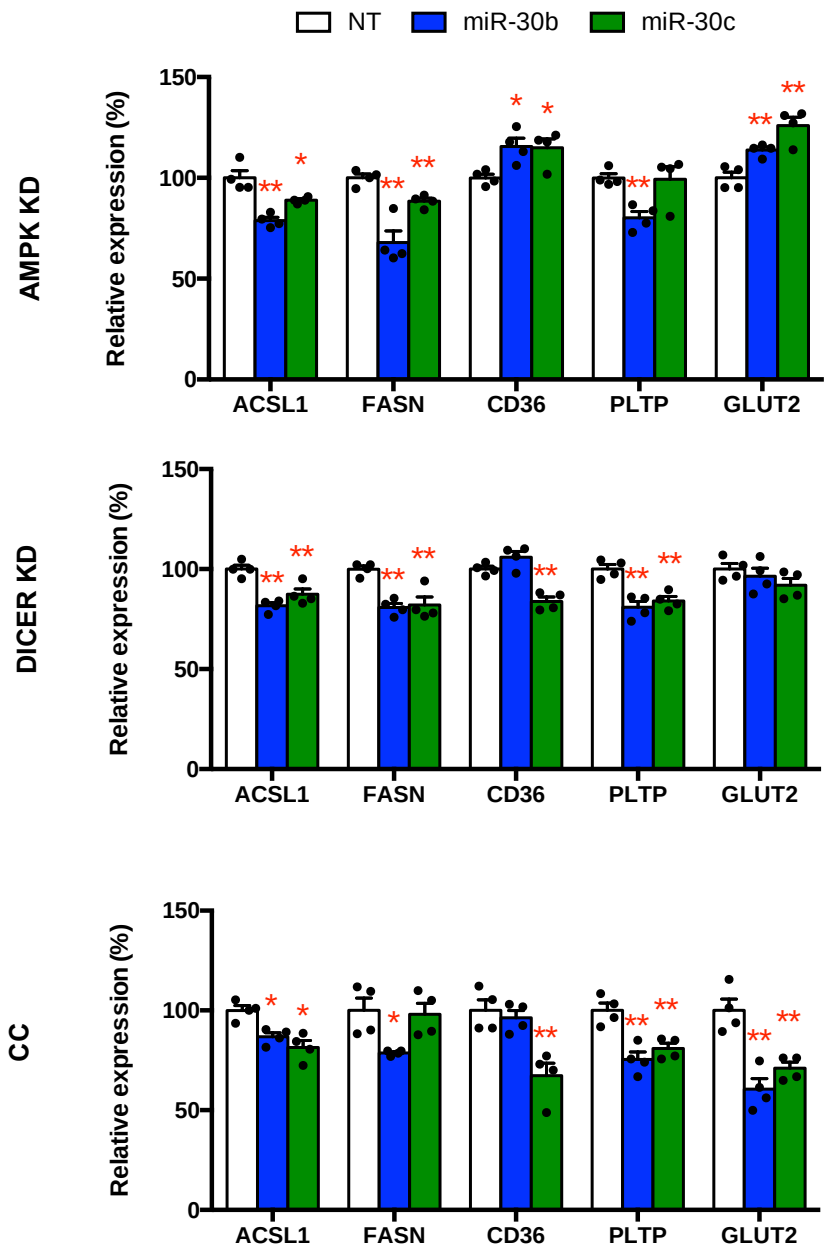

Figure 51. Recovery of miR-30b and miR-30c protects against FA deposition. Quantification of mRNA expression of genes related to lipid biosynthesis and glucose metabolism after mimic transfection in treatments leading to increased FA deposition (i.e. AMPK and DICER knockdown (KD), and Compound C). Mean ± SEM. *p<0.05, **p<0.01.

5.3.6. Expression of hepatic miR-30b and miR-30c is associated with NAFLD

With regard to the translation to humans, qRT-PCR analysis performed in liver samples from obese women with or without NAFLD confirmed significant downregulation in miR-16, miR-30b and miR-30c, together with increased *ACSL1* and decreased *DICER* and *PRKAA1* mRNA in subjects with NAFLD (**Figure 52**).

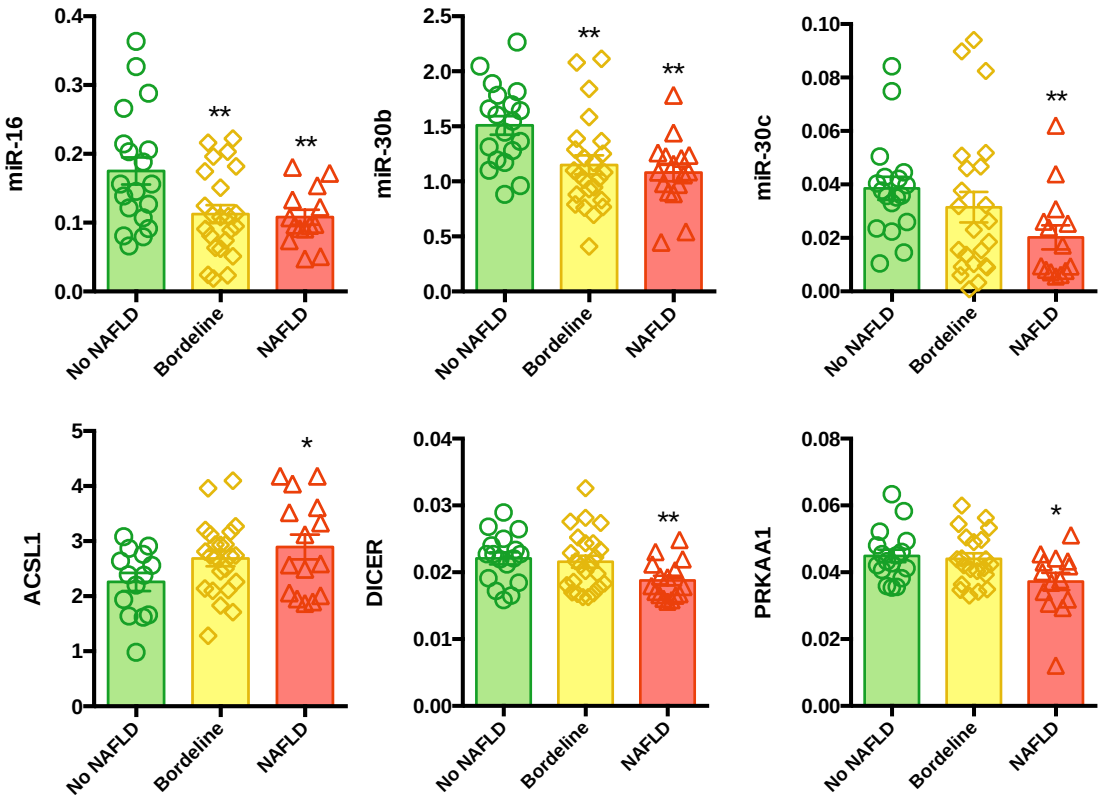

Figure 52. Gene and miRNA expression in no-NAFLD, Borderline and NAFLD. Expression of miR-16, miR-30b, miR-30c, ACSL1 and DICER in liver biopsies. Mean ± SEM. * p<0.05, ** p<0.01.

Moreover, the quantities of the three miRNAs assessed in liver samples were inversely correlated with body mass index and fasting triglycerides, further emphasizing the relevance of these miRNAs as novel candidates to control fatty liver through modulation of FA homeostasis in hepatocytes (**Figure 53**).

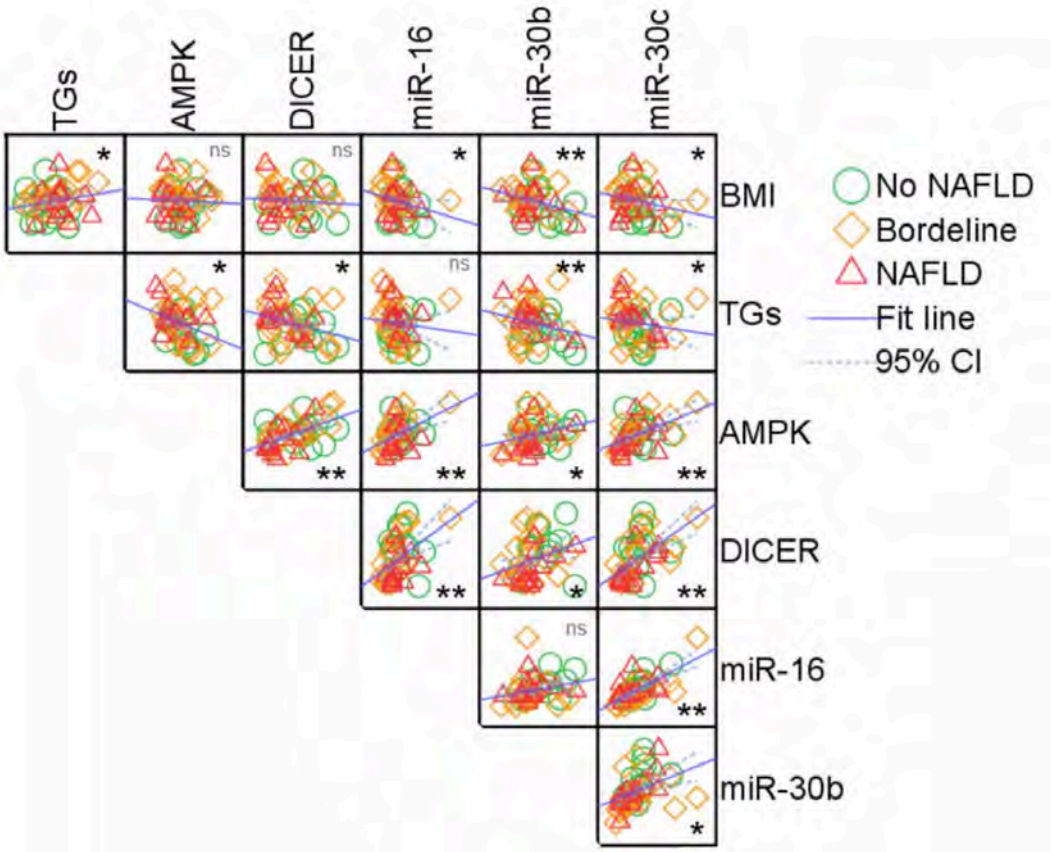

Figure 53. Correlations between miRNAs, genes and clinical parameters in liver biopsies. Spearman's correlations between miRNA and gene expression levels and body mass index (BMI) and fasting triglycerides (TGs). * $p<0.05$, ** $p<0.01$, *ns* stands for non-significant.

6. DISCUSSION

NAFLD is characterized by an extensive reprogramming of hepatic metabolism, where microRNAs can play a major role as epigenetic modulators. The discovery and characterization of miRNAs in pathological conditions has been considered a major biomedical breakthrough[287], since these small molecules can bind complementary regions in coding RNAs, leading to translational repression of several genes[196]. Many of the studies based on miRNA research have focused their potential as biomarkers of systemic diseases, describing specific signatures in different disorders such as obesity[288], type 2 diabetes[289] and NAFLD[199]. Besides being valuable biomarkers found in circulation, miRNAs can also be potential therapeutic targets. Being their regulatory activity coupled to the decreased expression of many target genes, and linearly dependent on the number of target sites harboured by each gene[290,291], a number of studies have unravelled the important role of miRNAs in the knowledge of aspects of health and disease, endorsing their potential as therapeutical targets[198].

In this thesis we provide evidence that NAFLD is associated with altered hepatic miRNA expression, which is tightly connected to AMPK activity. In fact, we postulated that AMPK may regulate FA metabolism through miRNA availability. Considering that potential targets of differentially expressed miRNAs are involved in molecular mechanisms commonly deregulated in NAFLD such as DNL or FA oxidation, the modification of miRNA expression might contribute to improved homeostasis in the liver. Hence, their involvement in NAFLD pathogenesis has been validated by the ectopic replenishment of miRNAs known to be downregulated in NAFLD status, rescuing FA overload and modifying lipid profiles within hepatocytes.

6.1. DECREASED LIPID METABOLISM BUT INCREASED FATTY ACID BIOSYNTHESIS ARE COUPLED WITH CHANGES IN LIVER miRNAs IN OBESE SUBJECTS WITH NAFLD

We provided the cross-sectional identification of at least five hepatic miRNAs significantly associated with NAFLD in obese subjects. Herein, differences between subjects with and without NAFLD included decreased expressions of miR-139-5p, miR-30b-5p, miR-122-5p and miR-422a, and increased miR-146b-5p, running in parallel to impaired histology and circulating liver enzymes. Of note, discriminant analysis revealed that hepatic downregulation of two miRNAs, miR-139-5p and miR-122-5p, may explain more than 29% of NAFLD diagnosis. Indeed, concomitant changes in miRNAs

and measures of gene expression imply the possibility of modulating liver FA through the application of miRNAs, inducing molecular changes with metabolic implications, such as lipogenesis and FA uptake, oxidation and glucose metabolism in hepatocytes. We provide here additional evidence and validation on the association of liver miRNAs with NAFLD pathophysiology, paving the way for further investigations targeting the potential for therapies based on miRNA-related hepatic transcriptional regulation. In miRNA functional studies, cellular models mimicking NAFLD condition disclosed PA and CC *in vitro* treatments as the best models triggering FA accumulation within hepatocytes, which have enabled to gain knowledge of the molecular mechanisms related to progression of NAFLD, coupled to miRNA expression patterns:

- *Increased hepatic FA biosynthesis coupled with changes in miRNAs*

Increased DNL, mainly characterized by enhanced *FASN* and *ACSL1* gene expression in HepG2 cells and HH supplemented with either saturated PA or CC has been identified. Consistent with current results, increased *de novo* FA biosynthesis and enhanced expression of lipogenic enzymes has been reported in liver samples from NAFLD/NASH subjects[292–295]. Previous studies in hepatocytes have also disclosed increased expression of lipogenic enzymes and transcription factors after PA[296] or CC[128] administration. Notwithstanding this, additional research endorsing the evaluation of the expression of lipogenic transcription factors and enzymes involved in FA biosynthesis disclosed that extremely obese subjects may show diminished hepatic lipogenesis during advanced stages of SS, disclosing decreased levels of key proteins such as SREBP1c or FASN[292]. Even though molecular mechanisms are still unclear, experimental studies have reported in mice models that IR can be translated into the inability to stimulate FA biosynthesis, leading to decreased expression of genes involved in the aforementioned pathway[140]. In fact, we could also detect this expression pattern in *FASN* expression levels in the population studied during this doctoral thesis, also comprised by severe obese patients. Despite that, the utilization of saturated FA or CC in hepatocytes is aimed at the increase of DNL commonly found in early NAFLD stages, which is mainly accomplished *in vitro* under these conditions. Besides *FASN* and *ACSL1*, *LPL* mRNA expression has also been detected to be significantly higher. Liver LPL hydrolyses TAGs, contributing to greater increase in hepatic uptake and re-esterification and therefore, worsening SS. In agreement with our data, higher LPL activity in the liver from morbidly obese patients has been reported to contribute to NAFLD[297].

Concomitantly with changes in gene expression patterns, decreased liver miR-139-5p and miR-122-5p in the current study and previous reports[203,293] suggest the potential involvement of miRNAs in NAFLD and changes in liver gene expression modifying FA biosynthesis and glucose metabolism. While miR-139-5p and miR-122-5p have been previously found to be downregulated in fatty liver disease[293], no previous reports have associated miR-30b-5p and miR-422a with NAFLD. So far, the miR-122-5p, a recognized liver-specific miRNA[210], has been widely studied, being significantly decreased in liver samples from NAFLD/NASH patients[293] and mice models of this kind of diseases[298], as well as in obese and diabetic mice[299]. Regulatory miR-122 is known to impact genes involved in hepatic cholesterol and lipid metabolism, having a central role in maintaining FA and glucose homeostasis in liver. Currently, the putative recognition sequences for miR-122 and miR-422a, also decreased in NAFLD samples (current findings) and in HCC[300], were localized in the 3'UTR of human cholesterol 7α-hydroxylase, an enzyme that plays a critical role in cholesterol metabolism and the regulation of bile acid synthesis in the liver[301]. There are also controversial results, reporting that increased miR-122 leads to the progression to advanced stages of fatty liver disease and such comorbidities. As a proof of concept, inhibition of miR-122 results in reduction of circulating cholesterol in both mice[302] and chimpanzees[212]. Previously it was also reported that treatments of PA may trigger increased miR-122 expression levels in parallel to increased *SREPB1c*, *FASN* and *ACACA* in HepG2 cells[303]. Discrepancies in this sense may arise from differences regarding experimental conditions, considering both time and dose exposure, together with the fine-tuned regulation of regulatory elements such as miRNAs. In this respect, Pirola *et al*. found that miR-122 was increased in liver samples of subjects with simple steatosis, followed by systematic downregulation in NASH patients[207]. This suggests that miR-122 could be characterized by significant fluctuations within hepatocytes depending on the state of disease and fat deposition. Noteworthy, changes in this respect did not modify the impact in FA accumulation and the expression of lipogenic genes such as *ChREBP*, *FASN* and *ACACA* in isolated hepatocytes, suggesting alternative mechanisms of regulation. Changes in inflammation, proliferation, FA transport and β-oxidation may be at the crossroad of these associations. So far, the lack of consistency among several studies calls for a broader view of this paradigm, and the evaluation of other pathways, genes and miRNAs that may explain such discrepancies.

- *Impaired glucose and lipid metabolism in association with variations in miRNAs*

According to current data and previous reports, NAFLD and PA or CC-conducted changes in HepG2 and HH are associated with downregulation of miRNAs and genes that are involved in aspects of hepatocytes metabolism, including decreased DNL through alternative mechanisms, such as expression of *NR1H4*, *NR1H3* and *PPP2R5C*, impaired FA transport (*PGC1α*) and oxidation (*PPARα*) and decreased glucose metabolism (*PEPCK* or *G6PC*). As an example, studies on *NR1H4*, a transcription factor involved in bile acid synthesis and transport also known as *FXR*, have demonstrated that it exerts hepatoprotective effects, suppressing lipid accumulation in hepatocytes[304]. It is worth stressing that gluconeogenesis is reported to be increased in NAFLD subjects[305], but we found a significant decrease in gluconeogenic genes in NAFLD, especially *PEPCK* and *G6PC*. Since it has been previously indicated that mice with diminished *PEPCK* expression develop lipid metabolism abnormalities such as hepatic steatosis[306], measuring protein activity should be considered.

The involvement of the FA-induced inflammatory response does not seem to explain miRNA changes by their own, since HH, apparently less resilient to FA than HepG2 cells, disclosed similar findings regarding miRNA expression changes. Indeed, expression values of pro-inflammatory macrophage-related genes such as *ITGAX* and *FABP4* were inversely associated with miR-30b-5p, which was also lowered in both HepG2 and HH upon treatment with FA. In agreement, lower liver miR-30b expression has been reported in HCC[307], and in Huh7 cells after hepatitis C virus infection[308], two conditions that involve inflammation and impaired metabolism. Perhaps, hepatic miR-30b responds negatively to the inflammatory profile of NAFLD, fat deposition and the presence of macrophages in the liver, as further supported by its inverse association with C reactive protein. It should be noted that, although hepatic miR-30b has not been associated with human NAFLD before, previous studies have reported the close association with adipogenesis in fat cells[309]. Accordingly, the circulating presence of miR-30b seems to be inversely correlated with inflammation, IR and impaired metabolism, since obese mice following high-fat diet also disclosed decreased circulating miR-30b levels, being restored after normal re-feeding[310].

Our data indicated decreased liver miR-139-5p and increased miR-146b in NAFLD samples, in concordance with previous findings[293]. The miR-139-5p has been pointed as

a tumour suppressor miRNA, controlling cellular growth through the regulation of c-Myc and c-fos[311]. This evidence, together with current inverse associations between miR-139-5p and *TNFα* mRNA levels in liver may hint into the decreased expressions found in HCC[311], also involving inflammation. On the other hand, the miR-146b showed opposite patterns *in vivo* (increased in NAFLD samples) vs. *in vitro* (decreased upon PA treatment in HepG2 and HH). In agreement with current results, additional controversies are found in the literature, since increased hepatic miR-146b was found in NASH patients[293], but treatments with this miRNA ameliorated HFD-induced NASH in mice[312]. It should be noted that miR-146b is mainly expressed in macrophages and rat liver Kupffer cells[312], being more likely identified as an immune system regulator[313]. This conclusion was further confirmed through increased expression in HepG2 treated with a lipid mixture coupled with pro-inflammatory cytokines such as TNFα and IL-6[314], and agrees with the inverse associations found with high-density lipoprotein and the lack of a positive response in HepG2 and HH upon PA treatment.

Controversies between studies can be attributed to changes in the study groups. As a proof of concept, it should be noted the overlap identified between current results and those reported by *Cheung et al.*, where miRNA expression pattern is analysed in the background of the metabolic syndrome (that is, subjects with obesity, dyslipidaemia and/or impaired glucose tolerance). Additionally, differences between samples analysed have to be also taken into account, since some miRNAs have been reported to show opposite changes between liver and plasma samples[315].

Altogether, this thesis gives promising evidence for studies using miRNAs to examine the pathophysiology of NAFLD, narrowing the selection of miRNA candidates for paving the way leading to further investigations targeting the potential for genomic therapies based on the activity of miRNA-related hepatic transcriptional regulation. As well, significant associations with clinical parameters and gene expression markers both *in vivo* and i*n vitro* led to develop new hypothesis based on the involvement of miRNAs in disease progression.

6.2. IMPAIRED AMPK FUNCTION COMPROMISES THE BIOSYNTHESIS OF HEPATIC miRNAs REQUIRED TO MAINTAIN LIPID HOMEOSTASIS

This doctoral thesis demonstrates that treatments of PA and CC may mirror NAFLD features *in vitro*, triggering increased expression of genes related to lipid deposition. Both models are able to inhibit AMPK activity. While saturated FA palmitate blocks AMPK phosphorylation and, therefore increases FA biosynthesis[316,317], CC, also called dorsomorphin, has been widely used in cell-based assays as a AMPK inhibitor[234]. CC is the most used agent to study physiological functions of AMPK[318]. The participation of AMPK in the fatty liver arena is well recognized[319]. It integrates hormonal and nutritional signals to promote energy balance by switching off ATP-consuming pathways by the impact on regulatory proteins, the control of enzymes involved in lipid metabolism and changes in gene expression patterns[320]. Activation of AMPK in hepatocytes leads to the stimulation of FA uptake and oxidation, while switches off the anabolic pathways[319]. Therefore, NAFLD long-lasting metabolic impairment affecting DNL, FA uptake, and β-oxidation can be modulated by AMPK function. In this section, we demonstrated impaired miRNA regulation after direct/indirect AMPK modulation in cultured hepatocytes and rodent models with impaired AMPK activity. AMPK inhibition accomplished by PA or CC led to an overall downregulation of the miRNA profile, while its activation with metformin triggered mostly an upregulated pattern. Accordingly, tail-vein injected mice with lentiviral particles harbouring dominant negative isoforms of AMPKα were characterized by an overall downregulation of analysed miRNAs compared to controls. Of note, candidate miRNAs described previously to be downregulated in NAFLD subjects disclosed the same modulation in HepG2 and HH challenged with steatotic agents. The findings highlight the contribution of AMPK to hepatic miRNA biosynthesis by means of its pharmacological and genetic modifications accomplished both *in vivo* and *in vitro*. As CC has been postulated to trigger off-target effects due to its ability to inhibit a broad variety of kinases[280], lentiviral particles inducing AMPKα1/2 knockdown were employed to assign miRNA modulation to this kinase itself. Not only AMPK inhibition was able to impact on miRNA expression, but also triggered an increase in genes involved in FA biosynthesis. Considering the effects of AMPK silencing, and taking into account that AMPK itself has been widely reported to inhibit FA biosynthesis, DICER knockdown, an enzyme clearly involved in miRNA biosynthesis[195], was investigated to test whether expected miRNA downregulation impacted on genes involved in lipid metabolism, and consequently

allow to define an AMPK-miRNA-lipid homeostasis crosstalk. Consistently, genetic modulation of DICER in hepatocytes demonstrated that its downregulation was intrinsically coupled to significant changes in miRNA profiles and increased FA overload, being both miRNA and gene expression values similar to those happening in HepG2 challenged with AMPKα1/2 lentiviral particles, and subsequently suggesting a plausible involvement of miRNAs in the modulation of genes that belong to FA biosynthesis pathway. Therefore, we postulated a scenario where AMPK may regulate FA metabolism in hepatocytes through miRNAs availability. Accordingly, the interplay between AMPK and hepatic miRNA profiles leading to changes in FA metabolism was sustained by i) the reduced AMPK activity/expression coupled to decreased miRNA abundance and expression of genes related to miRNA biosynthesis, and ii) consistent decrease of miRNA candidates in either AMPKα1/2 or DICER knockdown coinciding with increased FA accumulation. In line with our results, previous data had already disclosed the interplay between DICER and miRNA profiles, controlling the epithelial-mesenchymal transition during oncogenic events[321], and increased DICER after treatments modulating AMPK activity in both mice and humans[322,323]. Additionally, previous research performed in dietary-induced NASH mouse model reported a significant decrease of hepatic Dicer[324]. Further research should be employed to comprehend this scenario, where there is a high likelihood of additional elements participating in the pathway, or that AMPK impacted post-transcriptionally on DICER enzyme. In fact, as DICER knockdown triggered FA accumulation within hepatocytes, and metformin treatment reduced lipid accumulation through AMPK activation, the combination of both could elucidate its interplay, where if metformin is not able to reduce FA deposition in DICER knockdown hepatocytes, it will imply that DICER and consequently, miRNAs, are essential to accomplish metformin beneficial effects. Previous research also revealed the presence of multiple E2F DNA-binding sites in the DICER promoter that were influenced by metformin treatment, disclosing an increase in DICER protein levels[323]. Besides that, and to consistently verify the AMPK-miRNAs-lipid homeostasis axis, more investigation is required to address the underlying molecular mechanisms.

Referring to miRNAs appearing consistently regulated in the extended miRNA profiles analysed *in vitro*, new candidates prospectively associated with NAFLD came up, together with the candidates assessed in human samples. Many of the miRNAs found herein have been already reported to be associated with NAFLD pathophysiology or

lipid homeostasis. It has to be mentioned the presence of controversial data about miRNA expression patterns throughout studies. For instance, miR-34a together with miR-222 and miR-16 have been reported as upregulated in NAFLD[293]. The family comprising miR-146a and miR-146b has also been in the spotlight[325,326]. In agreement with our own results, mice with NAFLD induced with methionine-choline deficient diet presented miR-146a as the most downregulated, and its role was involved in suppressing the activation and proliferation of hepatic stellate cells during the progression of NAFLD[325]. However, a high-fat and high-cholesterol diet-induced rat model of NAFLD showed increased levels of hepatic miR-146a/b, and high expression was reported in HepG2 challenged with FFAs and proinflammatory factors[327]. Our findings about miR-26a were reinforced with previous findings, which postulated its relationship with insulin sensitivity and metabolism of glucose and lipids. In those, mice infected with lentivirus carrying miR-26a were protected from glucose dysmetabolism and presented decreased total liver weight and hepatic triglyceride deposition[328]. Consistencies were also found for miR-30c, which has been described to be downregulated in the liver of leptin receptor-deficient mice[329], as well as in plasma samples of patients with NAFLD[330]. And despite the fact that no previous reports pointed at the role of miR-16 in NAFLD, *FASN* has been validated experimentally to be a direct target of miR-16, giving importance to its ability to decrease FA biosynthesis[331].

Overall, by approaches performed both *in vivo* and *in vitro*, we confirmed that treatments mirroring NAFLD and leading to AMPK disruption compromises hepatic miRNA biosynthesis, while knockdown of the miRNA-processing enzyme DICER exhibits a substantial increase in lipid deposition.

6.3. miR-30b AND miR-30b AS A POTENTIAL AVENUE FOR THE TREATMENT OF NAFLD

Genes related to DNL and FA uptake were identified as plausible targets for some of the miRNA candidates identified during this work. The overall outcome of their regulation under conditions mimicking NAFLD, also characterized by decreased AMPK activity, would be translated into decreased miRNA expression and the disability to actively repress specific target genes. As a consequence, this would result in altered expression patterns, lipid metabolism, and the acquisition of NAFLD traits. Specifically, miR-16,

miR-30b and miR-30c were reported to be consistently involved in lipid homeostasis, as demonstrated by studies assessing organelle structure, gene expression, mitochondrial function, and mass spectrometric analysis of the hepatocyte lipidome. Thereby, replenishment of these miRNA candidates led to i) decreased lipid droplet accumulation, ii) impaired expression of genes related to the synthesis of triglycerides, and iii) in the case of miR-30b and miR-30c, enhanced mitochondrial function coupled with increased *CPT1α* expression and modulation of genes related to the lipidome. Accordingly, *ACSL1* was validated as a direct target, which is known to dynamically drive FA metabolism in hepatocytes[332]. *ACSL1* is the predominant isoform in the liver and its activity accounts for 50% of total hepatic ACSL1 activity[333]. Indeed, previous research suggested that ACSL1 channels radiolabelled oleate towards diacylglycerol, phosphatidylethanolamine, phosphatidylinositol, and phosphatidylcholine, diminishing cholesterol esterification in hepatocytes and the liver[334,335]. On the contrary, ACSL1 deficiency led to reduced FA biosynthesis and enabled β-oxidation[333]. Our results point out the higher expression of hepatic *ACSL1* in NAFLD patients and under conditions mimicking enhanced FA deposition and decreased miRNA expression in hepatocytes, while the control exercised by miR-30b and miR-30c was coupled with increased mitochondrial function and decreased *de novo* lipogenesis.

On the other hand, lipidome-wide quantitative assessment performed in hepatocytes shortlisted key differences between the activity exercised by mimic miR-16, miR-30b and miR-30c. HepG2 cells challenged by miR-30b and miR-30c disclosed a reduction of ceramides coinciding with an elevation of sphingomyelins, while these changes were not visible with miR-16 treatments. It should be noted that an increase in hepatic ceramides is associated with steatosis and IR[336], and that ACSL1 can induce excess synthesis of total acyl derived long chain ceramides[337], thus reinforcing the causal implication of our current results. On the other hand, sphingomyelins have been reported to attenuate hepatic steatosis in high-fat-diet-induced obese mice, proving beneficial effects[338]. Hence, the analysis of the lipidome in hepatocytes challenged with miRNA candidates reinforced the potential therapeutic utility of the ectopic recovery of miR-30b and miR-30c in the fatty liver arena, restoring lipid homeostasis in hepatocytes. To strengthen the potential usage of these miRNAs, they were supplied to hepatocytes under conditions of FA accumulation, to test whether the ectopic replenishment of either hepatic miR-30b or miR-30c were able to rescue FA overload. Strikingly, both AMPK and DICER knockdown HepG2 cells, phenotypically characterized by increased FA

deposition in hepatocytes, were partially counteracted by rescue of the diminished expression of two of the miRNA species most consistently affected: miR-30b and miR-30c. As it has been previously mentioned, consistent results have been already reported with regard to hepatic miR-30c, which showed decreased expression in the liver of leptin receptor-deficient mice[329], and in the plasma of NAFLD subjects[330]. miR-30c has also been linked to lipid metabolism, disclosing its ability to dampen lipid biosynthesis and lipoprotein secretion, and being postulated as potential therapeutic target against hyperlipidaemia and related diseases[339,340]. Recently, miR-30b has been found to be positively associated with IR and catalogued as a non-invasive biomarker of NAFLD in rats[341]. Of note, despite the fact that miRNAs show high conservation between species, 3'UTR regions are highly variable, which can yield totally different results even though the miRNA sequences are identical[198]. As a proof of concept, while miR-30b in humans is widely predicted to be involved in FA biosynthesis and metabolism, neither mice nor rat miR-30b is apparently involved in lipid pathways. Therefore, candidate target genes should be experimentally validated taking into account the specie.

Altogether, our data unravel the activity of miR-30b and miR-30c in tackling inadequate FA accumulation in hepatocytes, offering a potential avenue for the treatment of NAFLD.

6.4. GENERAL DISCUSSION

NAFLD is known to be the most common cause of chronic liver disease in Western countries. Global epidemic of the disease is increasing at the same rate as obesity and diabetes epidemics[53]. Preceding worsen stages such as liver cirrhosis or hepatocellular carcinoma, and being in close association with cardiovascular events, it is predicted to become the most frequent indication for liver transplantation within the next decades[342]. At the moment, liver biopsy constitutes the gold standard approach for diagnosis and staging of NAFLD[93].

Although knowledge of the disease is rapidly increasing, molecular mechanisms involved in NAFLD progression are not clearly understood. Therefore, focusing on the identification of pathogenic pathways and developing screening approaches and proper diagnosis tools is crucial for further investigations based on new therapeutic agents to tackle the disease.

NAFLD occurs when there is an imbalance between lipid acquisition and removal, triggered by DNL and FA uptake, and FA β-oxidation and VLDL secretion, respectively. All these processes are directly or indirectly regulated by AMPK, a master metabolic regulator that inhibits lipogenesis and other ATP-consuming processes[269], and also by miRNAs, post-transcriptional key regulators of gene expression involved in a wide range of processes[198]. The association between the epigenetic regulation exercised by hepatic miRNAs and NAFLD is being increasingly recognized[202,204,207], as well as the close interplay between AMPK disruption and fatty liver disease[276,343]. By treatments mirroring NAFLD and modulating AMPK activity *in vitro* we confirmed significant downregulation of candidate miRNAs, coupled to increased FA deposition within hepatocytes. Additionally, impaired DICER expression is also coupled to decreased miRNA profile and increase FA overload, thus reinforcing miRNA role in controlling hepatocytes lipid homeostasis. The interplay between AMPK and hepatic miRNA expression leading to changes in FA homeostasis was sustained by: i) a reduced AMPK expression is coupled to decreased miRNA abundance, ii) consistent decrease of miRNA candidates together with enhanced FA deposition, and iii) ectopic replenishment of hepatic miR-30b and miR-30c rescuing FA overload and modifying lipid profiles within hepatocytes. miR-30b/c, sharing the seed region, were able to downregulate *ACSL1* (experimentally validated), *ELOVL5, SCD1, AGPAT4, DGAT1* and *DGAT2*, at the same time that upregulate *CPT1α* (**Figure 54**). We herein stress the potential of miR-30b and miR-30c in combating fatty liver disease, thus making them attractive epigenetic regulators to combat human NAFLD.

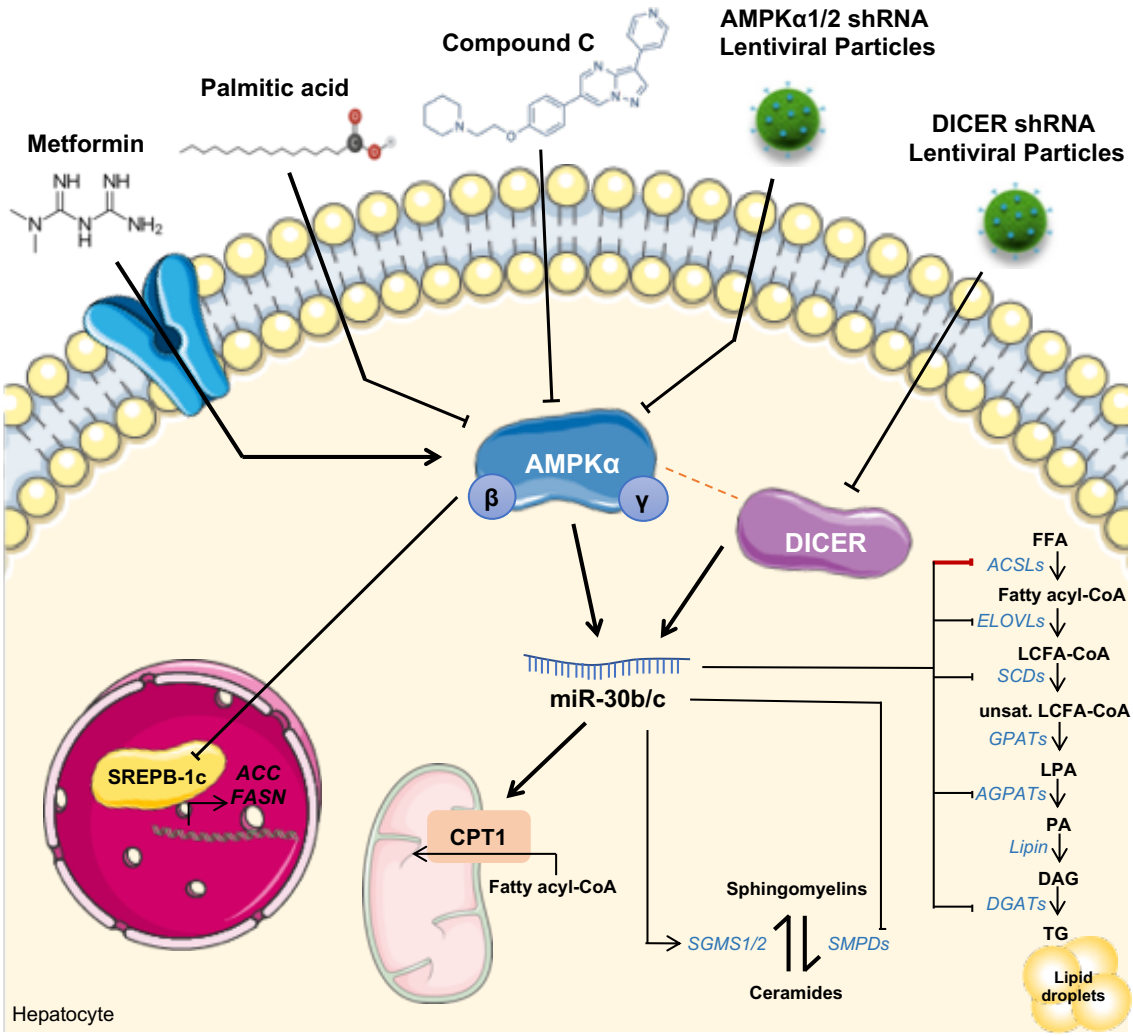

Figure 54. Molecular mechanisms involving hepatic AMPK, DICER and miR-30b/c. Treatments modulating AMPK (metformin as an inducer, and palmitic acid, compound C and AMPK shRNA lentiviral particles as inhibitors) or DICER (DICER shRNA lentiviral particles) activities were used to test miRNA expression profiles. In particular, either miR-30b or miR-30c were able to dampen lipid droplet accumulation (by specifically regulating ACSL1, ELOVL5, SCD1, AGPAT4, DGAT1 and DGAT2), increase sphingomyelin/ceramide ratio and enhancing FA mitochondrial oxidation (through increased CPT1a expression), globally ameliorating lipid homeostasis within the hepatocyte. *J Latorre (2019).*

Nowadays, there is no treatment for NAFLD besides lifestyle modification, based on healthy habits (comprising diet and exercise) and focused on ameliorating risk factors such as IR and obesity with the aim of preventing from disease progression[344]. Linking NAFLD management with our results, *Zhang R et al.* reported that caloric restriction induced a global increase of miRNAs expression in mice, improving mitochondrial function[345]. At the same time, both caloric restriction and physical activity have been extensively reported to be physiological activators of AMPK activity[172,346,347], being these statements reinforcing our data, where miRNAs could be the critical mediators in controlling FA metabolism.

Nevertheless, this thesis presents some limitations that deserve special mention. Although we have observed an overall downregulated profile of miRNA under conditions mirroring NAFLD, which is highly related to FA deposition in hepatocytes, a better mechanistic understanding of how AMPK and DICER interplay would help to dissect the importance of hepatic miRNAs in mediating FA metabolism. It is worth stressing that researching on miRNA represents a major challenge since expression and function of a specific miRNA can be widely variable depending on cell type and energetic status[348]. It has been specifically demonstrated that, in different NAFLD stages, significant fluctuations of miRNA expression pattern within hepatocytes makes them tough to characterize[207]. In fact, only few miRNA targets have been thoroughly validated experimentally due to complexity of miRNA-based approaches to elucidate their specific functions[348].

Overall, careful characterization of human samples and cell cultures challenged with different compounds disclosed the link between NAFLD and miRNA biosynthesis. Accordingly, while decreased hepatic miRNA expression is closely coupled to enhanced DNL, transient transfection with specific miRNA candidates such as miR-30b and miR-30c controls impaired lipid deposition and rescues mitochondrial activity in hepatocytes, offering a potential avenue for the treatment of NAFLD.

7. CONCLUSIONS

1. The hepatic miRNA patterns of obese NAFLD cases and age, gender, and weight-matched controls with normal liver histology disclose the identification of specific miRNA candidates significantly associated with variations in gene expression and impaired glucose and lipid metabolism.

2. The metabolic modifications observed in primary human hepatocytes and HepG2 cells after treatments with palmitate, palmitate plus oleate, and high glucose and insulin demonstrate that components of this profile are regulated in parallel to changes in glucose and FA metabolism.

3. This study, including expanded miRNA-profile, values of gene expression, and experiments *in vitro*, consolidate the relevance of increased miR-146b, and decreased miR-139-5p, miR-122-5p, miR-30b, and miR-422a in obese subjects with NAFLD.

4. Conditions mimicking NAFLD in human hepatocytes depict similar changes in miRNA patterns. Namely, *in silico* prediction categorized genes related to *de novo* lipogenesis and FA uptake as plausible targets for differentially expressed miRNA candidates.

5. The overall outcome of their downregulation under conditions mimicking NAFLD, also characterized by decreased AMPK activity, would be translated into decreased miRNA expression and the disability to actively repress targets genes. As a consequence, this could result in impaired expression patterns, disruption of lipid homeostasis, and the acquisition of NAFLD traits.

6. AMPK regulates FA metabolism through miRNA availability. The interplay between AMPK and hepatic miRNA patterns leading to changes in FA metabolism was sustained by the reduced AMPK expression coupled to decreased miRNA abundance and expression of genes related to miRNA biosynthesis, and consistent decrease of miRNA candidates coinciding with increased FA accumulation

7. As a proof of concept, hepatic AMPK activation through metformin leads to increased miRNA biosynthesis, while its disruption through either palmitic acid, compound C, or AMPKα1/2 knockdown leads to reduced miRNA biosynthesis.

8. Hepatic DICER disruption leads to reduced miRNA biosynthesis, coupled to increased FA overload, reinforcing the involvement of miRNAs in the modulation of genes related to the synthesis and accumulation of FA. Therefore, decreased miRNA in hepatocytes is coupled to enhanced *de novo* lipogenesis.

9. Specifically, miR-16, miR-30b and miR-30c were involved in controlling the deposition of fatty acids, as demonstrated by studies assessing organelle structure, gene expression, mitochondrial function, and mass spectrometric analysis of the hepatocyte lipidome.

10. Ectopic replenishment of these miRNA candidates led to i) decreased lipid droplet accumulation, ii) impaired expression of genes related to the synthesis of triglycerides, and iii), in the case of mimic miR-30b and miR-30c, enhanced mitochondrial function and a significant increase in CPT1α, involved in higher FA oxidation activity.

11. ACSL1, known to dynamically drive FA metabolism within hepatocytes, has been catalogued as an experimental validated target of miR-30b and miR-30c.

12. Lipidome-wide quantitative assessment performed in hepatocytes shortlisted key differences between the activity exercised by mimic miR-16, miR-30b, and miR-30c, a reduction of ceramides coinciding with an elevation of sphingomyelins, accomplished by miR-30b and miR-30c but not by miR-16. Indeed, transient transfection with miR-30b or miR-30c increases the sphingomyelin/ceramide ratio, being related to the improvement of insulin sensitivity, also supported by increased *GLUT2* in human hepatocytes.

13. Our data unravel the activity of miR-30b and miR-30c in tackling inadequate FA accumulation in hepatocytes, offering a potential avenue for the treatment of NAFLD.

8. REFERENCES

1. Than NN, Newsome PN. A concise review of non-alcoholic fatty liver disease. *Atherosclerosis*. 2015;239(1):192-202. doi:10.1016/j.atherosclerosis.2015.01.001
2. Bugianesi E. EASL–EASD–EASO Clinical Practice Guidelines for the management of non-alcoholic fatty liver disease: disease mongering or call to action? *Diabetologia*. 2016;59(6):1145-1147. doi:10.1007/s00125-016-3930-7
3. European Association for the Study of the Liver (EASL), European Association for the Study of Diabetes (EASD), European Association for the Study of Obesity (EASO). EASL-EASD-EASO Clinical Practice Guidelines for the management of non-alcoholic fatty liver disease. *J Hepatol*. 2016. doi:10.1016/j.jhep.2015.11.004
4. Chalasani N, Younossi Z, Lavine JE, et al. The diagnosis and management of non-alcoholic fatty liver disease: Practice Guideline by the American Association for the Study of Liver Diseases, American College of Gastroenterology, and the American Gastroenterological Association. *Hepatology*. 2012. doi:10.1002/hep.25762
5. Cobbina E, Akhlaghi F. Non-alcoholic fatty liver disease (NAFLD)–pathogenesis, classification, and effect on drug metabolizing enzymes and transporters. *Drug Metab Rev*. 2017. doi:10.1080/03602532.2017.1293683
6. Long-term mortality in nonalcoholic fatty liver disease. Is liver histology of any prognostic significance? (Hepatology (2010) 51 (373-375)). *Hepatology*. 2010. doi:10.1002/hep.23677
7. Vernon G, Baranova A, Younossi ZM. Systematic review: The epidemiology and natural history of non-alcoholic fatty liver disease and non-alcoholic steatohepatitis in adults. *Aliment Pharmacol Ther*. 2011;34(3):274-285. doi:10.1111/j.1365-2036.2011.04724.x
8. Younossi Z, Anstee QM, Marietti M, et al. Global burden of NAFLD and NASH: Trends, predictions, risk factors and prevention. *Nat Rev Gastroenterol Hepatol*. 2018;15(1):11-20. doi:10.1038/nrgastro.2017.109
9. Yu Y, Cai J, She Z, Li H. Insights into the Epidemiology, Pathogenesis, and Therapeutics of Nonalcoholic Fatty Liver Diseases. *Adv Sci*. 2019. doi:10.1002/advs.201801585
10. Byrne CD, Targher G. NAFLD: A multisystem disease. *J Hepatol*. 2015. doi:10.1016/j.jhep.2014.12.012
11. Leite NC, Salles GF, Araujo ALE, Villela-Nogueira CA, Cardoso CRL. Prevalence and associated factors of non-alcoholic fatty liver disease in patients with type-2 diabetes mellitus. *Liver Int*. 2009. doi:10.1111/j.1478-3231.2008.01718.x
12. Katsiki N, Mikhailidis DP, Mantzoros CS. Non-alcoholic fatty liver disease and dyslipidemia: An update. *Metabolism*. 2016. doi:10.1016/j.metabol.2016.05.003
13. Marchesini G, Brizi M, Blanchi G, et al. Nonalcoholic Fatty Liver Disease: A Feature of the Metabolic Syndrome. *Diabetes*. 2001. doi:10.2337/diabetes.50.8.1844
14. Adams LA, Anstee QM, Tilg H, Targher G. Non-Alcoholic fatty liver disease and its relationship with cardiovascular disease and other extrahepatic diseases. *Gut*. 2017. doi:10.1136/gutjnl-2017-313884
15. Rinella ME, Sanyal AJ. Management of NAFLD: A stage-based approach. *Nat Rev*

Gastroenterol Hepatol. 2016. doi:10.1038/nrgastro.2016.3

16. Cohen JC, Horton JD, Hobbs HH. Human fatty liver disease: Old questions and new insights. *Science (80-)*. 2011;332(6037):1519-1523. doi:10.1126/science.1204265
17. Fabbrini E, Sullivan S, Klein S. Obesity and nonalcoholic fatty liver disease: Biochemical, metabolic, and clinical implications. *Hepatology*. 2010. doi:10.1002/hep.23280
18. Treeprasertsuk S, Lopez-Jimenez F, Lindor KD. Nonalcoholic fatty liver disease and the coronary artery disease. *Dig Dis Sci*. 2011. doi:10.1007/s10620-010-1241-2
19. Day CP, James OFW. Steatohepatitis: A tale of two "Hits"? *Gastroenterology*. 1998. doi:10.1016/S0016-5085(98)70599-2
20. Peverill W, Powell LW, Skoien R. Evolving concepts in the pathogenesis of NASH: Beyond steatosis and inflammation. *Int J Mol Sci*. 2014. doi:10.3390/ijms15058591
21. Fang YL, Chen H, Wang CL, Liang L. Pathogenesis of non-alcoholic fatty liver disease in children and adolescence: From "two hit theory" to "multiple hit model." *World J Gastroenterol*. 2018. doi:10.3748/wjg.v24.i27.2974
22. Buzzetti E, Pinzani M, Tsochatzis EA. The multiple-hit pathogenesis of non-alcoholic fatty liver disease (NAFLD). *Metabolism*. 2016. doi:10.1016/j.metabol.2015.12.012
23. Bugianesi E, Moscatiello S, Ciaravella MF, Marchesini G. Insulin Resistance in Nonalcoholic Fatty Liver Disease. *Curr Pharm Des*. 2010. doi:10.2174/138161210791208875
24. Guilherme A, Virbasius J V., Puri V, Czech MP. Adipocyte dysfunctions linking obesity to insulin resistance and type 2 diabetes. *Nat Rev Mol Cell Biol*. 2008. doi:10.1038/nrm2391
25. Cusi K. Role of Insulin Resistance and Lipotoxicity in Non-Alcoholic Steatohepatitis. *Clin Liver Dis*. 2009. doi:10.1016/j.cld.2009.07.009
26. Delarue J, Lallès JP. Nonalcoholic fatty liver disease: Roles of the gut and the liver and metabolic modulation by some dietary factors and especially long-chain n-3 PUFA. *Mol Nutr Food Res*. 2016. doi:10.1002/mnfr.201500346
27. Kirpich IA, Marsano LS, McClain CJ. Gut-liver axis, nutrition, and non-alcoholic fatty liver disease. *Clin Biochem*. 2015. doi:10.1016/j.clinbiochem.2015.06.023
28. Lee UE, Friedman SL. Mechanisms of hepatic fibrogenesis. *Best Pract Res Clin Gastroenterol*. 2011. doi:10.1016/j.bpg.2011.02.005
29. Czaja MJ, Weiner FR, Flanders KC, et al. In vitro and in vivo association of transforming growth factor-β1 with hepatic fibrosis. *J Cell Biol*. 1989. doi:10.1083/jcb.108.6.2477
30. Wong L, Yamasaki G, Johnson RJ, Friedman SL. Induction of β-platelet-derived growth factor receptor in rat hepatic lipocytes during cellular activation in vivo and in culture. *J Clin Invest*. 1994. doi:10.1172/JCI117497
31. Friedman SL, Arthur MJP. Activation of cultured rat hepatic lipocytes by Kupffer cell conditioned medium. Direct enhancement of matrix synthesis and stimulation of cell proliferation via induction of platelet-derived growth factor receptors. *J Clin Invest*. 1989. doi:10.1172/JCI114362
32. Tanaka H, Leung PSC, Kenny TP, Gershwin ME, Bowlus CL. Immunological

orchestration of liver fibrosis. *Clin Rev Allergy Immunol*. 2012. doi:10.1007/s12016-012-8323-1

33. Samuel VT, Liu ZX, Qu X, et al. Mechanism of hepatic insulin resistance in non-alcoholic fatty liver disease. *J Biol Chem*. 2004. doi:10.1074/jbc.M313478200
34. Magkos F, Su X, Bradley D, et al. Intrahepatic diacylglycerol content is associated with hepatic insulin resistance in obese subjects. *Gastroenterology*. 2012. doi:10.1053/j.gastro.2012.03.003
35. Savage DB, Petersen KF, Shulman GI. Disordered Lipid Metabolism and the Pathogenesis of Insulin Resistance. *Physiol Rev*. 2007. doi:10.1152/physrev.00024.2006
36. Petersen MC, Shulman GI. Roles of Diacylglycerols and Ceramides in Hepatic Insulin Resistance. *Trends Pharmacol Sci*. 2017;38(7):649-665. doi:10.1016/j.tips.2017.04.004
37. Yilmaz Y. Review article: Is non-alcoholic fatty liver disease a spectrum, or are steatosis and non-alcoholic steatohepatitis distinct conditions? *Aliment Pharmacol Ther*. 2012. doi:10.1111/apt.12046
38. Younossi ZM, Koenig AB, Abdelatif D, Fazel Y, Henry L, Wymer M. Global epidemiology of nonalcoholic fatty liver disease—Meta-analytic assessment of prevalence, incidence, and outcomes. *Hepatology*. 2016. doi:10.1002/hep.28431
39. Araújo AR, Rosso N, Bedogni G, Tiribelli C, Bellentani S. Global epidemiology of non-alcoholic fatty liver disease/non-alcoholic steatohepatitis: What we need in the future. *Liver Int*. 2018. doi:10.1111/liv.13643
40. Loomba R, Sanyal AJ. The global NAFLD epidemic. *Nat Rev Gastroenterol Hepatol*. 2013. doi:10.1038/nrgastro.2013.171
41. Williamson RM, Price JF, Glancy S, et al. Prevalence of and risk factors for hepatic steatosis and nonalcoholic fatty liver disease in people with type 2 diabetes: The Edinburgh type 2 diabetes study. *Diabetes Care*. 2011. doi:10.2337/dc10-2229
42. Machado M, Marques-Vidal P, Cortez-Pinto H. Hepatic histology in obese patients undergoing bariatric surgery. *J Hepatol*. 2006. doi:10.1016/j.jhep.2006.06.013
43. Gaggini M, Morelli M, Buzzigoli E, DeFronzo RA, Bugianesi E, Gastaldelli A. Non-alcoholic fatty liver disease (NAFLD) and its connection with insulin resistance, dyslipidemia, atherosclerosis and coronary heart disease. *Nutrients*. 2013. doi:10.3390/nu5051544
44. Chalasani N, Younossi Z, Lavine JE, et al. The diagnosis and management of non-alcoholic fatty liver disease: Practice Guideline by the American Association for the Study of Liver Diseases, American College of Gastroenterology, and the American Gastroenterological Association. *Hepatology*. 2012;55(6):2005-2023. doi:10.1002/hep.25762
45. Byrne CD, Targher G. EASL–EASD–EASO Clinical Practice Guidelines for the management of non-alcoholic fatty liver disease: is universal screening appropriate? *Diabetologia*. 2016. doi:10.1007/s00125-016-3910-y
46. Pan JJ, Fallon MB. Gender and racial differences in nonalcoholic fatty liver disease. *World*

J Hepatol. 2014. doi:10.4254/wjh.v6.i5.274

47. Chen Z, Chen L, Dai H, Chen J, Fang L. Relationship between alanine aminotransferase levels and metabolic syndrome in nonalcoholic fatty liver disease. *J Zhejiang Univ Sci B*. 2008. doi:10.1631/jzus.b0720016
48. Papatheodoridis G V., Goulis J, Christodoulou D, et al. High prevalence of elevated liver enzymes in blood donors: Associations with male gender and central adiposity. *Eur J Gastroenterol Hepatol*. 2007. doi:10.1097/MEG.0b013e328011438b
49. Ong JP, Elariny H, Collantes R, et al. Predictors of nonalcoholic steatohepatitis and advanced fibrosis in morbidly obese patients. *Obes Surg*. 2005. doi:10.1381/0960892053576820
50. Ruhl CE, Everharty JE. Determinants of the association of overweight with elevated serum alanine aminotransferase activity in the United States. *Gastroenterology*. 2003. doi:10.1053/gast.2003.50004
51. Browning JD, Szczepaniak LS, Dobbins R, et al. Prevalence of hepatic steatosis in an urban population in the United States: Impact of ethnicity. *Hepatology*. 2004. doi:10.1002/hep.20466
52. Ballestri S, Nascimbeni F, Baldelli E, Marrazzo A, Romagnoli D, Lonardo A. NAFLD as a Sexual Dimorphic Disease: Role of Gender and Reproductive Status in the Development and Progression of Nonalcoholic Fatty Liver Disease and Inherent Cardiovascular Risk. *Adv Ther*. 2017. doi:10.1007/s12325-017-0556-1
53. Vernon G, Baranova A, Younossi ZM. Systematic review: The epidemiology and natural history of non-alcoholic fatty liver disease and non-alcoholic steatohepatitis in adults. *Aliment Pharmacol Ther*. 2011. doi:10.1111/j.1365-2036.2011.04724.x
54. Ong JP, Pitts A, Younossi ZM. Increased overall mortality and liver-related mortality in non-alcoholic fatty liver disease. *J Hepatol*. 2008. doi:10.1016/j.jhep.2008.06.018
55. Adams LA, Lymp JF, St. Sauver J, et al. The natural history of nonalcoholic fatty liver disease: A population-based cohort study. *Gastroenterology*. 2005. doi:10.1053/j.gastro.2005.04.014
56. Ascha MS, Hanouneh IA, Lopez R, Tamimi TAR, Feldstein AF, Zein NN. The incidence and risk factors of hepatocellular carcinoma in patients with nonalcoholic steatohepatitis. *Hepatology*. 2010. doi:10.1002/hep.23527
57. Kallwitz ER, Kumar M, Aggarwal R, et al. Ethnicity and nonalcoholic fatty liver disease in an obesity clinic: The impact of triglycerides. *Dig Dis Sci*. 2008. doi:10.1007/s10620-008-0234-x
58. Speliotes EK, Yerges-Armstrong LM, Wu J, et al. Genome-wide association analysis identifies variants associated with nonalcoholic fatty liver disease that have distinct effects on metabolic traits. *PLoS Genet*. 2011. doi:10.1371/journal.pgen.1001324
59. Romeo S, Kozlitina J, Xing C, et al. Genetic variation in PNPLA3 confers susceptibility to nonalcoholic fatty liver disease. *Nat Genet*. 2008. doi:10.1038/ng.257

60. Simmons RK, Alberti KGMM, Gale EAM, et al. The metabolic syndrome: Useful concept or clinical tool? Report of a WHO expert consultation. *Diabetologia*. 2010. doi:10.1007/s00125-009-1620-4
61. Yki-Järvinen H. Non-alcoholic fatty liver disease as a cause and a consequence of metabolic syndrome. *Lancet Diabetes Endocrinol*. 2014. doi:10.1016/S2213-8587(14)70032-4
62. Koehler EM, Schouten JNL, Hansen BE, et al. Prevalence and risk factors of non-alcoholic fatty liver disease in the elderly: Results from the Rotterdam study. *J Hepatol*. 2012;57(6):1305-1311. doi:10.1016/j.jhep.2012.07.028
63. Anstee QM, Targher G, Day CP. Progression of NAFLD to diabetes mellitus, cardiovascular disease or cirrhosis. *Nat Rev Gastroenterol Hepatol*. 2013. doi:10.1038/nrgastro.2013.41
64. Li L, Liu DW, Yan HY, Wang ZY, Zhao SH, Wang B. Obesity is an independent risk factor for non-alcoholic fatty liver disease: Evidence from a meta-analysis of 21 cohort studies. *Obes Rev*. 2016. doi:10.1111/obr.12407
65. Cani PD, Amar J, Iglesias MA, et al. Metabolic endotoxemia initiates obesity and insulin resistance. *Diabetes*. 2007;56(7):1761-1772. doi:10.2337/db06-1491
66. Safari Z, Gérard P. The links between the gut microbiome and non-alcoholic fatty liver disease (NAFLD). *Cellular and Molecular Life Sciences*. 2019.
67. Paolella G, Mandato C, Pierri L, Poeta M, Di Stasi M, Vajro P. Gut-liver axis and probiotics: Their role in non-alcoholic fatty liver disease. *World J Gastroenterol*. 2014. doi:10.3748/wjg.v20.i42.15518
68. Dunstan DW, Salmon J, Healy GN, et al. Association of television viewing with fasting and 2-h postchallenge plasma glucose levels in adults without diagnosed diabetes. *Diabetes Care*. 2007. doi:10.2337/dc06-1996
69. Zelber-Sagi S, Nitzan-Kaluski D, Goldsmith R, et al. Role of leisure-time physical activity in nonalcoholic fatty liver disease: A population-based study. *Hepatology*. 2008. doi:10.1002/hep.22525
70. Perseghin G, Lattuada G, De Cobelli F, et al. Habitual physical activity is associated with intrahepatic fat content in humans. *Diabetes Care*. 2007. doi:10.2337/dc06-2032
71. Soman VR, Koivisto VA, Deibert D, Felig P, DeFronzo RA. Increased Insulin Sensitivity and Insulin Binding to Monocytes after Physical Training. *N Engl J Med*. 2010. doi:10.1056/nejm197911293012203
72. Bae JC, Suh S, Park SE, et al. Regular Exercise Is Associated with a Reduction in the Risk of NAFLD and Decreased Liver Enzymes in Individuals with NAFLD Independent of Obesity in Korean Adults. *PLoS One*. 2012. doi:10.1371/journal.pone.0046819
73. Rabol R, Petersen KF, Dufour S, Flannery C, Shulman GI. Reversal of muscle insulin resistance with exercise reduces postprandial hepatic de novo lipogenesis in insulin resistant individuals. *Proc Natl Acad Sci*. 2011. doi:10.1073/pnas.1110105108
74. al-Eryani L, Wahlang B, Falkner KC, et al. Identification of Environmental Chemicals

Associated with the Development of Toxicant-associated Fatty Liver Disease in Rodents. *Toxicol Pathol*. 2015. doi:10.1177/0192623314549960

75. Tomaru M, Takano H, Inoue KI, et al. Pulmonary exposure to diesel exhaust particles enhances fatty change of the liver in obese diabetic mice. *Int J Mol Med*. 2007;19(1):17-22.
76. Tarantino G, Capone D, Finelli C. Exposure to ambient air particulate matter and non-alcoholic fatty liver disease. *World J Gastroenterol*. 2013;19(25):3951-3956. doi:10.3748/wjg.v19.i25.3951
77. Arciello M, Gori M, Maggio R, et al. Environmental pollution: A tangible risk for NAFLD pathogenesis. *Int J Mol Sci*. 2013;14(11):22052-22066. doi:10.3390/ijms141122052
78. al-Eryani L, Wahlang B, Falkner KC, et al. Identification of Environmental Chemicals Associated with the Development of Toxicant-associated Fatty Liver Disease in Rodents. *Toxicol Pathol*. 2015;43(4):482-497. doi:10.1177/0192623314549960
79. Kahali B, Halligan B, Speliotes EK. Insights from Genome-Wide Association Analyses of Nonalcoholic Fatty Liver Disease. *Semin Liver Dis*. 2015. doi:10.1055/s-0035-1567870
80. Cardon LR, Bell JI. Association study designs for complex diseases. *Nat Rev Genet*. 2001. doi:10.1038/35052543
81. Hirschhorn JN. Genomewide Association Studies — Illuminating Biologic Pathways. *N Engl J Med*. 2009. doi:10.1056/nejmp0808934
82. Kozlitina J, Smagris E, Stender S, et al. Exome-wide association study identifies a TM6SF2 variant that confers susceptibility to nonalcoholic fatty liver disease. *Nat Genet*. 2014. doi:10.1038/ng.2901
83. Anstee QM, Seth D, Day CP. Genetic Factors That Affect Risk of Alcoholic and Nonalcoholic Fatty Liver Disease. *Gastroenterology*. 2016. doi:10.1053/j.gastro.2016.01.037
84. Luukkonen PK, Zhou Y, Hyötyläinen T, et al. The MBOAT7 variant rs641738 alters hepatic phosphatidylinositols and increases severity of non-alcoholic fatty liver disease in humans. *J Hepatol*. 2016. doi:10.1016/j.jhep.2016.07.045
85. Eslam M, Valenti L, Romeo S. Genetics and epigenetics of NAFLD and NASH: Clinical impact. *J Hepatol*. 2018. doi:10.1016/j.jhep.2017.09.003
86. Pirazzi C, Adiels M, Burza MA, et al. Patatin-like phospholipase domain-containing 3 (PNPLA3) I148M (rs738409) affects hepatic VLDL secretion in humans and in vitro. *J Hepatol*. 2012. doi:10.1016/j.jhep.2012.07.030
87. Kumari M, Schoiswohl G, Chitraju C, et al. Adiponutrin functions as a nutritionally regulated lysophosphatidic acid acyltransferase. *Cell Metab*. 2012. doi:10.1016/j.cmet.2012.04.008
88. Del Campo JA, Gallego-Durán R, Gallego P, Grande L. Genetic and epigenetic regulation in nonalcoholic fatty liver disease (NAFLD). *Int J Mol Sci*. 2018;19(3). doi:10.3390/ijms19030911
89. Mancina RM, Dongiovanni P, Petta S, et al. The MBOAT7-TMC4 Variant rs641738 Increases Risk of Nonalcoholic Fatty Liver Disease in Individuals of European Descent.

Gastroenterology. 2016. doi:10.1053/j.gastro.2016.01.032

90. Santoro N, Zhang CK, Zhao H, et al. Variant in the glucokinase regulatory protein (GCKR) gene is associated with fatty liver in obese children and adolescents. *Hepatology*. 2012. doi:10.1002/hep.24806
91. Hashimoto E, Taniai M, Tokushige K. Characteristics and diagnosis of NAFLD/NASH. *J Gastroenterol Hepatol*. 2013;28(S4):64-70. doi:10.1111/jgh.12271
92. Vuppalanchi R, Chalasani N. Nonalcoholic fatty liver disease and nonalcoholic steatohepatitis: Selected practical issues in their evaluation and management. *Hepatology*. 2009. doi:10.1002/hep.22603
93. E. H. Clinical diagnosis of NAFLD/NASH. *Hepatol Int*. 2012;6(1):12. http://ovidsp.ovid.com/ovidweb.cgi?T=JS&PAGE=reference&D=emed10&NEWS=N&AN=70811832.
94. Gariani K, Philippe J, Jornayvaz FR. Non-alcoholic fatty liver disease and insulin resistance: From bench to bedside. *Diabetes Metab*. 2013;39(1):16-26. doi:10.1016/j.diabet.2012.11.002
95. Rinella ME. Nonalcoholic fatty liver disease a systematic review. *JAMA - J Am Med Assoc*. 2015. doi:10.1001/jama.2015.5370
96. Mofrad P, Contos MJ, Haque M, et al. Clinical and histologic spectrum of nonalcoholic fatty liver disease associated with normal ALT values. *Hepatology*. 2003. doi:10.1053/jhep.2003.50229
97. Yki-Järvinen H. Diagnosis of nonalcoholic fatty liver disease (NAFLD). *Duodecim*. 2016.
98. Fitzpatrick E, Dhawan A. Noninvasive biomarkers in non-alcoholic fatty liver disease: Current status and a glimpse of the future. *World J Gastroenterol*. 2014. doi:10.3748/wjg.v20.i31.10851
99. Ballestri S, Romagnoli D, Nascimbeni F, Francica G, Lonardo A. Role of ultrasound in the diagnosis and treatment of nonalcoholic fatty liver disease and its complications. *Expert Rev Gastroenterol Hepatol*. 2015;9(5):603-627. doi:10.1586/17474124.2015.1007955
100. Boursier J, Calès P. Controlled attenuation parameter (CAP): a new device for fast evaluation of liver fat? *Liver Int*. 2012;32(6):875-877. doi:10.1111/j.1478-3231.2012.02824.x
101. Zeb I, Li D, Nasir K, Katz R, Larijani VN, Budoff MJ. Computed Tomography Scans in the Evaluation of Fatty Liver Disease in a Population Based Study. The Multi-Ethnic Study of Atherosclerosis. *Acad Radiol*. 2012;19(7):811-818. doi:10.1016/j.acra.2012.02.022
102. Abd El-Kader SM, El-Den Ashmawy EMS. Non-alcoholic fatty liver disease: The diagnosis and management. *World J Hepatol*. 2015;7(6):846-858. doi:10.4254/wjh.v7.i6.846
103. Bohte AE, Van Werven JR, Bipat S, Stoker J. The diagnostic accuracy of US, CT, MRI and 1H-MRS for the evaluation of hepatic steatosis compared with liver biopsy: A meta-analysis. *Eur Radiol*. 2011;21(1):87-97. doi:10.1007/s00330-010-1905-5
104. Yilmaz Y, Kedrah AE, Ozdogan O. Cytokeratin-18 fragments and biomarkers of the metabolic syndrome in nonalcoholic steatohepatitis. *World J Gastroenterol*.

2009;15(35):4387-4391. doi:10.3748/wjg.15.4387

105. Feldstein AE, Wieckowska A, Lopez AR, Liu YC, Zein NN, McCullough AJ. Cytokeratin-18 fragment levels as noninvasive biomarkers for nonalcoholic steatohepatitis: A multicenter validation study. *Hepatology*. 2009;50(4):1072-1078. doi:10.1002/hep.23050
106. Bedossa P. Histological Assessment of NAFLD. *Dig Dis Sci*. 2016;61(5):1348-1355. doi:10.1007/s10620-016-4062-0
107. European Association for the Study of the Liver (EASL), European Association for the Study of Diabetes (EASD), European Association for the Study of Obesity (EASO). EASL-EASD-EASO Clinical Practice Guidelines for the management of non-alcoholic fatty liver disease. *J Hepatol*. 2016;64(6):1388-1402. doi:10.1016/j.jhep.2015.11.004
108. Kleiner DE, Brunt EM, Van Natta M, et al. Design and validation of a histological scoring system for nonalcoholic fatty liver disease. *Hepatology*. 2005;41(6):1313-1321. doi:10.1002/hep.20701
109. Stanger BZ. Cellular Homeostasis and Repair in the Mammalian Liver. *Annu Rev Physiol*. 2015. doi:10.1146/annurev-physiol-021113-170255
110. Trefts E, Gannon M, Wasserman DH. The liver. *Curr Biol*. 2017. doi:10.1016/j.cub.2017.09.019
111. Schulze RJ, Schott MB, Casey CA, Tuma PL, McNiven MA. The cell biology of the hepatocyte: A membrane trafficking machine. *J Cell Biol*. 2019. doi:10.1083/jcb.201903090
112. Weibel ER, Stäubli W, Gnägi HR, Hess FA. Correlated morphometric and biochemical studies on the liver cell. I. Morphometric model, stereologic methods, and normal morphometric data for rat liver. *J Cell Biol*. 1969. doi:10.1083/jcb.42.1.68
113. Kanuri G, Bergheim I. In vitro and in vivo models of non-alcoholic fatty liver disease (NAFLD). *Int J Mol Sci*. 2013;14(6):11963-11980. doi:10.3390/ijms140611963
114. Cole BK, Feaver RE, Wamhoff BR, Dash A. Non-alcoholic fatty liver disease (NAFLD) models in drug discovery. *Expert Opin Drug Discov*. 2018;13(2):193-205. doi:10.1080/17460441.2018.1410135
115. C. Chavez-Tapia N, Rosso N, Tiribelli C. In Vitro Models for the Study of Non-Alcoholic Fatty Liver Disease. *Curr Med Chem*. 2011;18(7):1079-1084. doi:10.2174/092986711794940842
116. Janorkar A V., Harris LM, Murphey BS, Sowell BL. Use of three-dimensional spheroids of hepatocyte-derived reporter cells to study the effects of intracellular fat accumulation and subsequent cytokine exposure. *Biotechnol Bioeng*. 2011;108(5):1171-1180. doi:10.1002/bit.23025
117. Deboyser D, Goethals F, Krack G, Roberfroid M. Investigation into the mechanism of tetracycline-induced steatosis: Study in isolated hepatocytes. *Toxicol Appl Pharmacol*. 1989;97(3):473-479. doi:10.1016/0041-008X(89)90252-4
118. Tilg H, Hotamisligil GS. Nonalcoholic Fatty Liver Disease: Cytokine-Adipokine Interplay and Regulation of Insulin Resistance. *Gastroenterology*. 2006.

doi:10.1053/j.gastro.2006.05.054

119. Bujanda L, Hijona E, Hijona L, Arenas JI. Inflammatory mediators of hepatic steatosis. *Mediators Inflamm*. 2010. doi:10.1155/2010/837419
120. Girard J, Lafontan M. Impact of visceral adipose tissue on liver metabolism and insulin resistance. Part II: Visceral adipose tissue production and liver metabolism. *Diabetes Metab*. 2008. doi:10.1016/j.diabet.2008.04.002
121. Pusl T, Wild N, Vennegeerts T, et al. Free fatty acids sensitize hepatocytes to bile acid-induced apoptosis. *Biochem Biophys Res Commun*. 2008. doi:10.1016/j.bbrc.2008.04.113
122. Joshi-Barve S, Barve SS, Amancherla K, et al. Palmitic acid induces production of proinflammatory cytokine interleukin-8 from hepatocytes. *Hepatology*. 2007. doi:10.1002/hep.21752
123. Grasselli E, Canesi L, Portincasa P, Voci A, Vergani L, Demori I. Models of non-Alcoholic Fatty Liver Disease and Potential Translational Value: the Effects of 3,5-L-diiodothyronine. *Ann Hepatol*. 2017;16(5):707-719. doi:10.5604/01.3001.0010.2713
124. Smith BK, Marcinko K, Desjardins EM, Lally JS, Ford RJ, Steinberg GR. Treatment of nonalcoholic fatty liver disease: role of AMPK. *Am J Physiol Metab*. 2016. doi:10.1152/ajpendo.00225.2016
125. Wei C-C, Wu K, Gao Y, Zhang L-H, Li D-D, Luo Z. Magnesium Reduces Hepatic Lipid Accumulation in Yellow Catfish (Pelteobagrus fulvidraco) and Modulates Lipogenesis and Lipolysis via PPARA, JAK-STAT, and AMPK Pathways in Hepatocytes . *J Nutr*. 2017. doi:10.3945/jn.116.245852
126. Tang H, Yu R, Liu S, Huwatibieke B, Li Z, Zhang W. Irisin Inhibits Hepatic Cholesterol Synthesis via AMPK-SREBP2 Signaling. *EBioMedicine*. 2016. doi:10.1016/j.ebiom.2016.02.041
127. Bort A, Sánchez BG, Mateos-Gómez PA, Díaz-Laviada I, Rodríguez-Henche N. Capsaicin targets lipogenesis in hepG2 cells through AMPK activation, AKT inhibition and ppars regulation. *Int J Mol Sci*. 2019. doi:10.3390/ijms20071660
128. Xiong J, Yang H, Wu L, et al. Fluoxetine suppresses AMP-activated protein kinase signaling pathway to promote hepatic lipid accumulation in primary mouse hepatocytes. *Int J Biochem Cell Biol*. 2014;54:236-244. doi:10.1016/j.biocel.2014.07.019
129. Fullerton MD, Galic S, Marcinko K, et al. Single phosphorylation sites in Acc1 and Acc2 regulate lipid homeostasis and the insulin-sensitizing effects of metformin. *Nat Med*. 2013. doi:10.1038/nm.3372
130. Um JH, Park SJ, Kang H, et al. AMP-activated protein kinase-deficient mice are resistant to the metabolic effects of resveratrol. *Diabetes*. 2010. doi:10.2337/db09-0482
131. Shu T, Song X, Cui X, Ge W, Gao R, Wang J. Fc gamma receptor IIb expressed in hepatocytes promotes lipid accumulation and gluconeogenesis. *Int J Mol Sci*. 2018. doi:10.3390/ijms19102932
132. Fontana J, Kučera O, Anděl M, Červinková Z. Effect of glucagon-like peptide-1 analogue

liraglutide on primary cultures of rat hepatocytes isolated from lean and steatotic livers. *Gen Physiol Biophys*. 2019. doi:10.4149/gpb_2019016

133. Lau JKC, Zhang X, Yu J. Animal models of non-alcoholic fatty liver disease: current perspectives and recent advances. *J Pathol*. 2017. doi:10.1002/path.4829
134. Rui L. Energy metabolism in the liver. *Compr Physiol*. 2014;4(1):177-197. doi:10.1002/cphy.c130024
135. Koliaki C, Roden M. Hepatic energy metabolism in human diabetes mellitus, obesity and non-alcoholic fatty liver disease. *Mol Cell Endocrinol*. 2013. doi:10.1016/j.mce.2013.06.002
136. Ipsen DH, Lykkesfeldt J, Tveden-Nyborg P. Molecular mechanisms of hepatic lipid accumulation in non-alcoholic fatty liver disease. *Cell Mol Life Sci*. 2018. doi:10.1007/s00018-018-2860-6
137. Saltiel AR, Kahn CR. Insulin signalling and the regulation of glucose and lipid metabolism. *Nature*. 2001. doi:10.1038/414799a
138. Brown MS, Goldstein JL. The SREBP pathway: Regulation of cholesterol metabolism by proteolysis of a membrane-bound transcription factor. *Cell*. 1997. doi:10.1016/S0092-8674(00)80213-5
139. Titchenell PM, Quinn WJ, Lu M, et al. Direct Hepatocyte Insulin Signaling Is Required for Lipogenesis but Is Dispensable for the Suppression of Glucose Production. *Cell Metab*. 2016. doi:10.1016/j.cmet.2016.04.022
140. Brown MS, Goldstein JL. Selective versus Total Insulin Resistance: A Pathogenic Paradox. *Cell Metab*. 2008;7(2):95-96. doi:10.1016/j.cmet.2007.12.009
141. Bugianesi E, Gastaldelli A, Vanni E, et al. Insulin resistance in non-diabetic patients with non-alcoholic fatty liver disease: Sites and mechanisms. *Diabetologia*. 2005;48(4):634-642. doi:10.1007/s00125-005-1682-x
142. Yamamoto Y, Hiasa Y, Murakami H, et al. Rapid alternative absorption of dietary long-chain fatty acids with upregulation of intestinal glycosylated CD36 in liver cirrhosis. *Am J Clin Nutr*. 2012. doi:10.3945/ajcn.111.033084
143. Kawano Y, Cohen DE. Mechanisms of hepatic triglyceride accumulation in non-alcoholic fatty liver disease. *J Gastroenterol*. 2013. doi:10.1007/s00535-013-0758-5
144. Kawano Y, Cohen DE. Mechanisms of hepatic triglyceride accumulation in non-alcoholic fatty liver disease. *J Gastroenterol*. 2013;48(4):434-441. doi:10.1007/s00535-013-0758-5
145. Byrne CD. Ectopic fat, insulin resistance and non-alcoholic fatty liver disease. *Proc Nutr Soc*. 2013. doi:10.1017/s0029665113001249
146. Diraison F, Moulin PH, Beylot M. Contribution of hepatic de novo lipogenesis and reesterification of plasma non esterified fatty acids to plasma triglyceride synthesis during non-alcoholic fatty liver disease. *Diabetes Metab*. 2003;29(5):478-485. doi:10.1016/S1262-3636(07)70061-7
147. Donnelly KL, Smith CI, Schwarzenberg SJ, Jessurun J, Boldt MD, Parks EJ. Sources of fatty acids stored in liver and secreted via lipoproteins in patients with nonalcoholic fatty liver

disease. *J Clin Invest*. 2005;115(5):1343-1351. doi:10.1172/JCI23621

148. Ameer F, Scandiuzzi L, Hasnain S, Kalbacher H, Zaidi N. De novo lipogenesis in health and disease. *Metabolism*. 2014;63(7):895-902. doi:10.1016/j.metabol.2014.04.003
149. Rui L. Energy metabolism in the liver. *Compr Physiol*. 2014. doi:10.1002/cphy.c130024
150. Listenberger LL, Han X, Lewis SE, et al. Triglyceride accumulation protects against fatty acid-induced lipotoxicity. *Proc Natl Acad Sci U S A*. 2003. doi:10.1073/pnas.0630588100
151. Uyeda K, Repa JJ. Carbohydrate response element binding protein, ChREBP, a transcription factor coupling hepatic glucose utilization and lipid synthesis. *Cell Metab*. 2006;4(2):107-110. doi:10.1016/j.cmet.2006.06.008
152. Ferré P, Foufelle F. Hepatic steatosis: A role for de novo lipogenesis and the transcription factor SREBP-1c. *Diabetes, Obes Metab*. 2010. doi:10.1111/j.1463-1326.2010.01275.x
153. Sanders FWB, Griffin JL. De novo lipogenesis in the liver in health and disease: More than just a shunting yard for glucose. *Biol Rev*. 2016. doi:10.1111/brv.12178
154. McGarry JD, Woeltje KF, Kuwajima M, Foster DW. Regulation of ketogenesis and the renaissance of carnitine palmitoyltransferase. *Diabetes Metab Rev*. 1989. doi:10.1002/dmr.5610050305
155. Serra D, Mera P, Malandrino MI, Mir JF, Herrero L. Mitochondrial Fatty Acid Oxidation in Obesity. *Antioxid Redox Signal*. 2012. doi:10.1089/ars.2012.4875
156. Arafat AM, Kaczmarek P, Skrzypski M, et al. Glucagon increases circulating fibroblast growth factor 21 independently of endogenous insulin levels: A novel mechanism of glucagon-stimulated lipolysis? *Diabetologia*. 2013. doi:10.1007/s00125-012-2803-y
157. Nakamuta M, Kohjima M, Morizono S, et al. Evaluation of fatty acid metabolism-related gene expression in nonalcoholic fatty liver disease. *Int J Mol Med*. 2005.
158. Perla FM, Prelati M, Lavorato M, Visicchio D, Anania C. The Role of Lipid and Lipoprotein Metabolism in Non-Alcoholic Fatty Liver Disease. *Children*. 2017;4(6):46. doi:10.3390/children4060046
159. Shelness GS, Sellers JA. Very-low-density lipoprotein assembly and secretion. *Curr Opin Lipidol*. 2001. doi:10.1097/00041433-200104000-00008
160. Schonfeld G, Patterson BW, Yablonskiy DA, et al. Fatty liver in familial hypobetalipoproteinemia: roles of the APOB defects, intra-abdominal adipose tissue, and insulin sensitivity. *J Lipid Res*. 2003. doi:10.1194/jlr.m200342-jlr200
161. Berriot-Varoqueaux N, Aggerbeck L, Samson-Bouma ME, Wetterau JR. The role of the microsomal triglygeride transfer protein in abetalipoproteinemia. *Annu Rev Nutr*. 2000.
162. Raabe M, Véniant MM, Sullivan MA, et al. Analysis of the role of microsomal triglyceride transfer protein in the liver of tissue-specific knockout mice. *J Clin Invest*. 1999. doi:10.1172/JCI6576
163. Fabbrini E, Mohammed BS, Magkos F, Korenblat KM, Patterson BW, Klein S. Alterations in Adipose Tissue and Hepatic Lipid Kinetics in Obese Men and Women With Nonalcoholic Fatty Liver Disease. *Gastroenterology*. 2008. doi:10.1053/j.gastro.2007.11.038

164. Choi SH, Ginsberg HN. Increased very low density lipoprotein (VLDL) secretion, hepatic steatosis, and insulin resistance. *Trends Endocrinol Metab*. 2011. doi:10.1016/j.tem.2011.04.007

165. Bradbury MW. Lipid Metabolism and Liver Inflammation. I. Hepatic fatty acid uptake: possible role in steatosis. *Am J Physiol Liver Physiol*. 2006. doi:10.1152/ajpgi.00413.2005

166. Doege H, Stahl A. Protein-Mediated Fatty Acid Uptake: Novel Insights from In Vivo Models. *Physiology*. 2006. doi:10.1152/physiol.00014.2006

167. Zhou J, Zhai Y, Mu Y, et al. A novel pregnane X receptor-mediated and sterol regulatory element-binding protein-independent lipogenic pathway. *J Biol Chem*. 2006. doi:10.1074/jbc.M511116200

168. Doege H, Baillie RA, Ortegon AM, et al. Targeted Deletion of FATP5 Reveals Multiple Functions in Liver Metabolism: Alterations in Hepatic Lipid Homeostasis. *Gastroenterology*. 2006;130(4):1245-1258. doi:10.1053/j.gastro.2006.02.006

169. Hajri T, Han XX, Bonen A, Abumrad NA. Defective fatty acid uptake modulates insulin responsiveness and metabolic responses to diet in CD36-null mice. *J Clin Invest*. 2002. doi:10.1172/JCI0214596

170. Bu SY, Mashek DG. Hepatic long-chain acyl-CoA synthetase 5 mediates fatty acid channeling between anabolic and catabolic pathways. *J Lipid Res*. 2010. doi:10.1194/jlr.m009407

171. Xiao B, Heath R, Saiu P, et al. Structural basis for AMP binding to mammalian AMP-activated protein kinase. *Nature*. 2007. doi:10.1038/nature06161

172. Smith BK, Marcinko K, Desjardins EM, Lally JS, Ford RJ, Steinberg GR. Treatment of nonalcoholic fatty liver disease: role of AMPK. *Am J Physiol Metab*. 2016;311(4):E730-E740. doi:10.1152/ajpendo.00225.2016

173. Cho YS, Lee J Il, Shin D, et al. Molecular mechanism for the regulation of human ACC2 through phosphorylation by AMPK. *Biochem Biophys Res Commun*. 2010. doi:10.1016/j.bbrc.2009.11.029

174. McGarry JD, Foster DW. Regulation of Hepatic Fatty Acid Oxidation and Ketone Body Production. *Annu Rev Biochem*. 2003. doi:10.1146/annurev.bi.49.070180.002143

175. McGarry JD, Takabayashi Y, Foster DW. The role of malonyl-CoA in the coordination of fatty acid synthesis and oxidation in isolated rat hepatocytes. *J Biol Chem*. 1978.

176. Schmid AI, Szendroedi J, Chmelik M, Krššák M, Moser E, Roden M. Liver ATP synthesis is lower and relates to insulin sensitivity in patients with type 2 diabetes. *Diabetes Care*. 2011. doi:10.2337/dc10-1076

177. Steinberg GR, Michell BJ, van Denderen BJW, et al. Tumor necrosis factor α-induced skeletal muscle insulin resistance involves suppression of AMP-kinase signaling. *Cell Metab*. 2006. doi:10.1016/j.cmet.2006.11.005

178. Mazza A, Fruci B, Garinis GA, Giuliano S, Malaguarnera R, Belfiore A. The role of metformin in the management of NAFLD. *Exp Diabetes Res*. 2012.

doi:10.1155/2012/716404

179. Lee RC, Feinbaum RL, Ambros V. The C. elegans heterochronic gene lin-4 encodes small RNAs with antisense complementarity to lin-14. *Cell*. 1993;75(5):843-854. doi:10.1016/0092-8674(93)90529-Y
180. Reinhart BJ, Slack FJ, Basson M, et al. The 21-nucleotide let-7 RNA regulates developmental timing in Caenorhabditis elegans. *Nature*. 2000. doi:10.1038/35002607
181. Lagos-Quintana M, Rauhut R, Lendeckel W, Tuschl T. Identification of novel genes coding for small expressed RNAs. *Science (80-)*. 2001;294(5543):853-858. doi:10.1126/science.1064921
182. Lau NC, Lim LP, Weinstein EG, Bartel DP. An abundant class of tiny RNAs with probable regulatory roles in Caenorhabditis elegans. *Science (80-)*. 2001;294(5543):858-862. doi:10.1126/science.1065062
183. Lee RC, Ambros V. An extensive class of small RNAs in Caenorhabditis elegans. *Science (80-)*. 2001;294(5543):862-864. doi:10.1126/science.1065329
184. Ambros V. The functions of animal microRNAs. *Nature*. 2004;431(7006):350-355. doi:10.1038/nature02871
185. Bartel DP. MicroRNAs: Genomics, Biogenesis, Mechanism, and Function. *Cell*. 2004;116(2):281-297. doi:10.1016/S0092-8674(04)00045-5
186. Kozomara A, Birgaoanu M, Griffiths-Jones S. MiRBase: From microRNA sequences to function. *Nucleic Acids Res*. 2019. doi:10.1093/nar/gky1141
187. Lewis BP, Shih I, Jones-Rhoades MW, Bartel DP, Burge CB. Prediction of mammalian microRNA targets. *Cell*. 2003.
188. Friedman RC, Farh KKH, Burge CB, Bartel DP. Most mammalian mRNAs are conserved targets of microRNAs. *Genome Res*. 2009. doi:10.1101/gr.082701.108
189. Agarwal V, Bell GW, Nam JW, Bartel DP. Predicting effective microRNA target sites in mammalian mRNAs. *Elife*. 2015. doi:10.7554/eLife.05005
190. Wang XW, Heegaard NHH, Orum H. MicroRNAs in liver disease. *Gastroenterology*. 2012;142(7):1431-1443. doi:10.1053/j.gastro.2012.04.007
191. Remsburg C, Konrad K, Sampilo NF, Song JL. Analysis of microRNA functions. *Methods Cell Biol*. 2019;151:323-334. doi:10.1016/bs.mcb.2018.10.005
192. Bhaskaran M, Mohan M. MicroRNAs: History, Biogenesis, and Their Evolving Role in Animal Development and Disease. *Vet Pathol*. 2014. doi:10.1177/0300985813502820
193. Lee Y, Ahn C, Han J, et al. The nuclear RNase III Drosha initiates microRNA processing. *Nature*. 2003. doi:10.1038/nature01957
194. Yi R, Qin Y, Macara IG, Cullen BR. Exportin-5 mediates the nuclear export of pre-microRNAs and short hairpin RNAs. *Genes Dev*. 2003. doi:10.1101/gad.1158803
195. Ha M, Kim VN. Regulation of microRNA biogenesis. *Nat Rev Mol Cell Biol*. 2014. doi:10.1038/nrm3838
196. Bartel DP. Metazoan MicroRNAs. *Cell*. 2018.

197. Riffo-Campos ÁL, Riquelme I, Brebi-Mieville P. Tools for sequence-based miRNA target prediction: What to choose? *Int J Mol Sci*. 2016. doi:10.3390/ijms17121987

198. Gjorgjieva M, Sobolewski C, Dolicka D, Correia de Sousa M, Foti M. miRNAs and NAFLD: from pathophysiology to therapy. *Gut*. July 2019. doi:10.1136/gutjnl-2018-318146

199. Liu C-H, Ampuero J, Gil-Gomez A, et al. miRNAs in patients with non-alcoholic fatty liver disease: A systematic review and meta-analysis. *J Hepatol*. 2018;69(6):1335-1348. doi:10.1016/j.jhep.2018.08.008

200. He Z, Hu C, Jia W. miRNAs in non-alcoholic fatty liver disease. *Front Med*. 2016;10(4):389-396. doi:10.1007/s11684-016-0468-5

201. Otsuka M, Kishikawa T, Yoshikawa T, et al. MicroRNAs and liver disease. *J Hum Genet*. 2017. doi:10.1038/jhg.2016.53

202. Cheung O, Puri P, Eicken C, et al. Nonalcoholic steatohepatitis is associated with altered hepatic MicroRNA expression. *Hepatology*. 2008. doi:10.1002/hep.22569

203. Pirola CJ, Fernández Gianotti T, Castaño GO, et al. Circulating microRNA signature in non-alcoholic fatty liver disease: from serum non-coding RNAs to liver histology and disease pathogenesis. *Gut*. 2015;64(5):800-812. doi:10.1136/gutjnl-2014-306996

204. Leti F, Malenica I, Doshi M, et al. High-throughput sequencing reveals altered expression of hepatic microRNAs in nonalcoholic fatty liver disease-related fibrosis. *Transl Res*. 2015;166(3):304-314. doi:10.1016/j.trsl.2015.04.014

205. Soronen J, Yki-Järvinen H, Zhou Y, et al. Novel hepatic microRNAs upregulated in human nonalcoholic fatty liver disease. *Physiol Rep*. 2016. doi:10.14814/phy2.12661

206. Guo Y, Xiong Y, Sheng Q, Zhao S, Wattacheril J, Flynn CR. A micro-RNA expression signature for human NAFLD progression. *J Gastroenterol*. 2016;51(10):1022-1030. doi:10.1007/s00535-016-1178-0

207. Pirola CJ, Gianotti TF, Castaño GO, et al. Circulating microRNA signature in non-alcoholic fatty liver disease: From serum non-coding RNAs to liver histology and disease pathogenesis. *Gut*. 2015. doi:10.1136/gutjnl-2014-306996

208. Szabo G, Csak T. Role of MicroRNAs in NAFLD/NASH. *Dig Dis Sci*. 2016;61(5):1314-1324. doi:10.1007/s10620-015-4002-4

209. Tessitore A, Cicciarelli G, Del Vecchio F, et al. MicroRNA expression analysis in high fat diet-induced NAFLD-NASH-HCC progression: study on C57BL/6J mice. *BMC Cancer*. 2016. doi:10.1186/s12885-015-2007-1

210. Tsai WC, Hsu S Da, Hsu CS, et al. MicroRNA-122 plays a critical role in liver homeostasis and hepatocarcinogenesis. *J Clin Invest*. 2012. doi:10.1172/JCI63455

211. Moore KJ, Rayner KJ, Suárez Y, Fernández-Hernando C. The Role of MicroRNAs in Cholesterol Efflux and Hepatic Lipid Metabolism. *Annu Rev Nutr*. 2011. doi:10.1146/annurev-nutr-081810-160756

212. Esau C, Davis S, Murray SF, et al. miR-122 regulation of lipid metabolism revealed by in vivo antisense targeting. *Cell Metab*. 2006. doi:10.1016/j.cmet.2006.01.005

213. Horie T, Nishino T, Baba O, et al. MicroRNA-33 regulates sterol regulatory element-binding protein 1 expression in mice. *Nat Commun*. 2013. doi:10.1038/ncomms3883

214. Ding J, Li M, Wan X, et al. Effect of MIR-34a in regulating steatosis by targeting PPARα expression in nonalcoholic fatty liver disease. *Sci Rep*. 2015. doi:10.1038/srep13729

215. Salvoza NC, Klinzing DC, Gopez-Cervantes J, Baclig MO. Association of circulating serum MIR-34a and MIR-122 with dyslipidemia among patients with non-alcoholic fatty liver disease. *PLoS One*. 2016. doi:10.1371/journal.pone.0153497

216. Loyer X, Paradis V, Hénique C, et al. Liver microRNA-21 is overexpressed in non-alcoholic steatohepatitis and contributes to the disease in experimental models by inhibiting PPARα expression. *Gut*. 2016. doi:10.1136/gutjnl-2014-308883

217. Trajkovski M, Hausser J, Soutschek J, et al. MicroRNAs 103 and 107 regulate insulin sensitivity. *Nature*. 2011;474(7353):649-653. doi:10.1038/nature10112

218. C. R, G.-W. U, K. B, et al. Micro-RNA profiling reveals a role for miR-29 in human and murine liver fibrosis. *Hepatology*. 2011;53(1):209-218. doi:http://dx.doi.org/10.1002/hep.23922

219. Deng Z, He Y, Yang X, et al. MicroRNA-29: A Crucial Player in Fibrotic Disease. *Mol Diagnosis Ther*. 2017;21(3):285-294. doi:10.1007/s40291-016-0253-9

220. Jampoka K, Muangpaisarn P, Khongnomnan K, Treeprasertsuk S, Tangkijvanich P, Payungporn S. Serum miR-29a and miR-122 as Potential Biomarkers for Non-Alcoholic Fatty Liver Disease (NAFLD). *MicroRNA*. 2018;7(3):215-222. doi:10.2174/2211536607666180531093302

221. Csak T, Bala S, Lippai D, et al. microRNA-122 regulates hypoxia-inducible factor-1 and vimentin in hepatocytes and correlates with fibrosis in diet-induced steatohepatitis. *Liver Int*. 2015. doi:10.1111/liv.12633

222. Coulouarn C, Factor VM, Andersen JB, Durkin ME, Thorgeirsson SS. Loss of miR-122 expression in liver cancer correlates with suppression of the hepatic phenotype and gain of metastatic properties. *Oncogene*. 2009;28(40):3526-3536. doi:10.1038/onc.2009.211

223. Iliopoulos D, Hirsch HA, Struhl K. An Epigenetic Switch Involving NF-κB, Lin28, Let-7 MicroRNA, and IL6 Links Inflammation to Cell Transformation. *Cell*. 2009;139(4):693-706. doi:10.1016/j.cell.2009.10.014

224. Kota J, Chivukula RR, O'Donnell KA, et al. Therapeutic microRNA Delivery Suppresses Tumorigenesis in a Murine Liver Cancer Model. *Cell*. 2009;137(6):1005-1017. doi:10.1016/j.cell.2009.04.021

225. Trajkovski M, Hausser J, Soutschek J, et al. MicroRNAs 103 and 107 regulate insulin sensitivity. *Nature*. 2011;474(7353):649-653. doi:10.1038/nature10112

226. C. R, G.-W. U, K. B, et al. Micro-RNA profiling reveals a role for miR-29 in human and murine liver fibrosis. *Hepatology*. 2011;53(1):209-218. doi:http://dx.doi.org/10.1002/hep.23922

227. Deurenberg P, Weststrate JA, Seidell JC. Body mass index as a measure of body fatness:

age- and sex-specific prediction formulas. *Br J Nutr*. 1991. doi:10.1079/BJN19910073

228. Bonora E, Targher G, Alberiche M, et al. Homeostasis model assessment closely mirrors the glucose clamp technique in the assessment of insulin sensitivity: Studies in subjects with various degrees of glucose tolerance and insulin sensitivity. *Diabetes Care*. 2000. doi:10.2337/diacare.23.1.57
229. Aguilo F, Zhang F, Sancho A, et al. Coordination of m6A mRNA Methylation and Gene Transcription by ZFP217 Regulates Pluripotency and Reprogramming. *Cell Stem Cell*. 2015;17(6):689-704. doi:10.1016/j.stem.2015.09.005
230. Costantini S, Di Bernardo G, Cammarota M, Castello G, Colonna G. Gene expression signature of human HepG2 cell line. *Gene*. 2013. doi:10.1016/j.gene.2012.12.106
231. Kasai F, Hirayama N, Ozawa M, Satoh M, Kohara A. HuH-7 reference genome profile: complex karyotype composed of massive loss of heterozygosity. *Hum Cell*. 2018. doi:10.1007/s13577-018-0212-3
232. Mayer CM, Belsham DD. Palmitate attenuates insulin signaling and induces endoplasmic reticulum stress and apoptosis in hypothalamic neurons: Rescue of resistance and apoptosis through adenosine 5′ monophosphate-activated protein kinase activation. *Endocrinology*. 2010;151(2):576-585. doi:10.1210/en.2009-1122
233. Chlouverakis C, Harris P. Composition of the free fatty acid fraction in the plasma of human arterial blood. *Nature*. 1960;188(4756):1111-1112. doi:10.1038/1881111a0
234. Liu X, Chhipa RR, Nakano I, Dasgupta B. The AMPK Inhibitor Compound C Is a Potent AMPK-Independent Antiglioma Agent. *Mol Cancer Ther*. 2014. doi:10.1158/1535-7163.mct-13-0579
235. Bailey CJ. Metformin: historical overview. *Diabetologia*. 2017. doi:10.1007/s00125-017-4318-z
236. Anastasov N, Höfig I, Mall S, Krackhardt AM, Thirion C. Optimized lentiviral transduction protocols by use of a poloxamer enhancer, spinoculation, and scFv-antibody fusions to VSV-G. In: *Methods in Molecular Biology*. ; 2016. doi:10.1007/978-1-4939-3753-0_4
237. Geier GE, Modrich P. Recognition sequence of the dam methylase of Escherichia coli K12 and mode of cleavage of Dpn I endonuclease. *J Biol Chem*. 1979.
238. Dheda K, Huggett JF, Bustin SA, Johnson MA, Rook G, Zumla A. Validation of housekeeping genes for normalizing RNA expression in real-time PCR. *Biotechniques*. 2004.
239. Biederman J, Yee J, Cortes P. Validation of internal control genes for gene expression analysis in diabetic glomerulosclerosis. *Kidney Int*. 2004. doi:10.1111/j.1523-1755.2004.66016.x
240. Silver N, Best S, Jiang J, Thein SL. Selection of housekeeping genes for gene expression studies in human reticulocytes using real-time PCR. *BMC Mol Biol*. 2006. doi:10.1186/1471-2199-7-33
241. Thal SC, Wyschkon S, Pieter D, Engelhard K, Werner C. Selection of endogenous control

genes for normalization of gene expression analysis after experimental brain trauma in mice. *J Neurotrauma*. 2008. doi:10.1089/neu.2007.0497

242. Radonić A, Thulke S, Mackay IM, Landt O, Siegert W, Nitsche A. Guideline to reference gene selection for quantitative real-time PCR. *Biochem Biophys Res Commun*. 2004. doi:10.1016/j.bbrc.2003.11.177
243. Livak KJ, Schmittgen TD. Analysis of relative gene expression data using real-time quantitative PCR and the 2-ΔΔCT method. *Methods*. 2001. doi:10.1006/meth.2001.1262
244. Imbernon M, Beiroa D, Vázquez MJ, et al. Central melanin-concentrating hormone influences liver and adipose metabolism via specific hypothalamic nuclei and efferent autonomic/JNK1 pathways. *Gastroenterology*. 2013. doi:10.1053/j.gastro.2012.10.051
245. Bligh EG, Dyer WJ. A rapid method of total lipid extraction. *Can J Biochem Physiol*. 1959;37(8):911-917. doi:10.1145/3163918
246. Liebisch G, Lieser B, Rathenberg J, Drobnik W, Schmitz G. High-throughput quantification of phosphatidylcholine and sphingomyelin by electrospray ionization tandem mass spectrometry coupled with isotope correction algorithm. *Biochim Biophys Acta - Mol Cell Biol Lipids*. 2004;1686(1-2):108-117. doi:10.1016/j.bbalip.2004.09.003
247. Liebisch G, Binder M, Schifferer R, Langmann T, Schulz B, Schmitz G. High throughput quantification of cholesterol and cholesteryl ester by electrospray ionization tandem mass spectrometry (ESI-MS/MS). *Biochim Biophys Acta - Mol Cell Biol Lipids*. 2006;1761(1):121-128. doi:10.1016/j.bbalip.2005.12.007
248. Liebisch G, Drobnik W, Lieser B, Schmitz G. High-throughput quantification of lysophosphatidylcholine by electrospray ionization tandem mass spectrometry. *Clin Chem*. 2002;48(12):2217-2224.
249. Matyash V, Liebisch G, Kurzchalia T V, Shevchenko A, Schwudke D. methods Lipid extraction by methyl-tert-butyl ether for high-throughput lipidomics. *J Lipid Res*. 2008;49:1137-1146. doi:10.1194/jlr.D700041-JLR200
250. Zemski Berry KA, Murphy RC. Electrospray ionization tandem mass spectrometry of glycerophosphoethanolamine plasmalogen phospholipids. *J Am Soc Mass Spectrom*. 2004;15(10):1499-1508. doi:10.1016/j.jasms.2004.07.009
251. Liebisch G, Drobnik W, Reil M, et al. Quantitative measurement of different ceramide species from crude cellular extracts by electrospray ionization tandem mass spectrometry (ESI-MS/MS). *J Lipid Res*. 1999;40(8):1539-1546. http://www.ncbi.nlm.nih.gov/pubmed/10428992.
252. Liebisch G, Vizcaino JA, Koefeler H, et al. Shorthand Notation for Lipid Structures Derived from Mass Spectrometry. *J Lipid Res*. 2013;54. doi:10.1194/jlr.M033506
253. Höring M, Ejsing CS, Hermansson M, Liebisch G. Quantification of Cholesterol and Cholesteryl Ester by Direct Flow Injection High Resolution FTMS Utilizing Species-Specific Response Factors. *Anal Chem*. 2019. doi:10.1021/acs.analchem.8b05013
254. Husen P, Tarasov K, Katafiasz M, et al. Analysis of lipid experiments (ALEX): A software

framework for analysis of high-resolution shotgun lipidomics data. *PLoS One*. 2013;8(11). doi:10.1371/journal.pone.0079736

255. Lewis BP, Burge CB, Bartel DP. Conserved seed pairing, often flanked by adenosines, indicates that thousands of human genes are microRNA targets. *Cell*. 2005;120(1):15-20. doi:10.1016/j.cell.2004.12.035
256. Vlachos IS, Zagganas K, Paraskevopoulou MD, et al. DIANA-miRPath v3.0: Deciphering microRNA function with experimental support. *Nucleic Acids Res*. 2015. doi:10.1093/nar/gkv403
257. Huang DW, Sherman BT, Lempicki RA. Systematic and integrative analysis of large gene lists using DAVID bioinformatics resources. *Nat Protoc*. 2009;4(1):44-57. doi:10.1038/nprot.2008.211
258. Huang DW, Sherman BT, Lempicki RA. Bioinformatics enrichment tools: Paths toward the comprehensive functional analysis of large gene lists. *Nucleic Acids Res*. 2009;37(1):1-13. doi:10.1093/nar/gkn923
259. Beck JR, Shultz EK. The use of relative operating characteristic (ROC) curves in test performance evaluation. *Arch Pathol Lab Med*. 1986;110(1):13-20.
260. Vandesompele J, Preter D, Pattyn F, et al. Accurate normalization of real-time quantitative RT-PCR data by geometric averaging of multiple internal control genes. *Genome Biol*. 2002;3(7):2-12. doi:10.1186/gb-2002-3-7-research0034
261. Auguet T, Berlanga A, Guiu-Jurado E, et al. Altered fatty acid metabolism-related gene expression in liver from morbidly obese women with non-alcoholic fatty liver disease. *Int J Mol Sci*. 2014. doi:10.3390/ijms151222173
262. Walle P, Takkunen M, Männistö V, et al. Fatty acid metabolism is altered in non-alcoholic steatohepatitis independent of obesity. *Metabolism*. 2016. doi:10.1016/j.metabol.2016.01.011
263. Baranova A, Schlauch K, Elariny H, et al. Gene expression patterns in hepatic tissue and visceral adipose tissue of patients with non-alcoholic fatty liver disease. *Obes Surg*. 2007.
264. Younossi ZM, Baranova A, Ziegler K, et al. A genomic and proteomic study of the spectrum of nonalcoholic fatty liver disease. *Hepatology*. 2005. doi:10.1002/hep.20838
265. Chen X, Li L, Liu X, et al. Oleic acid protects saturated fatty acid mediated lipotoxicity in hepatocytes and rat of non-alcoholic steatohepatitis. *Life Sci*. 2018. doi:10.1016/j.lfs.2018.04.022
266. Pfaffenbach KT, Gentile CL, Nivala AM, Wang D, Wei Y, Pagliassotti MJ. Linking endoplasmic reticulum stress to cell death in hepatocytes: Roles of C/EBP homologous protein and chemical chaperones in palmitate-mediated cell death. *Am J Physiol - Endocrinol Metab*. 2010. doi:10.1152/ajpendo.00642.2009
267. Zhou Y, Yu S, Cai C, Zhong L, Yu H, Shen W. LXRα participates in the mTOR/S6K1/SREBP-1c signaling pathway during sodium palmitate-induced lipogenesis in HepG2 cells. *Nutr Metab*. 2018. doi:10.1186/s12986-018-0268-9

268. Park WJ, Park JW, Merrill AH, Storch J, Pewzner-Jung Y, Futerman AH. Hepatic fatty acid uptake is regulated by the sphingolipid acyl chain length. *Biochim Biophys Acta - Mol Cell Biol Lipids*. 2014. doi:10.1016/j.bbalip.2014.09.009

269. Foretz M, Even PC, Viollet B. AMPK activation reduces hepatic lipid content by increasing fat oxidation in vivo. *Int J Mol Sci*. 2018. doi:10.3390/ijms19092826

270. Liu X, Chhipa RR, Nakano I, Dasgupta B. The AMPK inhibitor compound C is a potent AMPK-independent antiglioma agent. *Mol Cancer Ther*. 2014. doi:10.1158/1535-7163.MCT-13-0579

271. Stephenne X, Foretz M, Taleux N, et al. Metformin activates AMP-activated protein kinase in primary human hepatocytes by decreasing cellular energy status. *Diabetologia*. 2011. doi:10.1007/s00125-011-2311-5

272. Rena G, Hardie DG, Pearson ER. The mechanisms of action of metformin. *Diabetologia*. 2017. doi:10.1007/s00125-017-4342-z

273. Mansouri A, Gattolliat CH, Asselah T. Mitochondrial Dysfunction and Signaling in Chronic Liver Diseases. *Gastroenterology*. 2018. doi:10.1053/j.gastro.2018.06.083

274. Gan L, Xiang W, Xie B, Yu L. Molecular mechanisms of fatty liver in obesity. *Front Med*. 2015;9(3):275-287. doi:10.1007/s11684-015-0410-2

275. Li Y, Xu S, Mihaylova MM, et al. AMPK phosphorylates and inhibits SREBP activity to attenuate hepatic steatosis and atherosclerosis in diet-induced insulin-resistant mice. *Cell Metab*. 2011. doi:10.1016/j.cmet.2011.03.009

276. Day EA, Ford RJ, Steinberg GR. AMPK as a Therapeutic Target for Treating Metabolic Diseases. *Trends Endocrinol Metab*. 2017;28(8):545-560. doi:10.1016/j.tem.2017.05.004

277. Lin HZ, Yang SQ, Chuckaree C, Kuhajda F, Ronnet G, Diehl AM. Metformin reverses fatty liver disease in obese, leptin-deficient mice. *Nat Med*. 2000. doi:10.1038/79697

278. You M, Matsumoto M, Pacold CM, Cho WK, Crabb DW. The role of AMP-activated protein kinase in the action of ethanol in the liver. *Gastroenterology*. 2004. doi:10.1053/j.gastro.2004.09.049

279. Isakovic A, Harhaji L, Stevanovic D, et al. Dual antiglioma action of metformin: Cell cycle arrest and mitochondria-dependent apoptosis. *Cell Mol Life Sci*. 2007. doi:10.1007/s00018-007-7080-4

280. Bain J, Plater L, Elliott M, et al. The selectivity of protein kinase inhibitors: a further update. *Biochem J*. 2007. doi:10.1042/bj20070797

281. Yu P, Xu X, Zhang J, et al. Liraglutide Attenuates Nonalcoholic Fatty Liver Disease through Adjusting Lipid Metabolism via SHP1/AMPK Signaling Pathway. *Int J Endocrinol*. 2019. doi:10.1155/2019/1567095

282. Chen K, Chen X, Xue H, et al. Coenzyme Q10 attenuates high-fat diet-induced non-alcoholic fatty liver disease through activation of the AMPK pathway. *Food Funct*. 2019. doi:10.1039/c8fo01236a

283. López M, Nogueiras R, Tena-Sempere M, Diéguez C. Hypothalamic AMPK: A canonical

regulator of whole-body energy balance. *Nat Rev Endocrinol*. 2016. doi:10.1038/nrendo.2016.67

284. Dweep H, Gretz N, Sticht C. MiRWalk database for miRNA-target interactions. *Methods Mol Biol*. 2014. doi:10.1007/978-1-4939-1062-5_25
285. Kersten S. Angiopoietin-like 3 in lipoprotein metabolism. *Nat Rev Endocrinol*. 2017. doi:10.1038/nrendo.2017.119
286. Salo VT, Belevich I, Li S, et al. Seipin regulates ER–lipid droplet contacts and cargo delivery. *EMBO J*. 2016. doi:10.15252/embj.201695170
287. Bartel DP. MicroRNAs: Target Recognition and Regulatory Functions. *Cell*. 2009. doi:10.1016/j.cell.2009.01.002
288. Ortega FJ, Mercader JM, Catalán V, et al. Targeting the circulating microRNA signature of obesity. *Clin Chem*. 2013. doi:10.1373/clinchem.2012.195776
289. Ortega FJ, Mercader JM, Moreno-Navarrete JM, et al. Profiling of circulating microRNAs reveals common microRNAs linked to type 2 diabetes that change with insulin sensitization. *Diabetes Care*. 2014. doi:10.2337/dc13-1847
290. Lim LP, Lau NC, Garrett-Engele P, et al. Microarray analysis shows that some microRNAs downregulate large numbers of-target mRNAs. *Nature*. 2005;433(7027):769-773. doi:10.1038/nature03315
291. Nielsen CB, Shomron N, Sandberg R, Hornstein E, Kitzman J, Burge CB. Determinants of targeting by endogenous and exogenous microRNAs and siRNAs. *RNA*. 2007. doi:10.1261/rna.768207
292. Auguet T, Berlanga A, Guiu-Jurado E, et al. Altered fatty acid metabolism-related gene expression in liver from morbidly obese women with non-alcoholic fatty liver disease. *Int J Mol Sci*. 2014. doi:10.3390/ijms151222173
293. Cheung O, Puri P, Eicken C, et al. Nonalcoholic steatohepatitis is associated with altered hepatic MicroRNA expression. *Hepatology*. 2008;48(6):1810-1820. doi:10.1002/hep.22569
294. Kohjima M, Enjoji M, Higuchi N, et al. Re-evaluation of fatty acid metabolism-related gene expression in nonalcoholic fatty liver disease. *Int J Mol Med*. 2007.
295. Naik A, Košir R, Rozman D. Genomic aspects of NAFLD pathogenesis. *Genomics*. 2013. doi:10.1016/j.ygeno.2013.03.007
296. Iliopoulos D, Drosatos K, Hiyama Y, Goldberg IJ, Zannis VI. MicroRNA-370 controls the expression of MicroRNA-122 and Cpt1α and affects lipid metabolism. *J Lipid Res*. 2010. doi:10.1194/jlr.m004812
297. Pardina E, Baena-Fustegueras JA, Llamas R, et al. Lipoprotein lipase expression in livers of morbidly obese patients could be responsible for liver steatosis. *Obes Surg*. 2009. doi:10.1007/s11695-009-9827-5
298. Wang B, Majumder S, Nuovo G, et al. Role of microRNA-155 at early stages of hepatocarcinogenesis induced by choline-deficient and amino acid-defined diet in C57BL/6 mice. *Hepatology*. 2009. doi:10.1002/hep.23100

299. Li S, Chen X, Zhang H, et al. Differential expression of microRNAs in mouse liver under aberrant energy metabolic status. *J Lipid Res*. 2009. doi:10.1194/jlr.M800509-JLR200
300. Song K-H, Li T, Owsley E, Chiang JYL. A putative role of micro RNA in regulation of cholesterol 7α-hydroxylase expression in human hepatocytes. *J Lipid Res*. 2010. doi:10.1194/jlr.m004531
301. Zhang J, Yang Y, Yang T, et al. Double-negative feedback loop between MicroRNA-422a and forkhead box (FOX)G1/Q1/E1 regulates hepatocellular carcinoma tumor growth and metastasis. *Hepatology*. 2015. doi:10.1002/hep.27491
302. Krützfeldt J, Rajewsky N, Braich R, et al. Silencing of microRNAs in vivo with "antagomirs." *Nature*. 2005. doi:10.1038/nature04303
303. Wei S, Zhang M, Yu Y, et al. HNF-4α regulated miR-122 contributes to development of gluconeogenesis and lipid metabolism disorders in Type 2 diabetic mice and in palmitate-treated HepG2 cells. *Eur J Pharmacol*. 2016. doi:10.1016/j.ejphar.2016.08.038
304. Nie H, Song C, Wang D, et al. MicroRNA-194 inhibition improves dietary-induced non-alcoholic fatty liver disease in mice through targeting on FXR. *Biochim Biophys Acta - Mol Basis Dis*. 2017. doi:10.1016/j.bbadis.2017.09.020
305. Petersen MC, Vatner DF, Shulman GI. Regulation of hepatic glucose metabolism in health and disease. *Nat Rev Endocrinol*. 2017. doi:10.1038/nrendo.2017.80
306. She P, Burgess SC, Shiota M, et al. Mechanisms by which liver-specific PEPCK knockout mice preserve euglycemia during starvation. *Diabetes*. 2003. doi:10.2337/diabetes.52.7.1649
307. Huang YH, Lin KH, Chen HC, et al. Identification of postoperative prognostic microRNA predictors in hepatocellular carcinoma. *PLoS One*. 2012. doi:10.1371/journal.pone.0037188
308. Zhang X, Daucher M, Armistead D, Russell R, Kottilil S. MicroRNA Expression Profiling in HCV-Infected Human Hepatoma Cells Identifies Potential Anti-Viral Targets Induced by Interferon-α. *PLoS One*. 2013. doi:10.1371/journal.pone.0055733
309. Hilton C, Neville MJ, Karpe F. MicroRNAs in adipose tissue: Their role in adipogenesis and obesity. *Int J Obes*. 2013. doi:10.1038/ijo.2012.59
310. Hsieh CH, Rau CS, Wu SC, et al. Weight-reduction through a low-fat diet causes differential expression of circulating microRNAs in obese C57BL/6 mice. *BMC Genomics*. 2015. doi:10.1186/s12864-015-1896-3
311. Huang Y, Chen HC, Chiang CW, Yeh CT, Chen SJ, Chou CK. Identification of a two-layer regulatory network of proliferation-related microRNAs in hepatoma cells. *Nucleic Acids Res*. 2012. doi:10.1093/nar/gks789
312. Jiang W, Liu J, Dai Y, Zhou N, Ji C, Li X. MiR-146b attenuates high-fat diet-induced non-alcoholic steatohepatitis in mice. *J Gastroenterol Hepatol*. 2015. doi:10.1111/jgh.12878
313. Taganov KD, Boldin MP, Chang K-J, Baltimore D. NF- B-dependent induction of microRNA miR-146, an inhibitor targeted to signaling proteins of innate immune responses. *Proc Natl Acad Sci*. 2006. doi:10.1073/pnas.0605298103

314. Feng YY, Xu XQ, Ji CB, Shi CM, Guo XR, Fu JF. Aberrant hepatic MicroRNA expression in nonalcoholic fatty liver disease. *Cell Physiol Biochem*. 2014. doi:10.1159/000366394
315. Wang K, Zhang S, Marzolf B, et al. Circulating microRNAs, potential biomarkers for drug-induced liver injury. *Proc Natl Acad Sci*. 2009. doi:10.1073/pnas.0813371106
316. Kim K, Pyo S, Um SH. S6 kinase 2 deficiency enhances ketone body production and increases peroxisome proliferator-activated receptor alpha activity in the liver. *Hepatology*. 2012. doi:10.1002/hep.25537
317. Mihaylova MM, Shaw RJ. The AMPK signalling pathway coordinates cell growth, autophagy and metabolism. *Nat Cell Biol*. 2011. doi:10.1038/ncb2329
318. Rao E, Zhang Y, Li Q, et al. AMPK-dependent and independent effects of AICAR and compound C on T-cell responses. *Oncotarget*. 2016. doi:10.18632/oncotarget.9277
319. Li Y, Xu S, Mihaylova MM, et al. AMPK phosphorylates and inhibits SREBP activity to attenuate hepatic steatosis and atherosclerosis in diet-induced insulin-resistant mice. *Cell Metab*. 2011;13(4):376-388. doi:10.1016/j.cmet.2011.03.009
320. Hardie DG. AMPK: A key regulator of energy balance in the single cell and the whole organism. *Int J Obes*. 2008. doi:10.1038/ijo.2008.116
321. Martello G, Rosato A, Ferrari F, et al. A microRNA targeting dicer for metastasis control. *Cell*. 2010;141(7):1195-1207. doi:10.1016/j.cell.2010.05.017
322. Noren Hooten N, Martin-Montalvo A, Dluzen DF, et al. Metformin-mediated increase in DICER1 regulates microRNA expression and cellular senescence. *Aging Cell*. 2016;15(3):572-581. doi:10.1111/acel.12469
323. Blandino G, Valerio M, Cioce M, et al. Metformin elicits anticancer effects through the sequential modulation of DICER and c-MYC. *Nat Commun*. 2012;3. doi:10.1038/ncomms1859
324. Liu MX, Gao M, Li CZ, et al. Dicer1/miR-29/HMGCR axis contributes to hepatic free cholesterol accumulation in mouse non-alcoholic steatohepatitis. *Acta Pharmacol Sin*. 2017;38(5):660-671. doi:10.1038/aps.2016.158
325. Du J, Niu X, Wang Y, et al. MiR-146a-5p suppresses activation and proliferation of hepatic stellate cells in nonalcoholic fibrosing steatohepatitis through directly targeting Wnt1 and Wnt5a. *Sci Rep*. 2015;5. doi:10.1038/srep16163
326. Feng YY, Xu XQ, Ji CB, Shi CM, Guo XR, Fu JF. Aberrant hepatic MicroRNA expression in nonalcoholic fatty liver disease. *Cell Physiol Biochem*. 2014. doi:10.1159/000366394
327. Feng YY, Xu XQ, Ji CB, Shi CM, Guo XR, Fu JF. Aberrant hepatic MicroRNA expression in nonalcoholic fatty liver disease. *Cell Physiol Biochem*. 2014;34(6):1983-1997. doi:10.1159/000366394
328. He Q, Li F, Li J, et al. MicroRNA-26a-interleukin (IL)-6-IL-17 axis regulates the development of non-alcoholic fatty liver disease in a murine model. *Clin Exp Immunol*. 2017;187(1):174-184. doi:10.1111/cei.12838
329. Fan J, Li H, Nie X, et al. MiR-30c-5p ameliorates hepatic steatosis in leptin receptor-

deficient (db/db) mice via down-regulating FASN. *Oncotarget*. 2017;8(8):13450-13463. doi:10.18632/oncotarget.14561

330. Mehta R, Otgonsuren M, Younoszai Z, Allawi H, Raybuck B, Younossi Z. Circulating miRNA in patients with non-alcoholic fatty liver disease and coronary artery disease. *BMJ Open Gastroenterol*. 2016;3(1):e000096. doi:10.1136/bmjgast-2016-000096
331. Cao P, Zhang Q, Wan M, et al. Fatty acid synthase is a primary target of MiR-15a and MiR-16-1 in breast cancer. *Oncotarget*. 2016. doi:10.18632/oncotarget.12479
332. Young PA, Senkal CE, Suchanek AL, et al. Long-chain acyl-CoA synthetase 1 interacts with key proteins that activate and direct fatty acids into niche hepatic pathways. *J Biol Chem*. 2018. doi:10.1074/jbc.RA118.004049
333. Li LO, Ellis JM, Paich HA, et al. Liver-specific loss of long chain Acyl-CoA synthetase-1 decreases triacylglycerol synthesis and β-oxidation and alters phospholipid fatty acid composition. *J Biol Chem*. 2009. doi:10.1074/jbc.M109.022467
334. Li LO, Mashek DG, An J, Doughman SD, Newgard CB, Coleman RA. Overexpression of rat long chain acyl-CoA synthetase 1 alters fatty acid metabolism in rat primary hepatocytes. *J Biol Chem*. 2006. doi:10.1074/jbc.M604427200
335. Parkes HA, Carpenter L, Wood L, et al. Overexpression of acyl-CoA synthetase-1 increases lipid deposition in hepatic (HepG2) cells and rodent liver in vivo. *Am J Physiol Metab*. 2006. doi:10.1152/ajpendo.00112.2006
336. Luukkonen PK, Zhou Y, Sädevirta S, et al. Hepatic ceramides dissociate steatosis and insulin resistance in patients with non-alcoholic fatty liver disease. *J Hepatol*. 2016;64(5):1167-1175. doi:10.1016/j.jhep.2016.01.002
337. Goldenberg JR, Wang X, Lewandowski ED. Acyl CoA synthetase-1 links facilitated long chain fatty acid uptake to intracellular metabolic trafficking differently in hearts of male versus female mice. *J Mol Cell Cardiol*. 2016;94:1-9. doi:10.1016/j.yjmcc.2016.03.006
338. Norris GH, Porter CM, Jiang C, Millar CL, Blesso CN. Dietary sphingomyelin attenuates hepatic steatosis and adipose tissue inflammation in high-fat-diet-induced obese mice. *J Nutr Biochem*. 2017. doi:10.1016/j.jnutbio.2016.09.017
339. Soh J, Iqbal J, Queiroz J, Fernandez-Hernando C, Hussain MM. MicroRNA-30c reduces hyperlipidemia and atherosclerosis in mice by decreasing lipid synthesis and lipoprotein secretion. *Nat Med*. 2013;19(7):892-900. doi:10.1038/nm.3200
340. Irani S, Hussain MM. Role of microRNA-30c in lipid metabolism, adipogenesis, cardiac remodeling and cancer. *Curr Opin Lipidol*. 2015;26(2):139-146. doi:10.1097/MOL.0000000000000162
341. Dai L, Li S, Ma Y, et al. MicroRNA-30b regulates insulin sensitivity by targeting SERCA2b in non-alcoholic fatty liver disease. *Liver Int*. 2019. doi:10.1111/liv.14067
342. Khan RS, Newsome PN. Non-alcoholic fatty liver disease and liver transplantation. *Metabolism*. 2016. doi:10.1016/j.metabol.2016.02.013
343. Woods A, Williams JR, Muckett PJ, et al. Liver-Specific Activation of AMPK Prevents

Steatosis on a High-Fructose Diet. *Cell Rep*. 2017;18(13):3043-3051. doi:10.1016/j.celrep.2017.03.011

344. Romero-Gómez M, Zelber-Sagi S, Trenell M. Treatment of NAFLD with diet, physical activity and exercise. *J Hepatol*. 2017. doi:10.1016/j.jhep.2017.05.016
345. Zhang R, Wang X, Qu J-H, et al. Caloric Restriction Induces MicroRNAs to Improve Mitochondrial Proteostasis. *iScience*. 2019. doi:10.1016/j.isci.2019.06.028
346. Jeon SM. Regulation and function of AMPK in physiology and diseases. *Exp Mol Med*. 2016. doi:10.1038/emm.2016.81
347. Palacios OM, Carmona JJ, Michan S, et al. Diet and exercise signals regulate SIRT3 and activate AMPK and PGC-1alpha in skeletal muscle. *Aging (Albany NY)*. 2009. doi:10.18632/aging.100075
348. Sood P, Krek A, Zavolan M, Macino G, Rajewsky N. Cell-type-specific signatures of microRNAs on target mRNA expression. *Proc Natl Acad Sci*. 2006. doi:10.1073/pnas.0511045103

9. APPENDIX I

APPENDIX I

Megaplex™ Primer Pools, Human Pools Set v3.0 – Pool A

ASSAY NAME	1	2	3	4	5	6	7	8	9	10	11	12	13	14	15	16	17	18	19	20	21	22	23	24
A	let-7a	let-7c	let-7d	let-7e	let-7f	let-7g	miR-1	miR-9	miR-10a	miR-10b	U6 snRNA	U6 snRNA	miR-15a	miR-15b	miR-16	miR-17	miR-18a	miR-18b	miR-19a	miR-19b	miR-20a	miR-20b	miR-21	miR-22
B	miR-23a	miR-23b	miR-24	miR-25	miR-26a	miR-26b	miR-27a	miR-27b	miR-28-3p	miR-28	U6 snRNA	U6 snRNA	miR-29a	miR-29b	miR-29c	miR-30b	miR-30c	miR-31	miR-32	miR-33b	miR-34a	miR-34c	miR-92a	mmu-miR-93
C	miR-95	mmu-miR-96	miR-98	miR-99a	miR-99b	miR-100	miR-101	miR-103	miR-105	miR-106a	RNU44	miR-106b	miR-107	miR-122	mmu-miR-124a	miR-125a-3p	miR-125a-5p	miR-125b	miR-126	miR-127	miR-127-5p	miR-128a	mmu-miR-129-3p	miR-129
D	miR-130a	miR-130b	miR-132	miR-133a	miR-133b	mmu-miR-134	miR-135a	miR-135b	miR-136	mmu-miR-137	miR-138	miR-139-3p	miR-139-5p	miR-140-3p	mmu-miR-140	miR-141	miR-142-3p	miR-142-5p	miR-143	miR-145	miR-146a	miR-146b-3p	miR-146b	miR-147b
E	miR-148a	miR-148b	miR-149	miR-150	miR-152	mmu-miR-153	miR-154	miR-181a	miR-181c	miR-182	RNU48	miR-183	miR-184	miR-185	miR-186	mmu-miR-187	miR-188-3p	miR-190	miR-191	miR-192	miR-193a-3p	miR-193a-5p	miR-193b	miR-194
F	miR-195	miR-196b	miR-197	miR-198	miR-199a	miR-199a-3p	miR-199b	miR-200a	miR-200b	miR-200c	miR-202	miR-203	miR-204	miR-205	miR-208b	miR-210	miR-214	miR-215	miR-216a	miR-216b	miR-217	miR-218	miR-219	miR-221
G	miR-222	miR-223	miR-224	miR-296-3p	miR-296	miR-299-3p	miR-299-5p	miR-301	miR-301b	miR-302a	ath-miR159a	miR-302b	miR-302c	miR-320	miR-323-3p	miR-324-3p	miR-324-5p	miR-326	miR-328	miR-329	miR-330	miR-330-5p	miR-331	miR-331-5p
H	miR-335	miR-337-5p	miR-338-3p	miR-339-3p	miR-339-5p	miR-340	miR-155	let-7b	miR-342-3p	miR-342-5p	miR-345	miR-361	miR-362-3p	miR-362	miR-363	miR-365	miR-367	miR-369-3p	miR-369-5p	miR-370	miR-371-3p	miR-372	miR-373	miR-374
I	mmu-miR-374-5p	miR-375	miR-376a	miR-376b	miR-377	mmu-miR-379	miR-380-3p	miR-381	miR-382	miR-383	miR-409-5p	miR-410	miR-411	miR-422a	miR-423-5p	miR-424	miR-425-5p	miR-429	miR-431	miR-433	miR-449	miR-449b	miR-450a	miR-450b-3p
J	miR-450b-5p	mmu-miR-451	miR-452	miR-453	miR-454	miR-455-3p	miR-455	miR-483-5p	miR-484	miR-485-3p	miR-485-5p	miR-486-3p	miR-486	miR-487a	miR-487b	miR-488	miR-489	miR-490	miR-491-3p	mmu-miR-491	miR-493	miR-494	mmu-miR-495	mmu-miR-496
K	miR-499-3p	mmu-miR-499	miR-500	miR-501-3p	miR-501	miR-502-3p	miR-502	miR-503	miR-504	miR-505	miR-507	miR-508	miR-508-5p	miR-509-5p	miR-510	miR-512-3p	miR-512-5p	miR-513-5p	miR-515-3p	miR-515-5p	miR-516a-5p	miR-516b	miR-517a	miR-517c
L	miR-518a-3p	miR-518a-5p	miR-518b	miR-518c	miR-518d	miR-518d-5p	miR-518e	miR-518f	miR-519a	miR-519d	miR-519e	miR-520a	miR-520a#	miR-520d-5p	miR-520g	miR-521	miR-522	miR-523	miR-524-5p	miR-525-3p	miR-525	miR-526b	miR-532-3p	miR-532
M	miR-539	miR-541	miR-542-3p	miR-542-5p	miR-544	miR-545	miR-548a	miR-548a-5p	miR-548b	miR-548b-5p	miR-548c	miR-548c-5p	miR-548d	miR-548d-5p	miR-551b	miR-556-3p	miR-556-5p	miR-561	miR-570	miR-574-3p	miR-576-3p	miR-576-5p	miR-579	miR-582-3p
N	miR-582-5p	miR-589	miR-590-5p	miR-597	miR-598	mmu-miR-615	miR-615-5p	miR-616	miR-618	miR-624	miR-625	miR-627	miR-628-5p	miR-629	miR-636	miR-642	miR-651	miR-652	miR-653	miR-654-3p	miR-654	miR-655	miR-660	miR-671-3p
O	miR-672	miR-674	miR-708	miR-744	miR-758	miR-871	miR-872	miR-873	miR-874	miR-875-3p	miR-876-3p	miR-876-5p	miR-885-3p	miR-885-5p	miR-886-3p	miR-886-5p	miR-887	miR-888	miR-889	miR-890	miR-891a	miR-891b	miR-892a	miR-147
P	miR-208	miR-211	miR-212	miR-219-1-3p	miR-219-2-3p	miR-220	miR-220b	miR-220c	miR-298	miR-325	miR-346	miR-376c	miR-384	miR-412	miR-448	miR-492	miR-506	miR-509-3-5p	miR-511	miR-517b	miR-519c	miR-520b	miR-520e	miR-520f

ASSAY ID	1	2	3	4	5	6	7	8	9	10	11	12	13	14	15	16	17	18	19	20	21	22	23	24
A	000377	000379	002283	002406	000382	002282	002222	000583	000387	002218	001973	001973	000389	000390	000391	002308	002422	002217	000395	000396	000580	001014	000397	000398
B	000399	000400	000402	000403	000405	000407	000408	000409	002446	000411	001973	001973	002112	000413	000587	000602	000419	002279	002109	002085	000426	000428	000431	001090
C	000433	000186	000577	000435	000436	000437	002253	000439	002167	002169	001094	000442	000443	002245	001182	002199	002198	000449	002228	000452	002229	002216	001184	000590
D	000454	000456	000457	002246	002247	001186	000460	002261	000592	001129	002284	002313	002289	002234	001187	000463	000464	002248	002249	002278	000468	002361	001097	002262
E	000470	000471	002255	000473	000475	001191	000477	000480	000482	002334	001006	002269	000485	002271	002285	001193	002106	000489	002299	000491	002250	002281	002367	000493
F	000494	002215	000497	002273	000498	002304	000500	000502	002251	002300	002363	000507	000508	000509	002290	000512	002306	000518	002220	002326	002337	000521	000522	000524
G	002276	002295	002099	002101	000527	001015	000600	000528	002392	000529	000338	000531	000533	002277	002227	002161	000539	000542	000543	001101	000544	002230	000545	002233
H	000546	002156	002252	002184	002257	002258	002623	002619	002260	002147	002186	000554	002117	001273	001271	001020	000555	000557	001021	002275	002124	000560	000561	000563
I	001319	000564	000565	001102	000566	001138	000569	000571	000572	000573	002331	001274	001610	002297	002340	000604	001516	001024	001979	001028	001030	001608	002303	002208
J	002207	001141	002329	002318	002323	002244	001280	002338	001821	001277	001036	002093	001278	001279	001285	002357	002358	001037	002360	001630	002364	002365	001663	001953
K	002427	001352	002428	002435	001047	002083	001109	001048	002084	002089	001051	001052	002092	002235	002241	001823	001145	002090	002369	001112	002416	001150	002402	001153
L	002397	002396	001156	002401	001159	002389	002395	002388	002415	002403	002370	001167	001168	002393	001121	001122	002413	002386	001982	002385	001174	002382	002355	001518
M	001286	002201	001284	002240	002265	002267	001538	002412	001541	002408	001590	002429	001605	002237	001535	002345	002344	001528	002347	002349	002351	002350	002398	002399
N	001983	002409	001984	001551	001988	001960	002353	002414	001593	002430	002431	001560	002433	002436	002088	001592	001604	002352	002292	002239	001611	001612	001515	002322
O	002327	002021	002341	002324	001990	002354	002264	002356	002268	002204	002225	002205	002372	002296	002194	002193	002374	002212	002202	002209	002191	002210	002195	000469
P	000511	000514	000515	002095	002390	000523	002206	002211	002190	000540	000553	002122	000574	001023	001029	001039	001050	002155	001111	001152	001163	001116	001119	001120

APPENDIX I

Megaplex™ Primer Pools, Human Pools Set v3.0 – Pool B

ASSAY NAME	1	2	3	4	5	6	7	8	9	10	11	12	13	14	15	16	17	18	19	20	21	22	23	24
A	miR-7	miR-548I	miR-30a-3p	miR-30a-5p	miR-30d	miR-30e-3p	miR-34b	miR-126#	miR-154#	miR-182#	U6 snRNA	U6 snRNA	miR-206	miR-213	miR-302c#	miR-302d	miR-378	miR-380-5p	miR-1257	miR-200a#	miR-432	miR-432#	miR-497	miR-500
B	miR-1238	miR-488	miR-517#	miR-516-3p	miR-518c#	miR-519e#	miR-520h	miR-524	mmu-let-7d#	miR-363#	U6 snRNA	U6 snRNA	rno-miR-7#	miR-656	miR-549	miR-657	miR-658	miR-659	miR-551a	miR-552	miR-553	miR-554	miR-555	miR-557
C	miR-558	miR-559	miR-562	miR-563	miR-564	miR-566	miR-567	miR-569	miR-586	miR-587	RNU44	miR-588	miR-589	miR-550	miR-591	miR-592	miR-593	miR-596	miR-622	miR-599	miR-623	miR-600	miR-624	miR-601
D	miR-626	miR-629	miR-630	miR-631	miR-603	miR-604	miR-605	miR-606	miR-607	miR-608	miR-609	miR-633	miR-634	miR-635	miR-637	miR-638	miR-639	miR-640	miR-641	miR-613	miR-614	miR-616	miR-617	miR-643
E	miR-644	miR-645	miR-621	miR-646	miR-647	miR-648	miR-649	miR-650	miR-661	miR-662	RNU48	miR-571	miR-572	miR-573	miR-575	miR-578	miR-580	miR-581	miR-583	miR-584	miR-585	rno-miR-29c#	miR-766	miR-595
F	miR-668	miR-767-5p	miR-767-3p	miR-454#	miR-769-5p	miR-770-5p	miR-769-3p	miR-802	miR-675	miR-505#	miR-218-1#	miR-221#	miR-222#	miR-223#	miR-136#	miR-34b	miR-185#	miR-186#	miR-195#	miR-30c-1#	miR-30c-2#	miR-32#	miR-31#	miR-130b#
G	miR-26a-2#	miR-361-3p	let-7g#	miR-302b#	miR-302d#	miR-367#	miR-374a#	miR-23b#	miR-376a#	miR-377#	ath-miR159a	miR-30b#	miR-122#	miR-130a#	miR-132#	miR-148a#	miR-33a	miR-33a#	miR-92a-1#	miR-92a-2#	miR-93#	miR-96#	miR-99a#	miR-100#
H	miR-101#	miR-138-2#	miR-141#	miR-143#	miR-144#	miR-145#	miR-920	miR-921	miR-922	miR-924	miR-337-3p	miR-125b-2#	miR-135b#	miR-148b#	miR-146a#	miR-149#	miR-29b-1#	miR-29b-2#	miR-105#	miR-106a#	miR-16-2#	let-7i#	miR-15b#	miR-27b#
I	miR-933	miR-934	miR-935	miR-936	miR-937	miR-938	miR-939	miR-941	miR-335#	miR-942	miR-943	miR-944	miR-99b#	miR-124#	miR-541#	miR-875-5p	miR-888#	miR-892b	miR-9#	miR-411#	miR-378	miR-151-3p	miR-340#	miR-190b
J	miR-545#	miR-183#	miR-192#	miR-200b#	miR-200c#	miR-155#	miR-10a#	miR-214#	miR-218-2#	miR-129#	miR-22#	miR-425#	miR-30d#	let-7a#	miR-424#	miR-18b#	miR-20b#	miR-431#	miR-7-2#	miR-10b#	miR-34a#	miR-181a-2#	miR-744#	miR-452#
K	miR-409-3p	miR-181c#	miR-196a#	miR-483-3p	miR-708#	miR-92b#	miR-551b#	miR-202#	miR-193b#	miR-497#	miR-518e#	miR-543	miR-125b-1#	miR-194#	miR-106b#	miR-302a#	miR-519b-3p	miR-518f#	miR-374b#	miR-520c-3p	let-7b#	let-7c#	let-7e#	miR-550
L	miR-593	let-7f-1#	let-7f-2#	miR-15a#	miR-16-1#	miR-17#	miR-18a#	miR-19a#	miR-19b-1#	miR-625#	miR-628-3p	miR-20a#	miR-21#	miR-23a#	miR-24-1#	miR-24-2#	miR-25#	miR-26a-1#	miR-26b#	miR-27a#	miR-29a#	miR-151-5P	miR-765	miR-338-5P
M	miR-620	miR-577	miR-144	miR-590-3P	miR-191#	miR-665	miR-520D-3P	miR-1224-3P	miR-1305	miR-513C	miR-513B	miR-1226#	miR-1236	miR-1228#	miR-1225-3P	miR-1233	miR-1227	miR-1286	miR-548M	miR-1179	miR-1178	miR-1205	miR-1271	miR-1201
N	miR-548J	miR-1263	miR-1294	miR-1269	miR-1265	miR-1244	miR-1303	miR-1259	miR-548P	miR-1264	miR-1255B	miR-1282	miR-1255A	miR-1270	miR-1197	miR-1324	miR-548H	miR-1254	miR-548K	miR-1251	miR-1285	miR-1245	miR-1292	miR-1301
O	miR-1200	miR-1182	miR-1288	miR-1291	miR-1275	miR-1183	miR-1184	miR-1276	miR-320B	miR-1272	miR-1180	miR-1256	miR-1278	miR-1262	miR-1243	miR-663B	miR-1252	miR-1298	miR-1290	miR-1249	miR-1248	miR-1289	miR-1204	miR-1826
P	miR-1304	miR-1203	miR-1206	miR-548G	miR-1208	miR-548E	miR-1274A	miR-1274B	miR-1267	miR-1250	miR-548N	miR-1283	miR-1247	miR-1253	miR-720	miR-1260	miR-664	miR-1302	miR-1300	miR-1284	miR-548L	miR-1293	miR-1825	miR-1296

ASSAY ID	1	2	3	4	5	6	7	8	9	10	11	12	13	14	15	16	17	18	19	20	21	22	23	24
A	000268	002909	000416	000417	000420	000422	000427	000451	000478	000483	001973	001973	000510	000516	000534	000535	000567	000570	002910	001011	001026	001027	001043	001046
B	002927	001106	001113	001149	001158	001166	001170	001173	001178	001283	001973	001973	001338	001510	001511	001512	001513	001514	001519	001520	001521	001522	001523	001525
C	001526	001527	001529	001530	001531	001533	001534	001536	001539	001540	001094	001542	001543	001544	001545	001546	001547	001550	001553	001554	001555	001556	001557	001558
D	001559	001562	001563	001564	001566	001567	001568	001569	001570	001571	001573	001574	001576	001578	001581	001582	001583	001584	001585	001586	001587	001589	001591	001594
E	001596	001597	001598	001599	001600	001601	001602	001603	001606	001607	001006	001613	001614	001615	001617	001619	001621	001622	001623	001624	001625	001818	001986	001987
F	001992	001993	001995	001996	001998	002002	002003	002004	002005	002087	002094	002096	002097	002098	002100	002102	002104	002105	002107	002108	002110	002111	002113	002114
G	002115	002116	002118	002119	002120	002121	002125	002126	002127	002128	000338	002129	002130	002131	002132	002134	002135	002136	002137	002138	002139	002140	002141	002142
H	002143	002144	002145	002146	002148	002149	002150	002151	002152	002154	002157	002158	002159	002160	002163	002164	002165	002166	002168	002170	002171	002172	002173	002174
I	002176	002177	002178	002179	002180	002181	002182	002183	002185	002187	002188	002189	002196	002197	002200	002203	002213	002214	002231	002238	002243	002254	002259	002263
J	002266	002270	002272	002274	002286	002287	002288	002293	002294	002298	002301	002302	002305	002307	002309	002310	002311	002312	002314	002315	002316	002317	002325	002330
K	002332	002333	002336	002339	002342	002343	002346	002362	002366	002368	002371	002376	002378	002379	002380	002381	002384	002387	002391	002400	002404	002405	002407	002410
L	002411	002417	002418	002419	002420	002421	002423	002424	002425	002432	002434	002437	002438	002439	002440	002441	002442	002443	002444	002445	002447	002642	002643	002658
M	002672	002675	002676	002677	002678	002681	002743	002752	002867	002756	002757	002758	002761	002763	002766	002768	002769	002773	002775	002776	002777	002778	002779	002781
N	002783	002784	002785	002789	002790	002791	002792	002796	002798	002799	002801	002803	002805	002807	002810	002815	002816	002818	002819	002820	002822	002823	002824	002827
O	002829	002830	002832	002838	002840	002841	002842	002843	002844	002845	002847	002850	002851	002852	002854	002857	002860	002861	002863	002868	002870	002871	002872	002873
P	002874	002877	002878	002879	002880	002881	002883	002884	002885	002887	002888	002890	002893	002894	002895	002896	002897	002901	002902	002903	002904	002905	002907	002908

10. APPENDIX II

International Journal of Obesity (2017) **41,** 620–630

www.nature.com/ijo

ORIGINAL ARTICLE

Decreased lipid metabolism but increased FA biosynthesis are coupled with changes in liver microRNAs in obese subjects with NAFLD

J Latorre[1], JM Moreno-Navarrete[1,2], JM Mercader[3], M Sabater[1,2], Ò Rovira[1], J Gironès[4], W Ricart[1,2], JM Fernández-Real[1,2] and FJ Ortega[1,2]

BACKGROUND/OBJECTIVE: Many controversies regarding the association of liver miRNAs with obesity and nonalcoholic fatty liver diseases (NAFLD) call for additional validations. This study sought to investigate variations in genes and hepatic miRNAs in a sample of obese patients with or without NAFLD and human hepatocytes (HH).

SUBJECTS/METHODS: A total of 60 non-consecutive obese women following bariatric surgery were recruited. Subjects were classified as NAFLD ($n = 17$), borderline ($n = 24$) and controls ($n = 19$) with normal enzymatic profile, liver histology and ultrasound assessments. Profiling of 744 miRNAs was performed in 8 obese women with no sign of hepatic disease and 11 NAFLD patients. Additional validation and expression of genes related to *de novo* fatty acid (FA) biosynthesis, uptake, transport and β-oxidation; glucose metabolism, and inflammation was tested in the extended sample. Induction of NAFLD-related genes and miRNAs was examined in HepG2 cells and primary HH treated with palmitic acid (PA), a combination of palmitate and oleic acid, or high glucose, and insulin (HG) mimicking insulin resistance in NAFLD.

RESULTS: In the discovery sample, 14 miRNAs were associated with NAFLD. Analyses in the extended sample confirmed decreased miR-139-5p, miR-30b-5p, miR-122-5p and miR-422a, and increased miR-146b-5p in obese subjects with NAFLD. Multiple linear regression analyses disclosed that NAFLD contributed independently to explain miR-139-5p ($P = 0.005$), miR-30b-5p ($P = 0.005$), miR-122-5p ($P = 0.021$), miR-422a ($P = 0.007$) and miR-146a ($P = 0.033$) expression variance after controlling for confounders. Decreased miR-122-5p in liver was associated with impaired FA usage. Expression of inflammatory and macrophage-related genes was opposite to decreased miR-30b-5p, miR-139-5p and miR-422a, whereas increased miR-146b-5p was associated with FABP4 and decreased glucose metabolism and FA mobilization. In partial agreement, PA (but not HG) led to decreased miR-139-5p, miR-30b-5p, miR-422a and miR-146a *in vitro*, in parallel with increased lipogenesis and FA transport, decreased glucose metabolism and diminished FA oxidation.

CONCLUSION: This study confirms decreased liver glucose and lipid metabolism but increased FA biosynthesis coupled with changes in five unique miRNAs in obese patients with NAFLD.

International Journal of Obesity (2017) **41,** 620–630; doi:10.1038/ijo.2017.21

INTRODUCTION

Mounting evidence endorsing the relevance of microRNAs (miRNAs) in the regulation of metabolic issues points toward the future development of medical strategies in the field. Nonalcoholic fatty liver disease (NAFLD) represents a spectrum of disturbances encompassing fatty acid (FA) infiltration of the liver parenchyma (steatosis), fat deposition, inflammation (steatohepatitis) and cirrhosis.[1,2] NAFLD has been described as the hepatic manifestation of the metabolic syndrome,[3] being in close association with obesity and insulin resistance.[4] Given its physiological impact, the willingness to unravel the molecular pathways involved is growing exponentially. The link with metabolic disturbances has lead to the analysis of inflammatory pathways and genes related to lipid and glucose metabolism in liver as key contributors.[5] Emerging evidences suggest the involvement of epigenetic modulators such as miRNAs to the development of this disease.[6]

MiRNAs are small non-coding RNAs capable of modulating gene expression[7] either by translational inhibition or mRNA target degradation.[8] Their impact in gene expression profiles can modify a variety of biological functions, including glucose and lipid metabolism in adipose tissue, muscle and liver. With regard to the hepatic miRNA patterns, abnormal miRNA expressions have been reported in many liver diseases, including viral hepatitis,[9] cirrhosis, cancer,[10] and both alcoholic and nonalcoholic fatty liver.[6,11–14] The most recent reports unravel the abnormal expression of liver miRNAs in NAFLD patients, being the distinguishing hepatic miRNA profile associated with the global dysmetabolic disease state,[15] cardiovascular risk[16] and impaired FA accumulation in hepatocytes.[17]

Trying to provide insights into the potential involvement of miRNAs in NAFLD, Cheung *et al.*[12] profiled 474 mature miRNA species in liver samples from obese individuals with nonalcoholic steatohepatitis (NASH) and subjects with normal liver histology.

[1]Department of Diabetes, Endocrinology and Nutrition (UDEN), Institut d'Investigació Biomédica de Girona (IdIBGi), Hospital of Girona 'Dr Josep Trueta' Carretera de França s/n, Girona, Spain; [2]CIBER de la Fisiopatología de la Obesidad y la Nutrición (CIBERobn) and Instituto de Salud Carlos III (ISCIII), Madrid, Spain; [3]Joint BSC-CRG-IRB Research Program in Computational Biology, Barcelona Supercomputing Center, Barcelona, Spain and [4]Department of Surgery, Hospital Dr. Josep Trueta of Girona, Girona, Spain. Correspondence: Dr FJ Ortega, Department of Diabetes, Endocrinology and Nutrition (UDEN), Institut d'Investigació Biomédica de Girona (IDIBGI), Hospital of Girona 'Dr Josep Trueta' Carretera de França s/n, Girona, 17007 Spain.
E-mail: fortega@idibgi.org
Received 18 July 2016; revised 7 December 2016; accepted 11 January 2017; accepted article preview online 25 January 2017; advance online publication, 14 February 2017

They found that 46 miRNAs showed differential expression between groups. Among them, upregulation of miR-34a and miR-146b, and downregulation of miR-122 were confirmed in an extended sample of 50 subjects (18% men, age = 46 ± 9 years, body mass index (BMI) = 37.3 ± 3.2 kg m^{-2}).[12] Noteworthy, miRNA levels were not associated with NASH severity, suggesting a role in biological processes not related to fibrosis itself.[12] Another work[16] disclosed significant downregulation of two hepatic miRNA candidates (miR-122 and miR-192) in obese patients with NASH and/or NAFLD when compared to lean subjects with normal liver histology (n = 65; 43% men, age = 50 ± 6 years, BMI = 30.1 ± 4.2 kg m^{-2}). Additional profiles have analyzed miRNAs expression in liver samples from morbid obese females with (n = 15; age = 51 ± 8 years, BMI = 44.4 ± 6.6 kg m^{-2}) and without (n = 15; age = 47 ± 6 years, BMI = 41 ± 4.6 kg m^{-2}) hepatic fibrosis,[13] disclosing significant changes in miRNAs that completely differed from those reported before. More recently, the comprehensive work of Soronen *et al.*[14] identified a set of hepatic miRNAs linked to NAFLD (n = 30; 33% men, age = 48 ± 10 years, BMI = 45.9 ± 5.4 kg m^{-2}). Here again, the match with previous findings was scarce (Supplementary Table 1). In addition, many works have analyzed individual miRNAs in liver samples from animal models of impaired metabolism and/or NAFLD,[15,18] and cell systems.[17,19,20] These reports endorse the concept that miRNAs are involved in FA accumulation in hepatocytes, and the subsequent deleterious consequences affecting NAFLD progression and impaired metabolism. However, many controversies in the field call for further validation in extended human samples and additional *in vitro* models.

The current study sought to investigate variations in hepatic miRNAs in obese patients with or without NAFLD, and in hepatocytes under conditions inducing FA accumulation and/or insulin resistance. Thus, miRNA candidates were analyzed in a sample of 60 participants in association with clinical and biochemical parameters, and the hepatic expression of key genes related to glucose metabolism (GLUT2, G6PC, PEPCK), *de novo* FA biosynthesis (ChREBP, SREBP1c, LXRα, FXR, FASN, ACACA, PPP2R5C), FA uptake and transport (PPARγ, PGC1α, CD36, FABP4, FATP5, PTPL), FA oxidation (PPARα), inflammation (ITGAX, PPARδ, HAMP, TNFα) and endoplasmic reticulum stress (ATF6, DDIT3, HSPA5). Induction of NAFLD-related genes and miRNAs was also examined in cultured HepG2 cells and primary human hepatocytes (HH) treated with palmitate, a combination of palmitate and oleate representing the normal proportion of free FAs found in humans, and high glucose (HG) and insulin mimicking insulin resistance in NAFLD patients. We provide here additional evidence on the relevance of five miRNAs in liver pathophysiology, paving the way for investigations targeting the potential for genomic therapies based on miRNA-related transcriptional regulation.

MATERIALS AND METHODS

Study population

A total of 60 non-consecutive severe obese patients (20% male, age = 46 ± 9 years, BMI = 45.2 ± 6.6 kg m^{-2}) with (28.3%) or without NAFLD were recruited. Each subject underwent clinical assessment, radiological, hematological and biochemical testing prior to bariatric surgery (laparoscopic Roux-en-Y gastric bypass). NAFLD was suspected in those patients with either (1) abnormal liver enzymes and/or radiological evidence of fatty liver, coupled with negative study for other causes of liver disease and (2) absence of significant alcohol consumption (⩾20 g per day for women, and ⩾ 30 g per day for men). Subjects underwent a percutaneous core liver biopsy with a 15-gauge microvasive biopsy device and laparoscopic guidance. Liver samples were snap frozen in liquid nitrogen for genomic analyses, and fixed in formalin for histological assessment. Fixed samples were stained with hematoxylin–eosin and Masson's trichrome stain. All specimens were evaluated by the same pathologist and evaluated according to the NAFLD clinical research network criteria. Based on the laboratory and sonographic findings, subjects were classified as NAFLD patients, borderline or controls with normal liver histology, ultrasound and liver enzymes. Exclusion criteria included fatty liver alone, cirrhosis or bridging fibrosis, and the use of statins. The study protocol was approved by the Ethics Committee and the Committee for Clinical investigation (CEIC) of the Hospital Universitari Dr Josep Trueta. All subjects provided written informed consent before entering the study.

Clinical measurements

BMI was calculated as weight (in kilograms) divided by height (in meters) squared. Percent fat mass was measured using the Tanita BIA scale (Tanita Corporation, Tokyo, Japan). Blood pressure, fasting glucose, total serum cholesterol and triglycerides, and other routine laboratory tests were measured as previously.[21] Insulin sensitivity was assessed with the euglycemic hyperinsulinemic clamp technique, as previously described.[21] Patients were requested to withhold alcohol and caffeine during at least 12 h prior to the analyses.

Cell cultures and treatments

Human hepatoma HepG2 cells were purchased from American Type Culture Collection (ATCC) and cultured in Dulbecco's Modified Eagle's Medium (DMEM) supplemented with 10% fetal bovine serum (Gibco), 100 units ml^{-1} penicillin and streptomycin, 1% glutamine and 1% sodium pyruvate, at 37 °C and 5% CO_2 atmosphere. Cryopreserved primary HH were also commercially obtained (Innoprot, Bizkaia, Spain) and cultured with hepatocytes medium (Innoprot) supplemented with 5% fetal bovine serum, 1% hepatocytes growth supplement (that is, the combination of growth factors, hormones and proteins necessary for culture of primary hepatocytes), and 100 units ml^{-1} penicillin and streptomycin. HH grew on poly-L-lysine pre-coated cell dishes at 37 °C and 5% CO_2 atmosphere following manufacturer's recommendations. Treatments were performed in HepG2 and HH 24 h after seeding. FA accumulation was induced by palmitic acid (PA) exposure as follows: 27.84 mg of PA (Sigma, San Luis, MO) were dissolved in 1 ml sterile water to make a 100 mM stock solution. An aliquot of 5% bovine serum albumin (BSA) was prepared in serum-free DMEM. 100 mM PA stock solution and 5% BSA were mixed for at least 1 hour at 40 °C to obtain a 5 mM solution, as previously described.[22] Then, HepG2 cells (72 h) and HH (24 h) were treated with PA 500 and 200 μM, respectively. In addition, a combination of PA (200 μM) and oleic acid (OA, 300 μM) representing the normal proportion of free FA found in humans[23] was tested in HepG2. Insulin resistance conditions (HG) were tempted by a combination of HG (33 mM) and insulin (100 nM), as previously.[24–26] HepG2 cells and/or HH were treated with PA, PA+OA, HG or with a combination of these treatments. BSA supplemented medium was used as control when necessary. After treatment, cells were washed with phosphate buffered saline and collected with Qiazol for RNA purification. Total RNA, including small RNAs, was extracted and purified using RNeasy Mini Kit (QIAgen, Gaithersburg, MD) according to the manufacturers' protocol. HepG2 cells grown in 12-well plates were also washed with phosphate buffered saline and fixed with paraformaldehyde 7% for 1 h. Cells were dipped in isopropanol 60% before completely dried and stained with Oil Red O (Sigma, Lyon, France) for 10 min at room temperature. Pictures were taken using an inverted microscope. For the analysis of HG-induced insulin resistance, HH were maintained in starvation for 1 h after 24 h treatment with glucose and insulin or control. Insulin 100 nM in serum-free DMEM media was used for stimulation of insulin pathway for 10 min. Then, cells were collected and homogenized in 50 μl of lysis buffer (Cell Signaling Technology, Barcelona, Spain), and cell debris were discarded by centrifugation (10 min, 15 000 r.p.m. at 4 °C). Protein content was determined using the Lowry assay (Biorad, Madrid, Spain). Phosphorylated (Ser473) Akt serine/threonine kinase (pAkt) and total Akt were measured using the PathScan Elisa Kit (Cell Signaling Technology), according to the manufacturer's indications. All experimental conditions were tested in ⩾ 3 biological replicates.

Profile of hepatic miRNAs

An identification sample (n = 19) of 8 obese women (age = 44 ± 9 years, BMI = 43.6 ± 8 kg m^{-2}) with normal liver histology, ultrasound and liver enzymes, and 11 obese and NAFLD female patients (age = 48 ± 6 years, BMI = 44.8 ± 7 kg m^{-2}, mean ± s.d., Supplementary Table 2) was selected for profiling miRNAs in liver using TaqMan Low-Density Arrays (Applied Biosystems, Darmstadt, Germany). Liver specimens from the extended sample of 60 Caucasian men (20%) and women (17 NAFLD, 24 borderline and 19 control obese participants with no signs of liver disease, Table 1)

Table 1. Anthropometric and biochemical data of study participants

Clinical outputs (units)	*No NAFLD* (n = *19*)	*Borderline* (n = *24*)	*NAFLD* (n = *17*)	*ANOVA*	*LSD*[a]
Sex (M/W)	2/17	6/18	4/13		
Fatty liver (yes/no)	1/18	4/20	2/15		
Dyslipidemia (yes/no)	7/12	8/16	6/11		
T2D (yes/no)	6/13	5/19	6/11		
NAFLD activity score (%5 grade)	0	0	12.5		
Lobular activity (>2 focus/field, %)	0	8.3	12.6		
Ballooning degeneration (%)	0	4.2	18.8		
Fibrosis staging (%)	0	16.7	43.7		
Age (years)	45.9 ± 9.6	47.1 ± 9.2	49.9 ± 6.4	0.376	0.172
BMI (kg m^{-2})	44.5 ± 7.6	46.4 ± 5.5	44.5 ± 6.9	0.538	0.999
SBP (mm Hg)	132.6 ± 17.6	139.0 ± 12.3	151.5 ± 19.4	**0.004**	**0.001**
DBP (mm Hg)	74.3 ± 10.3	76.5 ± 11.8	86.9 ± 13.7	**0.006**	**0.003**
Fat mass (%, densitometry)	44.9 ± 5	47.5 ± 6.5	44.7 ± 4.5	0.205	0.881
Fasting glucose (mg dl^{-1})	98.3 ± 17.7	107.3 ± 32.4	125.2 ± 54.2	0.092	**0.032**
Fasting insulin (μIU ml^{-1})	10.6 ± 4.2	23.9 ± 24.9	31.1 ± 41	0.074	**0.026**
Glycated hemoglobin (%)	5.66 ± 0.56	6.04 ± 1.25	6.49 ± 1.38	0.092	**0.030**
HOMA-IR index	2.63 ± 1.54	7.69 ± 14.24	13.43 ± 25.46	0.148	0.052
M (mg (kg min)$^{-1}$)	5.2 ± 3.16	3.32 ± 1.62	2.4 ± 1.23	**0.003**	**0.001**
Cholesterol (mg dl^{-1})	179.9 ± 30.5	201.1 ± 36.2	186.3 ± 27.9	0.095	0.558
HDL cholesterol (mg dl^{-1})	47.2 ± 10.4	46.0 ± 9.6	48.1 ± 15	0.852	0.817
LDL cholesterol (mg dl^{-1})	113.3 ± 26.5	129.7 ± 33.8	108.9 ± 22.7	0.053	0.646
Triglycerides (mg dl^{-1})	97.7 ± 36.7	126.7 ± 47.5	146.4 ± 52	**0.008**	**0.002**
GGT (IU l^{-1})	20.3 ± 7.7	28.7 ± 12.7	43.2 ± 38	**0.011**	**0.003**
GPT (IU l^{-1})	23.9 ± 15.3	27.6 ± 19.7	30.4 ± 17.6	0.554	0.282
CRP (mg dl^{-1})	0.63 ± 0.42	0.92 ± 0.57	0.96 ± 0.82	0.196	0.105
LBP (μg dl^{-1})	26.7 ± 10.3	23.7 ± 8.1	30.4 ± 13.4	0.160	0.302
miR-139-5p (r.u.)	1.43 ± 0.54	1 ± 0.37	1.08 ± 0.47	**0.009**	**0.023**
miR-30b-5p (r.u.)	1.48 ± 0.39	1.15 ± 0.42	1.18 ± 0.43	**0.028**	**0.036**
miR-122-5p (r.u.)	715.1 ± 361	499.9 ± 261.9	494.8 ± 253.7	**0.038**	**0.032**
miR-146b-5p (r.u.)	5.23 ± 1.66	5.64 ± 1.65	6.82 ± 2.3	**0.038**	**0.014**
miR-422a (r.u.)	3.96 ± 1.69	2.8 ± 1.52	2.92 ± 1.44	**0.042**	**0.048**

Abbreviations: ANOVA, analysis of variance; BMI, body mass index; CRP, C reactive protein; DBP, diastolic blood pressure; GGT, gamma-glutamyl transferase; GPT, glutamate pyruvate transaminase; HDL, high-density lipoprotein; HOMA-IR, homeostasis model assesment- insulin resistant index; LBP, lipopolysaccharide binding lipoprotein; LDL, low-density lipoprotein; LSD, least significant difference; M, insulin action measured using hyperinsulinemic-euglycemic clamp; NAFLD, nonalcoholic fatty liver disease; r.u., relative units; SBP, systolic blood pressure; T2D, type 2 diabetes. Values represent the mean ± s.d. [a]Fisher's LSD *post hoc* test was performed by comparing NAFLD vs no NAFLD participants. Bold indicates significant results (*P*-value < 0.05) and r.u.

were obtained from non-consecutive obese patients following bariatric surgery in the Surgery Service of the Hospital Universitari Dr Josep Trueta (Girona, Spain). Total RNA was purified from liver samples and cell debris using miRNeasy Mini Kit (QIAgen, Gaithersburg, MD), as previously explained.[27] Liver samples (~50 mg) were homogenized in 0.6 ml of QIAzol Lysis Reagent (QIAgen) before RNA extraction. High quality RNA concentrations were assessed with a Nanodrop ND-1000 Spectrophotometer (Thermo Fischer Scientific, Wilmington, DE). RNA integrity was checked with the Nano lab-on-a-chip assay for total eukaryotic RNA using Bioanalyzer 2100 (Agilent Technologies, Palo Alto, CA). An aliquot of 3 μg of purified RNA was used into the RT using the TaqMan miRNA Reverse Transcription Kit, and the TaqMan miRNA Multiplex RT Assays, which are required to run the TaqMan Array human MicroRNA A+B Cards Set v2.0 (Life Technology, Darmstadt, Germany). Then, TaqMan miRNAs arrays, covering a profile of 744 miRNA species, were applied to samples from the subcohort of 19 women (identification sample), as previously explained.[21] Normalized values were obtained as the raw Ct value—average of raw Cts for all miRNAs with reliable results (Ct values ⩽35) in each sample (Supplementary Figure 1).

Validation analyses

Total messenger RNA was reverse transcribed to cDNA using High Capacity cDNA Archive Kit, and miRNAs were specify reverse transcribed by TaqMan MicroRNA Reverse Transcription Kit (Applied Biosystems, Darmstadt, Germany). Pre-validated TaqMan primer/probe sets (Applied Biosystems) were used for gene expression in a real-time PCR using the LightCycler480 Real-Time PCR System (Roche Diagnostics, Barcelona, Spain). The reaction was performed in a final volume of 7 μl, as previously.[27] Gene and miRNA expression results are ratio relative to preselected and validated endogenous control (that is, cyclophilin A (PPIA) for gene expressions, and RNU6b for miRNAs in liver samples and cells). Replicates and positive and negative controls were included.

Statistical methods

The statistical association between clinical and biochemical outputs and changes in miRNA and gene expression was assessed using the program SPSS (SPSS v12 Inc., Chicago, IL, USA). Before statistical analysis, normal distribution and homogeneity of the variances were evaluated using Levene's test. One-way analysis of variance for multiple comparisons was used to compare groups (no NAFLD, borderline or NAFLD) with respect to continuous variables, using *post hoc* by Fisher's least significant difference (LSD) procedures for two by two comparisons. The level of significance was set at *P*-value < 0.05. The semi-quantitative expressions for miRNAs were correlated (Spearman) with clinical parameters. Receiver-operating characteristics (ROC) curves were generated to evaluate the ability of chosen miRNAs to distinguish between borderline participants and NAFLD patients vs controls with no sign of liver disease.[28] Statistical analyses were performed with the SPSS (SPSS V12.0, Inc., Chicago, IL), and R Statistical Software (http://www.r-project.org/). The SL qPCRNorm Package (Bioconductor) was used for the analysis of arrays, as previously.[29]

RESULTS

Comprehensive miRNA profiling in liver samples

Liver miRNA profiling was performed in a subgroup of 19 obese women. Previous surgery and histological evaluation, eleven of these participants (58%) were suspected of NAFLD based on the laboratory and sonographic findings. Histological assessment confirmed NAFLD in all these subjects. NAFLD patients and age, sex and weight-matched controls with no sights of hepatic

Table 2. Single correlations with clinical outputs and multiple linear regressions of the hepatic miRNAs highlighted in NAFLD after correcting for confounders such as gender, age, BMI, dyslipidemia (HDL, LDL) and/or systemic inflammation (CRP, LBP)

	BMI (kg m^{-2})		*HDL (mg dl^{-1})*		*LDL (mg dl^{-1})*		*LBP (μg ml^{-1})*		*CRP (mg dl^{-1})*	
	r	P	r	P	r	P	r	P	r	P
let-7a	**−0.326**	**0.011**	−0.055	0.674	−0.143	0.275	**−0.299**	**0.024**	−0.098	0.463
miR-125b	**−0.324**	**0.012**	−0.06	0.648	**0.301**	**0.020**	0.012	0.931	−0.022	0.867
miR-122-5p	**−0.291**	**0.025**	**0.290**	**0.026**	−0.064	0.628	−0.234	0.083	−0.144	0.284
miR-422a	**−0.281**	**0.029**	−0.112	0.396	0.178	0.172	−0.077	0.57	−0.211	0.112
miR-378	**−0.276**	**0.033**	−0.093	0.480	< 0.001	0.998	−0.260	0.051	−0.147	0.27
miR-30b	−0.221	0.09	−0.059	0.657	< 0.001	0.998	−0.161	0.231	**−0.270**	**0.04**
miR-204	−0.197	0.132	0.019	0.888	0.093	0.482	0.002	0.99	**−0.271**	**0.04**
miR-146b	0.185	0.16	**−0.262**	**0.045**	0.001	0.994	0.241	0.073	0.004	0.976
miR-155	−0.146	0.271	−0.038	0.778	**0.278**	**0.033**	−0.229	0.09	−0.048	0.724
miR-34a	−0.05	0.708	**0.543**	**< 0.001**	−0.049	0.711	−0.161	0.236	0.029	0.828
miR-139-5p	0.029	0.826	−0.197	0.132	0.003	0.982	0.171	0.203	−0.146	0.274

	miR-139-5p		*miR-30b-5p*		*miR-122-5p*		*miR-146b-5p*		*miR-422a*	
	Beta	P	*Beta*	P	*Beta*	P	*Beta*	P	*Beta*	P
Gender	0.018	0.887	−0.222	0.081	−0.083	0.526	0.09	0.501	−0.15	0.227
Age (years)	−0.12	0.343	0.049	0.693	−0.012	0.928	0	0.998	−0.073	0.56
BMI (kg m^{-2})	0.021	0.868	−0.191	0.129	**−0.288**	**0.05**	0.286	0.059	**−0.285**	**0.022**
HDL (mg dl^{-1})	−0.179	0.167			0.214	0.112	**−0.273**	**0.045**	−0.082	0.52
LDL (mg dl^{-1})									0.221	0.078
CRP (mg dl^{-1})					0.193	0.22	−0.289	0.082		
LBP (μg ml^{-1})			−0.13	0.297	−0.239	0.063	0.229	0.071		
NAFLD[a]	**−0.37**	**0.005**	**−0.368**	**0.005**	**−0.348**	**0.021**	**0.3**	**0.033**	**−0.342**	**0.007**
Adjusted R^2	**13% ($P = 0.028$)**		**15.3% ($P = 0.018$)**		**18.8% ($P = 0.018$)**		**15.4% ($P = 0.037$)**		**17.7% ($P = 0.011$)**	

Abbreviations: BMI, body mass index; CRP, C reactive protein; DBP, diastolic blood pressure; HDL, high-density lipoprotein; LBP, lipopolysaccharide binding lipoprotein; LDL, low-density lipoprotein; NAFLD, nonalcoholic fatty liver disease. Beta is the standardized regression coefficient, which allows evaluating the relative significance of the each independent variable in multiple linear regression analyses. Adjusted R^2 express the percentage of the variance explained by the independent variables in the different models (that is, 0.50 is 50%). Significant associations are indicated in bold. [a]NAFLD variable group is defined here as borderline + NAFLD vs control.

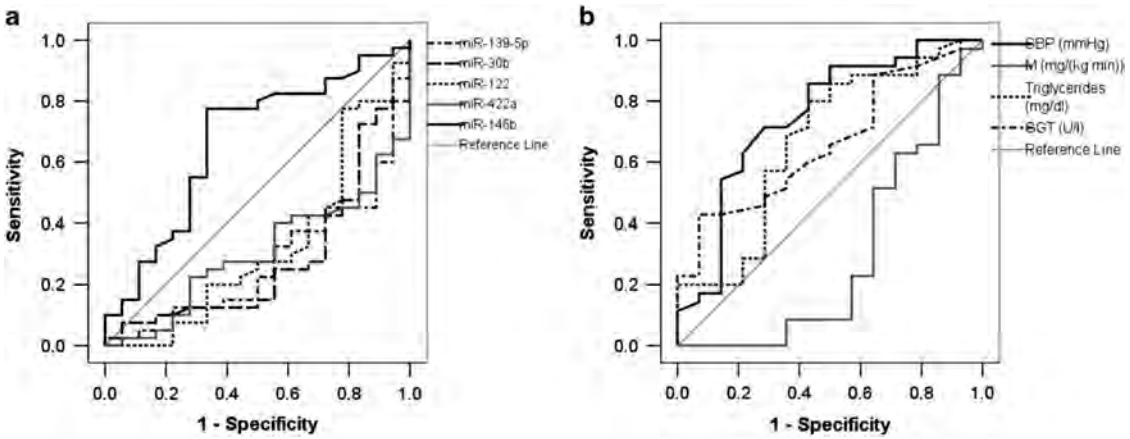

Figure 1. Continuous line: ROC curve for liver miRNAs as a diagnostic indicator for NAFLD (borderline + NAFLD), based on the laboratory, sonographic and histological findings. Gray continued line: diagonal indicating area under the curve (AUC) = 0.5.

disturbances also differed in parameters of insulin resistance, such as homeostasis model assesment- insulin resistant index (4.4 ± 2.8 and 2 ± 0.8, $P = 0.036$) and M-clamp (3.1 ± 1.5 and 6.6 ± 2.9 mg (kg min)$^{-1}$, $P = 0.011$, mean ± s.d., Supplementary Table 2). Concurrently with increased insulin resistance and signs of NAFLD (that is, increased NAFLD activity score, lobular activity, ballooning degeneration and/or fibrosis staging), deregulated expression of 14 hepatic miRNAs was identified (Supplementary Table 2).

Association with clinical outputs

All miRNA candidates (14 miRNAs) were analyzed using TaqMan miRNAs hydrolysis probes in liver biopsies from the extended validation sample of 60 participants, including the subjects selected for the identification sample. The validation shortlisted five hepatic miRNAs that differed significantly between NAFLD patients and controls (Table 1). Decreased expression of miR-139-5p, miR-30b-5p, miR-122-5p and miR-422a, and increased

Table 3. Gene expression in liver

Gene expression (r.u.)	*No NAFLD (n = 19)*	*Borderline (n = 24)*	*NAFLD (n = 17)*	*ANOVA*	*Ratio*	*LSD[a]*
Glucose metabolism						
GLUT2	0.9980 ± 0.256	1.005 ± 0.373	0.621 ± 0.232	**< 0.0001**	0.62	**0.001**
G6PC	0.465 ± 0.215	0.417 ± 0.234	0.237 ± 0.175	**0.007**	0.51	**0.003**
PEPCK	2.92 ± 1.05	2.24 ± 1.63	1.22 ± 0.69	**0.001**	0.42	**< 0.0001**
De novo FA biosynthesis						
ChREBP	0.466 ± 0.108	0.42 ± 0.104	0.398 ± 0.16349	0.265	0.85	0.115
SREBP1c	0.0024 ± 0.0008	0.0024 ± 0.0007	0.0026 ± 0.0011	0.842	1.06	0.611
NR1H4	0.02 ± 0.007	0.019 ± 0.007	0.015 ± 0.005	0.062	0.75	**0.028**
NR1H3	0.05 ± 0.011	0.046 ± 0.014	0.04 ± 0.014	0.145	0.82	**0.049**
FASN	0.052 ± 0.049	0.083 ± 0.096	0.042 ± 0.038	0.166	0.82	0.701
ACACA	0.02 ± 0.01	0.023 ± 0.009	0.02441 ± 0.017	0.496	1.23	0.268
PPP2R5C	0.026 ± 0.008	0.026 ± 0.008	0.019 ± 0.006	**0.012**	0.73	**0.01**
FA uptake and transport						
PPARγ	0.00036 ± 0.00013	0.00042 ± 0.00014	0.00033 ± 0.00012	0.111	0.92	0.512
PGC1α	0.082 ± 0.052	0.067 ± 0.031	0.049 ± 0.016	**0.037**	0.60	**0.01**
CD36	0.108 ± 0.04	0.114 ± 0.033	0.086 ± 0.027	**0.046**	0.80	0.069
FABP4	0.0034 ± 0.003	0.0064 ± 0.0105	0.0095 ± 0.0085	0.111	2.79	**0.037**
FATP5	0.609 ± 0.158	0.472 ± 0.128	0.409 ± 0.169	**0.001**	0.67	**< 0.0001**
PLTP	0.011 ± 0.005	0.012 ± 0.005	0.008 ± 0.004	0.059	0.73	0.054
FA Oxidation						
PPARα	0.132 ± 0.051	0.114 ± 0.028	0.099 ± 0.03	**0.036**	0.75	**0.011**
Inflammation						
ITGAX	0.0045 ± 0.0016	0.0063 ± 0.0028	0.0072 ± 0.0046	0.056	1.6	**0.021**
PPARδ	0.013 ± 0.003	0.0157 ± 0.0054	0.0119 ± 0.003	**0.020**	0.94	0.6
HAMP	0.724 ± 0.553	0.898 ± 0.668	0.693 ± 0.599	0.517	0.96	0.885
TNFα	0.0023 ± 0.0024	0.0038 ± 0.0034	0.0037 ± 0.0034	0.276	1.60	0.213
ER stress						
ATF6	0.025 ± 0.014	0.022 ± 0.0087	0.025 ± 0.013	0.433	0.88	0.339
DDIT3	0.01 ± 0.006	0.0082 ± 0.0042	0.0138 ± 0.0136	0.134	1.0	0.992
HSPA5	0.072 ± 0.044	0.066 ± 0.031	0.079 ± 0.033	0.524	0.98	0.93
Others						
ARL6IP1	0.402 ± 0.109	0.322 ± 0.048	0.325 ± 0.064	**0.003**	0.81	**0.005**
SULT1A2	12,009 ± 2,578	9,370 ± 2,546	9,176 ± 3,139	**0.016**	0.76	**0.009**

Abbreviations: ACACA, acetyl-CoA carboxylase alpha; ARL6IP1, ADP-ribosylation factor-like 6 interacting protein 1; ATF6, activating transcription factor 6; CD36, CD36 molecule; ChREBP, carbohydrate-responsive element-binding protein; DDIT3, DNA damage inducible transcript 3; FABP4, fatty acid binding protein 4; FASN, fatty acid synthase; FATP5, fatty acid transport protein 5; GLUT2, glucose transporter 2; G6PC, glucose 6-phosphatase subunit; HAMP, hepcidin; HSPA5, heat shock protein family A (Hsp70) member 5; ITGAX, integrin subunit alpha X; PEPCK, phosphoenolpyruvate carboxykinase 1; NR1H4, nuclear receptor subfamily 1 group H member 3 (or farnesoid X receptor, FXR); NR1H3, nuclear receptor subfamily 1 group H member 3 (also known as liver X receptor alpha, LXRA); PPARα, peroxisome proliferator activated receptor alpha; PPARδ, peroxisome proliferator activated receptor delta; PPARγ, peroxisome proliferator activated receptor gamma; PGC1α, PPARG coactivator 1 alpha; PLTP, phospholipid transfer protein; PPP2R5C, protein phosphatase 2, regulatory subunit B', gamma; r.u., relative units; SREBP1, sterol regulatory element-binding protein 1; SULT1A2, sulfotransferase 1A2; TNFα, tumor necrosis factor alpha. Values represent the mean ± s.d. Ratio shows values in NAFLD divided by results in no NAFLD samples. [a]Fisher's LSD *post hoc* test was performed by comparing NAFLD vs no NAFLD participants. Bold indicates significant results (*P*-value < 0.05).

miR-146b-5p was confirmed in obese NAFLD patients and/or borderline subjects, when compared to gender, age and weight-matched controls. On the other hand, expression in liver samples of selected miRNAs was associated with anthropometric and clinical measures such as BMI (that is, let-7a, miR-125b, miR-122-5p, miR-422a and miR-378, all of them inversely associated with increased weight), high-density lipoprotein (miR-122-5p and miR-34a, and miR-146, that showed inverse relationship with high-density lipoprotein), low-density lipoprotein (miR-125b and miR-155, with direct association) and circulating levels of inflammatory markers, such as lipopolysaccharide binding protein (inversely related to hepatic let-7a) and protein C-reactive (that shown negative association with hepatic miR-30b and miR-204, Table 2). Noteworthy, in multiple linear regression models NAFLD plus borderline participants (the so-called NAFLD variable group in Table 2) contributed to explain the variance of miR-139-5p (13%, $P = 0.028$), miR-30b-5p (15.3%, $P = 0.018$), miR-122-5p (18.8%, $P = 0.018$), miR-146b-5p (15.4%, $P = 0.037$) and miR-422a (17.7%, $P = 0.011$), after adjusting for gender, age, weight, dyslipidemia (that is, circulating high-density lipoprotein and/or low-density lipoprotein) and inflammation (lipopolysaccharide binding protein and/or protein C-reactive concentrations; Table 2). Only decreased miR-139-5p ($P = 0.03$) and miR-122-5p ($P = 0.006$) in liver explained together 29.2% ($P = 0.005$) of the variance of NAFLD (borderline +NAFLD patients) after correcting for many confounders.

In order to determine the level of discrimination provided by each hepatic miRNA, we estimated the area under the curve and their CI (Figure 1a). All highlighted miRNAs presented discriminatory capacity between subjects with signs of NAFLD and gender, sex and BMI-matched controls (miR-139-5p: area = 0.74 (95% CI = 0.61–0.87), $P = 0.003$; miR-30b: 0.71 (0.57–0.85), $P = 0.008$; miR-122: 0.68 (0.53–0.83), $P = 0.028$; miR-422a: 0.7 (0.57–0.84), $P = 0.013$; and miR-146b: 0.67 (0.51–0.82), $P = 0.041$). It should be noted that, among clinical outputs, only systolic blood pressure (0.75 (0.59–0.92), $P = 0.006$) and M-clamp (0.7 (0.51–0.89), $P = 0.027$) provided significant discriminatory capacity for NAFLD

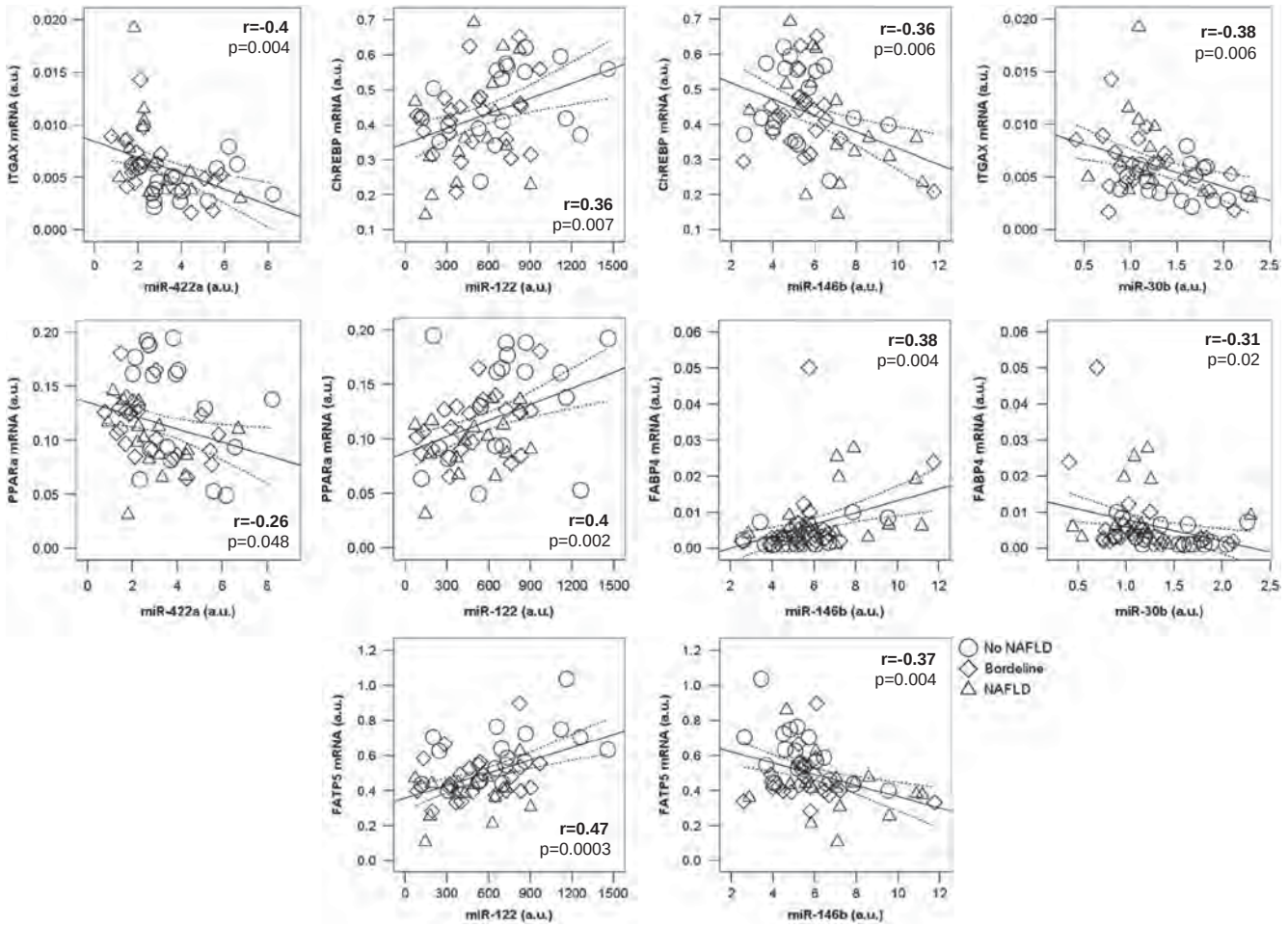

Figure 2. Linear relationships between gene expressions and hepatic miRNA candidates. Values for control subjects are represented as empty circles (○); borderline are empty diamonds (◇); and empty triangles for NAFLD patients (Δ).

variance (Figure 1b). However, no significant associations were identified between hepatic miRNAs and parameters of insulin resistance, triglycerides, systolic or diastolic blood pressure and plasma liver enzymes.

Association with gene expression

The expression of NAFLD-related key genes was also investigated. First, a set of genes expressed in association with fatty liver disease was identified. Then, gene expression measures were assessed in the whole cohort (qRT-PCR). The 'DeltaCt' normalized values were obtained as the raw Ct value for each gene—the raw Cts for the endogenous control (PPIA) in each sample. Associations with clinical outputs and/or NAFLD was tested for genes related to glucose metabolism (GLUT2, G6PC, PEPCK), *de novo* FA biosynthesis (ChREBP, SREBP1c, LXRα, FXR, FASN, ACACA, PPP2R5C), FA uptake and transport (PPARγ, PGC1α, CD36, FABP4, FATP5, PLTP), FA oxidation (PPARα), inflammation (ITGAX, PPARδ, HAMP, TNFα) and endoplasmic reticulum stress (ATF6, DDIT3, HSPA5). In addition, ARL6IP1 and SULT1A2, two genes that have been reported in close association with NAFLD,[30,31] were analyzed, showing significant variations in NAFLD patients vs controls (Table 3). These measurements disclosed the significant modification of at least 15 genes in liver samples from NAFLD patients when compared to sex, age and weight-matched controls (Table 3).

Of note, significant regulation of genes appeared to be in close association with changes in miRNAs (Figure 2). Currently, decreased miR-122-5p in NAFLD was associated with decreased FA metabolism and transport in liver, including lower ChREBP ($r=0.36$, $P=0.007$), PPARγ ($r=0.27$, $P=0.048$), PPARα ($r=0.398$, $P=0.002$), LXRα ($r=0.32$, $P=0.016$) and FATP5 ($r=0.47$, $P=0.0003$, Figure 2) genes expression. On the other hand, increased macrophages-related genes such as ITGAX ($r=-0.381$, $P=0.006$) and FABP4 ($r=-0.310$, $P=0.018$) associated with decreased miR-30b-5p (Figure 2). ITGAX was also inversely associated with miR-422a expression ($r=-0.4$, $P=0.004$), while increased miR-146b-5p expression was related to FABP4 ($r=0.38$, $P=0.004$), and decreased GLUT2 ($r=-0.34$, $P=0.011$), FATP5 ($r=-0.37$, $P=0.004$), FABP4 ($r=-0.38$, $P=0.004$) and ChREBP ($r=-0.36$, $P=0.006$, Figure 2). Expressions of miR-139-5p were associated with liver TNFα mRNA ($r=-0.34$, $P=0.01$, data not shown).

Analyses *in vitro*

To further validate cross-sectional findings in liver samples, and to test whether values of miRNA candidates for NAFLD respond to the FA deposition and insulin resistance in hepatocytes, the miRNAs of interest were analyzed in a model of FA-induced steatosis and conditions of HG and insulin mimicking insulin resistance in both HepG2 cells and HH. First, gene expression measures were obtained in order to see whether expression profiles were representative of *in vivo* findings (Table 4). Twenty-eight genes were tested in HepG2 and HH treated or not with PA, PA+OA and/or HG. Among the genes evaluated, fourteen showed significant changes upon PA in HepG2 cells (Table 4), including higher expressions of genes codifying for key enzymes in FA

Table 4. Gene and miRNA expressions in HepG2 and HH following treatments with HG (glucose 33 mM and insulin 100 nM in both cell models), PA (500 μM and 200 μM, respectively) or a combination of monounsaturated (300 μM OA) and saturated (200 μM PA) FA in HepG2, and HG+PA (200 μM PA) in HH

	HepG2 cells						*HH*					
	HG-24 h		*PA-72 h*		*OA+PA-72 h*		*HG-24 h*		*PA-24 h*		*HG+PA-24 h*	
	Ratio	P-*value*	*Ratio*	P-*value*	*Ratio*	P-*value*	*Ratio*	P-*value*	*Ratio*	P-*value*	*Ratio*	P-*value*[a]
Glucose metabolism												
GLUT2	1.12	0.065	1.1	0.482	0.70	**0.012**	0.79	**0.038**	0.47	< **0.0001**	0.79	**0.019**
G6PC	4.38	**0.001**	1.1	0.447	0.89	0.139	1.67	0.19	0.61	0.103	1.03	0.922
PEPCK	0.34	**0.003**	0.39	**0.009**	0.72	**0.030**	1.22	0.552	0.66	0.252	0.84	0.612
De novo FA biosynthesis												
ChREBP	1.3	**0.004**	1.63	**0.006**	0.68	**0.003**	0.65	0.091	1.19	0.201	1.34	0.06
SREBP1c	0.82	**0.004**	0.92	0.569	0.81	**0.034**	0.83	0.067	1.04	0.636	1.11	0.233
NR1H4	0.76	0.074	0.73	0.118	0.99	0.952	1.07	0.498	0.87	0.113	1.17	0.108
NR1H3	1.19	0.185	0.89	0.337	1.50	**0.041**	1.06	0.551	1.09	0.463	1.32	**0.009**
FASN	1.13	0.259	3.73	< **0.0001**	1.13	0.194	0.84	0.183	1.19	**0.046**	1.23	0.05
ACACA	0.93	0.483	1.71	**0.044**	0.83	**0.048**	0.8	0.125	0.85	0.283	0.93	0.479
PPP2R5C	0.99	0.866	0.72	0.154	1.02	0.808	0.85	**0.015**	1.03	0.468	0.9	0.089
FA uptake and transport												
PPARγ	0.36	**0.001**	0.33	**0.003**	0.81	**0.012**	0.9	0.162	1.1	0.435	1.09	0.472
PGC1α	0.68	**0.021**	0.45	**0.025**	0.50	**0.005**	0.61	**0.003**	1.26	**0.001**	1.18	0.155
CD36	1.08	0.343	1.79	**0.006**	0.61	**0.003**	0.88	0.134	1.66	< **0.0001**	1.65	< **0.0001**
FABP4	ND	NA	ND	NA	ND	NA	0.96	0.849	7.06	< **0.0001**	7.31	**0.003**
FATP5	1.31	0.234	1.04	0.704	0.55	< **0.0001**	1.06	0.787	1.7	0.105	1.6	**0.043**
PLTP	0.96	0.863	1.71	**0.002**	0.84	0.235	0.93	0.528	1.35	**0.003**	1.41	**0.01**
FA Oxidation												
PPARα	0.92	0.279	0.6	**0.026**	0.58	**0.003**	0.88	0.128	1.48	**0.002**	1.44	**0.002**
Inflammation												
ITGAX	ND	NA	ND	NA	ND	NA	0.75	0.053	5.36	< **0.0001**	2.82	< **0.0001**
PPARδ	1.09	0.7	0.67	0.094	0.25	**0.006**	0.93	0.502	1.02	0.764	1.04	0.719
HAMP	0.5	**0.028**	0.54	0.072	0.49	**0.004**	0.97	0.85	1.25	**0.023**	1.62	**0.005**
TNFα	0.73	0.429	0.73	0.119	0.32	**0.002**	1.04	0.84	2.51	< **0.0001**	2.5	**0.003**
ER stress												
ATF6	0.87	0.622	0.58	**0.002**	0.63	**0.029**	0.87	0.111	1.35	**0.018**	1.13	0.146
DDIT3	0.49	0.079	0.57	**0.001**	0.31	**0.015**	1.02	0.852	4.99	< **0.0001**	4.08	**0.004**
HSPA5	1.01	0.978	0.7	**0.021**	0.80	0.494	0.96	0.679	2.8	< **0.0001**	2.04	**0.003**
Others												
ARL6IP1	1.05	0.863	0.78	**0.033**	0.70	0.063	0.94	0.36	0.92	0.258	0.93	0.384
SULT1A2	1.04	0.898	1.59	**0.001**	0.37	< **0.0001**	0.89	0.319	1.18	0.179	1.37	0.069
miRNAs												
miR-139-5p	0.68	0.134	0.23	**0.041**	0.89	0.419	0.9	0.496	0.38	< **0.0001**	0.33	< **0.0001**
miR-30b-5p	0.95	0.801	0.27	**0.009**	0.48	**0.020**	0.84	0.354	0.72	**0.001**	0.49	**0.006**
miR-122-5p	0.82	0.227	0.88	0.762	0.73	0.111	0.76	0.258	0.77	**0.012**	0.45	**0.006**
miR-146b	0.84	0.585	0.23	**0.001**	0.77	**0.019**	0.7	0.052	0.84	**0.041**	0.55	**0.008**
miR-422a	0.74	0.054	0.56	**0.03**	0.84	**0.015**	0.77	0.1	0.71	**0.042**	0.48	**0.004**

Abbreviations: ACACA, acetyl-CoA carboxylase alpha; ARL6IP1, ADP-ribosylation factor-like 6 interacting protein 1; ATF6, activating transcription factor 6; CD36, CD36 molecule; ChREBP, carbohydrate-responsive element-binding protein; DDIT3, DNA damage inducible transcript 3; ER, endoplasmic reticulum; FABP4, fatty acid binding protein 4; FASN, fatty acid synthase; FATP5, fatty acid transport protein 5; GLUT2, glucose transporter 2; G6PC, glucose 6-phosphatase subunit; HAMP, hepcidin; HG, high glucose; HH, human hepatocytes; HSPA5, heat shock protein family A (Hsp70) member 5; ITGAX, integrin subunit alpha X; NA, not available; ND, non-detectable; NR1H3, nuclear receptor subfamily 1 group H member 3 (also known as liver X receptor alpha, LXRA); NR1H4, nuclear receptor subfamily 1 group H member 3 (or farnesoid X receptor, FXR); PA, palmitic acid; PEPCK, phosphoenolpyruvate carboxykinase 1; PPARα, peroxisome proliferator activated receptor alpha; PPARγ, peroxisome proliferator activated receptor gamma; PGC1α, PPARG coactivator 1 alpha; PLTP, phospholipid transfer protein; PPARδ, peroxisome proliferator activated receptor delta; PPP2R5C, protein phosphatase 2, regulatory subunit B', gamma; OA, oleic acid; SREBP1, sterol regulatory element-binding protein 1; SULT1A2, sulfotransferase 1A2; TNFα, tumor necrosis factor alpha. Values represent the ratio vs controls; ⩾3 biological replicates were performed for each cell model and condition. [a]Student's *t*-test was performed by comparing treated cells vs control. Bold indicates significant results (*P*-value < 0.05).

biosynthesis (for example, FASN, ACACA and ChREBP, with fold changes of 3.7, 1.7 and 1.6, respectively, *P*-value < 0.05, Table 4). Similar findings were found in treatments with PA+OA (Table 4). This suggests that FAs (but not HG) induced *de novo* FA biosynthesis, which is a key feature in NAFLD progression.[32,33] In agreement, oil red staining confirmed increased FA accumulation in HepG2 upon treatments with PA or PA+OA (Supplementary Figure 2), and changes in FA uptake and lipid transport were

identified, including increased CD36 and PLTP accompanying decreased PPARγ and PGC1α in PA HepG2 (Table 4). Concomitantly, decreased expression of genes related to FA oxidation (that is, PPARα) and gluconeogenesis (PEPCK) was found in HepG2 cells treated with PA or PA+OA, while the expression of genes related to ER stress diminished (Table 4). In agreement, increased expression of the antiapoptotic Bcl-2, and decreased levels of the tumor suppressor gene Bax in both PA (2.5 and 0.5-fold change) and PA+OA (1.7 and 0.8-fold change, respectively, *P*-value < 0.05, data not shown) reflected changes in signaling pathways aimed at regulating cell growth and proliferation, which are opposite to the activation of apoptosis. Altogether, HepG2 cells treated with FA showed increased lipogenesis and decreased gluconeogenesis and FA oxidation, while no signs of inflammatory activation or apoptosis were identified. Concurrently with these changes, FA-induced significant decreased expression of the miRNAs of interest, except for miR-122-5p (both PA and PA+OA) and miR-139-5p (only PA+OA), which showed no significant variations in cells upon treatment (Table 4).

In partial agreement with HepG2, primary HH cultured under conditions of saturated PA, HG and insulin (HG) or a combination of both (PA+HG), showed increased fat overload upon treatments with PA, or with PA plus HG, but not with HG alone. These changes were coupled to significant variations in targeted hepatic miRNAs (Table 4). Noteworthy, HH stimulated with PA alone or in combination with HG showed very similar results for genes and miRNAs, suggesting that PA alone may be enough to simulate NAFLD-related variations in primary hepatocytes. As in HepG2, increased expression of genes associated with FA metabolism, uptake and transport, was identified, including significant changes of FASN, CD36, FABP4, FATP5, PLTP and PPARα. In addition, markers of inflammation (that is, ITGAX, HAMP, TNFα) and endoplasmic reticulum stress (ATF6, DDIT3, HSPA5) were increased (Table 4), indicating some degree of lipotoxicity in this *in vitro* model. On the other hand, the expression of genes related to the insulin pathway (for example, GLUT2) was decreased. This agreed with decreased phosphorylated Akt serine/threonine kinase vs total Akt upon HG in HH (−54%, $P < 0.0001$, Supplementary Figure 3). Concomitantly with variations in gene expression, decreased glucose and lipid metabolism and increased FA biosynthesis, HG (not significant), PA and PA plus HG, induced downregulation of hepatic target miRNAs in primary HH as well as in HepG2 cells (Table 4).

DISCUSSION

The discovery and characterization of miRNAs in pathological conditions is considered a major biomedical breakthrough,[34] since these small molecules can bind complementary regions in coding RNAs, leading to translational repression of several genes. Being their regulatory activity equivalent to the decreased expression of target genes, and linearly dependent on the number of target sites harbored by each gene,[35,36] many studies have unraveled the important role of miRNAs in the knowledge of aspects of health and disease, endorsing their potentiality as therapeutical targets.[37]

In the current work we postulated the presence of distinct liver miRNAs which may be relevant in NAFLD. We provide in obese subjects the cross-sectional identification of at least 5 hepatic miRNAs significantly associated with NAFLD. Thus, beyond deregulated histology and circulating liver enzymes, differences between subjects with NAFLD and weight, gender and age-matched controls with normal enzymatic profile, liver histology and ultrasound assessments, included decreased expressions of miR-139-5p, miR-30b-5p, miR-122-5p and miR-422a, and increased miR-146b-5p in liver. Of note, discriminant analyses revealed that the hepatic downregulation of two of them (miR-139-5p and miR-122-5p) may explain more than 29% of NAFLD variance. Indeed, concomitant changes in miRNAs and measures of gene expression, validations *in vitro* imply the possibility of modulating liver miRNAs through the application of FA, inducing molecular changes with metabolical implications, such as increased ChREBP-mediated lipogenesis and decreased FA uptake, oxidation and glucose metabolism in hepatocytes (Supplementary Table 3). We provide here additional evidence and validation on the association of liver miRNAs with NAFLD pathophysiology, paving the way for further investigations targeting the potential for genomic therapies based on miRNA-related hepatic transcriptional regulation.

Increased hepatic FA biosynthesis coupled with changes in miRNAs

Increased lipogenesis, including enhanced FASN and ACACA gene expression in HepG2 cells and primary HH supplemented with saturated PA, has been identified. Consistent with current results, increased *de novo* FA biosynthesis and enhanced expression of lipogenic enzymes has been reported many times in liver samples from NAFLD/NASH patients.[5,12,38,39] In hepatocytes, expression of lipogenic enzymes and transcription factors also increases after treatment with PA.[19,40] Indeed, the utilization of saturated FA in hepatocytes is aimed at the increase of *de novo* lipogenesis, mainly accomplished *in vitro* under these conditions. In this context, the participation of AMP-activated protein kinases (AMPK) is well recognized.[41] AMPK integrates hormonal and nutritional signals to promote energy balance by switching off ATP-consuming pathways by the impact on regulatory proteins, the control of enzymes involved in lipid metabolism and changes in gene expression patterns.[42] Activation of AMPK in hepatocytes leads to the stimulation of FA uptake and oxidation, while switches off the anabolic pathways, such as the synthesis of glucose, glycogen and lipids.[41] The saturated FA palmitate blocks AMPK phosphorylation and, thus, increases FA biosynthesis independently of insulin.[43,44] Concomitantly with these changes, decreased miR-139-5p and miR-122a-5p in the current study and previous reports[12,16] suggest the potential involvement of some miRNAs in NAFLD and changes in liver gene expression patterns modifying FA biosynthesis and glucose metabolism. So far, the miR-122a-5p, a recognized liver-specific miRNA,[45] has been widely studied, being significantly decreased in liver samples from NAFLD/NASH patients[12] and mice models for these diseases,[46] as well as in obese and diabetic mice.[15] Regulatory miR-122 is known to impact genes involved in hepatic cholesterol and lipid metabolism, having a central role in maintaining FA and glucose homeostasis in liver. Currently, the putative recognition sequences for miR-122a and miR-422a, also decreased in NAFLD samples (current findings) and in hepatocellular carcinoma,[47] were localized in the 3′-UTR of human Cholesterol 7α-hydroxylase, an enzyme that plays a critical role in cholesterol metabolism and the regulation of bile acid synthesis in liver.[48] As a proof of concept, inhibition of miR-122 results in reduction of circulating cholesterol in mice[49] and chimpanzees.[50]

Intriguingly, two studies reported that deletion of the miR-122 in mice leads to the development of liver disease.[51,52] Also in contrast with current results and previous findings, Wei *et al.*[19] reported the increase of miR-122 in HepG2 cells treated with PA, concomitantly with increased SREBP1c, FASN and ACACA. Discrepancies in this sense may arise from differences regarding experimentally conditions and the fine-tuned regulation of powerful regulatory elements such as miRNAs. For example, *in vitro* treatments lasted 72 h in the current study, but 24 h in the one of Wei *et al*. Also, the intensity of the treatment with PA (500 vs 300 μM) may explain to some extent such controversies. In this sense, Pirola *et al.*[16] found that miR-122 was increased in liver samples of subjects with simple steatosis, followed by systematic downregulation in NASH patients. Thus, miR-122 could be characterized by significant fluctuations in hepatocytes depending

on the state of disease and fat deposition. Noteworthy, changes in this respect did not modify the impact in FA accumulation and the expression of lipogenic genes such as ChREBP, FASN and ACACA in isolated hepatocytes, suggesting alternative mechanisms of regulation. Changes in inflammation, proliferation, FA transport (that is, the association with FATP5) and β-oxidation (PPARα) may be at the crossroad of these associations. So far, the lack of consistency among several studies calls for a broader view of the paradigm, and the evaluation of other pathways, genes and miRNAs that may be at the forefront of such discrepancies.

Impaired glucose and lipid metabolism in association with variations in miRNAs

According to current data and previous reports (Supplementary Table 3), NAFLD and PA-conducted changes in HH and hepatoma cells are associated with downregulation of miRNAs and genes that are involved in additional aspects of hepatocytes metabolism, including decreased *de novo* lipogenesis through alternative mechanisms (that is, expression of NR1H4, NR1H3 and PPP2R5C), impaired FA transport (PGC1α) and oxidation (PPARα) and decreased glucose metabolism (PEPCK). The involvement of the FA-induced inflammatory response, ER stress and other apoptotic issues do not explain these changes by their own, since primary hepatocytes, apparently less resilient to FA than hepatoma HepG2 cells, disclosed similar findings regarding miRNAs. Indeed, expression values of pro-inflammatory macrophage-related genes such as ITGAX and FABP4 were inversely associated with decreased miR-30b-5p, which was also lowered in both HepG2 and primary hepatocytes upon treatment with FA. In agreement, lower liver miR-30b has been reported in samples of hepatocellular carcinoma,[53] and in Huh7 hepatocytes after Hepatitis C virus infection,[54] two conditions that involve inflammation and impaired metabolism (Supplementary Table 3). Perhaps, hepatic miR-30b responds negatively to the inflammatory profile of nonalcoholic fatty liver, fat deposition and the presence of macrophages in liver, as further indicated by the inverse association found here with C reactive protein. It should be noted that, although this is the first time that liver miR-30b is associated with NAFLD, previous studies have reported the close association with lipo/adipogenesis in fat cells.[55] In this context, Hsieh *et al.*[56] reported decreased circulating miR-30b in obese mice following high-fat diet, being upregulated after normal re-feeding. Of note, the plasma presence of miR-30b was inversely correlated with inflammation, insulin resistance and impaired metabolism, further reinforcing current results, since NAFLD is closely related to insulin resistance.

Our data indicated decreased liver miR-139-5p and increased miR-146b in NAFLD samples, in concordance with previous findings.[12] The miR-139-5p has been pointed as a tumor suppressive miRNA, controlling cellular growth through the regulation of c-Myc and c-fos.[57] This fact and current inverse associations between miR-139-5p and TNFα mRNA levels in liver may hint into the decreased expressions found in hepatocellular carcinoma,[57] also involving inflammation and impaired metabolism. On the other hand, the miR-146b showed opposite patterns *in vivo* (increased in NAFLD samples) vs *in vitro* (decreased upon PA treatment in HepG2 and primary HH). In agreement with current results, additional controversies are found in the literature, since increased hepatic miR-146b was found in NASH patients,[12] but treatments with this miRNA ameliorated HFD-induced NASH in mice.[20] It should be noted that miR-146b is mainly expressed in macrophages and rat liver kupffer cells,[20] being more likely identified as an immune system regulator.[58] This conclusion was further confirmed through increased expressions in HepG2 treated with a lipid mixture coupled with pro-inflammatory cytokines such as TNFα and IL-6,[17] and agrees with the inverse associations found with high-density lipoprotein and the lack of a positive response in HepG2 and primary HH upon PA treatment.

CONCLUSIONS

This study provides a comparative profiling of hepatic miRNAs in obese NAFLD cases and age, gender and weight-matched controls with normal liver histology, and the identification of specific miRNAs in liver that are associated with changes in both gene expression and impaired glucose and lipid metabolism. The metabolic modifications observed in HepG2 and primary HH after treatments with palmitate, palmitate plus oleate and/or HG and insulin demonstrate that components of this profile are regulated in parallel to changes in glucose and/or FA metabolism. Of note, the association of hepatic miRNAs with NAFLD in humans has been explored in a few previous studies (Supplementary Table 1). Differences along the miRNAs found here, and those identified by other authors are most probably due to changes in the study groups. As a proof of concept, it should be noted the match identified between current results and those reported by Cheung *et al.*[12] The previous study, as well as the current results, is focused in the NAFLD-related altered hepatic miRNA expression pattern in the background of the metabolic syndrome (that is, subjects with obesity, dyslipidemia and/or impaired glucose tolerance). Therefore, only subjects with obesity and either normal liver or NAFLD (defined by enzymes, ultrasound and liver biopsy) were studied. As far as we are concerned, this validation study, including independent cohorts, increased miRNA-profile, values of gene expression and additional experiments *in vitro*, consolidate the great relevance of at least three hepatic miRNAs (increased miR-146b, and decreased miR-122 and miR-139-5p) in obese subjects. Thus, the findings reported here yield new insights and further confirmation into the pathologic mechanisms underlying NAFLD in subjects with obesity and impaired metabolism. The results obtained in the present study give promising evidence for studies using miRNAs to examine the pathophysiology of NAFLD, narrowing the selection of miRNA candidates and paving the way for further investigations targeting the potential for genomic therapies based on the synergic activity of miRNA-related hepatic transcriptional regulation. The associations reported here call for functional measurements of FA oxidation and *de novo* lipogenesis after treatment with these miRNA candidates.

CONFLICT OF INTEREST

The authors declare no conflict of interest.

ACKNOWLEDGEMENTS

This study was supported by the European Project FLORINASH-FP7-HEALTH-2009-2.4.5-1, the CIBER de la Fisiopatología de la Obesidad y la Nutrición (CIBERobn), by funds from the Agència de Gestió d'Ajuts Universitaris de Recerca (AGAUR, FI-DGR 2015 to Jèssica Latorre), and the Fondo Europeo de Desarrollo Regional (FEDER). The CIBERobn is an initiative from the Instituto de Salud Carlos III (ISCIII). This study is indebted to the IDIBGI Biobank, integrated in the Spanish National Biobank Network, for the sample and data procurement. Dr Josep M Mercader was supported by a Sara Borrell fellowship, also from the Instituto de Salud Carlos III (ISCIII). Dr Francisco J Ortega is the guarantor for this work as a whole, including study design, access to data and the decision to submit and publish the manuscript.

DISCLAIMER

All authors are aware of and agree to the content of the manuscript. The contents of this manuscript have not been copyrighted or published previously. There are no directly related manuscripts or abstracts, published or unpublished, by one or more authors of this manuscript. The contents of this manuscript are not now under consideration for publication elsewhere. The submitted manuscript nor any similar manuscript, in whole or in

part, will be neither copyrighted, submitted or published elsewhere while the Journal is under consideration.

AUTHOR CONTRIBUTIONS

All authors of this manuscript have directly participated in the execution and analysis of the study. JL wrote the manuscript, designed the study, conducted *in vitro* experiments, participated in the analysis of biochemical variables and performed the statistical analysis. JMM-N, OR, JG and MS analyzed biochemical variables. JMM helped with the study design and the statistical analysis. WR and JMF-R contributed to the conception and design of the study, and provided important intellectual content. FJO carried out the conception and coordination of the study, participated in the analysis of biochemical variables, performed the statistical analysis and wrote the manuscript. All authors have approved the final version submitted and their being listed as an author on the manuscript.

REFERENCES

1 Than NN, Newsome PN. A concise review of non-alcoholic fatty liver disease. *Atherosclerosis* 2015; **239**: 192–202.
2 Brown GT, Kleiner DE. Histopathology of nonalcoholic fatty liver disease and nonalcoholic steatohepatitis. *Metabolism* 2015; **65**: 1080–1086.
3 Yki-Jarvinen H. Non-alcoholic fatty liver disease as a cause and a consequence of metabolic syndrome. *Lancet Diabetes Endocrinol* 2014; **2**: 901–910.
4 Yki-Jarvinen H. Nutritional modulation of non-alcoholic fatty liver disease and insulin resistance. *Nutrients* 2015; **7**: 9127–9138.
5 Auguet T, Berlanga A, Guiu-Jurado E, Martinez S, Porras JA, Aragones G *et al.* Altered fatty acid metabolism-related gene expression in liver from morbidly obese women with non-alcoholic fatty liver disease. *Int J Mol Sci* 2014; **15**: 22173–22187.
6 Baffy G. MicroRNAs in nonalcoholic fatty liver disease. *J Clin Med* 2015; **4**: 1977–1988.
7 Ambros V. The functions of animal microRNAs. *Nature* 2004; **431**: 350–355.
8 Ying SY, Chang DC, Miller JD, Lin SL. The microRNA: overview of the RNA gene that modulates gene functions. *Methods Mol Biol* 2006; **342**: 1–18.
9 Louten J, Beach M, Palermino K, Weeks M, Holenstein G. MicroRNAs expressed during viral infection: biomarker potential and therapeutic considerations. *Biomark Insights* 2016; **10**: 25–52.
10 Bronte F, Bronte G, Fanale D, Caruso S, Bronte E, Bavetta MG *et al.* HepatomiRNoma: the proposal of a new network of targets for diagnosis, prognosis and therapy in hepatocellular carcinoma. *Crit Rev Oncol Hematol* 2016; **97**: 312–321.
11 Bettermann K, Hohensee T, Haybaeck J. Steatosis and steatohepatitis: complex disorders. *Int J Mol Sci* 2014; **15**: 9924–9944.
12 Cheung O, Puri P, Eicken C, Contos MJ, Mirshahi F, Maher JW *et al.* Nonalcoholic steatohepatitis is associated with altered hepatic MicroRNA expression. *Hepatology* 2008; **48**: 1810–1820.
13 Leti F, Malenica I, Doshi M, Courtright A, Van Keuren-Jensen K, Legendre C *et al.* High-throughput sequencing reveals altered expression of hepatic microRNAs in nonalcoholic fatty liver disease-related fibrosis. *Transl Res* 2015; **166**: 304–314.
14 Soronen J, Yki-Jarvinen H, Zhou Y, Sadevirta S, Sarin AP, Leivonen M *et al.* Novel hepatic microRNAs upregulated in human nonalcoholic fatty liver disease. *Physiol Rep* 2016; **4**: 1.
15 Li S, Chen X, Zhang H, Liang X, Xiang Y, Yu C *et al.* Differential expression of microRNAs in mouse liver under aberrant energy metabolic status. *J Lipid Res* 2009; **50**: 1756–1765.
16 Pirola CJ, Fernandez Gianotti T, Castano GO, Mallardi P, San Martino J, Mora Gonzalez Lopez Ledesma M *et al.* Circulating microRNA signature in non-alcoholic fatty liver disease: from serum non-coding RNAs to liver histology and disease pathogenesis. *Gut* 2015; **64**: 800–812.
17 Feng YY, Xu XQ, Ji CB, Shi CM, Guo XR, Fu JF. Aberrant hepatic microRNA expression in nonalcoholic fatty liver disease. *Cell Physiol Biochem* 2014; **34**: 1983–1997.
18 Zhang J, Zhang F, Didelot X, Bruce KD, Cagampang FR, Vatish M *et al.* Maternal high fat diet during pregnancy and lactation alters hepatic expression of insulin like growth factor-2 and key microRNAs in the adult offspring. *BMC Genomics* 2009; **10**: 478.
19 Wei S, Zhang M, Yu Y, Lan X, Yao F, Yan X *et al.* Berberine attenuates development of the hepatic gluconeogenesis and lipid metabolism disorder in type 2 diabetic mice and in palmitate-incubated HepG2 cells through suppression of the HNF-4alpha miR122 pathway. *PLoS ONE* 2016; **11**: e0152097.
20 Jiang W, Liu J, Dai Y, Zhou N, Ji C, Li X. MiR-146b attenuates high-fat diet-induced non-alcoholic steatohepatitis in mice. *J Gastroenterol Hepatol* 2015; **30**: 933–943.
21 Ortega FJ, Mercader JM, Moreno-Navarrete JM, Rovira O, Guerra E, Esteve E *et al.* Profiling of circulating microRNAs reveals common microRNAs linked to type 2 diabetes that change with insulin sensitization. *Diabetes Care* 2014; **37**: 1375–1383.
22 Listenberger LL, Ory DS, Schaffer JE. Palmitate-induced apoptosis can occur through a ceramide-independent pathway. *J Biol Chem* 2001; **276**: 14890–14895.
23 Hetherington AM, Sawyez CG, Zilberman E, Stoianov AM, Robson DL, Borradaile NM. Differential lipotoxic effects of palmitate and oleate in activated human hepatic stellate cells and epithelial hepatoma cells. *Cell Physiol Biochem* 2016; **39**: 1648–1662.
24 Gao F, Jian L, Zafar MI, Du W, Cai Q, Shafqat RA *et al.* 4-Hydroxyisoleucine improves insulin resistance in HepG2 cells by decreasing TNF-alpha and regulating the expression of insulin signal transduction proteins. *Mol Med Rep* 2015; **12**: 6555–6560.
25 Gorgani-Firuzjaee S, Meshkani R. SH2 domain-containing inositol 5-phosphatase (SHIP2) inhibition ameliorates high glucose-induced *de-novo* lipogenesis and VLDL production through regulating AMPK/mTOR/SREBP1 pathway and ROS production in HepG2 cells. *Free Radic Biol Med* 2015; **89**: 679–689.
26 Hwang YP, Choi JH, Kim HG, Lee HS, Chung YC, Jeong HG. Saponins from *Platycodon grandiflorum* inhibit hepatic lipogenesis through induction of SIRT1 and activation of AMP-activated protein kinase in high-glucose-induced HepG2 cells. *Food Chem* 2013; **140**: 115–123.
27 Ortega FJ, Moreno M, Mercader JM, Moreno-Navarrete JM, Fuentes-Batllevell N, Sabater M *et al.* Inflammation triggers specific microRNA profiles in human adipocytes and macrophages and in their supernatants. *Clin Epigenetics* 2015; **7**: 49.
28 Beck JR, Shultz EK. The use of relative operating characteristic (ROC) curves in test performance evaluation. *Arch Pathol Lab Med* 1986; **110**: 13–20.
29 Vandesompele J, De Preter K, Pattyn F, Poppe B, Van Roy N, De Paepe A *et al.* Accurate normalization of real-time quantitative RT-PCR data by geometric averaging of multiple internal control genes. *Genome Biol* 2002; **3**: RESEARCH0034.
30 Baranova A, Schlauch K, Elariny H, Jarrar M, Bennett C, Nugent C *et al.* Gene expression patterns in hepatic tissue and visceral adipose tissue of patients with non-alcoholic fatty liver disease. *Obes Surg* 2007; **17**: 1111–1118.
31 Younossi ZM, Baranova A, Ziegler K, Del Giacco L, Schlauch K, Born TL *et al.* A genomic and proteomic study of the spectrum of nonalcoholic fatty liver disease. *Hepatology* 2005; **42**: 665–674.
32 Moon YA, Liang G, Xie X, Frank-Kamenetsky M, Fitzgerald K, Koteliansky V *et al.* The Scap/SREBP pathway is essential for developing diabetic fatty liver and carbohydrate-induced hypertriglyceridemia in animals. *Cell Metab* 2012; **15**: 240–246.
33 Nakamura A, Tajima K, Zolzaya K, Sato K, Inoue R, Yoneda M *et al.* Protection from non-alcoholic steatohepatitis and liver tumourigenesis in high fat-fed insulin receptor substrate-1-knockout mice despite insulin resistance. *Diabetologia* 2012; **55**: 3382–3391.
34 Bartel DP. MicroRNAs: target recognition and regulatory functions. *Cell* 2009; **136**: 215–233.
35 Lim LP, Lau NC, Garrett-Engele P, Grimson A, Schelter JM, Castle J *et al.* Microarray analysis shows that some microRNAs downregulate large numbers of target mRNAs. *Nature* 2005; **433**: 769–773.
36 Nielsen CB, Shomron N, Sandberg R, Hornstein E, Kitzman J, Burge CB. Determinants of targeting by endogenous and exogenous microRNAs and siRNAs. *RNA* 2007; **13**: 1894–1910.
37 van Rooij E, Olson EN. MicroRNAs: powerful new regulators of heart disease and provocative therapeutic targets. *J Clin Invest* 2007; **117**: 2369–2376.
38 Kohjima M, Enjoji M, Higuchi N, Kato M, Kotoh K, Yoshimoto T *et al.* Re-evaluation of fatty acid metabolism-related gene expression in nonalcoholic fatty liver disease. *Int J Mol Med* 2007; **20**: 351–358.
39 Naik A, Kosir R, Rozman D. Genomic aspects of NAFLD pathogenesis. *Genomics* 2013; **102**: 84–95.
40 Iliopoulos D, Drosatos K, Hiyama Y, Goldberg IJ, Zannis VI. MicroRNA-370 controls the expression of microRNA-122 and Cpt1alpha and affects lipid metabolism. *J Lipid Res* 2010; **51**: 1513–1523.
41 Li Y, Xu S, Mihaylova MM, Zheng B, Hou X, Jiang B *et al.* AMPK phosphorylates and inhibits SREBP activity to attenuate hepatic steatosis and atherosclerosis in diet-induced insulin-resistant mice. *Cell Metab* 2011; **13**: 376–388.
42 Hardie DG. AMPK: a key regulator of energy balance in the single cell and the whole organism. *Int J Obes (Lond)* 2008; **32**: S7–S12.
43 Kim K, Pyo S, Um SH. S6 kinase 2 deficiency enhances ketone body production and increases peroxisome proliferator-activated receptor alpha activity in the liver. *Hepatology* 2012; **55**: 1727–1737.
44 Mihaylova MM, Shaw RJ. The AMPK signalling pathway coordinates cell growth, autophagy and metabolism. *Nat Cell Biol* 2011; **13**: 1016–1023.

45 Szabo G, Bala S. MicroRNAs in liver disease. *Nat Rev Gastroenterol Hepatol* 2013; **10**: 542–552.
46 Wang B, Majumder S, Nuovo G, Kutay H, Volinia S, Patel T *et al.* Role of microRNA-155 at early stages of hepatocarcinogenesis induced by choline-deficient and amino acid-defined diet in C57BL/6 mice. *Hepatology* 2009; **50**: 1152–1161.
47 Song KH, Li T, Owsley E, Chiang JY. A putative role of micro RNA in regulation of cholesterol 7alpha-hydroxylase expression in human hepatocytes. *J Lipid Res* 2010; **51**: 2223–2233.
48 Zhang J, Yang Y, Yang T, Yuan S, Wang R, Pan Z *et al.* Double-negative feedback loop between microRNA-422a and forkhead box (FOX)G1/Q1/E1 regulates hepatocellular carcinoma tumor growth and metastasis. *Hepatology* 2015; **61**: 561–573.
49 Krutzfeldt J, Rajewsky N, Braich R, Rajeev KG, Tuschl T, Manoharan M *et al.* Silencing of microRNAs *in vivo* with 'antagomirs'. *Nature* 2005; **438**: 685–689.
50 Esau C, Davis S, Murray SF, Yu XX, Pandey SK, Pear M *et al.* miR-122 regulation of lipid metabolism revealed by *in vivo* antisense targeting. *Cell Metab* 2006; **3**: 87–98.
51 Tsai WC, Hsu SD, Hsu CS, Lai TC, Chen SJ, Shen R *et al.* MicroRNA-122 plays a critical role in liver homeostasis and hepatocarcinogenesis. *J Clin Invest* 2012; **122**: 2884–2897.
52 Hsu SH, Wang B, Kota J, Yu J, Costinean S, Kutay H *et al.* Essential metabolic, anti-inflammatory, and anti-tumorigenic functions of miR-122 in liver. *J Clin Invest* 2012; **122**: 2871–2883.
53 Huang YH, Lin KH, Chen HC, Chang ML, Hsu CW, Lai MW *et al.* Identification of postoperative prognostic microRNA predictors in hepatocellular carcinoma. *PLoS ONE* 2012; **7**: e37188.
54 Zhang X, Daucher M, Armistead D, Russell R, Kottilil S. MicroRNA expression profiling in HCV-infected human hepatoma cells identifies potential anti-viral targets induced by interferon-alpha. *PLoS ONE* 2013; **8**: e55733.
55 Hilton C, Neville MJ, Karpe F. MicroRNAs in adipose tissue: their role in adipogenesis and obesity. *Int J Obes (Lond)* 2013; **37**: 325–332.
56 Hsieh CH, Rau CS, Wu SC, Yang JC, Wu YC, Lu TH *et al.* Weight-reduction through a low-fat diet causes differential expression of circulating microRNAs in obese C57BL/6 mice. *BMC Genomics* 2015; **16**: 699.
57 Huang Y, Chen HC, Chiang CW, Yeh CT, Chen SJ, Chou CK. Identification of a two-layer regulatory network of proliferation-related microRNAs in hepatoma cells. *Nucleic Acids Res* 2012; **40**: 10478–10493.
58 Taganov KD, Boldin MP, Chang KJ, Baltimore D. NF-kappaB-dependent induction of microRNA miR-146, an inhibitor targeted to signaling proteins of innate immune responses. *Proc Natl Acad Sci USA* 2006; **103**: 12481–12486.

Supplementary Information accompanies this paper on International Journal of Obesity website (http://www.nature.com/ijo)

Supplemental Figure 1

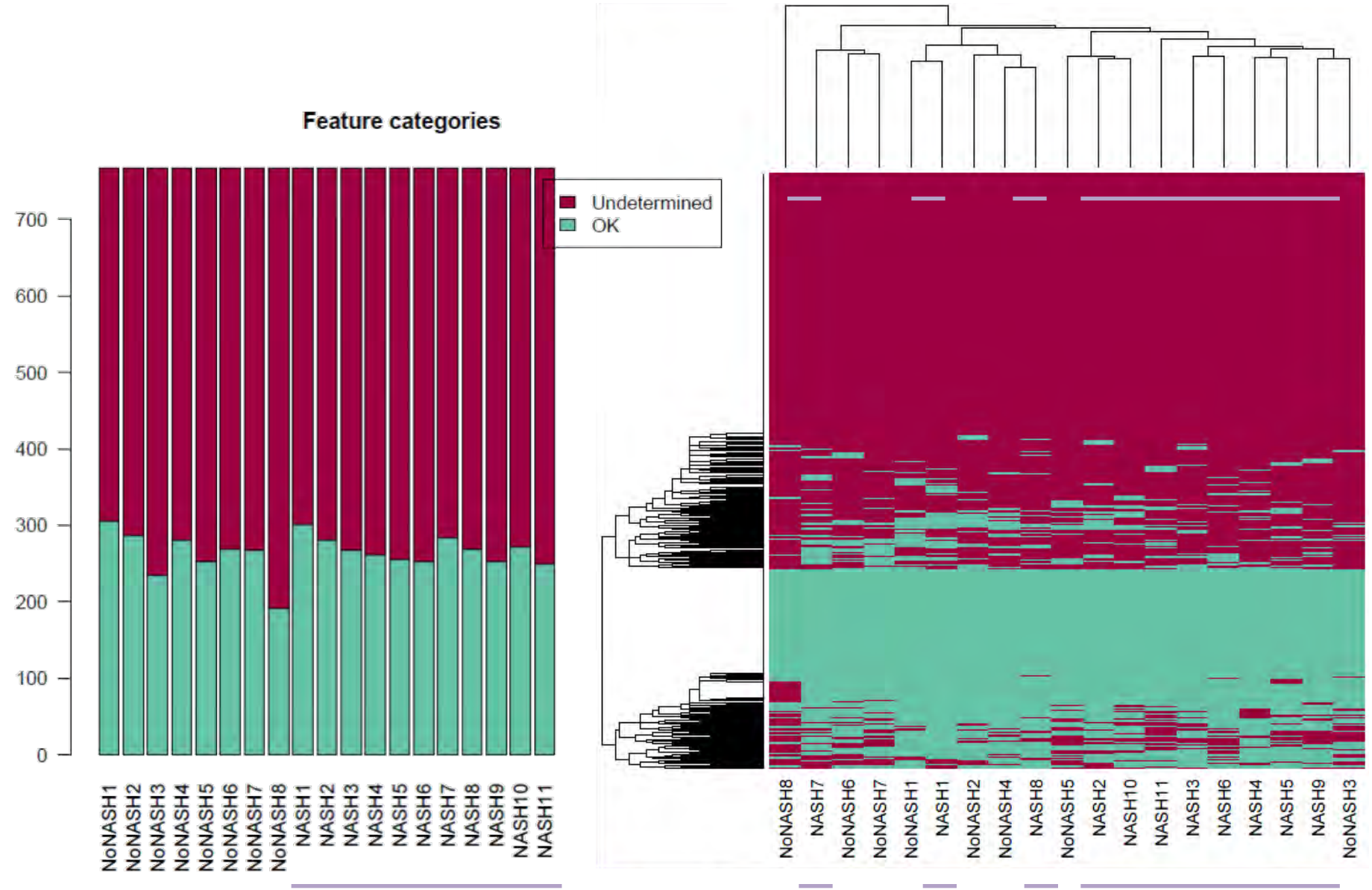

Supplemental Figure 2

Red Oil staining

Control (BSA) | + PA (0.5 mM) | + PA (0.2 mM) + OA (0.3 mM)

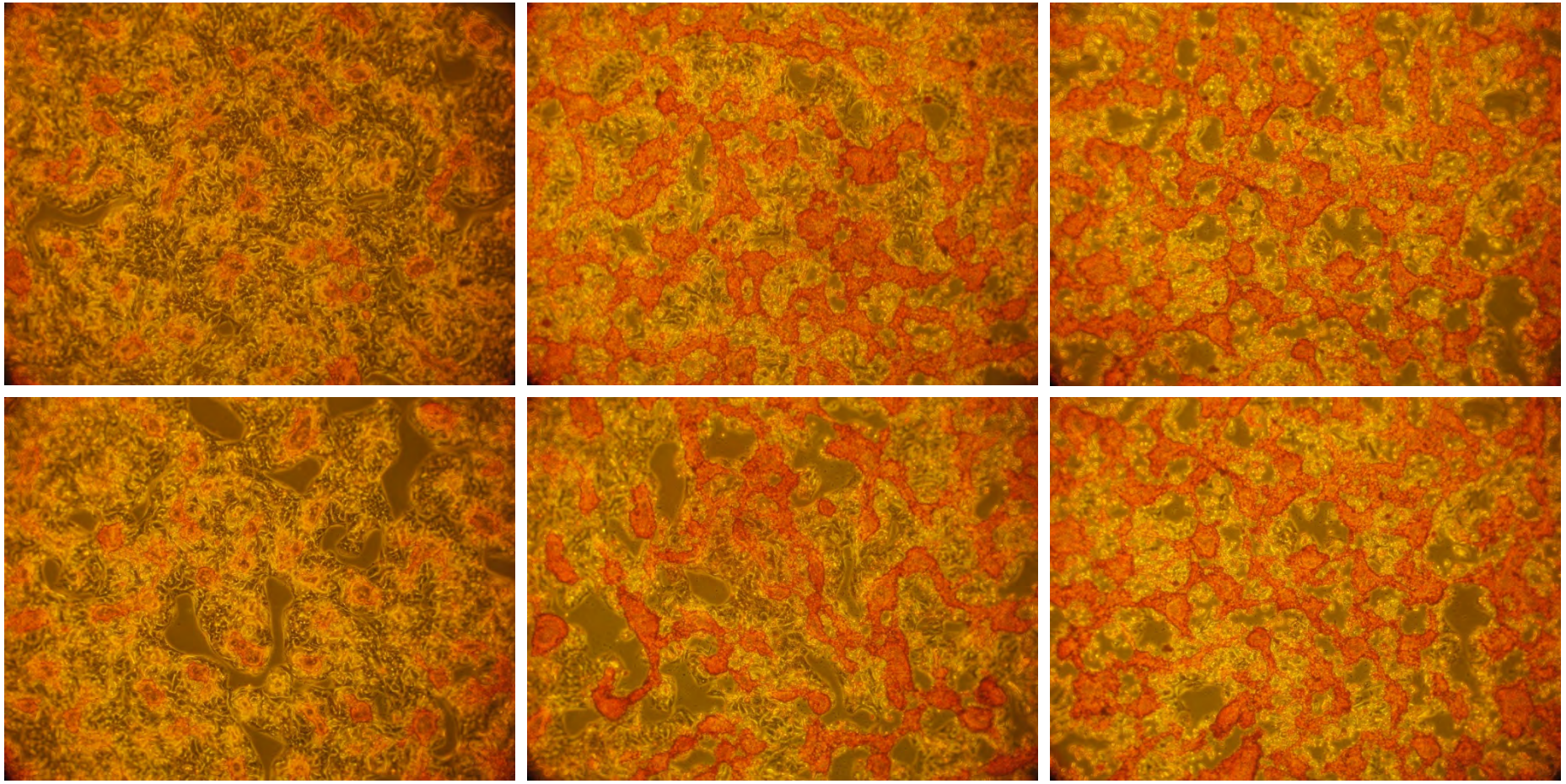

Supplemental Figure 3

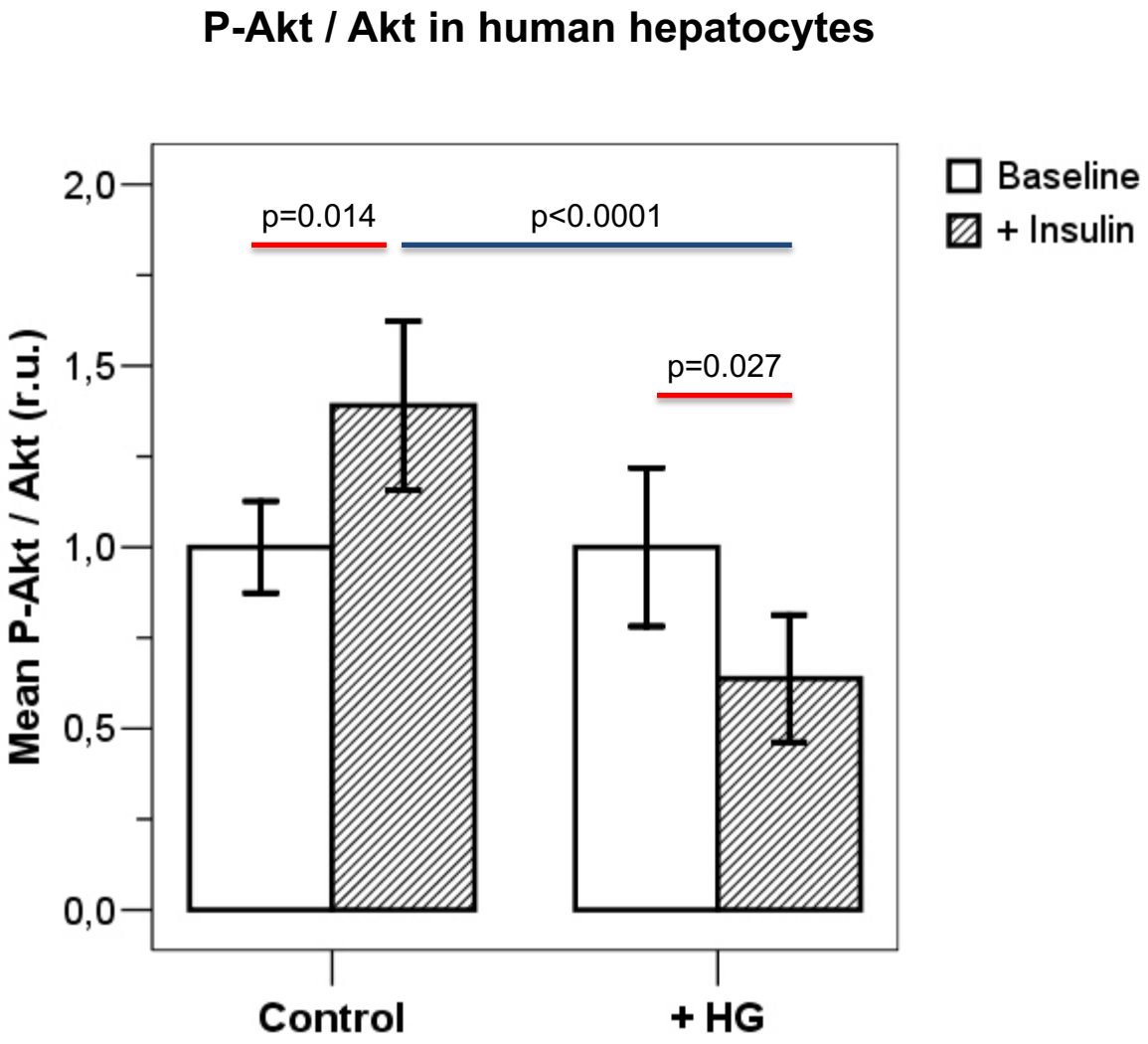

Supplemental Table 1 Summary of hepatic miRNA profiles previously associated with NAFLD in humans.

Study	*Hepatology*. 2008; 48(6):1810-20	*Gut*. 2015; 64(5):800-12	*Transl Res*. 2015; 166(3):304-14	*Physiol Rep*. 2016; 4(1). pii: e12661	*Present study*
N	50	65	30	30	60
Men/Women	9/41	28/37	0/30	10/20	12/48
Age (years)	46.4 ± 8.6	49.8 ± 5.7	49.2 ± 2.9	48 ± 10	47.5 ± 9
BMI (kg/m^2)	37.3 ± 3.2	30.1 ± 4.2	42.7 ± 2.4	45.9 ± 5.4	45.2 ± 6.6
Identification by (all miRNAs)	Microarray (474)	-	Sequencing	Microarray (1,438)	RT-PCR (744)
NAFLD/Controls (identification)	15/15	-	15/15	15/15	11/8
Validation by (miRNA candidates)	RT-PCR (4)	RT-PCR (2)	RT-PCR (11)	RT-PCR (8)	RT-PCR (14)
NAFLD/Controls (validation)	25/25	51/14	15/15	10/10	41/19[a]
Upregulated	miR-34a, **miR-146b**	-	miR-182, miR-183, miR-150, miR-224, miR-31	miR-103a-2*, miR-106b*, miR-576-5p, miR-892a	**miR-146b**
Downregulated	**miR-122**, **miR-139-5p**	**miR-122**, miR-192	miR-378i, miR-590, miR-17, miR-219	-	**miR-122**, miR-30b, miR-422a, **miR-139-5p**

Values represent the mean ± SD. **NAFLD**: non-alcoholic fatty liver disease, **BMI**: body mass index, **RT-PCR**: real-time polymerase chain reaction. [a] NAFLD as borderline plus NAFLD subjects. **Bold** indicate coincident results in more than one study.

Supplemental Table 2 Anthropometric and biochemical data of participants included in the identification sample.

Clinical outputs (units)	No NAFLD (n=8)	NAFLD (n=11)	Student t-test
Sex (M/W)	0/8	0/11	
Fatty liver (Yes/No)	0/8	0/11	
Dyslipidemia (Yes/No)	2/6	3/8	
T2D (Yes/No)	0/8	0/11	
NAFLD activity score (% 5 grade)	0	10.5	
Lobular activity (>2 focus/field, %)	0	26.4	
Ballooning degeneration (%)	0	0	
Fibrosis staging (%)	0	10.6	
Age (years)	44 ± 9	48 ± 6	0.251
BMI (kg/m2)	43.6 ± 8	44.8 ± 7	0.726
SBP (mmHg)	127.3 ± 24.4	143.1 ± 16.7	0.110
DBP (mmHg)	73.4 ± 12.4	82.9 ± 8.8	0.065
Fat mass (%, densitometry)	46 ± 3.1	47.2 ± 6	0.643
Fasting glucose (mg/dl)	93.1 ± 12.8	97.7 ± 10.2	0.395
Fasting insulin (μIU/ml)	9 ± 3	17.4 ± 10	**0.023**
Glycated hemoglobin (%)	5.3 ± 0.4	5.6 ± 0.4	0.193
HOMA-IR index	2 ± 0.8	4.4 ± 2.8	**0.036**
M (mg/(kg · min))	6.6 ± 2.9	3.1 ± 1.5	**0.011**
Cholesterol (mg/dl)	188 ± 37.2	198.7 ± 34.1	0.523
HDL Cholesterol (mg/dl)	48.8 ± 9.7	46.5 ± 12.1	0.665
LDL Cholesterol (mg/dl)	120 ± 29.3	126.2 ± 32.1	0.673
Triglycerides (mg/dl)	95.9 ± 44.7	130.6 ± 39	0.089
GGT (IU/l)	28.8 ± 22.8	30.5 ± 26.5	0.885
GPT (IU/l)	22.9 ± 9.5	23.8 ± 10.6	0.844
CRP (mg/dl)	0.62 ± 0.32	0.84 ± 0.45	0.259
LBP (μg/ml)	23.7 ± 6.1	26.9 ± 9.3	0.413

miR-155	0.284 ± 0.116	0.483 ± 0.173	**0.003**
miR-1201	0.083 ± 0.025	0.055 ± 0.023	**0.004**
miR-886-5p	0.051 ± 0.046	0.136 ± 0.076	**0.005**
miR-378	2.09 ± 0.45	1.34 ± 0.43	**0.015**
miR-30b-5p	5.68 ± 2.09	3.48 ± 1.04	**0.020**
miR-34a	0.346 ± 0.163	0.5 ± 0.188	**0.022**
miR-122-5p	89.8 ± 42.5	52.0 ± 20.6	**0.024**
miR-125b	2.79 ± 0.69	1.93 ± 0.41	**0.034**
miR-422a	0.34 ± 0.155	0.2 ± 0.081	**0.036**
miR-139-5p	1.45 ± 0.57	0.9 ± 0.52	**0.039**
miR-146b-5p	3.3 ± 1.6	5.6 ± 3.2	**0.044**
miR-204	0.137 ± 0.051	0.09 ± 0.03	**0.046**
miR-708	0.01 ± 0.004	0.023 ± 0.012	**0.047**
RNU48	28.3 ± 21.9	15.2 ± 11.2	**0.048**

Values represent the mean ± SD. **NAFLD:** non-alcoholic fatty liver disease, **BMI:** body mass index, **SBP:** systolic blood pressure, **DBP:** diastolic blood pressure, **HbA1C:** glycated hemoglobin, **HDL:** high-density lipoprotein, **LDL:** low-density lipoprotein, **GPT:** glutamate pyruvate transaminase, **GGT:** gamma-glutamyl transferase, **CRP:** C reactive protein, **LBP:** lipopolysaccharide binding lipoprotein. **Bold** indicates significant results (p-value < 0.05).

Supplemental Table 3 Gene and miRNA expressions changes.

	Liver (NAFLD vs. control)		HepG2 (PA vs. control)		Bibliography	
	Ratio	LSD[a]	Ratio	p-value[b]	References	Findings
Glucose metabolism						
GLUT2	0.62	**0.001**	1.10	0.482	Int J Mol Med. 2015;36(3):767-75	Decreased in NAFLD (rats)
G6PC	0.51	**0.003**	1.10	0.447	Hepatology. 2001;34(4 Pt 1):694-706 Biochem Biophys Res Com. 2015;467(3):527-33 PLoS One. 2016;11(3):e0152097	Decreased in NAFLD Decreased in HepG2 +PA Increased in HepG2 +PA
PEPCK	0.42	**<0.0001**	0.39	**0.009**	Hepatology. 2001;34(4 Pt 1):694-706 Biochem Biophys Res Com. 2015;467(3):527-33 PLoS One. 2016;11(3):e0152097	Decreased in NAFLD Decreased in HepG2 +PA Increased in HepG2 +PA
De novo fatty acid (FA) biosynthesis						
ChREBP	0.85	0.115	1.63	**0.006**	Genomics. 2013;102(2):84-95 J Clin Invest. 2012;122(6):2176-94 Hepatology. 2015;62(4):1086-100	Increased in NASH Increased in NASH (mice and humans) Increased in HepG2 +EtOH
SREBP1c	1.06	0.611	0.92	0.569	Hepatology. 2008;48(6):1810-20 Int J Mol Med. 2007;20(3):351-8 PloS One. 2016;11(3):e0152097 J Lipid Res. 2010;51(6):1513-23	Increased in NASH Increased in NAFLD Increased in HepG2 +PA Increased in HepG2 +PA
NR1H4	0.75	**0.028**	0.73	0.118	J Hepatol. 2014;60(4):847-54	Decreased in NAFLD (mice)
NR1H3	0.82	**0.049**	0.89	0.337	Hepatology. 2008;38(11):1122-9 Clin Sci. 2011;120(6):239-50	Increased in NAFLD Increased in NAFLD and HCV patients
FASN	0.82	0.701	3.73	**<0.0001**	Hepatology. 2008;48(6):1810-20 Int J Mol Sci. 2014;15(12):22173-87 Int J Mol Med. 2007;20(3):351-8 PloS One. 2016;11(3):e0152097 J Lipid Res. 2010;51(6):1513-23	Increased in NASH Increased in obese, NAFLD/NASH patients Increased in NAFLD Increased in HepG2 +PA Increased in HepG2 +PA
ACACA	1.23	0.268	1.71	**0.044**	Genomics. 2013;102(2):84-95 Int J Mol Med. 2007;20(3):351-8 PloS One. 2016;11(3):e0152097 J Lipid Res. 2010;51(6):1513-23	Increased in NASH Increased in NAFLD Increased in HepG2 +PA Increased in HepG2 +PA
PPP2R5C	0.73	0.01	0.72	0.154	PLoS Genet. 2015;11(10):e1005561	Increased in T2D/obese patients
FA uptake and transport						
PPARγ	0.92	0.512	0.33	**0.003**	Hepatology. 2003;38(4):1008-17 AIDS. 2006;20(3):387-95	PPARγ agonists improve IS in NASH patients Decreased in patients with IR
PGC1α	0.60	**0.01**	0.45	**0.025**	Cell Metab. 2013;18(2):296-302 Int J Med Sci. 2016;13(3):169-78	Decreased in NAFLD Increased in NAFLD and Huh-7 +PA
CD36	0.80	0.069	1.79	**0.006**	Am J Phy Gast Liv Phy. 2008;294(5):1281-7 Gut. 2011;60(10):1394-402	Increased in NAFLD Increased in NAFLD and HCV
FABP4	2.79	**0.037**	n.d.	n.a.	PloS One. 2012;7(11):e48605 Diabetes. 2007;56(11):2759-65 Biochim Biophys Acta. 2015;1853(11):2966-74	Increased in obese IR patients Increased in NAFLD patients Not found in HepG2 cells
FATP5	0.67	**<0.0001**	1.04	0.704	Hepatol Res. 2009;39(4):366-73 Gastroenterology. 2006;130(4):1245-58	Increased in NAFLD/decreased in NASH Involved in NAFLD progression (mice)
PLTP	0.73	0.054	1.71	**0.002**	J Lipid Res. 2003;44(9) Clin Endocrinol (Oxf). 2008;68(3):375-81 Atherosclerosis. 2007;190(1):114-23	Expressed and released by HepG2 cells Positively related to MetS (circulating) PLTP-KO impacts on hepatic lipogenesis
FA Oxidation						
PPARα	0.75	**0.011**	0.60	**0.026**	J Mol Endocrinol. 2014;53(3):393-403 J Hepatol. 2015;63(1):164-73	Decreased in NAFLD Decreased in NASH
Inflammation						
ITGAX	1.6	**0.021**	n.d.	n.a.	Clin Sci. 2015;129(9):797-808 Am J Phy Gast Liv Phy. 2016;310(2):117-27 Gastroenterology. 2015;149(3):635-48	Increased in mice MCD diet Increased in obese mice Increased in NASH patients
PPARδ	0.94	0.6	0.67	0.094	Int J Mol Med. 2015; 36(3):767-75 Diabetologia. 2012;55(3):743-51	PPARδ agonists restored NAFLD in HFD mice Activation prevented IR in HepG2 +PA
HAMP	0.96	0.885	0.54	0.072	Clin Gastroenterol Hepatol. 2014;12(7):1170-8 J Biol Chem. 2015;290(40):24178-89	Decreased circulating levels in obese subjects Increased in HepG2 +PA
TNFα	1.6	0.213	0.73	0.119	J Biol Chem. 2012;287(48):40161-40172 Metabolism. 2011;60(12):1781-9	Increased in NASH (mice) Increased in HepG2 +PA
Others						
ARL6IP1	0.81	**0.005**	0.78	**0.033**	Hepatology, 2005;42(3):665-674 Obes. Surg, 2007;17(8):1111-1118	Decreased in NAFLD Decreased in NAFLD
SULT1A2	0.76	**0.009**	1.59	**0.001**	Hepatology, 2005;42(3):665-674 Obes. Surg, 2007;17(8):1111-1118	Decreased in NAFLD Decreased in NAFLD
microRNAs						
miR-139-5p	0.76	**0.023**	0.23	**0.041**	Hepatology. 2008;48(6):1810-20 Oncotarget. 2015;6(35):37544-56 Nucleic Acids Res. 2012;40(20):10478-93	Decreased in NASH Decreased in HCC Increased in growth-arrested HepG2
miR-30b-5p	0.80	**0.036**	0.27	**0.009**	PLoS One. 2013;8(2):e55733 PLoS One. 2012;7(5):e37188 Transplantation. 2011;91(3):293-9	Decreased HCV Huh-7 Decreased in HCC Decreased after partial hepatectomy
miR-122-5p	0.69	**0.032**	0.88	0.762	Hepatology. 2008;48(6):1810-20 J Lipid Res. 2009;50(9):1756-65 J Lipid Res. 2010;51(6):1513-23 Transplantation. 2011;91(3):293-9 PLoS One. 2016;11(3):e0152097 Gut. 2015;64(5):800-12 Cell Metab. 2006;3:87–98.	Decreased in NASH Decreased in diabetic/obese mice Increased in HepG2 +PA Decreased after partial hepatectomy Increased in T2D and HepG2 +PA Decreased in NASH but increased in the circulation Inhibition modulate in FA biosynthesis in liver
miR-146b	1.3	**0.014**	0.23	**0.001**	Hepatology. 2008;48(6):1810-20 Cell Physiol Biochem. 2014;34(6):1983-97	Increased in NASH Increased in NAFLD and HepG2
miR-422a	0.74	**0.048**	0.56	**0.03**	n.a.	n.a.

Values represent the mean ± SD. **GLUT2:** glucose transporter 2, **G6PC:** glucose 6-phosphatase subunit, **PEPCK:** phosphoenolpyruvate carboxykinase 1, **ChREBP:** carbohydrate-responsive element-binding protein, **SREBP1:** sterol regulatory element-binding protein 1, **NR1H4:** nuclear receptor subfamily 1 group H member 3 (or farnesoid X receptor, FXR), **NR1H3:** nuclear receptor subfamily 1 group H member 3 (also known as liver X receptor alpha, LXRA), **FASN:** fatty acid synthase, **ACACA:** acetyl-CoA carboxylase alpha, **PPP2R5C:** protein phosphatase 2, regulatory subunit B', gamma, **PPARγ:** peroxisome proliferator activated receptor gamma, **PGC1α:** PPARG coactivator 1 alpha, **CD36:** CD36 molecule, **FABP4:** fatty acid binding protein 4, **FATP5:** fatty acid transport protein 5, **PLTP:** phospholipid transfer protein, **PPARα:** peroxisome proliferator activated receptor alpha, **ITGAX:** integrin subunit alpha X, **PPARδ:** peroxisome proliferator activated receptor delta, **HAMP:** hepcidin, **TNFα:** tumor necrosis factor alpha, **ARL6IP1:** ADP-ribosylation factor-like 6 interacting protein 1, **SULT1A2:** sulfotransferase 1A2. **NAFLD:** non-alcoholic fatty liver disease, **NASH:** nonalcoholic steatohepatitis, **HCC:** hepatocellular carcinoma. **Ratio** shows values in NAFLD divided by results in no NAFLD samples. [a] Fisher's least significant difference (LSD) post-hoc test was performed by comparing NAFLD vs. no NAFLD participants. [b] Student t-test was performed by comparing treated cells vs. control. **Bold** indicates significant results (p-value < 0.05), **r.u.** relative units, **n.d.** very low or non-detectable expression, and **n.a.** not available results.

Treatments mimicking NAFLD compromise the biosynthesis of microRNAs required to maintain lipid homeostasis in hepatocytes

Jèssica Latorre[1,2,3†], Francisco J. Ortega[1,2,3†*], Laura Liñares-Pose[4], José M. Moreno-Navarrete[1,2,3], Aina Lluch[1,3], Ferran Comas[1,2,3], Wifredo Ricart[1,2,3], Marcus Höring[5], You Zhou[6,7], Gerhard Liebisch[5], Nidhina Haridas PA[8], Vesa M. Olkkonen[8,9†], Miguel López[4†*], José M. Fernández-Real[1,2,3†*]

[1]*Institut d'Investigació Biomèdica de Girona (IDIBGI) – Girona, Spain*
[2]*CIBER de la Fisiología de la Obesidad y la Nutrición (CIBEROBN) – Madrid, Spain*
[3]*Department of Diabetes, Endocrinology and Nutrition (UDEN), Hospital of Girona "Dr Josep Trueta" – Girona, Spain*
[4]*Department of Physiology, CiMUS, University of Santiago de Compostela, Instituto de Investigación Sanitaria – Santiago de Compostela, Spain*
[5]*Institute of Clinical Chemistry and Laboratory Medicine, Regensburg University Hospital – Regensburg, Germany*
[6]*Systems Immunity Research Institute, Cardiff University – Cardiff, UK*
[7]*Division of Infection and Immunity, Cardiff University School of Medicine – Cardiff, UK*
[8]*Minerva Foundation Institute for Medical Research, Biomedicum 2U – Helsinki, Finland*
[9]*Department of Anatomy, Faculty of Medicine, University of Helsinki – Helsinki, Finland*

† Equal contribution

Running title: Hepatic microRNAs and lipid homeostasis

Keywords: MicroRNAs, epigenetics, hepatocytes, human, mice, energy expenditure, fatty acid homeostasis, metabolism, non-alcoholic fatty liver disease

Abstract word count: **188** words
Word count: **5,965** words
8 Figures

*Address for correspondence:
F. J. Ortega, Ph.D.; J. M. Fernández-Real, M.D., Ph.D.
Section of Diabetes, Endocrinology and Nutrition (UDEN), Hospital "Dr. Josep Trueta" of Girona, Spain
Institut d'Investigació Biomèdica de Girona (IDIBGI), and CIBEROBN
e-mail: fortega@idibgi.org, jmfreal@idibgi.org

M. López, Ph.D.
Department of Physiology, CiMUS, University of Santiago de Compostela, Spain
Instituto de Investigación Sanitaria de Santiago de Compostela, and CIBEROBN
e-mail: m.lopez@usc.es

ABSTRACT

While the impact of the antidiabetic drug metformin in hepatocytes leads to fatty acid (FA) oxidation and decreased lipogenesis, hepatic microRNAs (miRNA) have been associated with fat overload and impaired metabolism, contributing to the pathogenesis of non-alcoholic fatty liver disease (NAFLD). Here we investigated the expression of hundreds of mature miRNA and genes related to fatty liver disease in primary human hepatocytes challenged by chemical compounds mimicking NAFLD, palmitic acid and compound C (as inducers), and metformin (as an inhibitor). Analyses performed *in vitro* and in rodent models confirmed that treatments triggering fat accumulation and AMPK disruption may compromise the biosynthesis of hepatic miRNA, while the knockdown of the miRNA-processing enzyme Dicer exhibits a substantial increase in lipid deposition. After transient transfection with mimic miRNA candidates, lipid droplet staining, thin-layer chromatography, quantitative lipidome analysis, enzyme-linked immunosorbent assay for ApoB, gene expression, and mitochondrial activity in hepatocytes, miR-30b and miR-30c turned out to be the most potent miRNA, redirecting FA metabolism from energy storage to expenditure. Current findings unravel the biosynthesis of specific hepatic miRNA in tackling inadequate FA accumulation, offering a potential avenue for the treatment of NAFLD.

INTRODUCTION

Non-alcoholic fatty liver disease (NAFLD) is characterized by the excessive build-up of fat in the liver parenchyma that is not caused by alcohol consumption. It is estimated to afflict around one billion individuals worldwide [1], and represents a spectrum of disturbances encompassing fatty acid (FA) infiltration (steatosis), which often leads to the activation of inflammatory pathways (steatohepatitis) related to the induction of insulin resistance [2]. NAFLD is associated with obesity, hyperlipidemia, insulin resistance, type 2 diabetes, and a myriad of cardiovascular risk factors [3], being commonly described as the hepatic manifestation of metabolic syndrome [4,5]. Furthermore, NAFLD may precede more severe liver diseases such as cirrhosis and hepatocellular carcinoma [6].

The balance between FA biosynthesis, uptake and clearance is of utmost importance for maintaining lipid homeostasis in hepatocytes, the most common parenchyma cells in liver. Together with circulating FA intake, impaired β-oxidation occurring at the inner mitochondrial membrane [7], and *de novo* lipogenesis substantially contribute to hepatic FA deposition [8]. All these processes are directly or indirectly modulated by the energy sensor AMP-activated protein kinase (AMPK), a master metabolic regulator that blocks the transcription of lipogenic enzymes [9], while actively inhibits biosynthetic pathways and increases FA oxidation [10]. Therefore, a number of AMPK-activating compounds have been reported to have beneficial effects as therapeutic interventions in the fatty liver arena [11,12]. In particular, metformin, a common antidiabetic drug, can decrease hepatic steatosis in rodent models by activating hepatic AMPK [13–16]. Consistent with this notion, inhibition of AMPK leads to the activation of lipogenesis as a central event in the development of chemical-induced fatty liver [17]. In this context, the reagent called dorsomorphin or compound C, a pyrazolopyrimidine related to protein kinase inhibitors, is occasionally used as a cell-permeable ATP-competitive inhibitor of AMPK to rescue the positive effect of AICAR and metformin [18,19]. Despite the controversy about the selectivity of this reagent, known to inhibit a number of kinases other than AMPK [20], compound C is still being used to provide a proof of AMPK involvement in the regulation of lipid accumulation by other bioactive molecules both *in vivo* and *in vitro* [21–23].

MicroRNAs (miRNA) are small non-coding RNAs that regulate gene expression by specific binding to complementary regions in coding messenger RNAs, leading to their translational repression or decay [24]. Since the coordination of a large number of genes may be accomplished by a single miRNA [25], these factors have become attractive candidates to regulate cell fate decision in complex diseases [26]. In the context of impaired hepatic metabolism, the association between hepatic miRNA and NAFLD is being increasingly recognized [27,28]. For instance, our previous transcriptional analysis in the liver of obese subjects disclosed decreased glucose metabolism and increased FA biosynthesis coupled to significant variations of specific hepatic miRNA species in subjects with this condition [29].

Here we investigated the expression of hundreds of mature miRNA and genes related to fatty liver disease in primary human hepatocytes challenged by chemical

compounds mimicking NAFLD, palmitic acid and compound C (as inducers), and metformin (as an inhibitor). By approaches performed both *in vivo* and *in vitro*, we confirmed that treatments triggering fat accumulation and AMPK disruption may compromise hepatic miRNA biosynthesis, while the knockdown of the miRNA-processing enzyme DICER exhibited a substantial increase in lipid deposition. Then, we validated consistent downregulation of specific hepatic miRNAs, pointing the loss of a few unique miRNA candidates at the forefront of the imbalance affecting *de novo* lipogenesis and FA uptake, oxidation and transport in hepatocytes, leading to the acquisition of NAFLD traits. Finally, transient transfection with mimic miRNA candidates shortlisted the miR-30b and miR-30c as being capable of redirecting FA metabolism from energy storage to expenditure, tackling inadequate FA accumulation in human hepatocytes.

METHODS

Cell cultures

Commercially available primary human hepatocytes (HH) were grown on poly-L-lysine pre-coated dishes and cultured at 37°C and 5% CO_2 atmosphere in hepatocyte medium supplemented with 5% fetal bovine serum (FBS), 100 units/ml penicillin and streptomycin (P/S), and 1% of a commercially available combination of different growth factors and hormones (Innoprot, Bizkaia, Spain). HepG2 cells were purchased from the American Type Culture Collection (ATCC) and cultured under same conditions in Dulbecco's Modified Eagle's Medium (DMEM) supplemented with 10% FBS, 100 units/ml P/S, and 1% glutamine and sodium pyruvate (Thermo Fisher Scientific, Wilmington, DE). Huh7 cells were cultured in MEM AQ^{TM} Minimal essential Eagle Medium (Sigma-Aldrich, St. Louis, MO) with 10% FBS and 100 units/ml P/S. Decreased AMPK activity was induced by 10 μM compound C (CC). Exposure to 500 (HepG2) and 200 (HH) μM palmitic acid (PA) was accomplished as previously [29]. Transient AMPK activation was induced by 1 mM metformin (Sigma-Aldrich, St. Louis, MO).

Silencing of hepatic AMPK *in vivo*

10-weeks old C57BL6 mice were held in a specific restrainer for intravenous injections Tailveiner (TV-150, Bioseb, France). Tail-injections were carried out using a 27G X 3/8" (0.40 mm x 10 mm) syringe. Mice were injected with either 100 μl of null (sh-luciferase) or AMPKα1-DN lentiviral particles in saline solution. The protein-coding sequence of AMPKα1-DN was cloned from pVQAd SF1-AMPKα1-DN (reference number: 24603; ViraQuest Inc., North Liberty, IA) into the pSIN-Flag vector. To generate lentiviral particles, the pSIN-Flag vector containing AMPKα1-DN was co-transfected with packaging vectors (psPAX2 and pMD2G) into HEK293T, as previously [30]. psPAX2 and pMD2G vectors were a gift from Didier Trono (Addgene Plasmids, Cambridge, MA).

Human liver samples

A sample of 60 biopsy specimens was evaluated by a pathologist and scored using the NAFLD clinical research network criteria, considering the presence of steatosis, cytological ballooning and inflammation, as previously explained [29]. Based on laboratory, sonographic and histological findings, these nonconsecutive obese subjects were classified as NAFLD, borderline, or participants with normal hepatic histology, ultrasound, and liver enzymes. Exclusion criteria included cirrhosis or bridging fibrosis, a liver biopsy less than 2 cm long for histological characterization, and the use of statins. Gene expression and miRNA candidates were evaluated through prevalidated TaqMan primer/probe sets (Applied Biosystems, Darmstadt, Germany), as previously [29].

Depletion of AMPK and DICER in hepatocytes

Knockdown of AMPKα1/2 and DICER was performed by lentiviral particles expressing short hairpin (sh) interference RNA. HepG2 cells were plated and 1:1 viruses were added for 24 h, together with 7 μg/ml polybrene. Stable clones were selected via puromycin dihydrochloride (Santa Cruz Biotechnology Inc., Dallas, TX).

In vitro transfection of mimic miRNA

HepG2 and Huh7 cells were transfected for 48 h with 50 nM mimic miRNA candidates, or with non-targeting control using HiPerfect Transfection Reagent (Qiagen, Gaithersburg, MD).

Genomic analysis

Total RNA was purified using the RNeasy Mini Kit (QIAgen, Gaithersburg, MD). Concentrations were assessed by a Nanodrop ND-1000 Spectrophotometer (Thermo Fisher Scientific, Wilmington, DE). Total RNA was reversed transcribed to cDNA using High Capacity cDNA Archive Kit (Applied Biosystems, Darmstadt, Germany). 600 ng of total RNA was used as input for miRNA reverse transcription by the TaqMan miRNA Reverse Transcription Kit, and TaqMan miRNA Multiplex RT Assays, as previously [31]. Expression of 754 mature miRNA species was assessed by means of TaqMan low-density arrays (Life Technologies, Darmstadt, Germany). Real-time PCR was carried out in a QuantStudio 7 Flex Real-Time PCR. Results were analysed with the QuantStudioTM Real-Time PCR Software (ThermoFisher Scientific). Commercially available TaqMan hydrolysis probes (Applied Biosystems, Foster City, CA) and forward/reverse SYBR Green® paired primers were used to analyse the expression of genes and miRNA candidates in a Light Cycler 480 II (Roche Diagnostics SL, Barcelona, Spain). SDHA (succinate dehydrogenase complex, subunit A) and PPIA (peptidylpropyl isomerase A), and RNU6b were used as endogenous controls for gene and miRNA expression, respectively.

De novo lipogenesis

Transfected HepG2 cells were incubated for 3 h in complete media with 5 μCi/well of [^{3}H]-Acetic acid (Amersham, GE Healthcare, Thermo Fisher Scientific Inc.). Total lipids were extracted as explained in reference [32]. Samples were run on thin layer silica-based chromatography using hexane/diethyl ether/acetic acid/water (65:15:1:0.25) as solvent. TAG, DAG and CE standards were run along with samples to identify the corresponding species. The three lipid species were scraped, and the [^{3}H] radioactivity was measured by liquid scintillation counting. The results was normalized for total protein.

Lipidomics

Lipid extraction was performed as explained in reference [33]. The following lipid species were added as internal standards: PC 14:0/14:0, PC 22:0/22:0, PE 14:0/14:0, PE 20:0/20:0 (di-phytanoyl), PS 14:0/14:0, PS 20:0/20:0 (di-phytanoyl), PI 17:0/17:0, LPC 13:0, LPC 19:0, LPE 13:0, Cer d18:1/14:0, Cer 17:0, D7-FC, CE 17:0, and CE 22:0. The residues were dissolved in either in 10 mM ammonium acetate in methanol/chloroform (3:1, v/v) (for low mass resolution tandem mass spectrometry), or chloroform/methanol/2-propanol (1:2:4 v/v/v) with 7.5 mM ammonium formate (for high resolution mass spectrometry). The analysis of lipids was performed by direct flow injection analysis (FIA) using either a triple quadrupole mass spectrometer (FIA-MS/MS; QQQ triple quadrupole) [34,35] or a hybrid quadrupole-Orbitrap mass spectrometer (FIA-FTMS; high mass resolution) [36].

Lipid species were annotated according to the recently published proposal for shorthand notation [37]. Data processing details are described in [38]. The extracted data were further processed by self-programmed Macros.

Mitochondrial oxygen consumption rate

The oxygen consumption rate (OCR) was measured in HepG2 transfected with mimic miRNAs by means of a Seahorse XF96 Extracellular Flux Analyser (Agilent Technologies, Santa Clara, CA). Cells were cultured for 48 h with transfection complexes, followed by 60 min of culture with XF base medium supplemented with 1 mM pyruvate, 2 mM glutamine, and 10 mM glucose in a CO_2 free incubator. The OCR was measured using the XF Cell Mito Stress Test Kit (Agilent Technologies, Santa Clara, CA). OCR was then normalized to the total protein content, determined by Pierce™ BCA Protein Assay Kit (Thermo Fisher Scientific, Wilmington, DE).

Quantification of apolipoprotein B100

The media were analysed using Human Apolipoprotein B ELISA^{PRO} kit (3715-1HP-2, Mabtech, Sweden) according to manufacturer's protocol. The absorbance was measured at 450 nm in a Cytation 5 Cell Imaging Reader (BioTek Instruments, Winooski, VT).

Triglyceride and cholesterol analysis

HepG2 cells transfected for 72 h with 100 nM mimic miRNAs or non-targeting control were subjected to triglyceride and cholesterol analysis using the GPO-PAP Triglyceride assay kit and the CHOD-PAP Cholesterol assay kit (Cobas, Roche/Hitachi, Tokyo, Japan). Data was normalized for total protein.

Prediction of miRNA target sites

Putative miRNA binding sites in 3'UTR messenger RNA were assessed using TargetScan (http://www.targetscan.org), miRanda (http://www.microrna.org/), and miRWalk (http://zmf.umm.uni-heidelberg.de/apps/zmf/mirwalk2/). miRpath v.3 was employed to perform miRNA pathway analysis through experimentally validated miRNA interactions derived from DIANA-TarBase v6.0 [39]. Gene annotation enrichment analysis was performed by DAVID [40].

DNA constructs

Acyl-CoA synthetase long chain family member 1 (ACSL1) 3'UTR was amplified and inserted downstream of a firefly luciferase in the dual luciferase vector pEZX-MT06 (GeneCopoeia, Rockville, MD). Mutant ACSL1 3'UTR carrying a substitution of 7-8 nucleotides within the seed sequence of miRNA candidates was generated by oligonucleotide-directed PCR mutagenesis with Phusion High-Fidelity DNA Polymerase.

Luciferase assays

Huh7 cells were transfected for 48 h with the Luc-ACSL1 3'UTR wild-type or mutant constructs together with 200 nM mimic miRNAs by using Lipofectamine 2000™

(Invitrogen, Carlsbad, CA). Cell lysates were subjected to measurements of firefly and *Renilla* luciferase activities by using the Dual Luciferase Reporter Assay System (Promega, Madison, WI). The firefly signals were normalized by using the *Renilla* signals according to the manufacturer's instructions.

Lipid droplet staining

HepG2 and Huh7 cells were stained with 2 µM Bodipy 493/503 (Molecular Probes/Life Technologies, Eugene, OR). After washing, cover slips were mounted using Mowiol (Calbiochem, La Jolla, CA) containing 5 µg/ml DAPI (Thermo Scientific/Molecular Probes). Cells were imaged using Zeiss Axio Observer Z1 microscope (Carl Zeiss Imaging Solutions GmbH, Oberkochen, Germany), with the same exposure time for non-targeting control and mimic miRNAs. Staining was quantified using FIJI (Image J) software with a set cutoff threshold (total signal intensity/number of cells in the field). Treated and control HepG2 and primary HH were also fixed with paraformaldehyde 4%. Cells were dipped in 60% isopropanol before stained with Oil Red O (Sigma, Lyon, France) for 10 min at room temperature. Absorbance was measured at 500 nm.

Western blot

Equal amounts of total protein were loaded on 10% SDS-PAGE. After separation, proteins were transferred onto Nitrocellulose (BioRad, Hercules, CA). Antibodies against ACSL1 (Abcam, Cambridge, UK), AMPK, phospho and total ACC (Cell Signalling, Danvers, MA), FAS, and β-actin (Santa Cruz Biotechnology, Inc., Dallas, TX) were used. Blots were visualized by enhanced chemiluminescence (Thermo Fisher Scientific, Wilmington, DE) and signals were quantified by Image J software (https://imagej.nih.gov/ij/).

Statistics

Student's *t*-tests were performed to study differences between groups of treatments. Statistical associations between hepatic miRNA and clinical parameters was determined by Spearman's test. Data analyses were performed with the SPSS statistical software (SPSS v19.0, IBM, Chicago, IL), GraphPad Prism 6 (Graphpad Holdings, LLC), and the R Statistical Software (http://www.r-project.org/).

RESULTS

Treatments mimicking NAFLD increase FA deposition in hepatocytes

Our previous study established significant variations in primary human hepatocytes (HH) and HepG2 cells challenged with conditions that mimicked non-alcoholic fatty liver disease (NAFLD) [29]. Here, we performed additional experimental treatments aimed at evaluating the impact of specific compounds that may compromise fatty acid (FA) homeostasis in hepatocytes. For this, we exposed HH (**Figure 1a**) and HepG2 cells (**Figure 1b**) to palmitic acid (PA) and compound C (CC) as inducers, and to metformin (Mtf), which can mediate through or independently of AMPK-activation to alleviate fatty liver. First, we confirmed significant alterations in lipid deposition (oil red O lipid-droplet staining) and the expression of genes related to *de novo* FA biosynthesis, uptake and transport, as well as altered expression of genes involved in glucose intake and inflammation. On one hand, treatments with PA and CC enhanced lipid accumulation in HH and HepG2 cells (**Figure 1a** and **Figure 1b**), and shortlisted increased *ACSL1* and *FASN* mRNA, while *GLUT2* expression was compromised in both cell models. In parallel, inflammatory activation was evident in hepatocytes challenged with PA, as suggested by enhanced expression of *IL8* (HH), *ITGAX* (both), and *TNFα* (HepG2) (**Figure 1c** and **Figure 1d**). On the other hand, Mtf led to decreased lipid deposition in HH and HepG2 cells (**Figure 1a** and **Figure 1b**) coupled to a significant downregulation of *ACSL1* in both cell models, decreased *FATP5* and *CD36* in HepG2, and reduced *TNFα* mRNA in primary HH (**Figure 1c** and **Figure 1d**). These results confirmed chemical-induced molecular changes allowing lipid deposition in human hepatocytes, thus mirroring the onset of NAFLD *in vitro*.

Compounds that modulate FA homeostasis also modify miRNA biosynthesis

We used TaqMan Low Density Arrays (TLDA) to characterize the expression profile of 754 common mature microRNAs (miRNA) in primary HH challenged with PA, CC, or Mtf. First, we identified hepatic miRNA detectable (threshold Cts <35) in all samples. *In vitro* cultured HH expressed as many as 305 miRNA (40.5%), with a substantial increase upon PA and Mtf (67.3% and 70.9%, respectively), and an outstanding downregulation following the treatment with CC (-69.4%, **Figure 2a**). Indeed, chemical modulation of FA metabolism clearly impacted miRNA expression patterns, with 27 miRNA decreased under CC, and 18 miRNA significantly increased in hepatocytes treated with Mtf (**Figure 2a**). Such remarkable differences accounted in the context of 59 hepatic miRNA with significant variations upon at least one treatment (**Figure 2b**). Intriguingly, even though both PA and CC triggered lipid accumulation in cell models mimicking liver steatosis, quite few coincidences regarding miRNA deregulation were found between these two treatments (**Figure 2b**). However, validation of miRNA candidates accomplished in HepG2 confirmed significant downregulation of miR-26a, miR-30b, miR-30c, and miR-34a during both treatments, while reduced miR-29c, miR-146b, miR-222, and miR-422a accounted only upon PA, and miR-16 and miR-139a levels were significantly decreased in HepG2 challenged with CC (**Figure 2c**). Of note, Mtf led to enhanced expression of miR-16 and miR-30b (**Figure 2c**). Hence, treatments mirroring NAFLD and metformin-

induced lipogenesis inhibition in HH and HepG2 cells appear to have a significant impact on miRNA regulation.

AMPK and DICER may be required for the activity exercised by CC and Mtf

As miRNA profiles in hepatocytes were so widely affected by treatments leading to changes in FA metabolism, the expression of genes involved in miRNA biosynthesis was also investigated. Notably, decreased DROSHA and DICER in both HH and HepG2 cells upon PA and CC was further highlighted by the opposite upregulation exercised by Mtf in HH (**Figure 1c** and **Figure 1d**). As the activation of energy sensor AMP-activated protein kinase (AMPK, also known as PRKAA1) in hepatocytes drives FA oxidation and decreased lipogenesis, protecting against fatty liver disease [16], we aimed to investigate which mechanisms may underlie the observed effects through specific AMPK disruption. Thus, we assessed miRNA expression patterns and the metabolic commitment of cells subjected to AMPK knockdown. In agreement with our previous results, partial ablation of AMPK resulted in increased lipid deposition (**Figure 3a**) and enhanced lipogenesis (**Figure 3b**). Given that chemical induction of fatty liver resulted in impaired expression of the miRNA-processing enzyme DICER, we sought to study whether this key regulator was also involved in the hepatic accumulation of FA. Thus, partial knockdown of DICER was also accomplished in HepG2 cells, depicting similar effects as the knockdown of AMPK, including significant FA overload (**Figure 3a**), and enhanced expression of *ACSL1*, *FASN*, *CD36*, and *PLTP* (**Figure 3c**), leading to increased lipid deposition. Accordingly, altered gene expression patterns were coupled to an overall miRNA downregulation, with consistent decrease of miR-26a, miR-30b, miR-30c, miR-34a, miR-146b, and miR-222 in both models (**Figure 3d**). Thus, impaired AMPK and DICER expression and activity may play functional roles in decreased miRNA biosynthesis and the metabolic disruption affecting hepatocytes under conditions leading to increased FA deposition.

AMPK modulation impacts hepatic miRNA biosynthesis *in vivo*

To further confirm the contribution of AMPK activity to miRNA regulation in liver we applied lentiviral particles harboring dominant negative isoforms of AMPKα (AMPK-DN) in the tail vein of mice. Significantly reduced levels of phospho-ACC were identified following the injection of lentiviral particles harbouring AMPK-DN, when compared to control (**Figure 4a**). In keeping with the inhibition of liver AMPK and reduced phospho-ACC, increased hepatic triglyceride content (**Figure 4b-c**) was also detected. As expected, we found a marked increase in lipogenic genes such as *Acsl1* and *Fasn*, and decreased *Glut2* mRNA, coupled to the significant downregulation of genes relevant for miRNA biogenesis, namely *Drosha* and *Ago2* (**Figure 4d**). Notably, impaired AMPK expression also resulted in a significant deregulation of overall miRNA levels *in vivo* (**Figure 4e**), being tightly linked to increased FA metabolism. Hence, current results *in vivo* strongly support our findings *in vitro*, linking impaired AMPK activity to miRNA biosynthesis.

Overexpression of miRNA candidates improves lipid metabolism

To assess whether impaired hepatic miRNA expression is at the forefront of changes in gene expression and the deposition of FA in hepatocytes, HepG2 and Huh7 cells were transfected with mimic miRNA or a non-targeting (NT) control. We found that, among our twelve miRNA candidates, only treatments with mimic miR-16, miR-30b, and miR-30c led to a significant reduction in the content and size of lipid droplets in hepatocytes (**Figure 5a**). Accordingly, analysis performed by thin layer silica-based chromatography showed that the ectopic expression of these miRNA candidates drove reduced triglycerides, diacylglycerols, and cholesterol ester storage in transfected cells (**Figure 5b**), while the immunosorbent assessment of triglyceride and cholesterol in the growth media of the cells verified significant decreases when hepatocytes were treated with mimic miR-30b or miR-30c (but not with miR-16) (**Figure 5c**). Notably, quantitative analysis of the mitochondrial function (oxygen consumption rate, OCR) in HepG2 showed that cells transfected with mimic miR-30b and miR-30c accomplished 26% and 35% increase, respectively, while no significant change was found in human hepatocytes transfected with mimic miR-16 (**Figure 5d**). Additionally, treatments with mimic miR-30b and miR-30c led to decreased apolipoprotein B (apoB) levels in the media (**Figure 5e**). Altogether, current results point out decreased lipid deposition and significant recovery of mitochondrial activity in human hepatocytes after transient transfection with mimic miR-30b and miR-30c.

Hepatic miRNA candidates regulate proteins that control FA storage

In silico analysis pointed at a variety of predicted target genes related to glucose and FA metabolism (**Figure 5f**), many of which were experimentally tested. HepG2 cells transfected with mimic miR-16, miR-30b and miR-30c depicted decreased expression of genes coding for factors involved in the synthesis of triacylglycerols (**Figure 5g**). Of note, expression of two genes directly related to the development of NAFLD, angiopoietin like 3 (*ANGPTL3*), a liver-secreted protein recently identified as a marker of NAFLD in mice and humans [41], and the membrane-bound O-acyltransferase 7 (*MBOAT7*), the disruption of which is related to liver disease [42], showed significant down and upregulation, respectively (**Figure 5g**). In line with changes affecting mitochondrial activity, we found an increase of carnitine palmitoyltransferase 1 α (*CPT1α*) mRNA in cells treated with mimic miR-30b and miR-30c, while miR-16 did not impact its expression (**Figure 5g**). On the other hand, 3'UTR binding sites for these miRNA candidates were identified in the gene coding for acyl-CoA synthetase long chain family member 1 (*ACSL1*). Thus, *ACSL1* 3'UTR luciferase reporter constructs were transfected into Huh7 cells, showing a significant reduction of the luciferase signal upon transfection with mimic miRNA candidates (**Figure 5h**). Notably, luciferase activity was not modified in cells transfected with a mutated *ACSL1* 3'UTR reporter construct, hence confirming specific binding between the current miRNA candidates and *ACSL1* mRNA. Finally, ACSL1 protein analysis endorsed the luciferase results (**Figure 5i**), thus validating the causal relationship suggested by the complementary sequences (**Figure 5j**).

Mimic miR-30b and miR-30c modulate the sphingomyelin/ceramide ratio

To obtain an overview of the effects accomplished by mimic miRNA transfections on the lipid profile, we subjected lipids extracted from human hepatocytes to quantitative direct flow injection electrospray ionization tandem mass spectrometry. Notably, PCA and heatmap analysis (**Figure 6a**) discriminated the impact of mimic miR-16 from miR-30b and miR-30c. Consistent reduction of phosphatidylethanolamine plasmalogens and ceramides, together with an increase of sphingomyelins, were observed after the ectopic overexpression of miR-30b and miR-30c, the changes accomplished by miR-16 being less prominent (**Figure 6b**). These findings were strongly supported by consistent changes in the expression of key enzymes related to the synthesis/degradation of sphingomyelins and ceramides, namely elevated sphingomyelin synthase 1 and 2 (*SGMS1* and *SGMS2*), and decreased sphingomyelin phosphodiesterase 1 (*SMPD1*) in hepatocytes transfected with mimic miR-30b or miR-30c (**Figure 6c**). Noteworthy, the expression of genes involved in the formation and coating of lipid droplets (*PLIN1*, *SLC25A1*, and *MGAT1*) was also compromised by miR-30b and miR-30c, while miR-30b also reduced seipin (*BSCL2*) mRNA (**Figure 6c**), an endoplasmic reticulum-resident protein of key importance in neutral lipid storage [43].

Recovery of miR-30b and miR-30c acts against FA accumulation in hepatocytes

As consistent downregulation of hepatic miR-30b and miR-30c was found in association with NAFLD and treatments that mimicked this condition [29], pointing the loss of these unique miRNA species at the forefront of the imbalance of hepatic lipid homeostasis, we wanted to see whether their recovery restored lipid deposition after treatments triggering FA overload. As postulated, lipid droplet staining revealed the ability of miR-30b and miR-30c to reduce triglyceride storage in hepatocytes treated with CC, or upon the knockdown of *AMPK* and *DICER* (**Figure 7a**). Indeed, replenishment of miR-30b and miR-30c in hepatocytes with impaired *AMPK* or *DICER* activity, and treatments with either mimic miR-30b or miR-30c on HepG2 cells challenged with CC, reduced the lipid droplet area (**Figure 7b**). In concordance, transfection of mimic miR-30b and miR-30c (**Figure 7c**) decreased the expression of *ACSL1* and *FASN* (**Figure 7d**), and elevated *GLUT2* mRNA in human hepatocytes with impaired *AMPK* expression, suggesting partial restoration of glucose intake in this cell model.

Expression of hepatic miR-30b and miR-30c is associated with NAFLD

With regard to the clinical relevance of the results explained above, real time PCR performed in liver samples from obese women with or without NAFLD confirmed significant downregulation in miR-16, miR-30b and miR-30c, together with increased *ACSL1* mRNA, and decreased *DICER* and *AMPK* in subjects with NAFLD (**Figure 8a**). Indeed, *DICER* and *AMPK* gene expression levels in such liver biopsies were positive and significantly associated with current miRNA candidates (**Figure 8b**). Moreover, the quantities of these three miRNAs were inversely correlated with body mass index and fasting triglycerides (**Figure 8b**), further emphasizing their potential relevance as novel candidates to control fatty liver through the restauration of lipid homeostasis in liver.

DISCUSSION

Non-alcoholic fatty liver disease (NAFLD) is the main consequence of long-lasting metabolic impairment affecting hepatic *de novo* lipogenesis and fatty acid (FA) uptake, together with the inability to oxidize lipids that are gradually accumulated in hepatocytes [44]. Nowadays it is widely recognized that many of these procedures are mainly regulated by AMPK function [23,45,46]. Current findings highlight the apparent contribution of AMPK also to hepatic miRNA biosynthesis by means of its pharmacological modification and genetic blockade, accomplished both *in vitro* and *in vivo*. Indeed, as metformin [47] and compound C [48] have been postulated to trigger off-target effects, due to their ability to impact a broad variety of kinases that appear to be mediated by attenuation of biosynthetic and oxidative fluxes, lentiviral particles mediating specific AMPKα1/2 knockdown were employed. This confirmed, among others, miRNA downregulation as the result of diminished AMPK performance and impaired lipid homeostasis in human hepatocytes.

We next postulated that AMPK may regulate FA metabolism through miRNA availability. Accordingly, the interplay between AMPK and hepatic miRNA profiles leading to changes in FA metabolism was sustained by i) reduced AMPK activity/ expression coupled to decreased miRNA abundance and expression of genes related to miRNA biosynthesis, namely *DICER* and *DROSHA* under conditions mimicking NAFLD, ii) consistent decrease of miRNA candidates coinciding with increased FA accumulation, and iii) the ectopic replenishment of hepatic miR-30b and miR-30c, partially rescuing FA overload and modifying lipid profiles in human hepatocytes. In agreement, partial knockdown of *DICER* demonstrated that its downregulation is intrinsically coupled to significant changes in miRNA profiles and increased FA overload. This piece of data matches with previous studies reporting the interplay between DICER and miRNA profiles, controlling the epithelial-mesenchymal transition during oncogenic events [49], and increased DICER after treatments that modulate AMPK activity in both mice and humans [50,51]. Additionally, previous research performed in a dietary-induced NASH mouse model reported a significant decrease of hepatic *Dicer* [52]. Strikingly, both *AMPK* and *DICER* knockdown resulted in increased FA deposition in hepatocytes, which was partially counteracted by rescue of the diminished expression of two of the miRNA species most consistently affected, the miR-30b and miR-30c.

Variations in specific hepatic miRNA have been previously associated with NAFLD and lipid homeostasis [53–57]. Consistent results were reported with regard to miR-30c, which showed decreased expression in the liver of a leptin receptor-deficient mouse model [58], and in plasma from subjects with NAFLD [59]. miR-30c has been linked to lipid metabolism, disclosing its ability to dampen lipid biosynthesis and lipoprotein secretion, being postulated as a potential target against hyperlipidemia and related diseases [60,61]. Noteworthy, *in silico* prediction categorized genes related to *de novo* lipogenesis and FA uptake as plausible targets for the differentially expressed miRNA candidates (**Figure 5f**). The overall outcome of their downregulation under conditions mimicking NAFLD, also characterized by decreased AMPK activity, would be translated into decreased miRNA expression and the disability to actively repress

specific target genes. As a consequence, this may result in impaired expression patterns, anomalous lipid metabolism, and the acquisition of NAFLD traits.

Specifically, miR-16, miR-30b and miR-30c were consistently involved in lipid homeostasis, as demonstrated by studies assessing organelle structure, gene expression, mitochondrial function, and mass spectrometric analysis of the hepatocyte lipidome. Thereby, replenishment of these miRNA candidates led to i) decreased lipid droplet accumulation, ii) impaired expression of genes related to the synthesis of triglycerides, and iii), in the case of mimic miR-30b and miR-30c, enhanced mitochondrial function coupled with increased *CPT1α* expression and modulation of genes related to the lipidome. Accordingly, *ACSL1* was validated as a direct target, which is known to dynamically drive FA metabolism in hepatocytes [62]. Indeed, previous research suggested that *ACSL1* channels radiolabeled oleate towards diacylglycerol, phosphatidyl-ethanolamine, phosphatidylinositol, and phosphatidylcholine, diminishing cholesterol esterification [63,64]. On the contrary, ACSL1 deficiency led to reduced FA biosynthesis and enabled β-oxidation [65]. Our results point out the higher expression of hepatic *ACSL1* in NAFLD patients and under conditions mimicking enhanced FA deposition and decreased miRNA expression in hepatocytes, while the control exercised by miR-30b and miR-30c was coupled to increased mitochondrial function and decreased *de novo* lipogenesis.

Finally, lipidome-wide quantitative assessment shortlisted key differences between the activity exercised by mimic miR-16, miR-30b, and miR-30c, and a reduction of ceramides coinciding with an elevation of sphingomyelins, accomplished by miR-30b and miR-30c but not by miR-16. It should be noted that an increase in hepatic ceramides is associated with steatosis and insulin resistance [66], and that ACSL1 can induce excess synthesis of total acyl derived long chain ceramides [67], thus reinforcing the causal implications of our current results. On the other hand, sphingomyelins have been reported to attenuate hepatic steatosis in high-fat-diet-induced obese mice, proving beneficial effects [68]. Hence, the analysis of the lipidome in hepatocytes challenged with mimic miRNA candidates reinforced the potential therapeutic utility of the ectopic recovery of miR-30b and miR-30c in the fatty liver arena, restoring lipid homeostasis in hepatocytes. Altogether, our data unravel the activity of miR-30b and miR-30c in tackling inadequate FA accumulation in liver, offering a potential avenue for the treatment of NAFLD.

Financial support: This work was supported by research funds from the *Formación en Investigación en Salud* of the *Instituto de Salud Carlos III* (ISCIII; PI15-01934 to JMF-R, PI18-00550 to FJO); the *Pla Estratègic de Recerca i Innovació en Salut* and the *Govern de la Generalitat* (PERIS 2016), the *Catalan Association of Diabetes* (ACD 2019), and the *Spanish Society of Diabetes* (SED 2019) (to FJO); from the *Fondo Europeo de Desarrollo Regional* (FEDER), the *Xunta de Galicia* (2015-CP079 and 2016-PG068, to ML); the *Ministerio de Economía y Competitividad* (MINECO), also supported by the FEDER Program of EU (SAF2015-71026-R, and BFU2015-70454-REDT/Adipoplast), and the *CIBER de la Fisiopatología de la Obesidad y Nutrición* (CIBEROBN). The CIBEROBN is an initiative of the ISCIII.

Author Contribution: JL, FJO designed the experiments, analysed biochemical variables, performed the statistical analysis, and wrote the manuscript; JMM-N, AL, FC analysed biochemical variables and assisted with the setup of *in vitro* experiments; MH, YZ, GL, NHP also contributed to the performance and analyses of experiments, including lipidomics; WR obtained liver samples from volunteers, their clinical outputs, and the written consent of participants following bariatric surgery. LL-P, ML performed animal husbandry maintenance, treatment and characterization. VO, ML, JMF-R planned some of the experiments, revised the manuscript, and provided intellectual input.

Conflict of Interest: We certify that there is no conflict of interest to disclose regarding the material discussed in this manuscript. All authors of this manuscript have participated in the execution of this study. All authors are aware of and agree to the content of the manuscript, and have approved the final version submitted, being listed as authors on the manuscript. The contents of this manuscript have not been copyrighted or published previously. There are no directly related manuscripts or abstracts, published or unpublished, by one or more authors of this manuscript. The submitted manuscript nor any similar script, in whole or in part, will be neither copyrighted, submitted, or published elsewhere while the Journal is under consideration.

REFERENCES

[1] Loomba R, Sanyal AJ. The global NAFLD epidemic. Nat Rev Gastroenterol Hepatol 2013. doi:10.1038/nrgastro.2013.171.

[2] Brunt EM, Wong VW-S, Nobili V, Day CP, Sookoian S, Maher JJ, et al. Nonalcoholic fatty liver disease. Nat Rev Dis Prim 2015;1:15080.

[3] Byrne CD, Targher G. NAFLD: A multisystem disease. J Hepatol 2015. doi:10.1016/j.jhep.2014.12.012.

[4] Yki-Järvinen H. Non-alcoholic fatty liver disease as a cause and a consequence of metabolic syndrome. Lancet Diabetes Endocrinol 2014;2:901–10. doi:10.1016/S2213-8587(14)70032-4.

[5] Marchesini G, Brizi M, Blanchi G, Tomassetti S, Bugianesi E, Lenzi M, et al. Nonalcoholic Fatty Liver Disease: A Feature of the Metabolic Syndrome. Diabetes 2001. doi:10.2337/diabetes.50.8.1844.

[6] Than NN, Newsome PN. A concise review of non-alcoholic fatty liver disease. Atherosclerosis 2015;239:192–202. doi:10.1016/j.atherosclerosis.2015.01.001.

[7] Mansouri A, Gattolliat CH, Asselah T. Mitochondrial Dysfunction and Signaling in Chronic Liver Diseases. Gastroenterology 2018. doi:10.1053/j.gastro.2018.06.083.

[8] Gan L, Xiang W, Xie B, Yu L. Molecular mechanisms of fatty liver in obesity. Front Med 2015;9:275–87. doi:10.1007/s11684-015-0410-2.

[9] Li Y, Xu S, Mihaylova MM, Zheng B, Hou X, Jiang B, et al. AMPK phosphorylates and inhibits SREBP activity to attenuate hepatic steatosis and atherosclerosis in diet-induced insulin-resistant mice. Cell Metab 2011;13:376–88. doi:10.1016/j.cmet.2011.03.009.

[10] Day EA, Ford RJ, Steinberg GR. AMPK as a Therapeutic Target for Treating Metabolic Diseases. Trends Endocrinol Metab 2017;28:545–60. doi:10.1016/j.tem.2017.05.004.

[11] Smith BK, Marcinko K, Desjardins EM, Lally JS, Ford RJ, Steinberg GR. Treatment of nonalcoholic fatty liver disease: Role of AMPK. Am J Physiol - Endocrinol Metab 2016;311. doi:10.1152/ajpendo.00225.2016.

[12] Esquejo RM, Salatto CT, Delmore J, Albuquerque B, Reyes A, Shi Y, et al. Activation of Liver AMPK with PF-06409577 Corrects NAFLD and Lowers Cholesterol in Rodent and Primate Preclinical Models. EBioMedicine 2018. doi:10.1016/j.ebiom.2018.04.009.

[13] Lin HZ, Yang SQ, Chuckaree C, Kuhajda F, Ronnet G, Diehl AM. Metformin reverses fatty liver disease in obese, leptin-deficient mice. Nat Med 2000. doi:10.1038/79697.

[14] Zhou G, Myers R, Li Y, Chen Y, Shen X, Fenyk-Melody J, et al. Role of AMP-activated protein kinase in mechanism of metformin action. J Clin Invest 2001. doi:10.1172/JCI13505.

[15] Fullerton MD, Galic S, Marcinko K, Sikkema S, Pulinilkunnil T, Chen ZP, et al. Single phosphorylation sites in Acc1 and Acc2 regulate lipid homeostasis and the insulin-sensitizing effects of metformin. Nat Med 2013. doi:10.1038/nm.3372.

[16] Boudaba N, Marion A, Huet C, Pierre R, Viollet B, Foretz M. AMPK Re-Activation Suppresses Hepatic Steatosis but its Downregulation Does Not Promote Fatty Liver Development. EBioMedicine 2018. doi:10.1016/j.ebiom.2018.01.008.

[17] You M, Matsumoto M, Pacold CM, Cho WK, Crabb DW. The role of AMP-activated protein kinase in the action of ethanol in the liver. Gastroenterology 2004. doi:10.1053/j.gastro.2004.09.049.

[18] Isakovic A, Harhaji L, Stevanovic D, Markovic Z, Sumarac-Dumanovic M, Starcevic V, et al. Dual antiglioma action of metformin: Cell cycle arrest and mitochondria-dependent apoptosis. Cell Mol Life Sci 2007. doi:10.1007/s00018-007-7080-4.

[19] Tang YC, Williams BR, Siegel JJ, Amon A. Identification of aneuploidy-selective antiproliferation compounds. Cell 2011. doi:10.1016/j.cell.2011.01.017.

[20] Bain J, Plater L, Elliott M, Shpiro N, Hastie CJ, Mclauchlan H, et al. The selectivity of protein kinase inhibitors: A further update. Biochem J 2007. doi:10.1042/BJ20070797.

[21] Yu P, Xu X, Zhang J, Xia X, Xu F, Weng J, et al. Liraglutide Attenuates Nonalcoholic Fatty Liver Disease through Adjusting Lipid Metabolism via SHP1/AMPK Signaling Pathway. Int J Endocrinol 2019. doi:10.1155/2019/1567095.

[22] Chen K, Chen X, Xue H, Zhang P, Fang W, Chen X, et al. Coenzyme Q10 attenuates high-fat diet-induced non-alcoholic fatty liver disease through activation of the AMPK pathway. Food Funct 2019. doi:10.1039/c8fo01236a.

[23] Yao H, Tao X, Xu L, Qi Y, Yin L, Han X, et al. Dioscin alleviates non-alcoholic fatty liver disease through adjusting lipid metabolism via SIRT1/AMPK signaling pathway. Pharmacol Res 2018;131:51–60. doi:10.1016/j.phrs.2018.03.017.

[24] Baek D, Villén J, Shin C, Camargo FD, Gygi SP, Bartel DP. The impact of microRNAs on protein output. Nature 2008. doi:10.1038/nature07242.

[25] Lim LP, Lau NC, Garrett-Engele P, Grimson A, Schelter JM, Castle J, et al. Microarray analysis shows that some microRNAs downregulate large numbers of-target mRNAs. Nature 2005. doi:10.1038/nature03315.

[26] Selbach M, Schwanhäusser B, Thierfelder N, Fang Z, Khanin R, Rajewsky N. Widespread changes in protein synthesis induced by microRNAs. Nature 2008. doi:10.1038/nature07228.

[27] Ferreira DMS, Simão AL, Rodrigues CMP, Castro RE. Revisiting the metabolic syndrome and

paving the way for microRNAs in non-alcoholic fatty liver disease. FEBS J 2014;281:2503–24. doi:10.1111/febs.12806.
[28] Baffy G. MicroRNAs in Nonalcoholic Fatty Liver Disease. J Clin Med 2015;4:1977–88. doi:10.3390/jcm4121953.
[29] Latorre J, Moreno-Navarrete JM, Mercader JM, Sabater M, Rovira Ò, Gironès J, et al. Decreased lipid metabolism but increased FA biosynthesis are coupled with changes in liver microRNAs in obese subjects with NAFLD. Int J Obes 2017;41:620–30. doi:10.1038/ijo.2017.21.
[30] Aguilo F, Zhang F, Sancho A, Fidalgo M, Di Cecilia S, Vashisht A, et al. Coordination of m6A mRNA Methylation and Gene Transcription by ZFP217 Regulates Pluripotency and Reprogramming. Cell Stem Cell 2015;17:689–704. doi:10.1016/j.stem.2015.09.005.
[31] Ortega FJ, Moreno M, Mercader JM, Moreno-Navarrete JM, Fuentes-Batllevell N, Sabater M, et al. Inflammation triggers specific microRNA profiles in human adipocytes and macrophages and in their supernatants. Clin Epigenetics 2015;7. doi:10.1186/s13148-015-0083-3.
[32] Ruhanen H, Nidhina Haridas PA, Eskelinen EL, Eriksson O, Olkkonen VM, Käkelä R. Depletion of TM6SF2 disturbs membrane lipid composition and dynamics in HuH7 hepatoma cells. Biochim Biophys Acta - Mol Cell Biol Lipids 2017;1862:676–85. doi:10.1016/j.bbalip.2017.04.004.
[33] Bligh EG, Dyer WJ. A rapid method of total lipid extraction. Can J Biochem Physiol 1959;37:911–7. doi:10.1145/3163918.
[34] Liebisch G, Lieser B, Rathenberg J, Drobnik W, Schmitz G. High-throughput quantification of phosphatidylcholine and sphingomyelin by electrospray ionization tandem mass spectrometry coupled with isotope correction algorithm. Biochim Biophys Acta - Mol Cell Biol Lipids 2004;1686:108–17. doi:10.1016/j.bbalip.2004.09.003.
[35] Liebisch G, Binder M, Schifferer R, Langmann T, Schulz B, Schmitz G. High throughput quantification of cholesterol and cholesteryl ester by electrospray ionization tandem mass spectrometry (ESI-MS/MS). Biochim Biophys Acta - Mol Cell Biol Lipids 2006;1761:121–8. doi:10.1016/j.bbalip.2005.12.007.
[36] Höring M, Ejsing CS, Hermansson M, Liebisch G. Quantification of Cholesterol and Cholesteryl Ester by Direct Flow Injection High Resolution FTMS Utilizing Species-Specific Response Factors. Anal Chem 2019. doi:10.1021/acs.analchem.8b05013.
[37] Liebisch G, Vizcaino JA, Koefeler H, Troetzmueller M, Griffiths WJ, Schmitz G, et al. Shorthand Notation for Lipid Structures Derived from Mass Spectrometry. J Lipid Res 2013;54. doi:10.1194/jlr.M033506.
[38] Husen P, Tarasov K, Katafiasz M, Sokol E, Vogt J, Baumgart J, et al. Analysis of lipid experiments (ALEX): A software framework for analysis of high-resolution shotgun lipidomics data. PLoS One 2013;8. doi:10.1371/journal.pone.0079736.
[39] Vlachos IS, Zagganas K, Paraskevopoulou MD, Georgakilas G, Karagkouni D, Vergoulis T, et al. DIANA-miRPath v3.0: Deciphering microRNA function with experimental support. Nucleic Acids Res 2015. doi:10.1093/nar/gkv403.
[40] Huang DW, Sherman BT, Lempicki RA. Bioinformatics enrichment tools: Paths toward the comprehensive functional analysis of large gene lists. Nucleic Acids Res 2009;37:1–13. doi:10.1093/nar/gkn923.
[41] Kersten S. Angiopoietin-like 3 in lipoprotein metabolism. Nat Rev Endocrinol 2017. doi:10.1038/nrendo.2017.119.
[42] Eslam M, Valenti L, Romeo S. Genetics and epigenetics of NAFLD and NASH: Clinical impact. J Hepatol 2018. doi:10.1016/j.jhep.2017.09.003.
[43] Salo VT, Belevich I, Li S, Karhinen L, Vihinen H, Vigouroux C, et al. Seipin regulates ER–lipid droplet contacts and cargo delivery. EMBO J 2016. doi:10.15252/embj.201695170.
[44] Ferré P, Foufelle F. Hepatic steatosis: A role for de novo lipogenesis and the transcription factor SREBP-1c. Diabetes, Obes Metab 2010;12:83–92. doi:10.1111/j.1463-1326.2010.01275.x.
[45] Garcia D, Shaw RJ. AMPK: Mechanisms of Cellular Energy Sensing and Restoration of Metabolic Balance. Mol Cell 2017;66:789–800. doi:10.1016/j.molcel.2017.05.032.
[46] Woods A, Williams JR, Muckett PJ, Mayer F V., Liljevald M, Bohlooly-Y M, et al. Liver-Specific Activation of AMPK Prevents Steatosis on a High-Fructose Diet. Cell Rep 2017;18:3043–51. doi:10.1016/j.celrep.2017.03.011.
[47] Viollet B, Guigas B, Sanz Garcia N, Leclerc J, Foretz M, Andreelli F. Cellular and molecular mechanisms of metformin: An overview. Clin Sci 2012. doi:10.1042/CS20110386.
[48] Cohen P, Plater L, Bain J, Klevernic I, Arthur JSC, Mclauchlan H, et al. The selectivity of protein kinase inhibitors: a further update. Biochem J 2008;408:297–315. doi:10.1042/bj20070797.
[49] Martello G, Rosato A, Ferrari F, Manfrin A, Cordenonsi M, Dupont S, et al. A microRNA targeting dicer for metastasis control. Cell 2010;141:1195–207. doi:10.1016/j.cell.2010.05.017.
[50] Noren Hooten N, Martin-Montalvo A, Dluzen DF, Zhang Y, Bernier M, Zonderman AB, et al. Metformin-mediated increase in DICER1 regulates microRNA expression and cellular senescence. Aging Cell 2016;15:572–81. doi:10.1111/acel.12469.
[51] Blandino G, Valerio M, Cioce M, Mori F, Casadei L, Pulito C, et al. Metformin elicits anticancer effects through the sequential modulation of DICER and c-MYC. Nat Commun 2012;3. doi:10.1038/ncomms1859.
[52] Liu MX, Gao M, Li CZ, Yu CZ, Yan H, Peng C, et al. Dicer1/miR-29/HMGCR axis contributes to

hepatic free cholesterol accumulation in mouse non-alcoholic steatohepatitis. Acta Pharmacol Sin 2017;38:660–71. doi:10.1038/aps.2016.158.
[53] Cheung O, Puri P, Eicken C, Contos MJ, Mirshahi F, Maher JW, et al. Nonalcoholic steatohepatitis is associated with altered hepatic MicroRNA expression. Hepatology 2008. doi:10.1002/hep.22569.
[54] Du J, Niu X, Wang Y, Kong L, Wang R, Zhang Y, et al. MiR-146a-5p suppresses activation and proliferation of hepatic stellate cells in nonalcoholic fibrosing steatohepatitis through directly targeting Wnt1 and Wnt5a. Sci Rep 2015;5. doi:10.1038/srep16163.
[55] Feng YY, Xu XQ, Ji CB, Shi CM, Guo XR, Fu JF. Aberrant hepatic MicroRNA expression in nonalcoholic fatty liver disease. Cell Physiol Biochem 2014;34:1983–97. doi:10.1159/000366394.
[56] He Q, Li F, Li J, Li R, Zhan G, Li G, et al. MicroRNA-26a-interleukin (IL)-6-IL-17 axis regulates the development of non-alcoholic fatty liver disease in a murine model. Clin Exp Immunol 2017;187:174–84. doi:10.1111/cei.12838.
[57] Cao P, Zhang Q, Wan M, Wang J, Wang Y, Zhang Q, et al. Fatty acid synthase is a primary target of MiR-15a and MiR-16-1 in breast cancer. Oncotarget 2016. doi:10.18632/oncotarget.12479.
[58] Fan J, Li H, Nie X, Yin Z, Zhao Y, Chen C, et al. MiR-30c-5p ameliorates hepatic steatosis in leptin receptor-deficient (db/db) mice via down-regulating FASN. Oncotarget 2017;8:13450–63. doi:10.18632/oncotarget.14561.
[59] Mehta R, Otgonsuren M, Younoszai Z, Allawi H, Raybuck B, Younossi Z. Circulating miRNA in patients with non-alcoholic fatty liver disease and coronary artery disease. BMJ Open Gastroenterol 2016;3:e000096. doi:10.1136/bmjgast-2016-000096.
[60] Soh J, Iqbal J, Queiroz J, Fernandez-Hernando C, Hussain MM. MicroRNA-30c reduces hyperlipidemia and atherosclerosis in mice by decreasing lipid synthesis and lipoprotein secretion. Nat Med 2013;19:892–900. doi:10.1038/nm.3200.
[61] Irani S, Hussain MM. Role of microRNA-30c in lipid metabolism, adipogenesis, cardiac remodeling and cancer. Curr Opin Lipidol 2015;26:139–46. doi:10.1097/MOL.0000000000000162.
[62] Young PA, Senkal CE, Suchanek AL, Grevengoed TJ, Lin DD, Zhao L, et al. Long-chain acyl-CoA synthetase 1 interacts with key proteins that activate and direct fatty acids into niche hepatic pathways. J Biol Chem 2018. doi:10.1074/jbc.RA118.004049.
[63] Li LO, Mashek DG, An J, Doughman SD, Newgard CB, Coleman RA. Overexpression of rat long chain acyl-CoA synthetase 1 alters fatty acid metabolism in rat primary hepatocytes. J Biol Chem 2006. doi:10.1074/jbc.M604427200.
[64] Parkes HA, Carpenter L, Wood L, Ballesteros M, Furler SM, Kraegen EW, et al. Overexpression of acyl-CoA synthetase-1 increases lipid deposition in hepatic (HepG2) cells and rodent liver in vivo. Am J Physiol Metab 2006. doi:10.1152/ajpendo.00112.2006.
[65] Li LO, Ellis JM, Paich HA, Wang S, Gong N, Altshuller G, et al. Liver-specific loss of long chain Acyl-CoA synthetase-1 decreases triacylglycerol synthesis and β-oxidation and alters phospholipid fatty acid composition. J Biol Chem 2009. doi:10.1074/jbc.M109.022467.
[66] Luukkonen PK, Zhou Y, Sädevirta S, Leivonen M, Arola J, Orešič M, et al. Hepatic ceramides dissociate steatosis and insulin resistance in patients with non-alcoholic fatty liver disease. J Hepatol 2016;64:1167–75. doi:10.1016/j.jhep.2016.01.002.
[67] Goldenberg JR, Wang X, Lewandowski ED. Acyl CoA synthetase-1 links facilitated long chain fatty acid uptake to intracellular metabolic trafficking differently in hearts of male versus female mice. J Mol Cell Cardiol 2016;94:1–9. doi:10.1016/j.yjmcc.2016.03.006.
[68] Norris GH, Porter CM, Jiang C, Millar CL, Blesso CN. Dietary sphingomyelin attenuates hepatic steatosis and adipose tissue inflammation in high-fat-diet-induced obese mice. J Nutr Biochem 2017. doi:10.1016/j.jnutbio.2016.09.017.

FIGURE LEGENDS

Figure 1: Palmitate, compound C and metformin modify lipid deposition and gene expression in hepatocytes. Oil Red O staining in both **a)** primary human hepatocytes (HH) and **b)** HepG2 cells challenged with palmitate (PA), compound C (CC) and metformin (Mtf), and non-treated controls (Cnt). Optical density (OD) was measured at 500 nm and relative quantification of the Oil Red O staining is shown in plots. Results are expressed as mean ± SEM. Changes (% vs control) of gene expression in treated **c)** HH and **d)** HepG2 cells. Color-scale goes from red (increased) to green (decreased). n≥3 replicates/ cell/ treatment. * $p<0.05$, ** $p<0.01$.

Figure 2: Treatments mimicking NAFLD and metformin impact on miRNA expression patterns in hepatocytes. a) Volcano plots represent changes in miRNA expression profiles assessed in primary human hepatocytes (HH) challenged with palmitate (PA), compound C (CC) and metformin (Mtf). Red circles stand for statistically significant miRNAs ($p<0.05$). Venn diagrams plot the number of decreased/increased miRNA upon treatments with PA (blue), CC (red) and Mtf (green). The number of hepatic miRNAs showing significant alterations are depicted in the bar plots. **b)** Statistically significant variations detected in miRNA quantities with at least one treatment. Color-scale goes from red (increased) to green (decreased). n=3 replicates/ treatment. **c)** Altered expression levels of specific preselected miRNA candidates were also observed in HepG2. Results are expressed as mean ± SEM. * $p<0.05$, ** $p<0.01$.

Figure 3: *AMPK* and *DICER* knockdown (KD) enhances lipid accumulation in hepatocytes. a) Oil Red O staining of *AMPK* and *DICER* KD and control (Cnt) cells. Optical density (OD) was measured at 500 nm. **b)** Gene expression measures in *AMPK* (a.k.a. *PRKAA1*) KD vs control. **c)** Gene expression in *DICER* KD vs control. **d)** Impact of genetic modifications on the expression levels of miRNA candidates. Results are expressed as mean ± SEM. * $p<0.05$, ** $p<0.01$.

Figure 4: AMPK knockdown (KD) *in vivo*. a) Hepatic levels of phosphor(p)-ACC protein levels normalized by actin levels. **b)** Percentage of the Oil Red O stained area in liver. **c)** Triglyceride (TG) content in the liver normalized by grams of tissue. **d)** Gene and **e)** miRNA expression in mice subjected to tail-injection of AMPK sh-RNA lentivirus (AMPK-DN, n=9) vs vehicle (VH, n=7). Data is expressed as mean ± SEM. * $p<0.05$, ** $p<0.01$.

Figure 5: Impact of miRNA candidates on lipid metabolism. a) Lipid droplet staining in Huh7 cells transfected with non-targeting (NT) miRNA and different mimic miRNA candidates. Bar plots show average of lipid droplet area vs cell number. Bodipy 493/503 (green) and DAPI (blue) report lipid droplets and nuclei, respectively. **b)** Triglyceride, diacylglycerol, and cholesterol esters (c.p.m. per ng

protein) measured in transfected HepG2 by thin-layer chromatography. **c)** Triglycerides and cholesterol content (mmol/L per ng protein) in culture supernatants. **d)** Oxygen consumption rate (OCR) in NT control (orange dots), and HepG2 cells transfected with mimic miR-16 (green squares), miR-30b (straight red triangles), and miR-30c (inverted blue triangles). Seahorse quantification (pmol/ min/ µg protein) is shown in the plot. **e)** Apolipoprotein B (apoB) measures (ng/ µg cell protein) in transfected HepG2 and control cells. **f)** Heatmap showing predicted miRNA/pathways clusters interaction, according to DIANA-miRPath v3.0 and TarBase v7.0 algorithms. **g)** Expression of genes involved in lipid metabolism upon treatments with mimic miRNA candidates. **h)** Huh7 cells transfected with a wildtype control (WT) *ACSL1* 3'UTR dual Luc reporter or mutated *ACSL1* 3'UTR (MUT). Firefly Luc activity normalized for *Renilla* signal is shown. **i)** Western blot results for ACSL1 in HepG2 cells after transfection with NT control or mimic miRNA. The ACSL1 signal was quantified and normalized against total protein in 2 independent experiments. **j)** Predicted pairing of target region of *ACSL1* (wild-type and mutated) and miRNAs. Data in plots is expressed as mean ± SEM. * $p<0.05$, ** $p<0.01$.

Figure 6: Impact of miR-16, miR-30b and miR-30c on specific lipid species. **a)** Principal component analysis (PCA) of lipid classes and families significantly affected by treatment of mimic miRNA candidates in HepG2 cells. The color-scale indicates the intensity of detected changes (more red stands for more intense). **b)** Lipid species grouped in families significantly affected by mimic miR-16, miR-30b, and/or miR-30c. **c)** mRNA expression measures of genes related to the synthesis and degradation of phosphatidylethanolamine plasmalogens (PEP), sphingomyelins and ceramides, and those mainly related to the formation of lipid droplets (LD). n=6 replicates/ treatment. Data is expressed as mean ± SEM. * $p<0.05$, ** $p<0.01$.

Figure 7: Recovery of miR-30b and miR-30c in hepatocytes protects against lipid deposition. a) Lipid droplet staining in cells transfected with non-targeting control (NT), miR-30b and miR-30c. Bodipy 493/503 (green) and DAPI (blue) report lipid droplets and nuclei, respectively. **b)** Bar plots represent relative lipid droplet area per cell area, the value for NT being set at 100. **c)** Quantification of miRNA, and **d)** expression analysis of genes related to lipid biosynthesis and glucose metabolism after mimic transfection in treatments leading to increased FA deposition (i.e. *AMPK* and *DICER* knockdown (KD), and CC). Data is expressed as mean ± SEM. * $p<0.05$, ** $p<0.01$.

Figure 8: Gene and miRNA expression in subjects with and without NAFLD. **a)** Expression of miR-16, miR-30b, miR-30c, *ACSL1*, *DICER* and *AMPK* (a.k.a. PRKAA1) in liver biopsies from obese women with (NAFLD) or without non-alcoholic fatty liver disease. **b)** Spearman correlations between miRNA and gene

expression levels and body mass index (BMI) and fasting triglycerides (TGs). Data in bar plots is expressed as mean ± SD. * $p<0.05$, ** $p<0.01$.

Figure 1

a Primary human hepatocytes (HH)

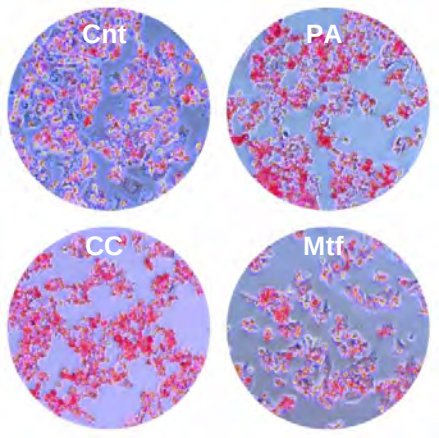

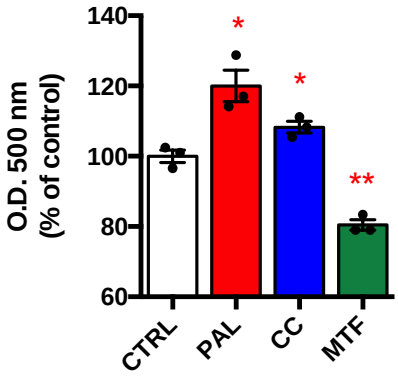

b HepG2 cells

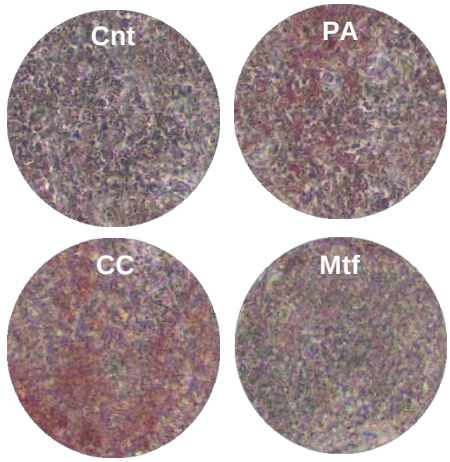

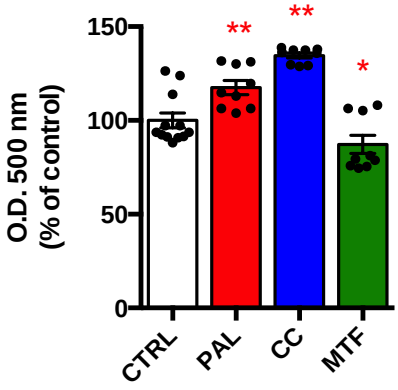

c

HH	PA	CC	Mtf
De novo fatty acid (FA) biosynthesis			
ACSL1	**154.9****	**37***	**-50.8***
FASN	**16.2****	**66.8***	22.5
LPL	6	**73.2****	22.2
FA uptake and transport			
FATP5	**115.8***	62.3	5.6
CD36	**56.0****	**-49.1****	-14.6
PLTP	**26.7****	**61.5***	-21.3
Glucose metabolism			
GLUT2	**-34,5****	**-16,6****	55.2
Inflammation			
TNFα	151.2	29.6	**-59.9***
ITGAX	**286.8****	-17.2	31.7
IL8	**635.6***	**-39.9***	12.6
miRNA processing machinery			
DROSHA	**-30.5****	**-31.9****	27
XPO5	**-16.0****	**-13.4***	**28.4***
DICER	**-28.8****	**-14.6***	**32.8***
AGO2	-13.5	-11.8	**48.2***

* p-val<0.05, ** p-val<0.01

d

HepG2	PA	CC	Mtf
De novo fatty acid (FA) biosynthesis			
ACSL1	**214.47****	**65.46****	**-15.37***
FASN	**29.84****	**116.76****	-3.63
LPL	**52.38****	55.16	-2.51
FA uptake and transport			
FATP5	**30.8***	**-77.7****	**-58.8***
CD36	**45.5****	**-79.5****	**-38.7****
PLTP	4.1	-12.6	-25.2
Glucose metabolism			
GLUT2	**-16.1***	**-74.3****	11.4
Inflammation			
TNFα	**227.8****	**162.0***	-21.4
ITGAX	**304.0***	56.2	5.2
IL8	19.7	-62.3	7.3
miRNA processing machinery			
DROSHA	**-19.9***	3.6	-13.3
XPO5	-4.5	-18.9	**-13.9***
DICER	**-11.7***	**-15.3****	1.1
AGO2	**63.4****	**266.2****	10.8

* p-val<0.05, ** p-val<0.01

Figure 2

a

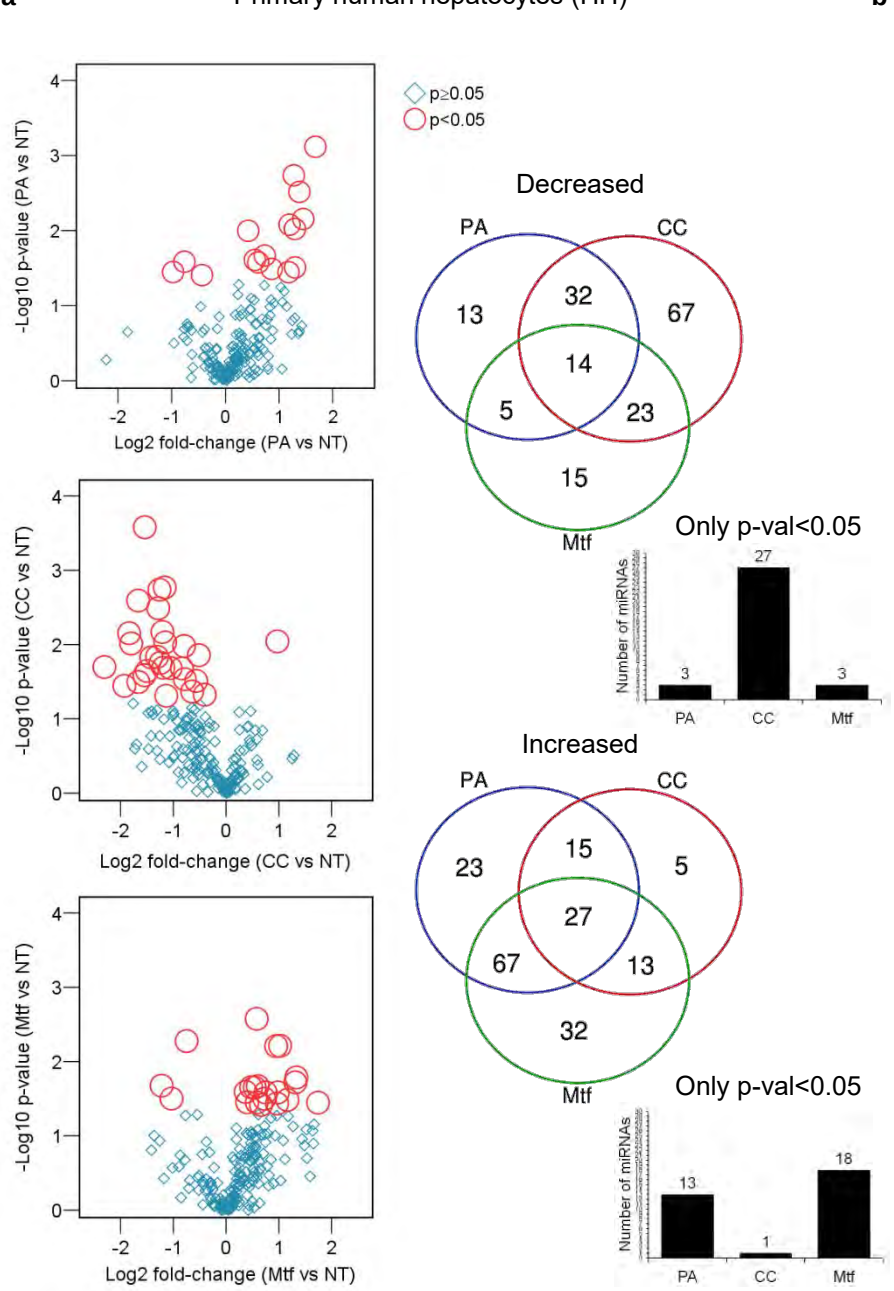

b

MicroRNAs	PA	CC	Mtf
hsa-let-7b	**-26.4***	19.0	-22.1
hsa-miR-100	20.4	**-68.8****	22.7
hsa-miR-106a	23.6	**-55.4****	40.8
hsa-miR-10a	59.6	**-71.9****	163.7
hsa-miR-1225-3P	**142.5****	-39.4	-41.1
hsa-miR-1227	-53.9	-37.4	**-52.2***
hsa-miR-1255B	**121***	-12.5	-14.2
hsa-miR-126	8.9	-33.9	**66***
hsa-miR-1274A	**175****	4.4	-0.5
hsa-miR-1274B	**143****	35.2	9
hsa-miR-1290	**68.1***	-26.1	-4
hsa-miR-130a	**34***	-31.1	-0.2
hsa-miR-130b	-41.8	**-56.7****	10.5
hsa-miR-132	2.9	0.1	**29.6***
hsa-miR-139-5p	-3.7	-13.3	**38.4***
hsa-miR-146a	107.7	**-59.1****	**146.2***
hsa-miR-146b	7.9	**-55.2****	95.2
hsa-miR-149#	**139.1***	18.9	98
hsa-miR-151-5P	19.1	-41.5	**92.2****
hsa-miR-152	**-50***	58	347.7
hsa-miR-16	34.9	**-72.7****	60.3
hsa-miR-17	13.7	**-58.5****	39.1
hsa-miR-199a-3p	14	**-67.1***	41.3
hsa-miR-200b	7.4	**-56***	20.8
hsa-miR-206	12.3	-29.1	**32.5***
hsa-miR-20a	10.8	**-60.2***	17.6
hsa-miR-20b	-15.4	-22.5	**104****
hsa-miR-21	8.3	**-58.5***	2.3
hsa-miR-22#	124.6	-74.7	**56.7***
hsa-miR-221	0.2	**-44.6***	**49.4****
hsa-miR-222	23.7	**-29.9***	26.3
hsa-miR-24	22.8	**-32.8***	44.3
hsa-miR-26a	5.1	**-52.2***	**96.8***
hsa-miR-27a	**52.8***	-21.5	**50.4***
hsa-miR-29a	20.9	**-36.6***	27.5
hsa-miR-30a-3p	48.9	-50.1	**51***
hsa-miR-30a-5p	-20.3	-49	**91.5***
hsa-miR-30b	18.9	**-42.2***	63.5
hsa-miR-30c	21.6	-32.7	**66.6***
hsa-miR-331-5p	-93.9	36	**-57.5***
hsa-miR-365	66.7	**-55.8***	55.4
hsa-miR-370	**162.2****	20.4	62.9
hsa-miR-374-5p	14.6	**-74.4***	-35.4
hsa-miR-375	**221.4****	13.4	-21.1
hsa-miR-376c	2.9	**-63.3***	0.5
hsa-miR-378	40.9	**-42.5***	**45.6***
hsa-miR-379	-39.6	-75.1	**258.9***
hsa-miR-411	**81.3***	**-67.2***	31.4
hsa-miR-432	**47.2***	-5.6	-1.4
hsa-miR-454	-25.3	**-65.9***	83.8
hsa-miR-489	**-40.8***	-5	-57
hsa-miR-505#	74.8	5.5	**129.9***
hsa-miR-532	95.4	-48.2	**151.4***
hsa-miR-655	-22.6	**-81.3***	26
hsa-miR-661	116.5	43.6	**-40.5****
hsa-miR-720	**128.9****	25.3	11.5
hsa-miR-744	18.5	**-24.7***	-31.8
hsa-miR-886-3p	46.5	**94.8****	-11.5
hsa-miR-99a	-3.4	**-65.6****	79.1

* p-val<0.05, ** p-val<0.01

c

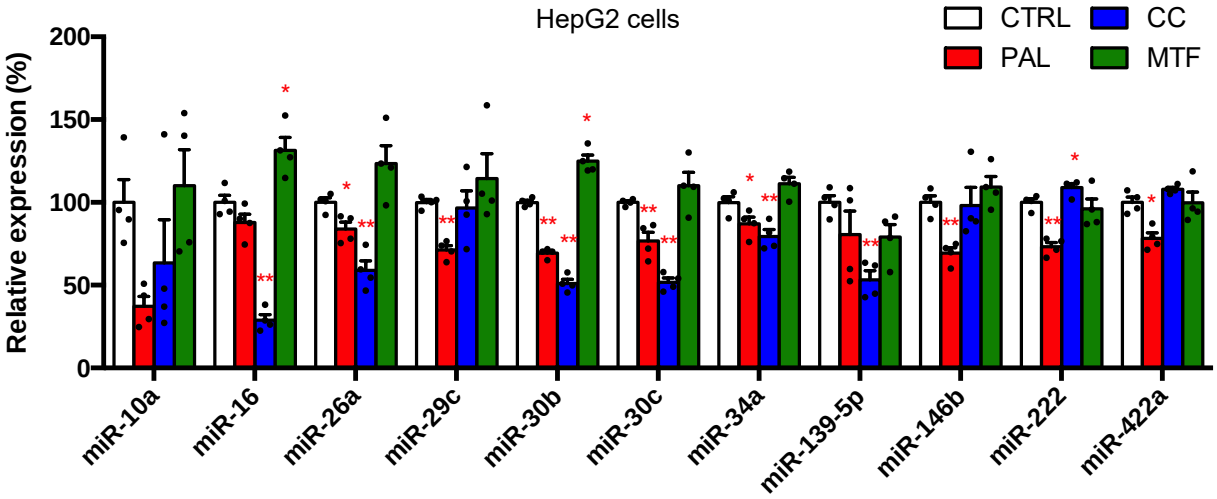

Figure 3

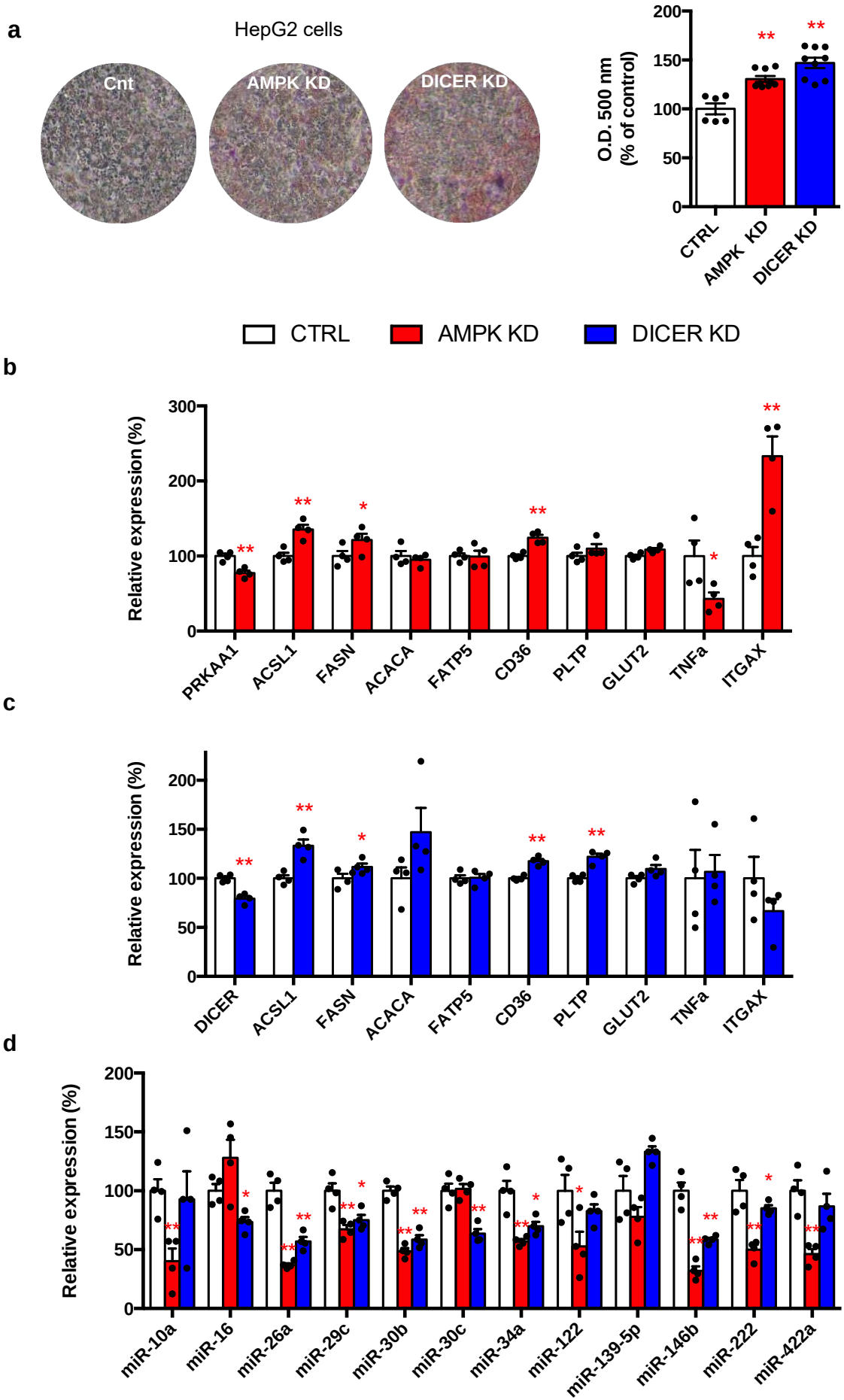
a
HepG2 cells
Cnt
AMPK KD
DICER KD
O.D. 500 nm (% of control)
CTRL
AMPK KD
DICER KD
b
Relative expression (%)
PRKAA1
ACSL1
FASN
ACACA
FATP5
CD36
PLTP
GLUT2
TNFa
ITGAX
c
Relative expression (%)
DICER
ACSL1
FASN
ACACA
FATP5
CD36
PLTP
GLUT2
TNFa
ITGAX
d
Relative expression (%)
miR-10a
miR-16
miR-26a
miR-29c
miR-30b
miR-30c
miR-34a
miR-122
miR-139-5p
miR-146b
miR-222
miR-422a

Figure 4

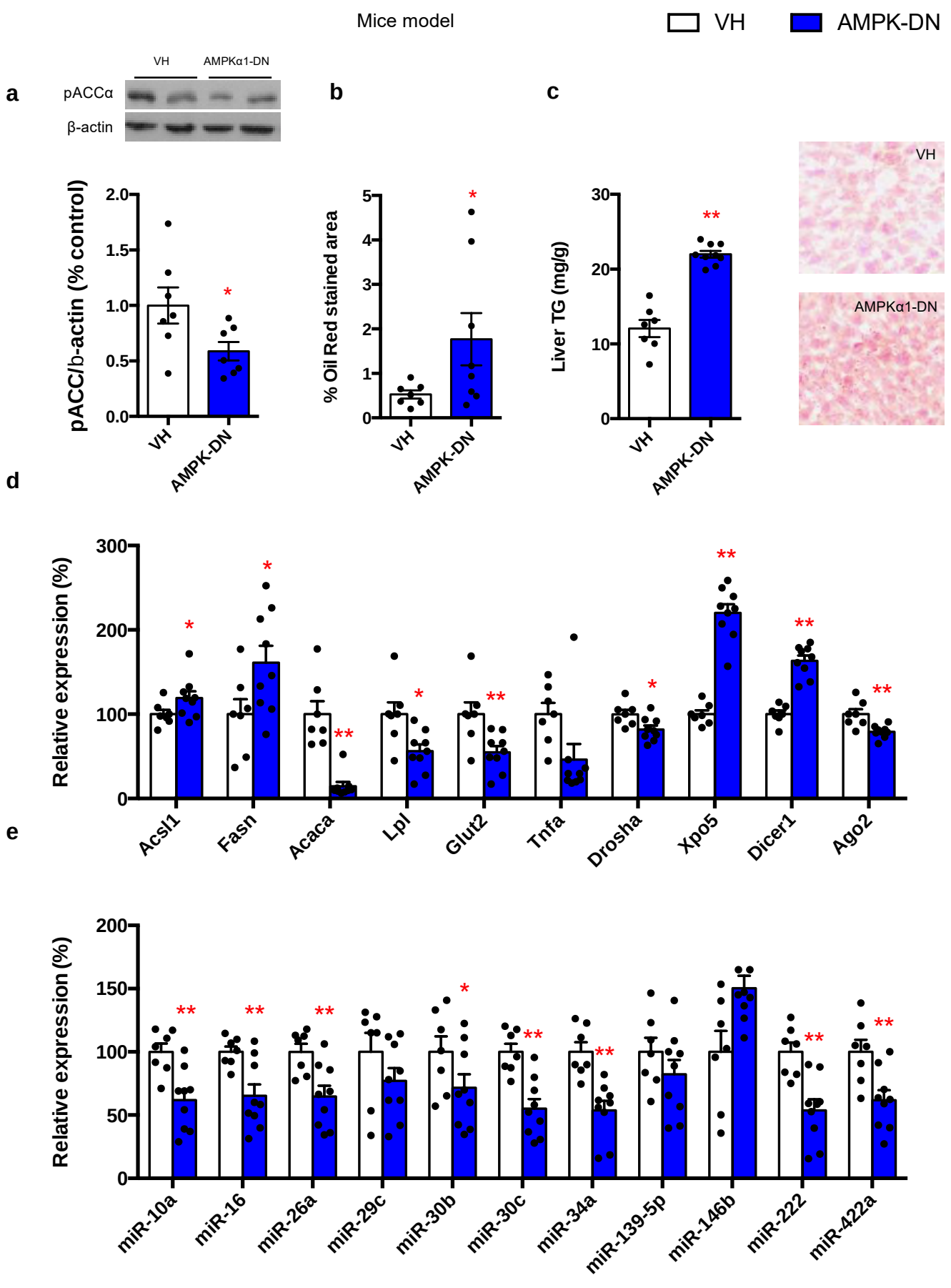
Mice model
VH
AMPK-DN
a
VH
AMPKα1-DN
pACCα
β-actin
b
c
pACC/b-actin (% control)
% Oil Red stained area
Liver TG (mg/g)
VH
AMPKα1-DN
d
Relative expression (%)
Acsl1
Fasn
Acaca
Lpl
Glut2
Tnfa
Drosha
Xpo5
Dicer1
Ago2
e
Relative expression (%)
miR-10a
miR-16
miR-26a
miR-29c
miR-30b
miR-30c
miR-34a
miR-139-5p
miR-146b
miR-222
miR-422a

Figure 5

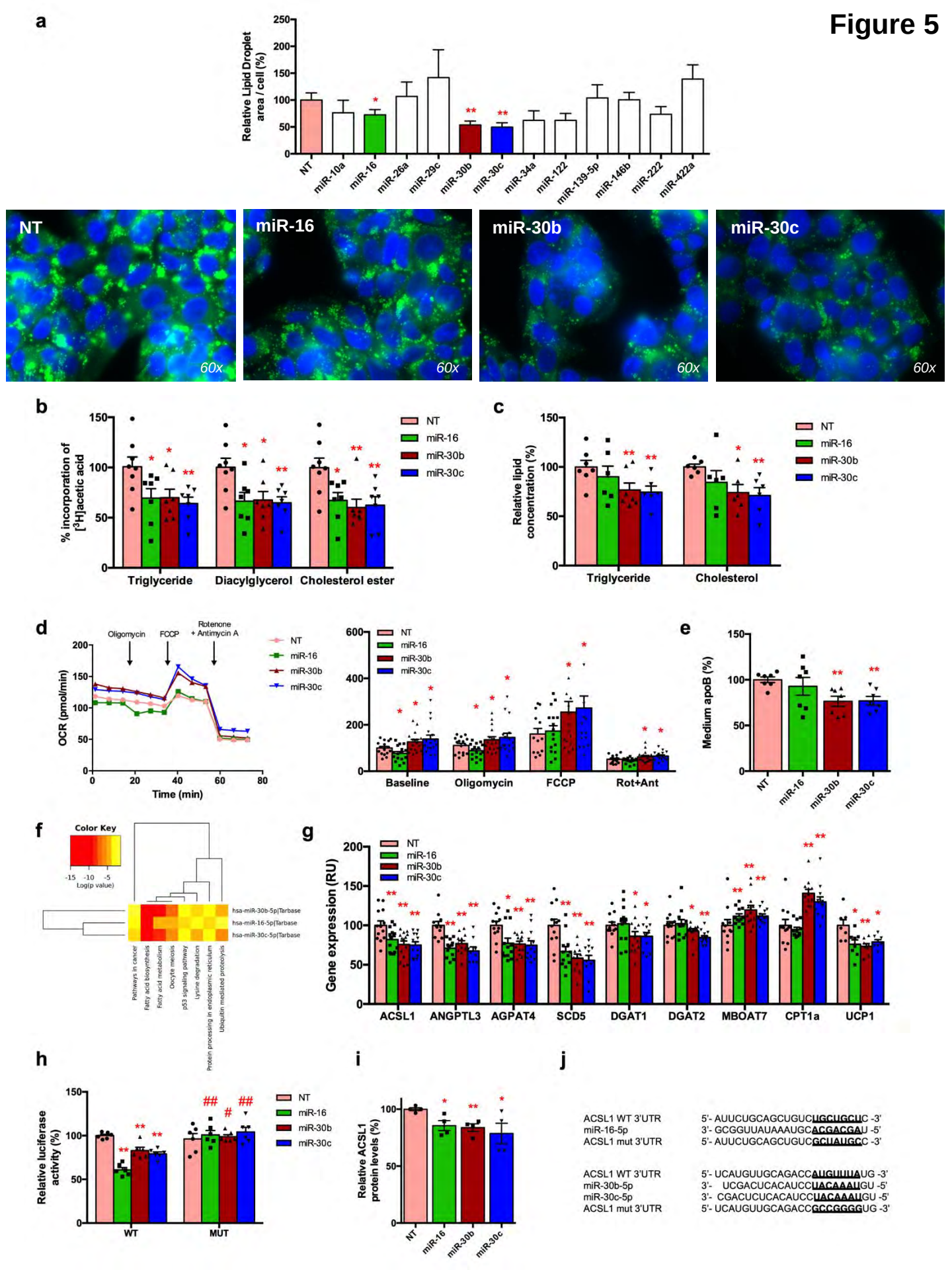
a
Relative Lipid Droplet area / cell (%)
NT
miR-10a
miR-16
miR-26a
miR-29c
miR-30b
miR-30c
miR-34a
miR-122
miR-139-5p
miR-146b
miR-222
miR-422a
NT
miR-16
miR-30b
miR-30c
60x
b
% incorporation of [3H]acetic acid
Triglyceride
Diacylglycerol
Cholesterol ester
c
Relative lipid concentration (%)
Triglyceride
Cholesterol
d
Oligomycin
FCCP
Rotenone + Antimycin A
OCR (pmol/min)
Time (min)
Baseline
Oligomycin
FCCP
Rot+Ant
e
Medium apoB (%)
f
Color Key
Log(p value)
hsa-miR-30b-5p|Tarbase
hsa-miR-16-5p|Tarbase
hsa-miR-30c-5p|Tarbase
Pathways in cancer
Fatty acid biosynthesis
Fatty acid metabolism
Oocyte meiosis
p53 signaling pathway
Lysine degradation
Protein processing in endoplasmic reticulum
Ubiquitin mediated proteolysis
g
Gene expression (RU)
ACSL1
ANGPTL3
AGPAT4
SCD5
DGAT1
DGAT2
MBOAT7
CPT1a
UCP1
h
Relative luciferase activity (%)
WT
MUT
i
Relative ACSL1 protein levels (%)
j
ACSL1 WT 3'UTR 5'- AUUCUGCAGCUGUCUGCUGCUC -3'
miR-16-5p 3'- GCGGUUAUAAAUGCACGACGAU -5'
ACSL1 mut 3'UTR 5'- AUUCUGCAGCUGUCGCUAUGCC -3'
ACSL1 WT 3'UTR 5'- UCAUGUUGCAGACCAUGUUUUAUG -3'
miR-30b-5p 3'- UCGACUCACAUCCUACAAAUGU -5'
miR-30c-5p 3'- CGACUCUCACAUCCUACAAAUGU -5'
ACSL1 mut 3'UTR 5'- UCAUGUUGCAGACCGCCGGGGUG -3'

Figure 6

a

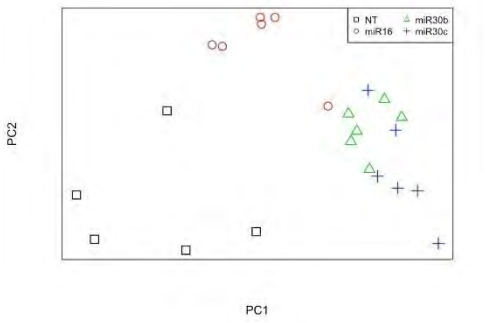

Lipid	Species	NT	16	30b	30c
LPE	20:3		*	*	*
	20:4		*	*	*
	22:6		**	*	**
PE	32:1		**		
	36:4			*	
	38:3		**		
	38:4		**		
	38:5		**		
	38:6		*		
	40:5		**		
	40:6		**		
PS	32:1			**	
	34:1			*	*
	34:2			*	*
	36:1			*	
	36:2		*	*	
	36:3		*	**	*
	36:4			*	*
	38:1			*	
	38:3		**		
	38:4		**		
	38:6				*
	40:3			**	*
	40:4		**	**	*
	40:6		**		
	42:5		*	**	
PI	34:1		*		*
	36:2		*		
	38:3		**		
	38:4		**		
	40:5		*		
PEP	16:0/16:0			**	**
	16:0/16:1			*	*
	16:0/18:0			**	**
	18:0/16:0		**	**	**
	16:0/18:1			**	*
	18:1/16:0			**	**
	18:0/16:1		**	**	**
	16:0/18:2			**	**
	18:1/16:1			*	
	18:0/18:0		*	**	**
	18:1/18:0			**	**
	18:0/18:1			**	**
	18:1/18:1		**	*	**
	18:0/18:2		**	**	**
	16:0/20:3			**	**
	18:1/18:2			**	**
	18:0/18:3		*	**	**
	16:0/20:4		**	**	**
	18:1/18:3			**	**
	16:0/20:5			*	*
	16:0/22:3		*	**	**
	18:0/20:3			*	**
	16:0/22:4			**	**
	18:1/20:3		**	*	**
	18:0/20:4			*	**
	16:0/22:5		*	**	**
	18:1/20:4		**	**	**
	18:1/20:5		**	*	**
	16:0/22:6			*	*
	18:1/20:5		*	**	**
	18:0/22:3			**	**
	18:0/22:5		**	**	**
	18:1/22:5		**	**	**
	18:0/22:6			**	**
	18:1/22:6			*	**
LPC	15:0			*	**
	16:0		*		
	16:1		**		
	18:0				*
LPC	18:1		*		
	18:2		*		
	18:3			*	**
	20:0			**	**
	20:3		*		
	20:4		*		
	20:5			*	**
	22:4				*
	22:5				*
	22:6				*
PC	32:0		*		
	32:2		*		
	34:1		**		
	34:2		**		
	34:3		**	**	**
	36:3		**		
	36:4		**	*	
	36:5		**	**	*
	38:2				**
	38:3		**		
	38:4		**		
	38:5		**		
	38:6		**		
	40:5		*		
	40:6		**		
PC O	32:0			*	
	32:1			**	
	34:0			**	*
	34:2		*		
	36:1			*	
	36:4		**	*	*
	38:4		**	*	*
SM	32:1		*		
	33:1		**		
	34:2		*		
	35:1		**	*	
	36:2		*	*	
	38:0		*		
	40:2		*		
	40:3				*
	42:1				**
	42:2		**	*	**
	42:3				*
Cer	18:1/16:0				*
	18:1/18:0				*
	18:1/18:1		*	**	**
	18:1/20:0			**	**
	18:1/22:1			*	**
	18:1/26:0		*	**	**
	18:1/26:1		*	*	**

Lipid	Species	NT	16	30b	30c
HexCer	18:1/12:0		*		
	18:1/23:0			*	*
	18:1/26:0			*	*
LPC	16:1			*	*
Cer	32:1;2			**	**
	42:1;2	*			
PC	31:0		*	**	**
	31:1			*	*
	31:2		*	*	
	32:0		**		
	32:1		**		
	32:2		**	*	
	33:1		**	**	**
	33:2			**	**
	34:1		**		
	34:2		**		
	34:3		**	**	*
	35:1		*		
	35:2		**		
	35:3		**		
	35:4		**		
	36:3		**		
	36:4		**		*
	36:5		**	**	
	38:2				**
	38:3		*		
	38:4		**		
	38:5		**		
	38:6		**		
	39:4			*	
	40:7		**		
PE	30:0			**	**
	32:1			*	
	32:2			**	*
	33:1			*	*
	34:3		*	*	*
	35:2		*	*	*
	36:4			*	
	36:5			**	
	37:3		*		
	37:4			*	
	38:3		*		
	38:4		**	*	
	38:5		*		
	38:6		**	*	
	38:7		**		
	40:6		*		
	40:7		**		
PG	34:2		*		
	36:2		*		*
	36:3		**		
PI	34:2			*	
	35:0		*		
	36:3			*	
	36:4			*	
	38:3		**	*	**
	38:4		*		
SM	34:1;2		**		
	42:1;2		*		*
	42:2;2		**	*	
CE	16:1			**	
	16:2		**		*
	18:2		**	*	
	20:1	**			*
	20:4	**			
	22:1			*	
DG	30:0				*
	30:3		**	*	**
	31:1			*	
	31:2			**	**
	31:3		*	**	**
	32:3		*	**	*
	33:1			*	
	33:2		*	**	**
	33:3		**	**	**
	34:2		*		**
	35:2				*
	36:2				**
	36:5		*	*	
	37:2				*
	37:3		*	*	*
	38:3		**	*	*
	38:5			*	
	38:8		*	*	*
	39:6		*	*	*
TG	41:4			*	
	44:0			*	**
	44:1				*
	46:1				**
	48:0		**		*
	48:1				**
	48:2		*		**
	48:3		*	*	
	48:4				*
	49:1				*
	49:2			*	
	50:1			*	**
	50:2		*		**
	50:3		**	*	
	50:4		**	*	
	51:2		**		
	51:3		**	**	
	52:2		**		**
	52:3		**		
	52:5		**	**	*
	53:2		**		
	53:3		**	*	
	53:4		**	**	*
	54:2		**	**	**
	54:3		**		
	54:4		**	*	
	54:5		**	*	
	55:3		**		
	55:4		**	**	**
	56:2				*
	56:3		**		*
	56:4		**		
	56:5		**		
	56:6		**		**
	58:5		*		
	58:7		*		
	60:2		*		*

* p-val<0.05, ** p-val<0.01

b

Abbrev.	Lipid Class	Lipid Category	Method	miR-16	miR-30b	miR-30c
LPE	Lysophosphatidylethanolamine	Glycerophospholipids	QQQ	37.6	34.7	34.1
PE	Phosphatidylethanolamine	Glycerophospholipids	QQQ	**7***	3.9	-0.3
PS	Phosphatidylserine	Glycerophospholipids	QQQ	**7.5***	2.6	-1.1
PG	Phosphatidylglycerol	Glycerophospholipids	QQQ	26.8	19.4	11.4
PI	Phosphatidylinositol	Glycerophospholipids	QQQ	**7.1***	4.1	0.2
PE P	based plasmalogens	Glycerophospholipids	QQQ	**-33.2****	**-51.6****	**-55.4****
LPC	Lysophosphatidylcholine	Glycerophospholipids	QQQ	**23.6***	-1.6	-7.6
PC	Phosphatidylcholine	Glycerophospholipids	FTMS	12.5	4.7	0.7
PC O	Phosphatidylcholine-ether	Glycerophospholipids	FTMS	-4.8	-19.7	-17
SM	Sphingomyelin	Sphingolipids	FTMS	**15.1****	**15.1***	**10.4***
Cer	Ceramide	Sphingolipids	QQQ	-1.7	-7	**-11.6***
HexCer	Hexosylceramide	Sphingolipids	QQQ	**-24.3****	**-25.6****	**-30.1****
CE	Cholesteryl Ester	Sterol Lipids	FTMS	1.5	6.9	2.2
DG	Diacylglycerol	Glycerolipids	FTMS	-6	-7.8	-9.4
TG	Triacylglycerol	Glycerolipids	FTMS	**10.8****	0.8	**-9****
FC	Free Cholesterol	Sterol Lipids	FTMS	-1.4	-3.6	-6.3

* p-val<0.05, ** p-val<0.01

c

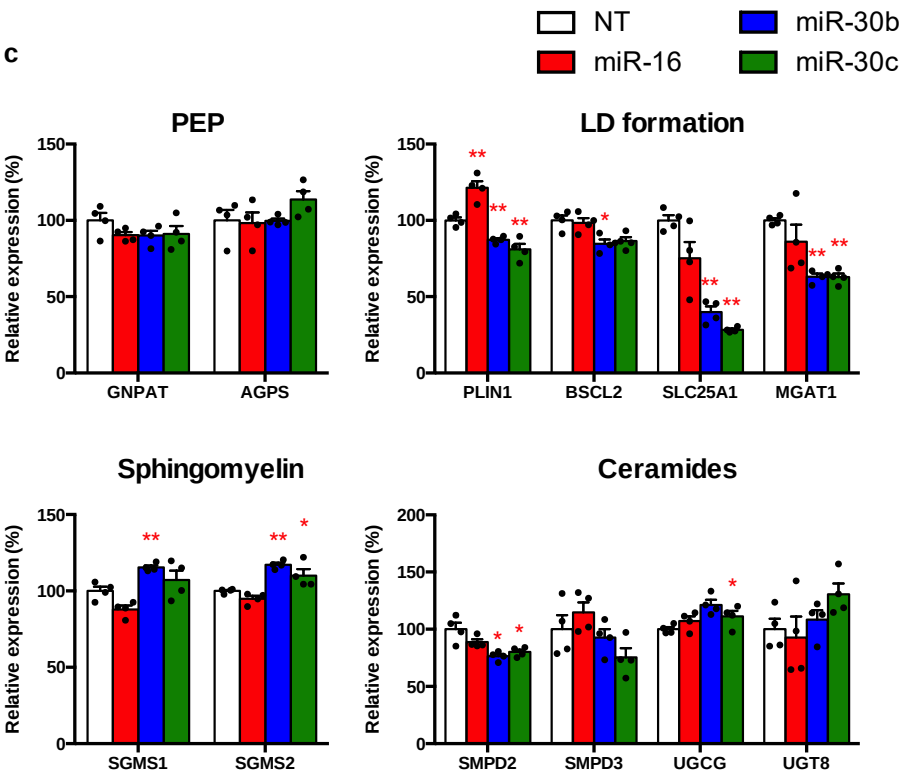

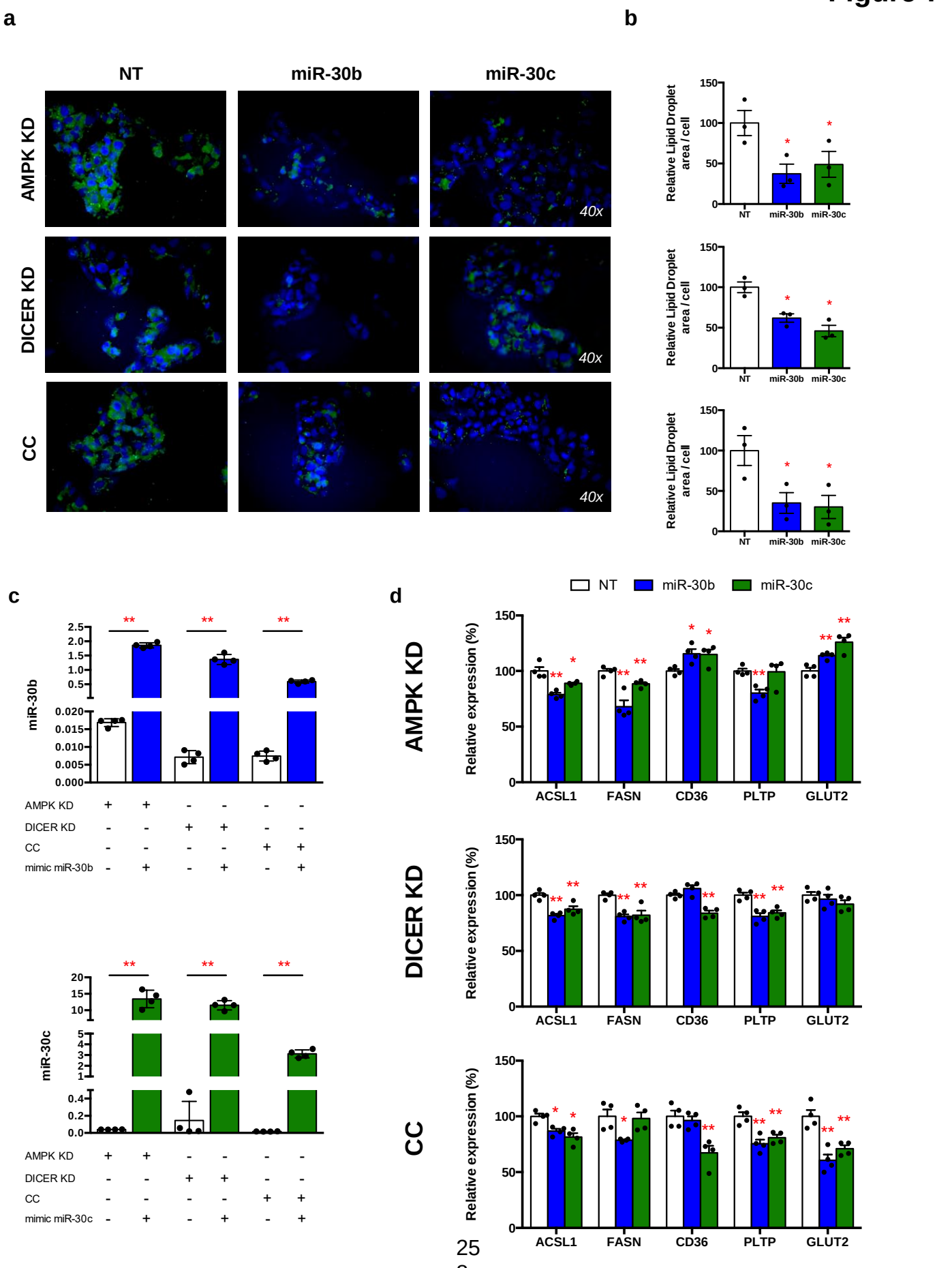
a
NT
miR-30b
miR-30c
AMPK KD
DICER KD
CC
40x
b
Relative Lipid Droplet area / cell
NT
miR-30b
miR-30c
c
miR-30b
miR-30c
AMPK KD
DICER KD
CC
mimic miR-30b
mimic miR-30c
d
NT
miR-30b
miR-30c
AMPK KD
DICER KD
CC
Relative expression (%)
ACSL1
FASN
CD36
PLTP
GLUT2

Figure 8

a

Human liver samples

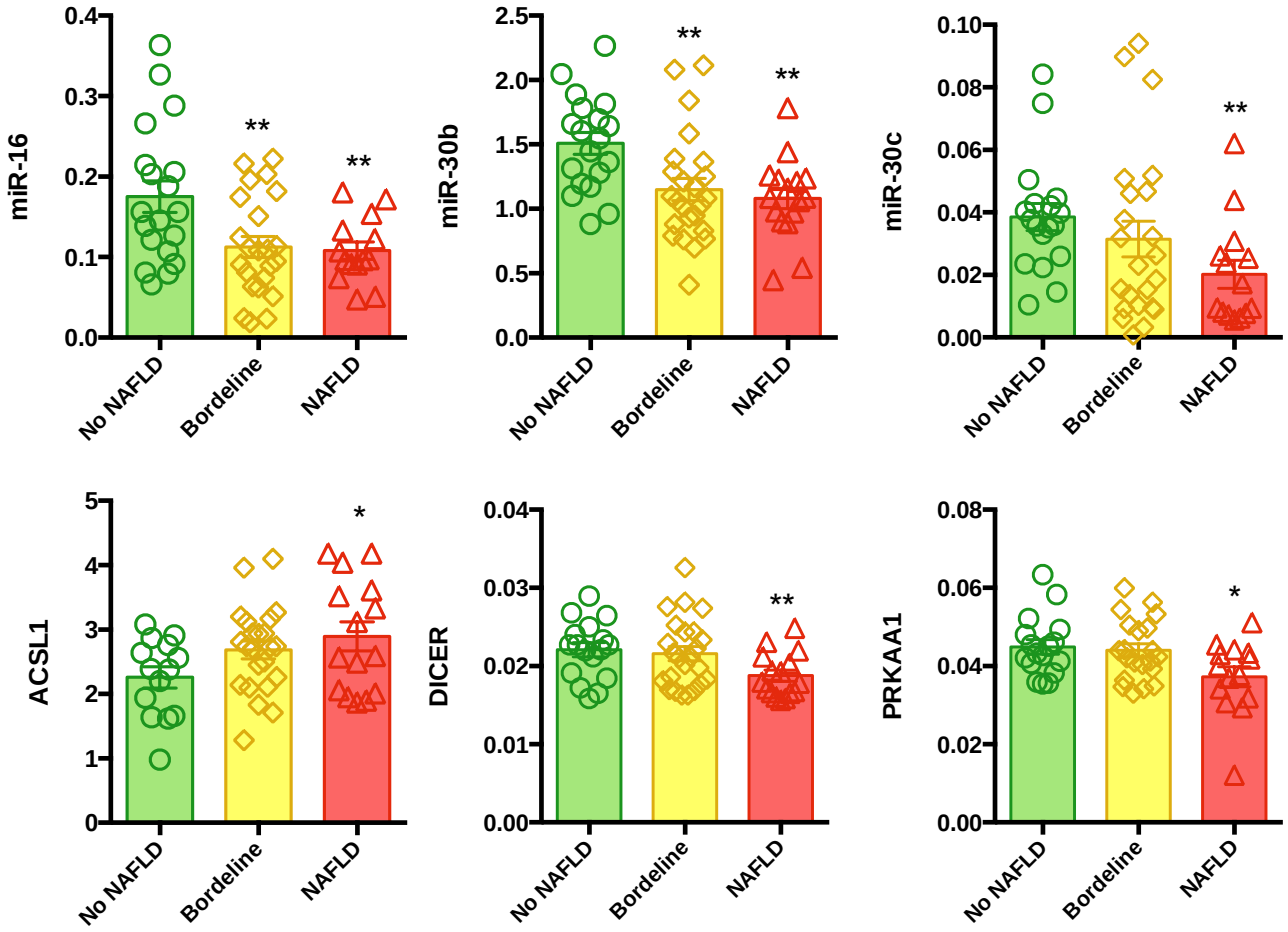

b